Patient-specific cardiovascular biomechanical modeling to augment interpretation of clinical data and assist planning interventions for patients with congenital heart disease

Maria Gusseva

INSTITUT POLYTECHNIQUE DE PARIS

NNT : 2022IPPAX007

Thèse de doctorat

ÉCOLE POLYTECHNIQUE

IP PARIS

Patient-specific cardiovascular biomechanical modeling to augment interpretation of clinical data and assist planning interventions for patients with congenital heart disease

Thèse de doctorat de l'Institut Polytechnique de Paris
préparée à l'École polytechnique

École doctorale n°626 École doctorale de l'Institut Polytechnique de Paris (EDIPP)
Spécialité de doctorat : Biomécanique

Thèse présentée et soutenue à Palaiseau, le 24 Mars 2022, par

MARIA GUSSEVA

Dr. Abdul Barakat Professor, LadHyX, École Polytechnique, France	Président
Dr. Jan Janoušek Professor of pediatric cardiology, Children's Heart Center, University Hospital Motol, Charles University, Prague, Czech Republic	Rapporteur
Dr. Alistair Young Professor, School of Biomedical Engineering and Imaging Sciences, King's College London, UK	Rapporteur
Dr. Vicky Y. Wang Research Scientist, Radiological Sciences Laboratory, Stanford University, CA, USA	Examinateur
Dr. Joost Lumens Professor, Department of Biomedical Engineering, Maastricht University, Netherlands	Examinateur
Dr. Eva Sammut Clinical lecturer in cardiology, Bristol Medical School, University of Bristol, UK	Examinateur
Dr. Dominique Chapelle Directeur de recherche, Inria, France	Directeur
Dr. Radomír Chabiniok Assistant professor, Department of Pediatrics, UT Southwestern Medical Center Dallas, TX, USA	Co-directeur
Dr. Tarique Hussain Professor of pediatric cardiology, Department of Pediatrics, UT Southwestern Medical Center Dallas, TX, USA	Co-directeur, Invité

This work was co-funded by Inria and University of Texas Southwestern (UTSW), and was performed at Inria Saclay-Ile-de-France within the MΞDISIM project team (joint with Institut Polytechnique de Paris and part of the LMS laboratory). The research was also funded by the Inria - UTSW Associated Team TOFMOD (Tetralogy of Fallot and Modeling of Diseases).

The research was supported by the W. B. Ellen Gordon Stuart Trust, The Communities Foundation of Texas and by the Pogue Family Distinguished Chair (award to Dr F. Gerald Greil in February, 2015). The work was in addition supported by the Ministry of Health of the Czech Republic [NV19-08-00071]. Research reported was supported by Children's Health^{SM}, but the content is solely the responsibility of the authors and does not necessarily represent the official views of Children's Health^{SM}.

UT Southwestern
Medical Center

Associated Research Team
TOFMOD

children's health

To the memory of my grandmother, Anna G.

Acknowledgements

This thesis has been a precious journey of three and a half years along which I have been immersed into a friendly, encouraging and intellectually stimulating environment. An environment created by people of great professionalism and kindness to whom I would like to express my sincere gratitude here.

First and foremost, I would like to thank my thesis supervisors, Radomír Chabiniok, Dominique Chapelle and Tarique Hussain. Thank you for initiating the collaboration between Inria (France) and University of Texas Southwestern Medical Center in Dallas (USA) – that I know took quite an effort to organize due to transatlantic location of the parties – and for honoring me with an opportunity to work within this collaboration towards developing new solutions for augmented patients' care. This PhD project was truly exciting and motivational for me right from reading the proposal. I would like to thank my supervisors for acknowledging my weaknesses and strengths and creating an environment where I was able to grow in a comfortable and enjoyable way. Thank you, Radek, for your continuous support, teaching and almost immediate availability every time I had a question. Thank you for your genuine interest, enthusiasm and professionalism in developing the subject of this thesis. I truly enjoyed our discussions on heart pathophysiology and biomechanics along all the journey of this work. In addition to that I would like to thank you for your contribution towards developing my scientific writing and presentation skills. Looking back, I see that when we started to work on our first article the level of my writing was rather feeble (compared to what it became at the end of the PhD). But thanks to your guidance and somewhat creative approach to the occurring problems I acquired a solid grasp of scientific writing style. Thank you, Dominique, for your professionalism in guiding my journey towards achieving a PhD degree. Thank you for your teaching and communication attitude, where you give your student enough space to be a leader of the project and at the same time provide rigorous professional and personal support. I truly admire your attention to details and ability to optimize every aspect of the work (and you have taught me to do so as well). All our progress meetings were efficient and educational, where I would always feel enriched with new knowledge and outlook on scientific research in general. Thank you, Tarique, for your genuine interest in translational research and providing a constant clinical outlook on our work. Your enthusiasm towards our results provided additional motivation along the journey. Thank you for all the advice, support and encouragement that you shared with me in these years.

I would also like to express my gratitude to the members of the jury. Firstly, to the examiners of my PhD manuscript, Alistair Young and Jan Janoušek. Thank you for taking your time to provide a thorough evaluation and review of my work. I thank Abdul Barakat for taking the responsibility of chairing the jury. In addition, I would like to thank other members of the jury, Joost Lumens, Eva Sammut, Vicky Y. Wang for your questions during the defense that triggered interesting discussion and provided me with a different viewpoint on possible interpretation of my results. Such an exchange is truly valuable.

Besides my PhD supervisors, I would like to thank clinical collaborators of this project, Gerald Greil, Animesh Tandon, Keren Hasbani, Daniel A. Castellanos, Joshua S. Greer, Mohamed Abdelghafar Hussein, Surendranath R. Veeram Reddy, for providing clinical data of the patients without which the research of this thesis would have been impossible. In addition, I would like to thank Camille Hancock Freisen for your enthusiasm in our results and for providing valuable clinical feedback that shaped the story of our papers acceptable for publication in clinical journal. Thank you, Gerald Greil, Animesh Tandon, and Daniel A. Castellanos for your encouragement, discussions and clinical outlook on our results.

My gratitude also goes to Philippe Moireau for development of CardiacLab cardiac simulation library (including specific components to this project: valve regurgitation & stenosis) – the tool that was fundamental for the development of this PhD research. In addition to that I thank you for hosting me at MΞDISIM team, for your help in solving all the organizational issues related to my circumstances.

I would like to thank Cécile Patte and Martin Genet for providing me with a motion tracking tool. I also thank Cécile Patte, Martin Genet, and Ezgi Berberoglu for introducing to me the fundamentals of MRI image segmentation in MeVisLab during the first year of my PhD.

My gratitude goes to my colleagues from the MΞDISIM team, with whom I was lucky to share this part of my scientific journey. I was surrounded by kind, friendly and dynamic people who are passionate about their work and at the same time care about the well-being of others. I thank the senior members of our team, Philippe Moireau, Patrick Le Tallec, Frédérique Clément, Sébastien Imperiale, Fabrice Vallée, Jean-Marc Allain, Martin Genet, Matthieu Caruel. Thank you for welcoming me at the team, it was a pleasure to share our team events with you. I would like to thank François Kimmig for your kindness and willingness to help with all sorts of problems – from administrative to scientific. Thank you for organizing VendrediSim with Arthur Le Gall that contributed to the dynamics of our team. I would like to thank François Kimmig, Arthur Le Gall, Federica Caforio, Cécile Patte, Nicole Tueni, Ezgi Berberoglu, Florent Wijanto, Chloé Giraudet, Hajer Methenni, Guillaume Balif and Jérôme Diaz. Most of you were there when I joined the team (or soon after), so I thank you for the welcoming and friendly atmosphere that you have created and I really enjoyed sharing an open space with you as well as our discussions during the coffee and lunch breaks. I would like to thank Jessica Manganotti for your company at open space, for taking care of the chouquette meetings and presents for our teammates. I also thank Mahdi Manoochehrtayebi, Mathieu Barre, Tiphaine Delaunay, André Dalmora, Jona Joachim, Giulia Merlini, Alice Peyraut for your company and scientific discussions. Finally, I would like to thank Bahar Carabetta for the administrative support and friendly communications.

My sincere gratitude goes to all members of the family whom I love endlessly. First of all, I would like to thank my dear husband, Temo, who has been supporting me along all the journey of this important chapter in my professional life. You have believed in me more than I have believed in myself. You have been creating such a space of unconditional love and support where all worries vanish and the mind renews for the new discoveries. Thank you Temo for giving me strength that nourished my growth and well-being. I would like to thank our daughter Ariana, who was born after the first year of my PhD and who has enlightened our life from inside out ever since. You were teaching me a healthy work-life balance by blocking me from work in the evenings and weekends. I would most sincerely like to thank my dear parents for your love, endless support and hard work that you have invested in raising me (and my 4 siblings). I thank my mom, Inna, for your endless optimism and encouragement, and for your trust in my dreams. I thank my dad, Sergei, for your love and belief in me that was a source of strength when I was thousands of kilometers away

from home all on my own. You have been holding my hand ever since I was a little girl and have been the proudest one of my small and big achievements (even if not showing that). I truly owe my achievements to my parents. I thank my sister, Anna, for your support and help with Ariana during the important events throughout my PhD. I thank my brother, Andrei, for your support, sense of humor and for calling me a Doctor way before I defended my PhD. I thank my youngest siblings, Misha and Dasha, for all the joyful moments that we spent together. I thank my aunt, Nadezda, for your support, love and kindness and tons of sweets that you had been packing me with so that "I did not feel sad abroad".

Contents

Introduction

Nothing in life is to be feared, it is only to be understood. Now is the time to understand more, so that we may fear less.
— Marie Curie

This PhD work was performed in the MΞDISIM team at Inria Saclay Ile-de-France and École Polytechnique, Palaiseau (France) jointly with University of Texas Southwestern (UTSW) Medical Center, Dallas (USA). It was supervised by Dr. Dominique Chapelle (Inria senior research scientist in the '**M**athematical and **M**echanical **M**odeling with **D**ata **I**nteraction im **SI**mulations for **M**edicine', MΞDISIM, team), Dr. Tarique Hussain (pediatric cardiologist at UTSW Medical Center Dallas) and Dr. Radomír Chabiniok (applied cardiac modeler connecting Inria and UTSW Medical Center).

The aim of this interdisciplinary project is to translate the cardiovascular biomechanical modeling to a clinical environment of patients with congenital heart disease. The advancement of this work was possible thanks to the close collaboration between the biomechanical modeling team at Inria and the department of pediatric cardiology at UTSW Medical Center, particularly within the Inria - UTSW Associated Team 'Tetralogy of Fallot and Modeling of Diseases' (TOFMOD).

Clinical management of congenital heart disease. Application to repaired tetralogy of Fallot

Congenital heart diseases (CHD) account for nearly a third of all congenital birth defects with an incidence of 1% of the total live births worldwide ($\approx$ 1.35 million annual births) [1; 2]. Accurate diagnosis and effective treatment of all types of congenital heart defects has dramatically improved over the past 50 years. Infant survival within the first year after birth with complex congenital heart defects increased from 67.4 % for the 1979-1993 birth cohort to 82.5 % for the 1994-2005 cohort [3]. Long-term survival of patients with CHD also improved with a mean decline of mortality rate by 34.5 % between 1990 and 2017 across all age groups (from birth to 50 years old) [4]. Increased survival of children with CHD has created a new cohort of population containing adolescents and adults who are at risk of suffering (or are suffering) from chronic heart disease. In 2010 in the USA it was estimated that the adult population exceeded the children population with CHD, with 1.4 million adults vs. 1.0 million children with CHD, and 300 000 of these adults had severe forms of CHD [5]. A growing population of adults with chronic life-long morbidity creates an associated burden on the healthcare systems over the world. This translates into increased financial expenses, increased need for educated professionals and the optimization of the existing and/or the development of new care strategies to ensure (1) the choice of the most efficient initial intervention for a given patient (e.g. to minimize a long-term detrimental effect of residual lesions), (2) a smooth transition from the pediatric to adult care, and (3) an adequate surveillance of sustained cardiovascular lesions to avoid uncontrolled deterioration of the heart function.

This thesis will primarily deal with the right ventricular congenital disease called tetralogy of Fallot (TOF), which is the most common cyanotic CHD with the incidence of 3.5 per 10 000 births [6] (e.g. $\approx$ 1660 babies with TOF are born in the USA every year [7]). Tetralogy of Fallot is a disease containing (Figure 1): (1) ventricular septal defect (VSD), (2) obstruction of the right ventricular outflow tract (RVOT), (3) overriding of the aorta (i.e. the aorta appears directly over VSD instead of over the left ventricle which makes blood from the right ventricle flow directly into the aorta), and (4) right ventricular hypertrophy. Complete surgical repair of TOF is usually performed within the first 1.5 years of life where the ventricular septal defect is closed and a transannular patch is inserted into the RVOT to enlarge the size of RVOT and pulmonary artery (PA).

Patients with repaired TOF (rTOF) show excellent survival rates after initial repair, e.g. 94.8 % and 92.8 % in the 10 and 25 years after the initial surgery [9], respectively. However,

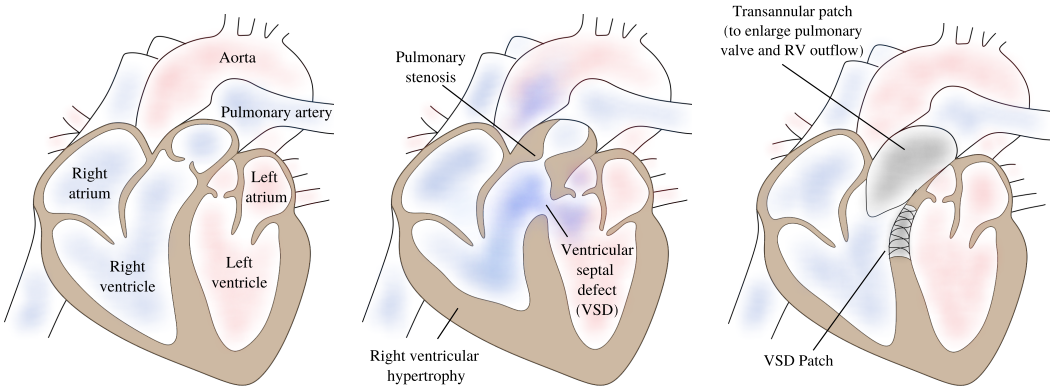

(a) Normal heart (b) Tetralogy of Fallot (TOF) (c) Repaired tetralogy of Fallot (rTOF)

Figure 1: Anatomy of the normal heart (a), tetralogy of Fallot (b), and tetralogy of Fallot after complete repair (rTOF) (c). Figure taken from [8].

their mortality rates are higher compared to normal population [10; 11] because some residual lesions could remain present after the initial surgery: (1) regurgitation through the PV (due to the insertion of the transannular patch), (2) stenosis on the RVOT, and (3) stenosis of the branched pulmonary arteries. RVOT obstruction and PV regurgitation create pressure- and/or volume- overload in the RV leading to ventricular remodeling, hypertrophy and/or dilatation of the ventricular chamber, respectively. In addition, rTOF RVs are prone to electrophysiological abnormalities caused either by the initial surgical repair [12] or developed later in the remodeled heart [13]. The most prevalent one is the right bundle branch block (RBBB) — a block along the electrical conduction system of the right ventricle that causes delay or blockage of the ventricular activation. It creates intraventricular (e.g. when the activation of RV is not homogeneous) or interventricular activation dyssynchrony (e.g. delayed activation of right with respect to the left ventricle). In such electrophysiological conditions RV contraction becomes delayed and mechanically less efficient. The patients tend to develop severe arrhythmias. If left untreated the rTOF RV function progressively diminishes and patients become at high risk of sudden death from cardiac arrest and arrhythmia. Park et al. [9] showed that at least 18%, 31% and 53 % of patients in 5, 10 and 20 years after the initial repair, respectively, require some type of reintervention – to correct the hemodynamic burden and/or to control the pathological RV remodeling and associated deterioration of electrophysiology.

Pulmonary valve replacement (PVR) is a common intervention that is performed to correct the hemodynamic burden and avoid deterioration of ventricular function. Predicting the correct timing for PVR is crucial. In the conditions of longstanding exposure to pressure- and volume overload the myocardium undergoes uncontrolled remodeling that at some point becomes irreversible. In addition, PVR has to be repeated throughout life as the lifespan of the implanted valve is typically up to ≈ 10 years. Therefore, PVR should be performed as late as possible but before the irreversible remodeling has occurred [14].

In clinical practice it is still unclear how to distinguish irreversible versus reversible myocardial remodeling and how to prevent or maintain a failing volume- and/or pressure-loaded RV [15]. Current decision-making protocols for interventional planning and monitoring of the functional response to the therapy of rTOF patients (as well as patients with other types of CHD [16; 17]) are vastly based on image-derived biomarkers [18; 19; 20]. The gold standard technique is cardiovascular magnetic resonance imaging (MRI) [16] that allows the quantification of ventricular volumes, mass and phase contrast flow through the valves.

However, the sensitivity and specificity of image-based biomarkers remain elusive, e.g. ≈ 40 % of rTOF patients show an unfavorable outcome post-PVR (i.e. normalization of ventricular volumes does not occur) [21; 22] suggesting that the timing of PVR was possibly incorrect [23].

Emerging need for personalized approaches in patient care of congenital heart disease

To date there is a knowledge gap regarding the underlying long-term mechanisms of a progression of congenital heart pathologies for a number of reasons:

1. Thanks to the ongoing progress in surgical techniques, children and adult populations with CHD continue to grow every year, creating a novel set of cardiovascular problems that were not seen before the era of progress of cardiac interventions [18]. As the longitudinal data of CHD progression had been quite sparse until recently, the current guidelines for the management of patients with CHD do not yet most adequately inform the therapy and follow-up planning.

2. Patients with CHD possess unique and complex anatomical arrangements with rare and varied lesions both prior to and after corrective surgery that trigger a long-term remodeling processes.

3. There is a lack of sensitivity and specificity of existing biomarkers.

The complexity of the CHD profiles necessitates the development of functional biomarkers that are (1) patient-specific, (2) capable of tracking the time-varying profile of the disease progression, and (3) capable of elucidating functional changes indicative of ventricular dysfunction. Existing biomarkers are primarily given by imaging and biochemical modalities. Practice shows that they are not sensitive enough to detect, track and assess the development of advanced pathological states. The loss of regulatory capacity of the heart to stress factors at tissue- and organ-level may well occur prior to the occurrence of detectable symptoms [24] (e.g. reduction in the ejection fraction). Hence, it is inherently challenging to spot the onset of failing organ. The ultimate goal is therefore to develop a patient-specific monitoring and surveillance tool that could consider an interaction between disease, therapy and time. Such a tool should integrate all levels of disease progression – from molecular to organ-level function and back – as well as take into account the lifestyle and the environment of a given patient. The development of monitoring tools of such a precision clearly necessitates an integration of collaborative efforts from multiple disciplines: applied mathematics, computer science, computational biology, biophysics, biomechanics, experimentation, and cardiovascular medicine (including imaging, surgery, cardiology). [25].

With an expansion of the availability of clinical data and accelerating progress of computer power, the creation of personalized monitoring tools containing a physiological representation of internal organ mechanics is becoming a reality [26]. A new era of digital medicine is developing with the emerging concept of 'digital twin', which could be defined as a virtual tool that coherently integrates the clinical data acquired over time by means of mechanistic and statistical models providing (1) augmented interpretation of existing clinical biomarkers, and (2) novel model-based patient-specific indices of heart function [25]. The schematics in Figure 2 demonstrates an example of a rTOF patient management profile, that in addition to conventional clinical biomarkers, could be augmented by novel mechanical and statistical model-derived indicators when e.g. evaluating the 'current state' of ventricular function prior to performing the PVR. In the sequel, we will briefly review the state of the art of existing modeling techniques.

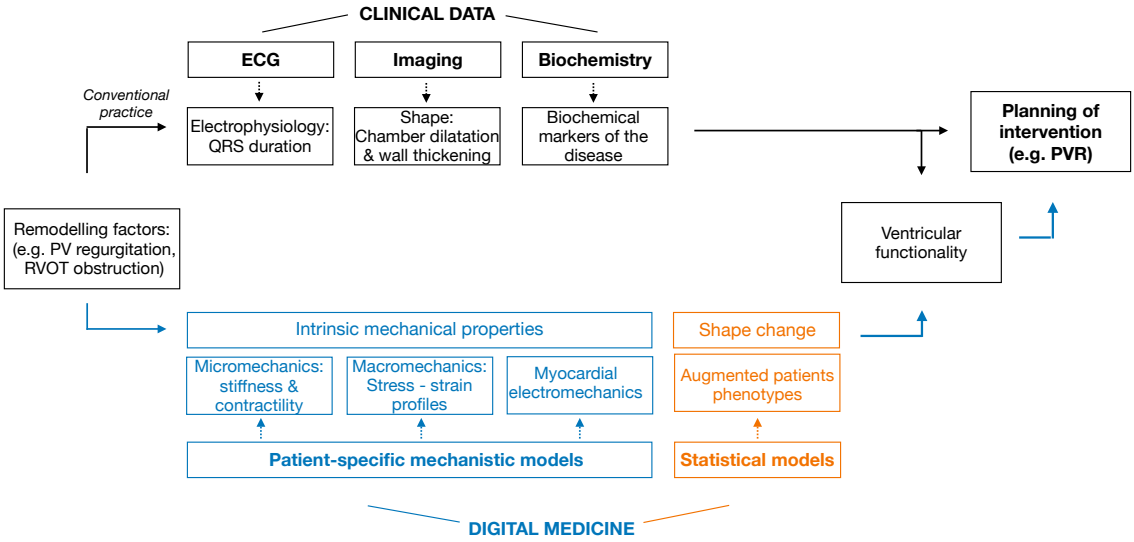

Figure 2: Clinical management of patients augmented by digital medicine tools, example of repaired tetralogy of Fallot patients. Black chart: current pipeline of the clinical decision-making; blue and orange charts: integration of model-derived indices into the clinical decision-making. ECG: electrocardiogram; PV: pulmonary valve; PVR: pulmonary valve replacement; RV: right ventricle; RVOT: right ventricular outflow tract obstruction.

Fundamental characteristics of cardiac anatomy, structure and function

The predominant role of the heart is to pump the blood through the vascular system to sustain the bodily demand in oxygen and nutrients. The function of the heart as a muscular pump arises from the orchestration of multiphysics processes occurring at various spatial scales.

The myocardium is a hierarchical structure. Its functional capacity is determined by the interaction between the electrical signal conducting system (e.g. sinus node and Purkinje system, Figure 3) and a force-generating unit of the myocardium (e.g. sarcomere, Figure 4). Sarcomeres are composed of thick and thin myofilaments (which contain myosin and actin filaments, respectively). Electrical activation of the myocytes triggers the release of the calcium ions from the sarcoplasmic reticulum into the cytoplasm. Calcium ions bind to the troponin-C (TN-C on Figure 4 (b)) causing the configurational change of the actin filament that unmasks the myosin binding sites. Myosin heads then attach to the actin filaments and produce the power stroke that pulls the Z-bands towards each other inducing the shortening of the sarcomere and the associated contraction of the myocardium. For a detailed description of excitation-contraction coupling of the cardiac myocytes see e.g the textbook of [27].

At the organ-level cardiac myocytes form the myofibers that are axially arranged into a three-dimensional (3D) structure [28] (Figure 5 (a)), and are wrapped by a 3D network of collagen connective tissue [29] (Figure 5 (b)). In addition, the tissue is organized in laminae – cleavage planes [29]. Such a structural organization of the tissue facilitates fast propagation of electrical waves in the direction of the fibers [30] and allows complex deformations of the myocardium that occur throughout the cardiac cycle [31].

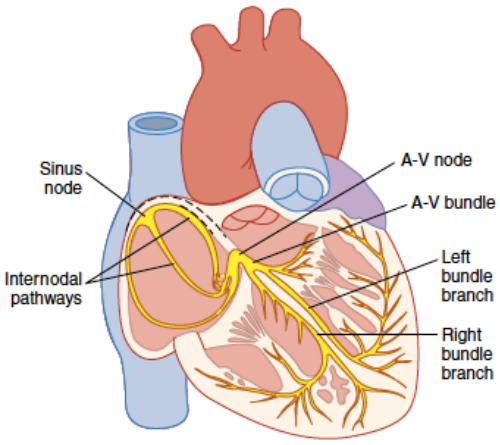

Figure 3: Electrical signal conducting system of the heart. Figure taken from [27]. Copyright Elsevier (2011) with permission.

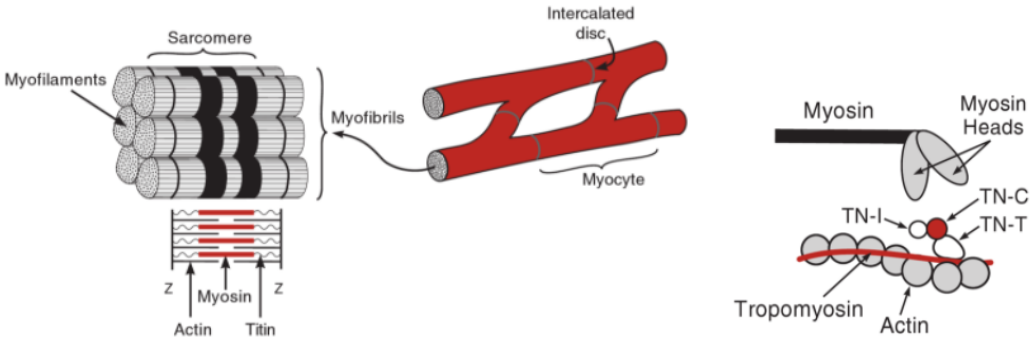

(a) Sarcomere

(b) Actin-myosin complex

Figure 4: Microstructural arrangement of cardiac myocytes. (a) At the tissue-level myofibers are composed of myocytes that are interconnected by intercalated discs. Myocytes are arranged into myofibrils that are divided into the functional compartments – sarcomeres. Sarcomeres are composed of thin and thick myofilaments (actin and myosin filaments, respectively), and are separeted by Z-discs. Protein titin anchors myosin filaments into the z-line (b) Microstructure of the sarcomere force producing region. Thick filaments are composed of myosin molecules that contain myosin heads. Thin filaments are composed of actin, tropomyosin that wraps the actin filament, and regulatory troponing complex (TN) proteins. TN-I: inhibits myosin binding to actin; TN-C: troponin-C, calcium ion binding cite; and TN-T: binds to tropomyosin. Excitation-contraction coupling with subsequent power stoke production arise via binding of the myosin head to the actin filaments. Attached myosin heads pulls the Z-bands towards each other producing the shortening of the sarcomere (contraction of the myocardium). Figure taken from [32]. Copyright Wolters Kluwer Health (2012) with permission.

Cardiac cycle

The mechanical pumping action of the heart is characterized by the cardiac cycle that describes the change in atrial and ventricular pressure and volume (Figure 6). The initiation of the cardiac cycle is determined by the generation of action potential in the sinus node and its propagation downstream the conducting system of the heart (see Figure 3). These electrophysiological events are reflected in the electrocardiogram (ECG) recording. The P-wave corresponds to the depolarization of the atria, triggered by the activation of the sinus node. The QRS complex represents the depolarization of the ventricles and corresponds to the signal propagation through the Purkinje network and ventricular myocardium, see Figure

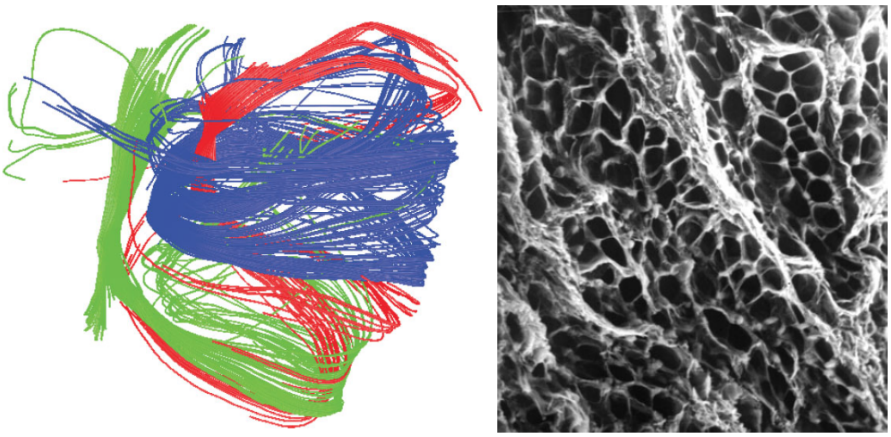

(a) 3D myofiber arrangements

(b) 3D fibrous matrix of the myocardium

Figure 5: Organ-level structural arrangements of the myocardial wall. (a) Directions of myocardial fibers reconstructed from diffusion tensor magnetic resonance imaging of porcine heart showing a three-dimensional (3D) myofiber arrangement within the myocardial wall. (b) Scanning electron microscope image of the cross section of the ventricular wall demonstrating the 3D structural arrangement of the extracellular matrix. Figures taken from [28] (open source).

6 and Figure 3. The travelling of the electrical signal throughout the myocardium induces an electro-mechanical coupling within the myocardium leading to an active contraction of the corresponding heart chambers, period called as atrial (ventricular) systole. Atrial (ventricular) systole is followed by the diastole when the repolarization of the myocardium occurs with associated relaxation of the tissue allowing the blood to fill up the chambers. The atrial physiological function is to facilitate an optimal filling of the ventricle with blood, while the ventricular function is to generate a major contractile force to pump the blood into the vascular tree [27].

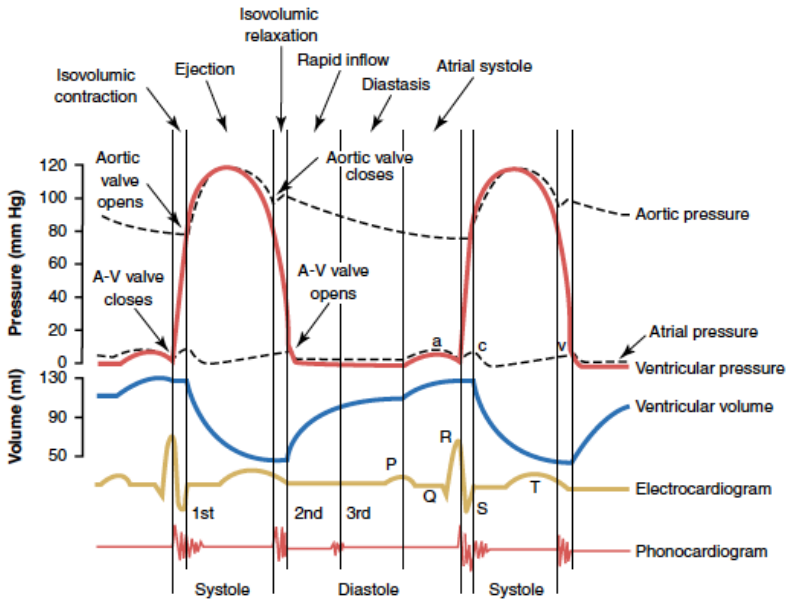

Figure 6: Orchestration of the events occurring during the cardiac cycle demonstrating changes in left atrial, left ventricular, and systemic circulation pressures, left ventricular volume, and electrocardiogram. Figure taken from [27]. Copyright Elsevier (2011) with permission.

Modeling of cardiovascular anatomy, physiology and function

An extended anatomical description of the cardiac compartments (e.g. ventricular chambers) could be obtained from the statistical shape models [33; 34; 35]. These models constitute population atlases based on the acquired patient-specific 3D image data of the pathology in question. Such an atlas contains the representation of a *mean shape* and *shape variations* around this mean for a given population. These metrics allow to detect correlative relationships between the specific geometrical features, which in turn could augment the phenotyping of a given pathology.

The representation of physiology (function) of various compartments of the cardiovascular system is a subject of biomechanical modeling studies. The major focus of these studies is to represent functional characteristics of the heart and cardiovascular system in order to provide additional mechanical perspective on the physiology and function that are not measurable *in vivo*. Considering a multiscale organization of the heart and interaction of the multiphysics processes on various spatial scales the modeling of the cardiovascular mechanics is a fundamentally complex task. The challenge is to achieve a balance between sufficient model complexity to represent the underlying physiology and (1) the availability of the numerical methods and computational techniques able to solve the associated system of equations and (2) the availability of the experimental data to estimate the parameters of the constitutive mechanical laws.

The mechanical behaviour of the heart and blood is often represented within the theory of continuum mechanics. The solution of the associated system of partial differential equations provides simulations of the tissue motion and blood flow. Mechanical actions of the heart (e.g. myocardial contraction and/or relaxation) can be represented by various formulations: (1) solid mechanics (modeling of myocardium), (2) fluid mechanics (flow of blood inside the cavity or vessels), (3) electrophysiology. These three can be coupled, e.g. fluid-structure interaction (blood inside heart cavities, or blood inside the coronary vessel tree modeled using porous material), electro-mechanical models (interaction between electrical signal propagation and subsequent mechanical action of the myocardium). Mechanical properties of the arteries (e.g. Young's modulus) and mechanical profile of the arterial blood flow (e.g. blood flow velocity) can be represented by the models of computational fluid dynamics.

The framework for formulating the biomechanical model of the heart within a theory of solid mechanics is of particular relevance to this thesis. In the sequel we provide a description of a formulation of such models. We also briefly mention a principle of integrating electrophysiology into solid mechanics.

General framework to formulate a biomechanical model of the heart

Cardiac biomechanics are often modeled with a theory of solid mechanics. An advancement of finite element methods and computers in the 1960s [36; 37] triggered the development of heart models with complex geometries where the solution of the prescribed non-linear constitutive equations became tractable [38]. First attempts to model a 3D function of the heart containing the description of underlying tissue-level mechanics date back to the 1970s in the works of P. J. Hunter [39; 40] and others [41; 42; 43; 44]. In order to model the 3D function of the heart the models need to contain the following constituents:

- A heart geometry with detailed description of myocardial tissue architecture
- Theoretical framework for the description of tissue motion
- Material constitutive laws that describe the mechanics of resting and contracting myocardium (derived from experimental measurements of tissue- and sarcomere-level

mechanics)

- Representation of electrical activation of the tissue
- Physiological boundary conditions that define an external loading and/or kinematic constraints acting on the deforming body
- Effective numerical method to solve the associated system of equations

Over the last decades, an advancement in imaging techniques has provided an accurate 3D description of patient-specific geometry. Acquired *in vivo* cardiac geometry could be directly deployed in the cardiac simulation pipeline. One of the common techniques is MRI thanks to its high spatial and temporal resolution and a high contrast between deforming myocardium and the surrounding tissues [45; 46]. In addition, MRI does not have any X-ray dose and can provide a wide variety of data (e.g. static high resolution anatomical, functional cine images, flow, tissue characterization – e.g. T1 weighted images, gadollinium late enhancement). Computed tomography and echocardiography are also widely used to extract hearts geometry, motion and flow.[1] The structural information about the spatial arrangement of the myofibers (e.g. fiber orientation, fiber angles) could be prescribed to the FE mesh [48; 49]. Patient-specific myocardial fiber architecture could be generated by processing diffusion tensor MRI data [50; 51; 52; 53]; however the accuracy of such data is still limited. In addition, the availability of patient-specific fiber data is hampered by the technical difficulty of their acquisition (e.g. only a few centers in the world are equipped for such exams) and practical difficulty (e.g. long acquisition time for patients). In the absence of patient-specific data the common practice is to assign fiber angles between 50 and 70° for endocardium and -50 and -70° for epicardium [54; 55; 56], the values being provided by the histological data [57].

A foundation for the formulation of mechanistic models of the heart is the theory of finite deformation elasticity. It characterizes myocardial deformations in space and time with prescribed stress-strain constitutive laws. The deformation acting on the material is given by the strain tensor. The stress acting on infinitesimally small planes within the material is given by the stress tensor. By solving the system of partial differential equations that govern the conservation of mass, momentum and energy it is possible to simulate the motion of the myocardial tissue [40; 58; 31].

Myocardium is commonly modeled as a viscoelastic, anisotropic (e.g. transversely isotropic) and incompressible material. Such a non-linear material behavior was observed in numerous experimental studies on tissue-mechanics (e.g. [59; 60], the review about the architecture of the myocardium by [61]) and was incorporated into the various forms of the elastic strain energy density function such as [62; 63; 64; 65; 60; 66]. The strain energy function is often expressed in terms of Piola-Kirchhoff stress to denote the passive stress tensor in the overall description of the constitutive law.

In order to model the active contraction of the myocardium the description of the active tension must be included. The active tension tensor, often in the form of second Piola-Kirchhoff stress, can be combined with the passive stress tensor to provide an overall description of active and passive constitutive law of the myocardium [58] – *active stress* framework. The representation of active tension within the myocardium can be either given by a single variable of active stress (such as in [67; 68; 49; 69; 70; 71]) or by integrating micro-

[1] After semiautomatic (e.g. Circle Cardiovascular Imaging, Calgary, Alberta, Canada) or manual contouring of the ventricular cavity (e.g. MeVisLab software) finite element (FE) mesh generation softwares (e.g. GMSH [47]) could be used to provide a patient-specific tetrahedral mesh that could be directly employed for subsequent simulations.

scale mechanics of actin-myosin interaction into the overall constitutive law of myocardial contraction (e.g. [72; 73; 74]).

One of the earliest constitutive model of active contraction of the myocardium was proposed by A. V. Hill [75] in 1938. He derived an empirical three-element rheological model of muscle contraction that consisted of a contractile element in series with a passive elastic element and both in parallel to the other passive elastic element. Elastic elements were considered as springs of a given stiffness while the contractile element constitutive law was in a form of force-velocity relationship. Another theoretical framework of active contraction modeling belongs to A. F. Huxley who proposed a sarcomere level contraction model [76]. In 1954 the experiments with skeletal muscle brought a sarcomere level description of location and arrangement of actin and myosin, with the contractile force being produced concurrently with the myosin sliding over the actin filaments. [77; 78]. Following that discovery in 1957 A. F. Huxley formulated a sliding filament theory of muscle contraction [76]. It considers all myosin heads as series of linear springs with a certain energy. Attachment of the myosin heads to the corresponding actin sites produces active tension and relative sliding of myosin over the actin causing shortening of the muscle. This theory was revolutionary to the field and later formed a basis for the other models of subcellular myocardial contraction, e.g. [79; 80; 81; 82; 83; 65; 84]. As more experimental data on subcellular myocyte physiology became available (e.g. calcium kinetics, passive propertied of cardiac muscles, length-dependent kinetics of the cross-bridges) Huxley's model of actin-myosin sliding was extended to account for the dynamics of calcium binding and passive properties of the myocytes [65; 68; 84] that allowed a more holistic description of myocardial physiology.

A model proposed by Bestel-Clément-Sorine (BCS) within Huxley's framework [84] is of particular relevance to this thesis. It is a model of a sarcomere level kinetics with chemically controlled (i.e. calcium concentration) constitutive law of actin-myosin mechanics in myofiber direction. The contractile component was coupled with passive component of visco-elastic type, and a set of differential equations provided a constitutive relation between stress and strain. The BCS model was further extended by Chapelle and colleagues in 2012 [72] to incorporate more physiological Frank-Starling mechanism (i.e. preload dependent property of the myocytes force generating capacity) of myocardial contraction and embed this model into an energy-consistent framework of continuum mechanics. This multi-scale model formulated by [72] is the biomechanical model used in this thesis in application to the modeling of cardiac mechanics of patients with CHD.

Electrical activation input to the mechanical model is often given by reaction-diffusion partial differential equations (e.g. bidomain, monodomain equations [85; 86; 87; 88]) that simulate the propagation of transmembrane potential over the 3D myocardium of the heart with subsequent intracellular calcium release. Calcium kinetics couple electrical and mechanical components in the model via embedding of the activation time or calcium concentration (output from the electrophysiological model) into the sarcomere-level constitutive model of active tension [68; 89; 90; 58; 73; 91; 92; 93]. However, if the modeled pathology is not related to electrical abnormalities the input variable of electrical activation duration could be directly prescribed into the sarcomere model of active tension. The electrical input is prescribed such that the timing of complete activation of the ventricular myocardial tissue corresponded to e.g. measured QRS duration [56; 94; 95; 96].

In the 3D space the boundary conditions define the displacement constraints on the deforming ventricle. They account for the presence of the surrounding anatomical structures: diaphragm, thoracic cage, and the lungs. One of the approaches is to consider viscoelastic boundary conditions [97] or sliding of the complementary surfaces [98]. Boundary conditions that define the external loading can be represented by a lumped-parameter model of the circulation coupled to the ventricular outflow tract [90; 99; 100; 93; 71].

Phenomenological model of the heart function

The simplest way to represent an organ-level pumping behavior of the heart is to consider the cardiac chamber as a generator of blood flow and pressure. A time-varying elastance model describes the time-variant changes of instantaneous intraventricular pressure and volume. It was originally proposed by H. Suga in the 1970s [101] and later extensively employed by others [102; 103; 104; 105; 106; 107; 108]. The model determines the ability of ventricular chamber to generate systolic pressure and flow against given vascular impedance [101]. It does not describe constitutive properties of underlying tissue-level mechanics, but gives a global organ-level function. Thanks to its simplicity the model has been used in clinical physiological studies to characterize organ-level cardiac performance [109; 110; 111].

Applied modeling to augment interpretation of clinical data

The development of the applied modeling workflow that may be directly employed in a clinical environment is a subject of ongoing research. The aim is to augment the interpretation of clinical data by model-derived characteristics of myocardial (vascular) mechanics (i.e. mechanical models) or by additional geometrical indices of the pathology (i.e. statistical shape models). Within a framework of mechanical modeling an augmented interpretation of clinical data is usually achieved by the following: (1) an appropriate choice of the model ingredients that sufficiently represent the pathophysiology in question; (2) the calibration of patient-specific parameters of the constitutive laws. The latter is achieved via matching the model prediction (e.g. output of the model in terms of ventricular pressure and/or volume curves) with the observed data – the so-called *data-model coupling*. The mathematical methods that enable a personalized *data-model coupling* are a vast area of research in applied mathematics. Briefly these methods are data assimilation (optimization) techniques [112; 113; 114; 115] that aim to find a balance between the two conditions: (1) a distance between the model prediction (defined by a given set of parameters) and the data, and (2) a confidence in the model (i.e. typically parameters cannot take arbitrary values). In application to cardiac modeling see e.g. [116; 71; 48; 56; 117].

As regards cardiac mechanics we can highlight some interesting approaches pertaining to model-augmented clinical data interpretation. Patient-specific diastolic and/or systolic mechanical properties may be extracted by coupling the 3D heart model with MRI data. The passive (active) constitutive law of the myocardium – i.e. that describes myocardial behavior during diastole (systole) – is prescribed to the 3D finite element model of the ventricle. The kinematics of the model are coupled to that given by CMR data by adjusting parameters of passive (active) constitutive law. Such a procedure provides patient-specific parameters of myocadial stiffness (active stress) that can be used to assess e.g. diastolic (systolic) heart failure in patients. Studies investigating the passive behavior of the myocardium are [48; 118; 119], and active behavior [120; 121; 56; 122]. Electromechanical models of the heart, where the electrophysiological input is embedded into the active constitutive law, allow to e.g. describe and predict the effect of cardiac resychronization therapy on ventricular contraction. Various patterns of electrical wave propagation are prescribed and the subsequent response of ventricular mechanics is studied, e.g. the models of [55; 74; 100; 69; 123; 93].

Whilst 3D finite element models allow modeling of the realistic multi-level and multi-physics phenomena, they require (1) high computational cost (e.g. in fluid structure interaction models simulation of one cardiac beat could be at the time-scale of days), and (2) adjustment of the large number of constitutive parameters. Such features limit their direct translation into clinical bench and make the studies of large patient cohorts almost

unattainable. Some approaches of a reduced geometrical representation of ventricular cavity exist that decrease the computational time of one cardiac beat to the duration of seconds. The family of CircAdapt models [124; 125; 70] – 1D models of cardiac mechanics – provide a global representation of a chamber-level stress-strain relationship. The geometry of the cavity is determined by the adaptation of the cavity to the imposed mechanical loading. Another approach was developed by Caruel et al. [126], where the geometry of a complete multi-scale 3D mechanical model [72] was reduced to a sphere while preserving all the constitutive laws (i.e. 0D model). The resulting 0D model preserves the sarcomere-level mechanical description but thanks to the only one radial displacement of the ventricular cavity the simulation of one cardiac beat takes around 10ms.

Modeling of patients with congenital heart disease

In this section we provide an overview of the biomechanical modeling techniques that can be coupled to the clinical data of patients with CHD. These models could be used in order to obtain biomechanical insight into the myocardial health. One of the first efforts to simulate the mechanical behaviour of the cardiovascular system of patients with CHD was in the early 2000s. Clinical data of patients with single-ventricle geometry was coupled to mechanical models of the heart and circulation. The pumping action of the heart was represented by a simple time-varying elastance model [104] that was coupled to the lumped parameter model of the circulation [127; 128; 129] (see also a later study in [130]). These models studied the influence of hemodynamic factors (e.g. resistance of the circulation) on the ability of the heart to generate cardiac output in rest and exercise. Despite a simple phenomenological representation of cardiac mechanics these models showed promising results in their ability to provide a global view on circulation dynamics of patients with single-ventricle physiology. A more mechanistic description of cardiac mechanics of patients with CHD was deployed by [131] for patients with single-ventricle physiology and by [132] with rTOF patients. The studies used CircAdapt models coupled to lumped parameter models of circulation. The model of the outflow valve allowed to incorporate the regurgitation into the system. The Bernoulli relation was used to model the pressure drop across the valve. The results of these studies reproduced the clinical nature of the complex pathophysiological patients conditions. Moreover, the study of [132] investigated a comparative effect of pulmonary regurgitation versus ventricular dyssynchrony on exercise capacity of rTOF patients. Another group used 3D finite element mechanical models coupled to the MRI data to study passive and active properties of RV myocardium of patients with rTOF [133; 134; 135]. The studies adjusted the parameters of the material law of the myocardium based on the direct measurements of the biaxial stress-strain data obtained from a cadaveric normal heart sample. The methods of obtaining biaxial mechanical dataset for ventricular tissue were previously developed by [136; 137]. The studies that compared active properties [133; 134] of the myocardium of rTOF pre- and post-PVR showed that patient-specific model-derived active stress pre-PVR was the best predictor of the outcome of PVR 6 months post-PVR. The study of [135] demonstrated that passive mechanical properties of rTOF patients pre-PVR were distinct from the healthy subjects substantiating the potential of the proposed method to discriminate patient-specific indices of myocardial health. In the study [138] a 3D biomechanical model of the heart coupled to pre-operative clinical data (stage 2 surgery) of a patient with single-ventricle physiology allowed to simulate various post-operative conditions of the cardiovascular system (i.e. virtual surgical planning). Mechanical properties of patients with single-ventricle geometry were extracted by coupling 0D model of the heart [126] with the clinical data of these patients. The framework provided patient-specific properties of myocardial stiffness, contractility and vascular resistance – the

indices that have clinical significance in studying potential mechanisms of failure of patients with Fontan circulation. Finally, various patterns of ventricular filling could be investigated by the models of ventricular fluid dynamics of e.g. patients with hypoplastic left heart syndrom [139; 140; 141]. These models provide an insight into e.g. filling efficiency, kinetic energy and viscous dissipation of the blood flow, and intraventricular pressure gradient.

Aims and objectives

The burden placed on the healthcare system due to the growing population of adults with CHD necessitates the development of new healthcare solutions. Often this cohort of patients requires lifelong monitoring of their cardiovascular health and repeated interventions. However, the complexity and uniqueness of their cardiovascular anatomy and function challenge the development of optimal diagnostic tools. It is particularly challenging to track the disease progression and elucidate the cut-off values of loss of functional capacity of the heart. Currently, clinical decision-making is driven by the image-based or biochemical biomarkers of the disease that are limited in their specificity and sensitivity to the advanced pathological states [24]. These biomarkers track the progression of the disease in terms of the change in organ's size and shape, or occurrence of biochemical agents in the blood (e.g. due to severe tissue-level remodeling). These changes however occur downstream sarcomere- and tissue-level remodeling. The latter in turn could be characterized in terms of associated changes in the myocardial mechanical properties (e.g. stiffness and contractility), that are difficult to access via standard clinical biomarkers.

Biomechanical modeling has a potential to provide an extended understanding of underlying tissue mechanics [30]. We have discussed above the ability of various types of models to provide an augmented description of various components of the cardiovascular system. Regardless of the variety of the modeling approaches available to date, studies demonstrating the translation of these models to a real clinical environment are lacking. Thus there is a need to explore the applicability of these modeling approaches in assisting clinical decision-making.

The aim of this PhD thesis is to apply biomechanical modeling in a cohort of patients with CHD to demonstrate its potential in assisting clinical decision-making. Firstly, we aim to provide patient-specific mechanical indicators of the pathology that may augment the interpretation of CMR and catheter pressure data in a cohort of patients with rTOF. Secondly, we aim to demonstrate the potential of the model to assist in clinical data processing – to ameliorate the interpretation of various data sources and data acquisition protocols – in a cohort of patients with single-ventricle geometry.

Objectives

The biomechanical model used in this thesis was developed at Inria by Chapelle et al. [72]. We use a 0D version of this model [126] in which the constitutive mechanical laws are preserved as in the full 3D model [72] but the geometry and kinematics are reduced to a sphere. The model also contains the valvular components to account for arterial and/or atrioventricular valve regurgitation and stenosis of the outflow tract (see valve law presented in [73] and proof-of-concept clinical studies e.g. [94; 95; 96]).

The clinical data (catherization pressures and MR images) were provided by the University of Texas Southwestern Medical Center, Dallas (USA) and the University of Texas, Austin (USA). We work with two cohort of patients with CHD: (1) rTOF prior to and after PVR, (2) patients with single-ventricle geometry prior to completing the Fontan circulation.

The following objectives are pursued:

I: Evaluate the mechanics of the right ventricle and pulmonary circulation in a patient-specific manner
We explore the ability of the model to represent RV and pulmonary circulation mechanics of rTOF patients pre- and post-PVR. These patients are subjected either to independent or combined effect of PV regurgitation and RVOT stenosis. We build patient-specific models of the cardiovascular system by calibrating the model to represent the measured data of these patients. We evaluate the mechanical response of the system (1) to the presence, and (2) to the immediate removal of PV regurgitation and RVOT stenosis.

II: Predict the evolution of ventricular mechanics under different loading conditions
The ability of the model to predict the evolution of RV mechanics under different loading conditions is explored. We use patient-specific models of RV calibrated considering the PV regurgitation and RVOT stenosis. We explore the ability of these models to predict an immediate response of RV contractility to acute changes of the level of RVOT resistance.

III: Develop a model-assisted time-synchronization technique of clinical pressure-volume data
We develop a model-assisted time-synchronization technique of clinical pressure-volume (P-V) data that can address the problem of P-V data dyssynchrony. The universality of the method for the variety of data acquisition protocols is demonstrated.

IV: Validate model-derived indices of ventricular systolic function against clinically accepted surrogate measures of systolic performance
We explore the correspondence of the indices of systolic performance directly obtained from the clinical measurements – maximum value of time-varying elastance ($E_{\max}$) and maximum time derivative of ventricular pressure ($\max(dP/dt)$) – with model-derived contractility and $\max(dP/dt)$. In addition, we confront data- vs. model-derived $\max(dP/dt)$ in order to show possible applications of model-derived $\max(dP/dt)$ as a model-based data-filter.

Thesis outline

This thesis manuscript is divided into four chapters.

Chapter 1: Biomechanical modeling to evaluate 'current mechanical state' of the myocardium in repaired tetralogy of Fallot patients.

The purpose of this chapter was to use the biomechanical model in a cohort of rTOF patients to assess comparative influences of residual right ventricular outflow tract obstruction (RVOTO) and pulmonary regurgitation on ventricular health. We analyzed 20 patients pre- and post-PVR. The data contained volume and phase contrast flow measurements given by CMR a few months prior to PVR, and catherization pressures obtained during PVR. The model was coupled to the patients' data to obtain patient-specific mechanical properties of the cardiovascular system. Thanks to the valvular component in the model we could incorporate PV regurgitation and stenosis into the calibration of constitutive mechanical properties of the myocardium. The results showed an increased contractility pre-PVR in all patients compared to normal RVs. After PVR the contractility significantly decreased in all patients. Patients with predominantly RVOTO showed higher levels of contractility and

stroke work decrease compared to those with predominantly PV regurgitation. This chapter shows the ability of the biomechanical model (1) to integrate multiple clinical data inputs, (2) to assess the influence of both combined and independent effects of PV regurgitation and RVOT stenosis on RV health, and (3) to augment clinical indicators of RV health in patient-specific manner.

This chapter was published as a clinical research article entitled 'Biomechanical modeling to inform pulmonary valve replacement in tetralogy of Fallot patients after complete repair' in the *Canadian Journal of Cardiology* [142]. An electronic supplementary material of the paper contains a detailed description of biomechanical heart model, model calibration procedure, and demographic and clinical details of the patients.

Chapter 2: Biomechanical modeling to evaluate the evolution of myocardial mechanical properties under different loading conditions

The purpose of this chapter was to explore the ability of the biomechanical model to predict the response of ventricular mechanics to the progressive decrease of the afterload in rTOF RVs that are predominantly affected by RVOTO. Patient-specific models pre-PVR created in chapter 1 were used, cessation of PV regurgitation and progressively decreasing RVOT resistance were assumed. Myocardial contractility was re-calibrated for the corresponding decrease in RVOT resistance. *In silico* relationships between the contractility and RVOT resistance post-PVR were built. The predictive value of these relationships was tested against the post-PVR models created from the actual post-PVR datasets in chapter 1. The resulting *in silico* relationships between contractility and RVOT resistance showed a linear form. *In silico* predicted contractility was in correspondence with post-PVR model-derived contractility. The chapter demonstrates that these relationships have the potential to inform clinicians about the hypothetical mechanical response of the ventricle based on the degree of pre-operative RVOTO.

This chapter was published as an original research article article entitled 'Prediction of ventricular mechanics after pulmonary valve replacement in tetralogy of Fallot by biomechanical modeling: A step towards precision healthcare' in the *Annals of Biomedical Engineering* [143].

Chapter 3: Model-assisted time-synchronization of clinical pressure-volume data

Clinical pressure-volume (P-V) data when acquired by different modalities (e.g. CMR and pressure catheter) are often subjected to time-synchronization errors. This yields acquired P-V loops with artificial shape, in particular skewed isovolumetric phases. These errors are inherent to data acquisition and data processing techniques. The prime motivation of this chapter was to develop a time-synchronization technique that could be directly employed in clinical settings, e.g. during a volume-challenge study (manipulating preload conditions of the heart via administration of fluid bolus) of patients with single-ventricle geometry prior to completing Fontan circulation. This chapter develops a model-assisted time-synchronization method for ventricular P-V signals from two types of data acquisition protocols: (1) P-V data with prospectively (N=24, single-ventricle patients) and (2) with retrospectively (N=45, predominantly rTOF left and right ventricular patients) ECG-triggered cine MRI sequences. The qualitative improvement of time-synchronized P-V loops is demonstrated by plotting the clinically acquired P-V loops and those obtained after the proposed time-synchronization. We use a metrics derived from cardiovascular physiology to demonstrate the physiologically meaningful quantitative improvement of time-synchronized P-V data. In particular, we statistically compare the original and time-synchronized

maximum time derivative of time-varying elastance ($E(t)$) – ($dE/dt_{\max}$) – in relation to max(dP/dt) derived from the original pressure signals. The proposed time-synchronization method produced high-quality P-V loops yielding statistically more accurate indices of myocardial energetics – max value of time-varying elastance ($E_{\max}$) and stroke work (area encompassed within P-V loop). This chapter demonstrated an ability of the model to assist in clinical data treatment during pre-interventional planning for e.g. patients with single-ventricle geometry.

The material of this chapter and the presented methods composed two publications that are in the appendices:

- Appendix 1 is an extended research letter to editor entitled 'Time-synchronization of invasive cardiovascular magnetic resonance data using a biomechanical model for pressure-volume loop analysis' that was accepted for publication in the *Journal of Magnetic Resonance Imaging*.

- Appendix 2 is a published peer-reviewed conference paper entitled 'Model-Assisted Time Synchronization of Cardiac MR Image and Catheter Pressure Data' in *Proc. of Functional Imaging and Modeling of Heart, FIMH 2021*. This work was a proof-of-concept study to demonstrate the model-assisted time-synchronization technique on 10 patients from rTOF left ventricular datasets.

Chapter 4: Conceptual link between model-derived measures of ventricular contractility and clinically accepted surrogate measures of ventricular systolic performance

Translation of novel model-derived indices into clinical practice necessitates their validation against existing clinically accepted biomarkers. In this chapter the goal is to explore a conceptual link between data- and model-derived indices of ventricular contractility. Time-synchronized datasets and calibrated models of all patients from Chapter 3 were used to (1) build statistical relationships between the aforemetioned indices, and (2) statistically compare model- and data-derived max(dP/dt). In addition, a thorough literature review on the clinical relevance of the presented indices of cardiac systolic function was performed. The results (1) showed significant correlation between all model- and data-derived indices, and (2) emphasized a potential application of model-derived max(dP/dt) as a model-based data filter of noisy values of clinical max(dP/dt). A literature review demonstrated that (1) the gold standard measure of ventricular contractility is challenging to use with the current physiological and biomechanical knowledge, and (2) some clinical scenarios might benefit from combining several indices of contractile performance.

Scientific contributions

Journal articles

- Gusseva, M., T. Hussain, C. H. Friesen, P. Moireau, A. Tandon, C. Patte, M. Genet, K. Hasbani, G. Greil, D. Chapelle, and R. Chabiniok. Biomechanical Modeling to Inform Pulmonary Valve Replacement in Tetralogy of Fallot Patients after Complete Repair. Canadian Journal of Cardiology, 37: pp.1798-1807, 2021.
- Gusseva, M., T. Hussain, C. H. Friesen, G. Greil, D. Chapelle, R. Chabiniok. Prediction of ventricular mechanics after pulmonary valve replacement in tetralogy of Fallot by biomechanical modeling: A step towards precision healthcare. Annals of Biomedical Engineering, 49: pp. 3339–3348, 2021.
- Gusseva, M., D. A. Castellanos, J. S. Greer, M. A. Hussein, K. Hasbani, G. Greil, S. R. Veeram Reddy, T. Hussain, D. Chapelle, and R. Chabiniok. Time-synchronization of invasive cardiovascular magnetic resonance data using a biomechanical model for pressure-volume loop analysis. Journal of Magnetic Resonance Imaging, 2022. *Accepted*.

Peer-reviewed conference proceedings

- Gusseva, M., J. S. Greer, D. A. Castellanos, M. A. Hussein, G. Greil, S. R. Veeram Reddy, T. Hussain, D. Chapelle, and R. Chabiniok. Model-Assisted Time- Synchronization of Cardiac MR Image and Catheter Pressure Data, Proc. of Functional Imaging and Modeling of Heart FIMH 2021, Volume 12738 of Lecture Notes in Computer Science (LNCS), pp. 362-372, Springer 2021.

Peer-reviewed book chapters

- Chabiniok, R., M. Gusseva, K. Škardová, R. Galabov, P.Eichler, J.Janoušek, R.Fučík, J. Tintěra, T. Oberhuber, T. Hussain. Translational Cardiovascular Modeling: Tetralogy of Fallot and Modeling of Diseases. A peer-reviewed book chapter in Modeling Biomaterials, 2021 (Birkhauser Science, editors Josef Málek and Endre Suli). *Accepted*

Conference presentations

- International Society for Magnetic Resonance in Medicine – ISMRM 2018 – Paris, France
  Electronic poster presentation: *Augmenting the interpretation of cardiac MRI by biomechanical modeling*
- International workshop on Tetralogy of Fallot and Modeling of Diseases - TOFMOD 2018 – Palaiseau, France
  Oral presentation: *Cardiac modelling for Tetralogy of Fallot*
- Virtual Physiological Human – VPH 2020 – Paris, France
  Poster presentation: *Biomechanical modeling to assess the functionality of right heart myocardium*
  Oral presentation at TOFMOD workshop: *Prediction of pulmonary valve replacement based on right ventricular mechanics. Application to repaired Tetralogy of Fallot*
- International Society for Magnetic Resonance in Medicine – ISMRM 2021 – Vancover, Canada
  Poster presentation: *Time resynchronization of data obtained during cardiovascular MRI combined with catherization using biophysical cardiac modeling*

- International Conference on Functional Imaging and Modeling of the Heart – FIMH 2021 – Stanford, USA
  Poster presentation: *Model-Assisted Time-Synchronization of Cardiac MR Image and Catheter Pressure Data*

Bibliography

[1] D. van der Linde, E. E. M. Konings, M. A. Slager, M. Witsenburg, W. A. Helbing, J. J. M. Takkenberg, and J. W. Roos-Hesselink, "Birth prevalence of congenital heart disease worldwide: a systematic review and meta-analysis," *Journal of the American College of Cardiology*, vol. 58, pp. 2241–2247, Nov. 2011.

[2] A. J. Marelli, A. S. Mackie, R. Ionescu-Ittu, E. Rahme, and L. Pilote, "Congenital heart disease in the general population: changing prevalence and age distribution," *Circulation*, vol. 115, pp. 163–172, Jan. 2007.

[3] M. E. Oster, K. A. Lee, M. A. Honein, T. Riehle-Colarusso, M. Shin, and A. Correa, "Temporal Trends in Survival Among Infants With Critical Congenital Heart Defects," *Pediatrics*, vol. 131, no. 5, pp. e1502–e1508, 2013.

[4] M. S. Zimmerman, A. G. C. Smith, C. A. Sable, M. M. Echko, L. B. Wilner, H. E. Olsen, H. T. Atalay, A. Awasthi, Z. A. Bhutta, J. L. Boucher, F. Castro, P. A. Cortesi, M. Dubey, F. Fischer, S. Hamidi, S. I. Hay, C. L. Hoang, C. Hugo-Hamman, K. J. Jenkins, A. Kar, I. A. Khalil, R. K. Kumar, G. F. Kwan, D. T. Mengistu, A. H. Mokdad, M. Naghavi, L. Negesa, I. Negoi, R. I. Negoi, C. T. Nguyen, H. L. T. Nguyen, L. H. Nguyen, S. H. Nguyen, T. H. Nguyen, M. R. Nixon, J. J. Noubiap, S. Patel, E. K. Peprah, R. C. Reiner, G. A. Roth, M.-H. Temsah, M. R. Tovani-Palone, J. A. Towbin, B. X. Tran, T. T. Tran, N. T. Truong, T. Vos, K. Vosoughi, R. G. Weintraub, K. G. Weldegwergs, Z. Zaidi, B. Zheleva, L. Zuhlke, C. J. L. Murray, G. R. Martin, and N. J. Kassebaum, "Global, regional, and national burden of congenital heart disease, 1990-2017: a systematic analysis for the Global Burden of Disease Study 2017," *The Lancet Child Adolescent Health*, vol. 4, no. 3, pp. 185–200, 2020.

[5] S. Gilboa, O. Devine, J. Kucik, M. Oster, T. Riehle-Colarusso, W. Nembhard, P. Xu, A. Correa, K. Jenkins, and A. Marelli, "Congenital Heart Defects in the United States: Estimating the Magnitude of the Affected Population in 2010," *Circulation*, vol. 134, no. 2, pp. 101–109, 2016.

[6] F. Bailliard and R. H. Anderson, "Tetralogy of Fallot," *Orphanet Journal of Rare Diseases*, vol. 4, pp. 1–10, Dec. 2009.

[7] S. E. Parker, C. T. Mai, M. A. Canfield, R. Rickard, Y. Wang, R. E. Meyer, P. Anderson, C. A. Mason, J. S. Collins, R. S. Kirby, and A. Correa, "Updated national birth prevalence estimates for selected birth defects in the United States, 2004–2006," *Birth Defects Research Part A: Clinical and Molecular Teratology*, vol. 88, pp. 1008–1016, Dec. 2010.

[8] R. Chabiniok, K. Škardová, R. Galabov, P. Eichler, M. Gusseva, J. Janoušek, R. Fučík, J. Tintěra, T. Oberhuber, and T. Hussain, "Translational Cardiovascular Modeling: Tetralogy of Fallot and Modeling of Diseases," in *Modeling Biomaterials*, 2021.

[9] C. S. Park, J. R. Lee, H.-G. Lim, W.-H. Kim, and Y. J. Kim, "The long-term result of total repair for tetralogy of Fallot," *European journal of cardio-thoracic surgery*

: official journal of the European Association for Cardio-thoracic Surgery, vol. 38, pp. 311–317, Sept. 2010.

[10] D. Benoist, V. Dubes, F. Roubertie, S. H. Gilbert, S. Charron, M. Constantin, D. Elbes, D. Vieillot, B. Quesson, H. Cochet, M. Haïssaguerre, C. Rooryck, P. Bordachar, J.-B. Thambo, and O. Bernus, "Proarrhythmic remodelling of the right ventricle in a porcine model of repaired tetralogy of Fallot," *Heart*, vol. 103, pp. 347–354, Mar. 2017.

[11] G. Nollert, T. Fischlein, S. Bouterwek, C. Böhmer, W. Klinner, and B. Reichart, "Long-Term Survival in Patients With Repair of Tetralogy of Fallot: 36-Year Follow-Up of 490 Survivors of the First Year After Surgical Repair," *Journal of the American College of Cardiology*, vol. 30, no. 5, pp. 1374–1383, 1997.

[12] P. Vojtovic, F. Kucera, P. Kubuš, R. Gebauer, T. Matejka, T. Tláskal, M. Ložek, J. Kovanda, and J. Janoušek, "Acute right ventricular resynchronization improves haemodynamics in children after surgical repair of tetralogy of Fallot.," *Europace : European pacing, arrhythmias, and cardiac electrophysiology : journal of the working groups on cardiac pacing, arrhythmias, and cardiac cellular electrophysiology of the European Society of Cardiology*, vol. 20, pp. 323–328, Feb. 2018.

[13] A. D'Andrea, P. Caso, B. Sarubbi, M. D'Alto, M. Giovanna Russo, M. Scherillo, M. Cotrufo, and R. Calabrò, "Right ventricular myocardial activation delay in adult patients with right bundle branch block late after repair of Tetralogy of Fallot.," *European journal of echocardiography : the journal of the Working Group on Echocardiography of the European Society of Cardiology*, vol. 5, pp. 123–131, Mar. 2004.

[14] C. Lee, E. S. Choi, and C.-H. Lee, "Long-term outcomes of pulmonary valve replacement in patients with repaired tetralogy of Fallot.," *European journal of cardio-thoracic surgery : official journal of the European Association for Cardio-thoracic Surgery*, vol. 58, pp. 246–252, Aug. 2020.

[15] G. P. L. Bossers, Q. A. J. Hagdorn, M. J. Ploegstra, M. A. J. Borgdorff, H. H. W. Silljé, R. M. F. Berger, and B. Bartelds, "Volume load-induced right ventricular dysfunction in animal models: insights in a translational gap in congenital heart disease," *European Journal of Heart Failure*, vol. 20, pp. 808–812, Apr. 2018.

[16] K. K. Stout, C. J. Daniels, J. A. Aboulhosn, B. Bozkurt, C. S. Broberg, J. M. Colman, S. R. Crumb, J. A. Dearani, S. Fuller, M. Gurvitz, P. Khairy, M. J. Landzberg, A. Saidi, A. M. Valente, and G. F. V. Hare, "2018 AHA/ACC Guideline for the Management of Adults With Congenital Heart Disease," *Journal of the American College of Cardiology*, vol. 73, no. 12, pp. e81–e192, 2019.

[17] C. K. Silversides, M. Kiess, L. Beauchesne, T. Bradley, M. Connelly, K. Niwa, B. Mulder, G. Webb, J. Colman, and J. Therrien, "Canadian Cardiovascular Society 2009 Consensus Conference on the management of adults with congenital heart disease: Outflow tract obstruction, coarctation of the aorta, tetralogy of Fallot, Ebstein anomaly and Marfan's syndrome," *Canadian Journal of Cardiology*, vol. 26, no. 3, pp. e80–e97, 2010.

[18] J. Therrien, Y. Provost, N. Merchant, W. Williams, J. Colman, and G. Webb, "Optimal timing for pulmonary valve replacement in adults after tetralogy of Fallot repair," *The American Journal of Cardiology*, vol. 95, no. 6, pp. 779–782, 2005.

[19] T. Oosterhof, A. van Straten, H. W. Vliegen, F. J. Meijboom, A. P. J. van Dijk, A. M. Spijkerboer, B. J. Bouma, A. H. Zwinderman, M. G. Hazekamp, A. de Roos, and B. J. M. Mulder, "Preoperative Thresholds for Pulmonary Valve Replacement in Patients With Corrected Tetralogy of Fallot Using Cardiovascular Magnetic Resonance," *Circulation*, July 2007.

[20] M. Hoelscher, F. Bonassin, A. Oxenius, B. Seifert, B. Leonardi, C. J. Kellenberger, and E. R. Valsangiacomo-Buechel, "Right ventricular dilatation in patients with pulmonary regurgitation after repair of tetralogy of Fallot: How fast does it progress?," *Annals of pediatric cardiology*, vol. 13, pp. 294–300, Oct. 2020.

[21] M. A. Quail, A. Frigiola, A. Giardini, V. Muthurangu, M. Hughes, P. Lurz, S. Khambadkone, J. E. Deanfield, V. Tsang, and A. M. Taylor, "Impact of Pulmonary Valve Replacement in Tetralogy of Fallot With Pulmonary Regurgitation: A Comparison of Intervention and Nonintervention," *The Annals of Thoracic Surgery*, vol. 94, no. 5, pp. 1619–1626, 2012.

[22] C. Lee, Y. M. Kim, C.-H. Lee, J. G. Kwak, C. S. Park, J. Y. Song, W.-S. Shim, E. Y. Choi, S. Y. Lee, and J. S. Baek, "Outcomes of Pulmonary Valve Replacement in 170 Patients With Chronic Pulmonary Regurgitation After Relief of Right Ventricular Outflow Tract Obstruction: Implications for Optimal Timing of Pulmonary Valve Replacement," *Journal of the American College of Cardiology*, Sept. 2012.

[23] J. P. Bokma, T. Geva, L. A. Sleeper, S. V. B. Narayan, R. Wald, K. Hickey, K. Jansen, R. Wassall, M. Lu, M. A. Gatzoulis, *et al.*, "A propensity score-adjusted analysis of clinical outcomes after pulmonary valve replacement in tetralogy of Fallot," *Heart*, vol. 104, no. 9, pp. 738–744, 2018.

[24] C. Ince, "Personalized physiological medicine," *Critical Care*, vol. 21, pp. 27–33, Dec. 2017.

[25] M. Alber, A. Buganza Tepole, W. R. Cannon, S. De, S. Dura-Bernal, K. Garikipati, G. Karniadakis, W. W. Lytton, P. Perdikaris, L. Petzold, and E. Kuhl, "Integrating machine learning and multiscale modeling—perspectives, challenges, and opportunities in the biological, biomedical, and behavioral sciences," *npj Digital Medicine*, vol. 2, pp. 1–11, Nov. 2019.

[26] J. Corral-Acero, F. Margara, M. Marciniak, C. Rodero, F. Loncaric, Y. Feng, A. Gilbert, J. F. Fernandes, H. A. Bukhari, A. Wajdan, M. V. Martinez, M. S. Santos, M. Shamohammdi, H. Luo, P. Westphal, P. Leeson, P. DiAchille, V. Gurev, M. Mayr, L. Geris, P. Pathmanathan, T. Morrison, R. Cornelussen, F. Prinzen, T. Delhaas, A. Doltra, M. Sitges, E. J. Vigmond, E. Zacur, V. Grau, B. Rodriguez, E. W. Remme, S. Niederer, P. Mortier, K. McLeod, M. Potse, E. Pueyo, A. Bueno-Orovio, and P. Lamata, "The 'Digital Twin' to enable the vision of precision cardiology," *European Heart Journal*, vol. 41, pp. 4556–4564, Mar. 2020.

[27] A. C. G. John E. Hall, *Textbook of Medical Physiology*. Saunders, 2011.

[28] R. H. Anderson, M. Smerup, D. Sanchez-Quintana, M. Loukas, and P. P. Lunkenheimer, "The three-dimensional arrangement of the myocytes in the ventricular walls," *Clinical Anatomy: The Official Journal of the American Association of Clinical Anatomists and the British Association of Clinical Anatomists*, vol. 22, no. 1, pp. 64–76, 2009.

[29] A. Young, I. Legrice, M. Young, and B. Smaill, "Extended confocal microscopy of myocardial laminae and collagen network," *Journal of microscopy*, vol. 192, no. 2, pp. 139–150, 1998.

[30] R. Chabiniok, V. Y. Wang, M. Hadjicharalambous, L. Asner, J. Lee, M. Sermesant, E. Kuhl, A. A. Young, P. Moireau, M. P. Nash, D. Chapelle, and D. A. Nordsletten, "Multiphysics and multiscale modelling, data–model fusion and integration of organ physiology in the clinic: ventricular cardiac mechanics," *Interface Focus*, Apr. 2016.

[31] K. D. Costa, J. W. Holmes, and A. D. McCulloch, "Modelling cardiac mechanical properties in three dimensions," *Philosophical Transactions of the Royal Society of London. Series A: Mathematical, Physical and Engineering Sciences*, June 2001.

[32] R. Klabunde, *Cardiovascular Physiology Concepts*. Lippincott Williams & Wilkins, 2007.

[33] T. Mansi, I. Voigt, B. Leonardi, X. Pennec, S. Durrleman, M. Sermesant, H. Delingette, A. M. Taylor, Y. Boudjemline, G. Pongiglione, *et al.*, "A statistical model for quantification and prediction of cardiac remodelling: Application to tetralogy of fallot," *IEEE transactions on medical imaging*, vol. 30, no. 9, pp. 1605–1616, 2011.

[34] B. Leonardi, A. M. Taylor, T. Mansi, I. Voigt, M. Sermesant, X. Pennec, N. Ayache, Y. Boudjemline, and G. Pongiglione, "Computational modelling of the right ventricle in repaired tetralogy of Fallot: can it provide insight into patient treatment?," *European Heart Journal–Cardiovascular Imaging*, vol. 14, no. 4, pp. 381–386, 2013.

[35] C. A. Mauger, S. Govil, R. Chabiniok, K. Gilbert, S. Hegde, T. Hussain, A. D. McCulloch, C. J. Occleshaw, J. Omens, J. C. Perry, *et al.*, "Right-left ventricular shape variations in tetralogy of Fallot: associations with pulmonary regurgitation," *Journal of Cardiovascular Magnetic Resonance*, vol. 23, no. 1, pp. 1–14, 2021.

[36] M. J. Turner, R. W. Clough, H. C. Martin, and L. Topp, "Stiffness and deflection analysis of complex structures," *journal of the Aeronautical Sciences*, vol. 23, no. 9, pp. 805–823, 1956.

[37] J. H. Argyris and S. Kelsey, *Energy theorems and structural analysis*, vol. 60. Springer, 1960.

[38] J. M. Guccione and A. D. McCulloch, *Finite Element Modeling of Ventricular Mechanics*, pp. 121–144. New York, NY: Springer New York, 1991.

[39] P. Hunter, *Finite Element Analysis of Cardiac Muscle Mechanics*. PhD thesis, University of Oxford, 1975.

[40] P. J. Hunter and B. H. Smaill, "The analysis of cardiac function: a continuum approach," *Progress in biophysics and molecular biology*, vol. 52, no. 2, pp. 101–164, 1988.

[41] P. Gould, D. Ghista, L. Brombolich, and I. Mirsky, "In vivo stresses in the human left ventricular wall: analysis accounting for the irregular 3-dimensional geometry and comparison with idealised geometry analyses," *Journal of biomechanics*, vol. 5, no. 5, pp. 521–539, 1972.

[42] R. F. Janz and A. F. Grimm, "Finite-Element Model for the Mechanical Behavior of the Left Ventricle: prediction of deformation in the potassium-arrested rat heart," *Circulation research*, vol. 30, no. 2, pp. 244–252, 1972.

[43] R. F. Janz, B. R. Kubert, T. F. Moriarty, and A. F. Grimm, "Deformation of the diastolic left ventricle—II. Nonlinear geometric effects," *Journal of biomechanics*, vol. 7, no. 6, pp. 509–516, 1974.

[44] S. Panda and R. Natarajan, "Finite-element method of stress analysis in the human left ventricular layered wall structure," *Medical and Biological Engineering and Computing*, vol. 15, no. 1, pp. 67–71, 1977.

[45] A. A. Young, B. R. Cowan, S. F. Thrupp, W. J. Hedley, and L. J. Dell'Italia, "Left ventricular mass and volume: fast calculation with guide-point modeling on MR images," *Radiology*, vol. 216, no. 2, pp. 597–602, 2000.

[46] A. Young and J. Prince, "Cardiovascular magnetic resonance: deeper insights through bioengineering," *Annual review of biomedical engineering*, vol. 15, pp. 433–461, 2013.

[47] C. Geuzaine and J.-F. Remacle, "Gmsh: A 3-D finite element mesh generator with built-in pre-and post-processing facilities," *International journal for numerical methods in engineering*, vol. 79, no. 11, pp. 1309–1331, 2009.

[48] V. Y. Wang, H. Lam, D. B. Ennis, B. R. Cowan, A. A. Young, and M. P. Nash, "Modelling passive diastolic mechanics with quantitative MRI of cardiac structure and function," *Medical image analysis*, vol. 13, no. 5, pp. 773–784, 2009.

[49] A. Krishnamurthy, C. T. Villongco, J. Chuang, L. R. Frank, V. Nigam, E. Belezzuoli, P. Stark, D. E. Krummen, S. Narayan, J. H. Omens, *et al.*, "Patient-specific models of cardiac biomechanics," *Journal of computational physics*, vol. 244, pp. 4–21, 2013.

[50] A. Nagler, C. Bertoglio, M. Gee, and W. Wall, "Personalization of cardiac fiber orientations from image data using the unscented Kalman filter," in *International Conference on Functional Imaging and Modeling of the Heart*, pp. 132–140, Springer, 2013.

[51] N. Toussaint, C. T. Stoeck, T. Schaeffter, S. Kozerke, M. Sermesant, and P. G. Batchelor, "In vivo human cardiac fibre architecture estimation using shape-based diffusion tensor processing," *Medical image analysis*, vol. 17, no. 8, pp. 1243–1255, 2013.

[52] C. T. Stoeck, C. von Deuster, M. Genet, D. Atkinson, and S. Kozerke, "Second-order motion-compensated spin echo diffusion tensor imaging of the human heart.," *Magnetic resonance in medicine*, vol. 75, pp. 1669–1676, Apr. 2016.

[53] J.-M. Peyrat, M. Sermesant, X. Pennec, H. Delingette, C. Xu, E. R. McVeigh, and N. Ayache, "A computational framework for the statistical analysis of cardiac diffusion tensors: application to a small database of canine hearts," *IEEE transactions on medical imaging*, vol. 26, no. 11, pp. 1500–1514, 2007.

[54] F. Sachse, R. Frech, C. Werner, and O. Dossel, "A model based approach to assignment of myocardial fibre orientation," in *Computers in Cardiology 1999. Vol. 26 (Cat. No. 99CH37004)*, pp. 145–148, IEEE, 1999.

[55] M. Sermesant, P. Moireau, O. Camara, J. Sainte-Marie, R. Andriantsimiavona, R. Cimrman, D. L. Hill, D. Chapelle, and R. Razavi, "Cardiac function estimation from mri using a heart model and data assimilation: advances and difficulties," *Medical Image Analysis*, vol. 10, no. 4, pp. 642–656, 2006.

[56] R. Chabiniok, P. Moireau, P.-F. Lesault, A. Rahmouni, J.-F. Deux, and D. Chapelle, "Estimation of tissue contractility from cardiac cine-MRI using a biomechanical heart model," *Biomechanics and modeling in mechanobiology*, vol. 11, no. 5, pp. 609–630, 2012.

[57] D. D. Streeter Jr, H. M. Spotnitz, D. P. Patel, J. Ross Jr, and E. H. Sonnenblick, "Fiber orientation in the canine left ventricle during diastole and systole," *Circulation research*, vol. 24, no. 3, pp. 339–347, 1969.

[58] D. Nordsletten, S. Niederer, M. Nash, P. Hunter, and N. Smith, "Coupling multi-physics models to cardiac mechanics," *Progress in biophysics and molecular biology*, vol. 104, no. 1-3, pp. 77–88, 2011.

[59] H. Ter Keurs, W. H. Rijnsburger, R. Van Heuningen, and M. J. Nagelsmit, "Tension development and sarcomere length in rat cardiac trabeculae. Evidence of length-dependent activation.," *Circulation research*, vol. 46, no. 5, pp. 703–714, 1980.

[60] S. Dokos, B. H. Smaill, A. A. Young, and I. J. LeGrice, "Shear properties of passive ventricular myocardium," *American Journal of Physiology-Heart and Circulatory Physiology*, vol. 283, no. 6, pp. H2650–H2659, 2002.

[61] S. H. Gilbert, A. P. Benson, P. Li, and A. V. Holden, "Regional localisation of left ventricular sheet structure: integration with current models of cardiac fibre, sheet and band structure," *European journal of cardio-thoracic surgery*, vol. 32, no. 2, pp. 231–249, 2007.

[62] Y.-C. Fung, "Mathematical representation of the mechanical properties of the heart muscle," *Journal of biomechanics*, vol. 3, no. 4, pp. 381–404, 1970.

[63] J. D. Humphrey, R. K. Strumpf, and F. C. Yin, "Determination of a constitutive relation for passive myocardium: I. A new functional form.," *Journal of biomechanical engineering*, vol. 112, pp. 333–339, Aug. 1990.

[64] J. M. Guccione, A. D. McCulloch, and L. K. Waldman, "Passive material properties of intact ventricular myocardium determined from a cylindrical model.," *Journal of biomechanical engineering*, vol. 113, pp. 42–55, Feb. 1991.

[65] P. J. Hunter, A. D. McCulloch, and H. Ter Keurs, "Modelling the mechanical properties of cardiac muscle," *Progress in biophysics and molecular biology*, vol. 69, no. 2-3, pp. 289–331, 1998.

[66] G. A. Holzapfel and R. W. Ogden, "Constitutive modelling of passive myocardium: a structurally based framework for material characterization," *Philosophical Transactions of the Royal Society A: Mathematical, Physical and Engineering Sciences*, vol. 367, no. 1902, pp. 3445–3475, 2009.

[67] T. Arts, T. Delhaas, P. Bovendeerd, X. Verbeek, and F. W. Prinzen, "Adaptation to mechanical load determines shape and properties of heart and circulation: the CircAdapt model," *American Journal of Physiology-Heart and Circulatory Physiology*, vol. 288, no. 4, pp. H1943–H1954, 2005.

[68] S. Niederer, P. Hunter, and N. Smith, "A quantitative analysis of cardiac myocyte relaxation: a simulation study," *Biophysical journal*, vol. 90, no. 5, pp. 1697–1722, 2006.

[69] R. Kerckhoffs, P. Bovendeerd, F. Prinzen, K. Smits, and T. Arts, "Intra-and interventricular asynchrony of electromechanics in the ventricularly paced heart," *Journal of Engineering Mathematics*, vol. 47, no. 3, pp. 201–216, 2003.

[70] J. Lumens, T. Delhaas, B. Kirn, and T. Arts, "Three-wall segment (TriSeg) model describing mechanics and hemodynamics of ventricular interaction," *Annals of biomedical engineering*, vol. 37, no. 11, pp. 2234–2255, 2009.

[71] L. Marx, M. A. Gsell, A. Rund, F. Caforio, A. J. Prassl, G. Toth-Gayor, T. Kuehne, C. M. Augustin, and G. Plank, "Personalization of electro-mechanical models of the pressure-overloaded left ventricle: fitting of windkessel-type afterload models," *Philosophical Transactions of the Royal Society A*, vol. 378, no. 2173, p. 20190342, 2020.

[72] D. Chapelle, P. L. Tallec, P. Moireau, and M. Sorine, "Energy-preserving muscle tissue model: formulation and compatible discretizations," *International Journal for Multiscale Computational Engineering*, vol. 10, no. 2, pp. 189–211, 2012.

[73] J. Sainte-Marie, D. Chapelle, R. Cimrman, and M. Sorine, "Modeling and estimation of the cardiac electromechanical activity," *Computers & Structures*, vol. 84, pp. 1743–1759, Nov. 2006.

[74] M. Sermesant, R. Chabiniok, P. Chinchapatnam, T. Mansi, F. Billet, P. Moireau, J.-M. Peyrat, K. Wong, J. Relan, K. Rhode, *et al.*, "Patient-specific electromechanical models of the heart for the prediction of pacing acute effects in CRT: a preliminary clinical validation," *Medical image analysis*, vol. 16, no. 1, pp. 201–215, 2012.

[75] A. V. Hill, "The heat of shortening and the dynamic constants of muscle," *Proceedings of the Royal Society of London. Series B - Biological Sciences*, vol. 126, pp. 136–195, Oct. 1938.

[76] A. Huxley, "Muscle structure and theories of contraction," *Prog. Biophys. Biophys. Chem*, vol. 7, pp. 255–318, 1957.

[77] A. F. Huxley and R. Niedergerke, "Structural changes in muscle during contraction: interference microscopy of living muscle fibres," *Nature*, vol. 173, no. 4412, pp. 971–973, 1954.

[78] H. Huxley and J. Hanson, "Changes in the cross-striations of muscle during contraction and stretch and their structural interpretation," *Nature*, vol. 173, no. 4412, pp. 973–976, 1954.

[79] A. Tözeren, "Continuum rheology of muscle contraction and its application to cardiac contractility," *Biophysical journal*, vol. 47, no. 3, pp. 303–309, 1985.

[80] J. M. Guccione and A. D. McCulloch, "Mechanics of Active Contraction in Cardiac Muscle: Part I—Constitutive Relations for Fiber Stress That Describe Deactivation," *Journal of biomechanical engineering*, vol. 115, pp. 72–81, Feb. 1993.

[81] P. J. Hunter, "Myocardial constitutive laws for continuum mechanics models of the heart," in *Molecular and subcellular cardiology*, pp. 303–318, Springer, 1995.

[82] G. Piazzesi and V. Lombardi, "A cross-bridge model that is able to explain mechanical and energetic properties of shortening muscle," *Biophysical journal*, vol. 68, no. 5, pp. 1966–1979, 1995.

[83] D. Smith, "A strain-dependent ratchet model for [phosphate]-and [ATP]-dependent muscle contraction," *Journal of Muscle Research & Cell Motility*, vol. 19, no. 2, pp. 189–211, 1998.

[84] J. Bestel, F. Clément, and M. Sorine, "A biomechanical model of muscle contraction," in *International Conference on Medical Image Computing and Computer-Assisted Intervention*, pp. 1159–1161, Springer, 2001.

[85] O. H. Schmitt, "Biological information processing using the concept of interpenetrating domains," in *Information processing in the nervous system*, pp. 325–331, Springer, 1969.

[86] R. Plonsey, "Bioelectric sources arising in excitable fibers (ALZA lecture)," *Annals of biomedical engineering*, vol. 16, no. 6, pp. 519–546, 1988.

[87] G. Plank, L. Zhou, J. L. Greenstein, S. Cortassa, R. L. Winslow, B. O'Rourke, and N. A. Trayanova, "From mitochondrial ion channels to arrhythmias in the heart: computational techniques to bridge the spatio-temporal scales," *Philosophical Transactions of the Royal Society A: Mathematical, Physical and Engineering Sciences*, vol. 366, no. 1879, pp. 3381–3409, 2008.

[88] A. Pullan, M. L. Buist, and L. K. Cheng, *Mathematically modelling the electrical activity of the heart: from cell to body surface and back again.* World Scientific Publishing Company, 2005.

[89] S. A. Niederer and N. P. Smith, "An improved numerical method for strong coupling of excitation and contraction models in the heart," *Progress in biophysics and molecular biology*, vol. 96, no. 1-3, pp. 90–111, 2008.

[90] N. A. Trayanova, "Whole-heart modeling: applications to cardiac electrophysiology and electromechanics," *Circulation research*, vol. 108, no. 1, pp. 113–128, 2011.

[91] D. Chapelle, M. A. Fernández, J.-F. Gerbeau, P. Moireau, J. Sainte-Marie, and N. Zemzemi, "Numerical simulation of the electromechanical activity of the heart," in *International Conference on Functional Imaging and Modeling of the Heart*, pp. 357–365, Springer, 2009.

[92] R. C. Kerckhoffs, S. N. Healy, T. P. Usyk, and A. D. McCULLOCH, "Computational methods for cardiac electromechanics," *Proceedings of the IEEE*, vol. 94, no. 4, pp. 769–783, 2006.

[93] V. Gurev, T. Lee, J. Constantino, H. Arevalo, and N. A. Trayanova, "Models of cardiac electromechanics based on individual hearts imaging data," *Biomechanics and modeling in mechanobiology*, vol. 10, no. 3, pp. 295–306, 2011.

[94] R. Chabiniok, P. Moireau, C. Kiesewetter, T. Hussain, R. Razavi, and D. Chapelle, "Assessment of atrioventricular valve regurgitation using biomechanical cardiac modeling," in *International Conference on Functional Imaging and Modeling of the Heart*, pp. 401–411, Springer, 2017.

[95] B. Ruijsink, K. Zugaj, J. Wong, K. Pushparajah, T. Hussain, P. Moireau, R. Razavi, D. Chapelle, and R. Chabiniok, "Dobutamine stress testing in patients with fontan circulation augmented by biomechanical modeling," *PloS one*, vol. 15, no. 2, p. e0229015, 2020.

[96] A. Le Gall, F. Vallée, K. Pushparajah, T. Hussain, A. Mebazaa, D. Chapelle, É. Gayat, and R. Chabiniok, "Monitoring of cardiovascular physiology augmented by a patient-specific biomechanical model during general anesthesia. A proof of concept study," *PLoS ONE*, vol. 15, p. e0232830, May 2020.

[97] P. Moireau, N. Xiao, M. Astorino, C. A. Figueroa, D. Chapelle, C. Taylor, and J.-F. Gerbeau, "External tissue support and fluid–structure simulation in blood flows," *Biomechanics and modeling in mechanobiology*, vol. 11, no. 1, pp. 1–18, 2012.

[98] M. R. Pfaller, J. M. Hörmann, M. Weigl, A. Nagler, R. Chabiniok, C. Bertoglio, and W. A. Wall, "The importance of the pericardium for cardiac biomechanics: from physiology to computational modeling," *Biomechanics and modeling in mechanobiology*, vol. 18, no. 2, pp. 503–529, 2019.

[99] R. C. Kerckhoffs, M. L. Neal, Q. Gu, J. B. Bassingthwaighte, J. H. Omens, and A. D. McCulloch, "Coupling of a 3D finite element model of cardiac ventricular mechanics to lumped systems models of the systemic and pulmonic circulation," *Annals of biomedical engineering*, vol. 35, no. 1, pp. 1–18, 2007.

[100] S. A. Niederer, G. Plank, P. Chinchapatnam, M. Ginks, P. Lamata, K. S. Rhode, C. A. Rinaldi, R. Razavi, and N. P. Smith, "Length-dependent tension in the failing heart and the efficacy of cardiac resynchronization therapy," *Cardiovascular research*, vol. 89, no. 2, pp. 336–343, 2011.

[101] H. Suga, "Theoretical analysis of a left-ventricular pumping model based on the systolic time-varying pressure/volume ratio," *IEEE Transactions on Biomedical Engineering,*, vol. 18, 1971.

[102] K. Sunagawa, W. L. Maughan, and K. Sagawa, "Effect of regional ischemia on the left ventricular end-systolic pressure-volume relationship of isolated canine hearts.," *Circulation Research*, Feb. 1983.

[103] W. C. Little and G. L. Freeman, "Description of LV pressure-volume relations by time-varying elastance and source resistance," *American Journal of Physiology-Heart and Circulatory Physiology*, July 1987.

[104] H. Suga, K. Sagawa, and A. A. Shoukas, "Load Independence of the Instantaneous Pressure-Volume Ratio of the Canine Left Ventricle and Effects of Epinephrine and Heart Rate on the Ratio," *Circulation Research*, Mar. 1973.

[105] H. Suga and K. Sagawa, "Instantaneous Pressure-Volume Relationships and Their Ratio in the Excised, Supported Canine Left Ventricle," *Circulation Research*, July 1974.

[106] W. C. Little, "The left ventricular dP/dtmax-end-diastolic volume relation in closed-chest dogs.," *Circulation Research*, June 1985.

[107] H. Senzaki, C. H. Chen, and D. A. Kass, "Single-beat estimation of end-systolic pressure-volume relation in humans. A new method with the potential for noninvasive application.," *Circulation*, vol. 94, pp. 2497–2506, Nov. 1996.

[108] A. Le Gall, F. Vallée, D. Chapelle, and R. Chabiniok, "Minimally-Invasive Estimation of Patient-Specific End-Systolic Elastance Using a Biomechanical Heart Model," in *Functional Imaging and Modeling of the Heart*, pp. 266–275, Springer, Cham, June 2019.

[109] H. Ishihara, M. Yokota, T. Sobue, and H. Saito, "Relation between ventriculoarterial coupling and myocardial energetics in patients with idiopathic dilated cardiomyopathy," *Journal of the American College of Cardiology*, Feb. 1994.

[110] M. R. Starling, M. M. Kirsh, D. G. Montgomery, and M. D. Gross, "Mechanisms for left ventricular systolic dysfunction in aortic regurgitation: Importance for predicting the functional response to aortic valve replacement," *Journal of the American College of Cardiology*, Mar. 1991.

[111] J. J. Schreuder, J. D. Biervliet, E. T. van der Velde, K. ten Have, A. D. van Dijk, N. G. Meyne, and J. Baan, "Systolic and diastolic pressure-volume relationships during cardiac surgery.," *Journal of cardiothoracic and vascular anesthesia*, vol. 5, pp. 539–545, Dec. 1991.

[112] D. Chapelle, M. Fragu, V. Mallet, and P. Moireau, "Fundamental principles of data assimilation underlying the Verdandi library: applications to biophysical model personalization within euHeart," *Medical & biological engineering & computing*, vol. 51, no. 11, pp. 1221–1233, 2013.

[113] P. Moireau, D. Chapelle, and P. Le Tallec, "Filtering for distributed mechanical systems using position measurements: perspectives in medical imaging," *Inverse problems*, vol. 25, no. 3, p. 035010, 2009.

[114] P. Moireau, D. Chapelle, and P. Le Tallec, "Joint state and parameter estimation for distributed mechanical systems," *Computer methods in applied mechanics and engineering*, vol. 197, no. 6-8, pp. 659–677, 2008.

[115] J. Mineroff, A. D. McCulloch, D. Krummen, B. Ganapathysubramanian, and A. Krishnamurthy, "Optimization framework for patient-specific cardiac modeling," *Cardiovascular engineering and technology*, vol. 10, no. 4, pp. 553–567, 2019.

[116] S. Niederer, Y. Aboelkassem, C. D. Cantwell, C. Corrado, S. Coveney, E. M. Cherry, T. Delhaas, F. H. Fenton, A. Panfilov, P. Pathmanathan, *et al.*, "Creation and application of virtual patient cohorts of heart models," *Philosophical Transactions of the Royal Society A*, vol. 378, no. 2173, p. 20190558, 2020.

[117] J. Xi, P. Lamata, W. Shi, S. Niederer, S. Land, D. Rueckert, S. G. Duckett, A. K. Shetty, C. A. Rinaldi, R. Razavi, *et al.*, "An automatic data assimilation framework for patient-specific myocardial mechanical parameter estimation," in *International Conference on Functional Imaging and Modeling of the Heart*, pp. 392–400, Springer, 2011.

[118] K. F. Augenstein, B. R. Cowan, I. J. LeGrice, P. M. Nielsen, and A. A. Young, "Method and apparatus for soft tissue material parameter estimation using tissue tagged magnetic resonance imaging," *J. Biomech. Eng.*, vol. 127, no. 1, pp. 148–157, 2005.

[119] J. Xi, P. Lamata, S. Niederer, S. Land, W. Shi, X. Zhuang, S. Ourselin, S. G. Duckett, A. K. Shetty, C. A. Rinaldi, *et al.*, "The estimation of patient-specific cardiac diastolic functions from clinical measurements," *Medical image analysis*, vol. 17, no. 2, pp. 133–146, 2013.

[120] J. C. Walker, M. B. Ratcliffe, P. Zhang, A. W. Wallace, E. W. Hsu, D. A. Saloner, and J. M. Guccione, "Magnetic resonance imaging-based finite element stress analysis after

linear repair of left ventricular aneurysm," *The Journal of thoracic and cardiovascular surgery*, vol. 135, no. 5, pp. 1094–1102, 2008.

[121] A. Krishnamurthy, C. T. Villongco, J. Chuang, L. R. Frank, V. Nigam, E. Belezzuoli, P. Stark, D. E. Krummen, S. Narayan, J. H. Omens, A. D. McCulloch, and R. C. Kerckhoffs, "Patient-specific models of cardiac biomechanics," *Journal of Computational Physics*, vol. 244, pp. 4–21, 2013. Multi-scale Modeling and Simulation of Biological Systems.

[122] L. Asner, M. Hadjicharalambous, R. Chabiniok, D. Peresutti, E. Sammut, J. Wong, G. Carr-White, P. Chowienczyk, J. Lee, A. King, *et al.*, "Estimation of passive and active properties in the human heart using 3D tagged MRI," *Biomechanics and modeling in mechanobiology*, vol. 15, no. 5, pp. 1121–1139, 2016.

[123] R. Kerckhoffs, P. Bovendeerd, J. Kotte, F. Prinzen, K. Smits, and T. Arts, "Homogeneity of cardiac contraction despite physiological asynchrony of depolarization: a model study," *Annals of biomedical engineering*, vol. 31, no. 5, pp. 536–547, 2003.

[124] T. Arts, P. Bovendeerd, F. W. Prinzen, and R. S. Reneman, "Relation between left ventricular cavity pressure and volume and systolic fiber stress and strain in the wall," *Biophysical journal*, vol. 59, no. 1, pp. 93–102, 1991.

[125] T. Arts, P. Bovendeerd, T. Delhaas, and F. Prinzen, "Modeling the relation between cardiac pump function and myofiber mechanics," *Journal of biomechanics*, vol. 36, no. 5, pp. 731–736, 2003.

[126] M. Caruel, R. Chabiniok, P. Moireau, Y. Lecarpentier, and D. Chapelle, "Dimensional reductions of a cardiac model for effective validation and calibration," *Biomechanics and Modeling in Mechanobiology*, vol. 13, pp. 897–914, Aug. 2014.

[127] G. Pennati, F. Migliavacca, G. Dubini, R. Pietrabissa, and M. R. de Leval, "A mathematical model of circulation in the presence of the bidirectional cavopulmonary anastomosis in children with a univentricular heart," *Medical engineering & physics*, vol. 19, no. 3, pp. 223–234, 1997.

[128] E. Magosso, S. Cavalcanti, and M. Ursino, "Theoretical analysis of rest and exercise hemodynamics in patients with total cavopulmonary connection," *American Journal of Physiology-Heart and Circulatory Physiology*, vol. 282, no. 3, pp. H1018–H1034, 2002.

[129] F. Migliavacca, G. Pennati, G. Dubini, R. Fumero, R. Pietrabissa, G. Urcelay, E. L. Bove, T.-Y. Hsia, and M. R. de Leval, "Modeling of the Norwood circulation: effects of shunt size, vascular resistances, and heart rate," *American Journal of Physiology-Heart and Circulatory Physiology*, vol. 280, no. 5, pp. H2076–H2086, 2001.

[130] F. Liang, K. Sughimoto, K. Matsuo, H. Liu, and S. Takagi, "Patient-specific assessment of cardiovascular function by combination of clinical data and computational model with applications to patients undergoing Fontan operation," *International journal for numerical methods in biomedical engineering*, vol. 30, no. 10, pp. 1000–1018, 2014.

[131] S. Pant, C. Corsini, C. Baker, T.-Y. Hsia, G. Pennati, I. E. Vignon-Clementel, M. of Congenital Hearts Alliance (MOCHA) Investigators, *et al.*, "Data assimilation and modelling of patient-specific single-ventricle physiology with and without valve regurgitation," *Journal of biomechanics*, vol. 49, no. 11, pp. 2162–2173, 2016.

[132] J. Lumens, C.-P. S. Fan, J. Walmsley, D. Yim, C. Manlhiot, A. Dragulescu, L. Grosse-Wortmann, L. Mertens, F. W. Prinzen, T. Delhaas, *et al.*, "Relative impact of right ventricular electromechanical dyssynchrony versus pulmonary regurgitation on right ventricular dysfunction and exercise intolerance in patients after repair of tetralogy of Fallot," *Journal of the American Heart Association*, vol. 8, no. 2, p. e010903, 2019.

[133] D. Tang, P. J. Del Nido, C. Yang, H. Zuo, X. Huang, R. H. Rathod, V. Gooty, A. Tang, Z. Wu, K. L. Billiar, *et al.*, "Patient-specific MRI-based right ventricle models using different zero-load diastole and systole geometries for better cardiac stress and strain calculations and pulmonary valve replacement surgical outcome predictions," *PLoS One*, vol. 11, no. 9, p. e0162986, 2016.

[134] D. Tang, C. Yang, J. Pedro, H. Zuo, R. H. Rathod, X. Huang, V. Gooty, A. Tang, K. L. Billiar, Z. Wu, *et al.*, "Mechanical stress is associated with right ventricular response to pulmonary valve replacement in patients with repaired tetralogy of Fallot," *The Journal of thoracic and cardiovascular surgery*, vol. 151, no. 3, pp. 687–694, 2016.

[135] H. Yu, J. Pedro, T. Geva, C. Yang, A. Tang, Z. Wu, R. H. Rathod, X. Huang, K. L. Billiar, and D. Tang, "Patient-specific in vivo right ventricle material parameter estimation for patients with tetralogy of Fallot using MRI-based models with different zero-load diastole and systole morphologies," *International journal of cardiology*, vol. 276, pp. 93–99, 2019.

[136] M. Sacks and C. Chuong, "Biaxial mechanical properties of passive right ventricular free wall myocardium," 1993.

[137] K. L. Billiar and M. S. Sacks, "Biaxial mechanical properties of the natural and glutaraldehyde treated aortic valve cusp—part I: experimental results," *J. Biomech. Eng.*, vol. 122, no. 1, pp. 23–30, 2000.

[138] A. Meoli, E. Cutrì, A. Krishnamurthy, G. Dubini, F. Migliavacca, T.-Y. Hsia, G. Pennati, M. of Congenital Hearts Alliance (MOCHA) Group, A. Taylor, A. Giardini, *et al.*, "A multiscale model for the study of cardiac biomechanics in single-ventricle surgeries: a clinical case," *Interface focus*, vol. 5, no. 2, p. 20140079, 2015.

[139] A. De Vecchi, A. Gomez, K. Pushparajah, T. Schaeffter, D. Nordsletten, J. Simpson, G. Penney, and N. Smith, "Towards a fast and efficient approach for modelling the patient-specific ventricular haemodynamics," *Progress in biophysics and molecular biology*, vol. 116, no. 1, pp. 3–10, 2014.

[140] A. De Vecchi, D. A. Nordsletten, E. W. Remme, H. Bellsham-Revell, G. Greil, J. M. Simpson, R. Razavi, and N. P. Smith, "Inflow typology and ventricular geometry determine efficiency of filling in the hypoplastic left heart," *The Annals of thoracic surgery*, vol. 94, no. 5, pp. 1562–1569, 2012.

[141] A. de Vecchi, D. A. Nordsletten, R. Razavi, G. Greil, and N. Smith, "Patient specific fluid–structure ventricular modelling for integrated cardiac care," *Medical & biological engineering & computing*, vol. 51, no. 11, pp. 1261–1270, 2013.

[142] M. Gusseva, T. Hussain, C. H. Friesen, P. Moireau, A. Tandon, C. Patte, M. Genet, K. Hasbani, G. Greil, D. Chapelle, *et al.*, "Biomechanical modeling to inform pulmonary valve replacement in tetralogy of Fallot patients after complete repair," *Canadian Journal of Cardiology*, vol. 37, pp. 1798–1807, 2021.

[143] M. Gusseva, T. Hussain, C. Hancock Friesen, G. Greil, D. Chapelle, and R. Chabiniok, "Prediction of Ventricular Mechanics After Pulmonary Valve Replacement in Tetralogy of Fallot by Biomechanical Modeling: A Step Towards Precision Healthcare," *Annals of Biomedical Engineering*, 2021.

CHAPTER 1

Biomechanical modeling to evaluate 'current mechanical state' of the myocardium in repaired tetralogy of Fallot patients

The purpose of this chapter was to use the biomechanical model in a cohort of rTOF patients to assess comparative influences of residual right ventricular outflow tract obstruction (RVOTO) and pulmonary regurgitation on ventricular health. We analyzed 20 patients pre- and post-PVR. The data contained volume and phase contrast flow measurements given by CMR a few months prior to PVR, and catherization pressures obtained during PVR. The model was coupled to the patients' data to obtain patient-specific mechanical properties of the cardiovascular system. Thanks to the valvular component in the model we could incorporate PV regurgitation and stenosis into the calibration of constitutive mechanical properties of the myocardium. The results showed an increased contractility pre-PVR in all patients compared to normal RVs. After PVR the contractility significantly decreased in all patients. Patients with predominantly RVOTO showed higher levels of contractility and stroke work decrease compared to those with predominantly PV regurgitation. This chapter shows the ability of the biomechanical model (1) to integrate multiple clinical data inputs, (2) to assess the influence of both combined and independent effects of PV regurgitation and RVOT stenosis on RV health, and (3) to augment clinical indicators of RV health in patient-specific manner.

Contents

Biomechanical Modeling to Inform Pulmonary Valve Replacement in Tetralogy of Fallot Patients After Complete Repair

Maria Gusseva[1,2], Tarique Hussain[3], Camille Hancock Friesen,[4], Philippe Moireau,[1,2], Animesh Tandon[3], Cécile Patte[1,2], Martin Genet[1,2], Keren Hasbani[5], Gerald Greil[3], Dominique Chapelle[1,2], Radomír Chabiniok[1,2,3,6,7]

[1]Inria, Palaiseau, France
[2]LMS, Ecole Polytechnique, CNRS, Institut Polytechnique de Paris, Palaiseau, France
[3]Division of Pediatric Cardiology, Department of Pediatrics, UT Southwestern Medical Center, Dallas, TX
[4]Division of Pediatric Cardiothoracic Surgery, Department of Pediatrics, UT Southwestern Medical Center, Dallas, Texas, USA
[5]Division of Pediatric Cardiology, Department of Pediatrics, Dell Medical School, University of Texas, Austin, Texas, USA
[6]School of Biomedical Engineering Imaging Sciences, St Thomas' Hospital, King's College London, London, United Kingdom
[7]Department of Mathematics, Faculty of Nuclear Sciences and Physical Engineering, Czech Technical University in Prague, Prague, Czech Republic

Canadian Journal of Cardiology 37: 1798-1807 (2021)

Abstract

Background: A biomechanical model of the heart can be used to incorporate multiple data sources (electrocardiography, imaging, invasive hemodynamics). The purpose of this study was to use this approach in a cohort of patients with tetralogy of Fallot after complete repair (rTOF) to assess comparative influences of residual right ventricular outflow tract obstruction (RVOTO) and pulmonary regurgitation on ventricular health.

Methods: Twenty patients with rTOF who underwent percutaneous pulmonary valve replacement (PVR) and cardiovascular magnetic resonance imaging were included in this retrospective study. Biomechanical models specific to individual patient and physiology (before and after PVR) were created and used to estimate the RV myocardial contractility. The ability of models to capture post-PVR changes of right ventricular (RV) end-diastolic volume (EDV) and effective flow in the pulmonary artery (Qeff) was also compared with expected values.

Results: RV contractility before PVR (mean 66 ± 16 kPa, mean ± standard deviation) was increased in patients with rTOF compared with normal RV (38-48 kPa) ($P < 0.05$). The contractility decreased significantly in all patients after PVR ($P < 0.05$). Patients with predominantly RVOTO demonstrated greater reduction in contractility (median decrease 35%) after PVR than those with predominant pulmonary regurgitation (median decrease 11%). The model

simulated post-PVR decreased EDV for the majority and suggested an increase of Q_{eff} both in line with published data.

Conclusions: This study used a biomechanical model to synthesize multiple clinical inputs and give an insight into RV health. Individualized modeling allows us to predict the RV response to PVR. Initial data suggest that residual RVOTO imposes greater ventricular work than isolated pulmonary regurgitation.

Keywords— translational research, cardiovascular modeling, myocardial contractility, tetralogy of Fallot, personalized medicine, cardiovascular magnetic resonance imaging

1.1 Introduction

Stenosis of the pulmonary valve is a relatively common congenital condition isolated, or as a part of the constellation of tetralogy of Fallot (TOF). The initial pressure overload is corrected surgically often using a transannular patch, causing varying degrees of pulmonary regurgitation (PR). Over time, valve-sparing techniques have been preferred, but at the cost of potentially higher rates of residual right ventricular outflow tract obstruction (RVOTO). Chronic RV volume overload leads to RV dilation and chronic RVOTO can cause RV hypertrophy. To avoid RV failure and even to allow reverse remodeling, patients undergo pulmonary valve replacement (PVR) in adolescence or early adult life. There is a robust debate regarding the optimal timing of PVR [1; 2; 3; 4; 5; 6; 7]. Among the main clinical indicators considered in decision making are the degree of RV dilation, RV ejection fraction (EF), and pulmonary valve regurgitation fraction (RF) [8]. However, the ability to predict post-PVR reverse remodeling remains elusive and is witnessed in only 60% of patients regardless of the threshold for intervention [2]. Upstream, the debate as to the optimal initial repair remains whether transannular patch with mild residual obstruction is preferable to annulus-sparing approaches in borderline valves. Current practice is to favor valve preservation, but recent long-term outcome data suggest [9] that RV hypertrophy may be a predictor of adverse events.

Although the current guidelines focus on the direct measures taken from imaging data, the underlying physiology is not the primary driver of interventions. Incorporating physical and physiologic assumptions of cardiovascular function in the framework of biomechanical modeling [10; 11] has the potential to augment the interpretation of clinical data, such as by estimating some clinically relevant functional quantities, eg, myocardial contractility [12; 13; 14]. The contractility in the present work represents the active stress generated by the myocardial sarcomere unit during contraction. The contractility in a given patient can be increased chronically (eg, in ventricular overloading such as due to a valvular defect) and adapts to the actual physiologic state by inotropic stimulation [14]. We remark that the level of myocardial contractilitydas used in this workdwas demonstrated to correlate with the maximum time derivative of ventricular pressure, $\max(dp/dt)$ [14], which is a widely accepted surrogate measure of global ventricular contractility. Assessing mechanical properties of the hearts of patients with tetralogy of Fallot after complete repair (rTOF) provides additional metrics which may provide new insight into the initial procedure choice in cases of borderline pulmonary valve annulus.

1.1.1 Objectives

The goal of this retrospective observational work was to quantify the level of RV myocardial contractility before PVR and immediately after PVR by coupling the available clinical data with a biomechanical model. We hypothesize that the RV contractility is chronically

increased in rTOF patients with PR or residual RVOTO and that it will decrease immediately after PVR. This reduction toward the normal values will also translate into the reduction of stroke work that the heart needs to exert.

1.2 Methods

1.2.1 Data

A group of 20 patients with rTOF who underwent percutaneous PVR were included in this retrospective study. The data collections were performed under the ethical approvals of Institutional Review Boards of the UT South- western Medical Center, Dallas (STU-2020-0023), and the University of Texas, Austin (IRB 2020-06-0128). The IRBs waived the need for a consent to use the anonymized retrospective data.

All patients underwent cardiovascular magnetic resonance (CMR) examination 4-6 months before PVR. CMR was processed semi-automatically by using the CVI42 software (Circle Cardiovascular Imaging, Calgary, Alberta, Canada) and a finite element method for image registration [15; 16]. The results of CMR analyses are RV time-vs-volume plots and time-vs-flow through the pulmonary artery (PA) together with the flow integrated throughout the cycle containing the forward and regurgitant components (Q_{for} and Q_{back}, respectively). The effective flow through the pulmonary circulation (ie, Q_{for} - Q_{back}) will be denoted as Q_{eff}.

During the percutaneous PVR, the right-heart pressures (containing right atrial, RV, and PA pressures) were taken before and after deploying the valve. Figure 1.1 displays an example of processed clinical data of a selected patient.

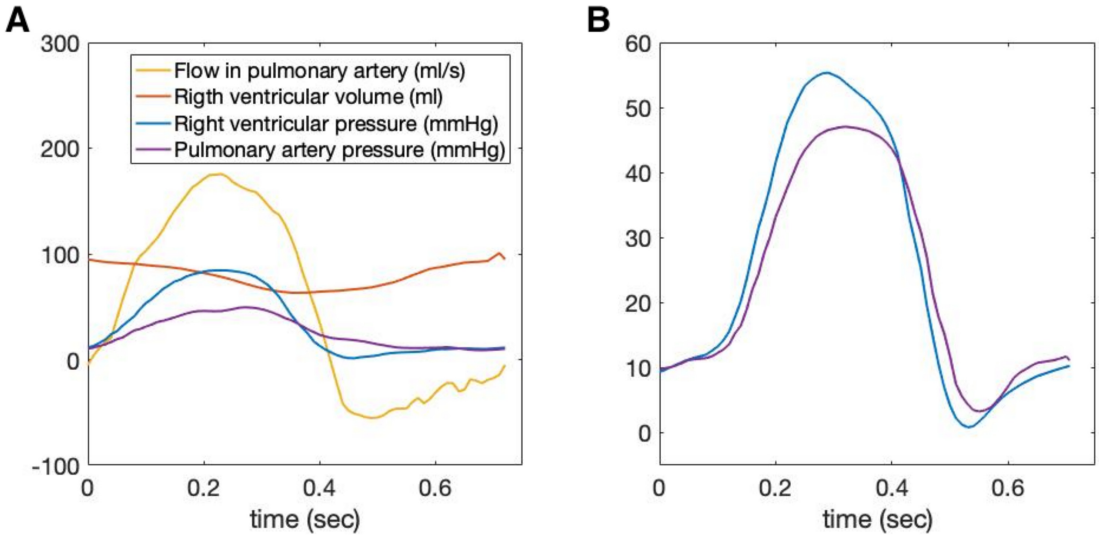

Figure 1.1: Example of processed clinical data (A) before and (B) after pulmonary valve replacement.

Supplemental Tables 1.4 and 1.3 provide information about the basic demographics, baseline anatomy, possible palliation, type and age of TOF repair, reintervention (if any), and the type of prosthesis in each patient.

Data of healthy subjects were obtained from a population study [17] that contained the values (weighted means) of RV and PA end-systolic pressures (ESPs), RV end-diastolic volume (EDV) and end-systolic volume (ESV), and RV myocardial mass.

1.2.2 Biomechanical model

The biomechanical heart model of reduced order [18; 19] was used. While the geometry and kinematics of RV are reduced, the constitutive mechanical laws are preserved as in the full 3D model [20] (Fig. 1.2). Specifically, myocardial tissue was modeled by a viscoelastic material with active contractile component representing the actin-myosin interaction (consistent with the sliding filament theory by A.F. Huxley [21; 22]). The myocardial internal stresses – passive (given by the tissue stiffness of the viscoelastic material) and active (generating the active shortening of the myocardial fibers leading to heart contraction) – are in equilibrium with the external loading (the pressure exerted on the endocardial surface) and inertia forces. The model of the RV was connected to a Windkessel model of the circulatory system [23], which consisted of proximal resistance and capacitance R_{prox}, C_{prox} (representing the main and branch pulmonary arteries) with pressure P_{ar}, distal resistance and capacitance R_{dist}, C_{dist} (representing the remaining pulmonary circulation) with pressure P_{dist}, and terminal venous pressure P_{vs}, as depicted in Figure 1.2. The detailed description of the model is provided in Supplemental Appendix, and rigorous formulations can be found in our previous work [18; 20; 24].

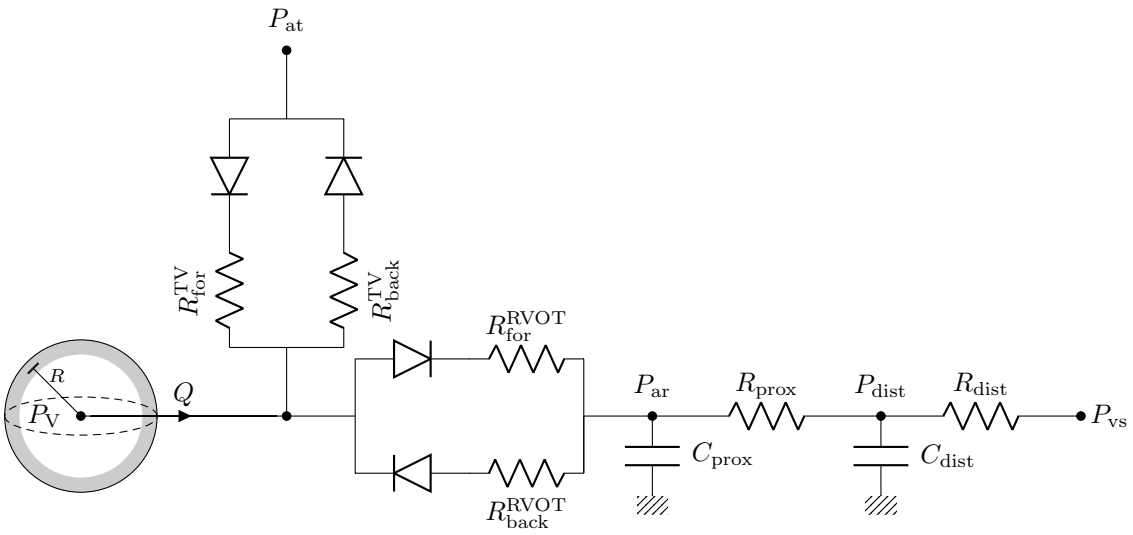

Figure 1.2: Model of right ventricle coupled with atrioventricular and arterial outflow valves and with circulation system represented by a Windkessel model. P_{V}, P_{at} , P_{ar}, P_{dist}, and P_{vs} stand for pressures in ventricle, atrium, large arteries, distal circulation, and venous system, respectively, $R_{\text{for}}^{\text{TV}}$, $R_{\text{back}}^{\text{TV}}$, $R_{\text{for}}^{\text{RVOT}}$ and $R_{\text{back}}^{\text{RVOT}}$ are forward and backward resistances of the tricuspid valve and forward and backward resistances of the ventricular outflow tract, respectively, and R_{prox}, R_{dist}, C_{prox}, and C_{dist} are proximal and distal resistances and capacitances of the circulation.

1.2.3 Model calibration to data of individual patients

The biomechanical model of RV and pulmonary circulation was adjusted manually to the data of each individual patient by a sequential calibration [19]. The pulmonary Windkessel model was adjusted while imposing the measured PA flow. Using cine magnetic resonance imaging, we prescribed the wall thickness and the ventricular volume in reference configuration (when zero intraventricular pressure is assumed) [25]. The RV preload was prescribed according to the measured RV pressure in diastole. Passive myocardial properties (ie, myocardial stiffness) were calibrated so that the simulated EDV matched the measurement. RVOT was modeled as an outlet valve allowing the forward and regurgitant

flow [24] (with resistances $R_{\text{for}}^{\text{RVOT}}$ and $R_{\text{back}}^{\text{RVOT}}$, respectively). The backward resistance $R_{\text{back}}^{\text{RVOT}}$ was adjusted to match the backward flow waveform. $R_{\text{back}}^{\text{RVOT}}$ was set to a high value if no PR was present (effectively zero backward conductance). Similarly, a negligible $R_{\text{for}}^{\text{RVOT}}$ was used if no pathologic RVOTO was present. The tricuspid valve (TV) was modeled as an inlet valve with resistances $R_{\text{for}}^{\text{TV}}$ and $R_{\text{back}}^{\text{TV}}$, respectively [26]. The myocardial contractility was adjusted according to the measured RV stroke volume (SV) and RV ESP. Physiologic assumptions of mechanochemical coupling of the actin-myosin complex in the sarcomere are translated into the mechanical system generating force – the active contractility – which combines with the passive viscoelastic properties of the tissue.

The post-PVR model was obtained by recalibrating the pre-PVR model with the aim to match the post-PVR pressure measurements. We preserved the passive myocardial properties, prescribed the preload as in the measurement, $R_{\text{back}}^{\text{RVOT}}$ was set to its maximum (to eliminate PR) and $R_{\text{for}}^{\text{RVOT}}$ adjusted to match the pressure difference between RV and PA. Finally, the contractility was adjusted so that the simulated RV ESP matched the data.

The mechanical parameters of these patient-specific models give an insight into the cardiovascular physiology of each patient. The simulated RV EDV and pulmonary flow after PVR were used to validate the model prediction against published data by Lurz et al. [27]. Further details of the model calibration, including quantitative values of parameters for each patient (Supplemental Table 1.5), are presented in the Supplemental Appendix 1.6.

1.2.4 Statistical analysis

Wilcoxon signed-rank tests were conducted for the changes in model-derived contractility and PA ESP at $P < 0.05$. Bland-Altman plots were constructed to evaluate the difference between simulated and measured functional indicators.

1.3 Results

1.3.1 Direct analysis of clinical data

The results of direct analysis of clinical data are summarized in Supplemental Table 1.3. Pre-PVR CMR revealed that 45% of patients had mild PR, with RF of 10%-30%, 15% of patients had moderate PR (RF 30%-40%), and 40% had severe PR (RF > 40%). Considering the RV size, 25% of patients had moderate RV dilation (EDV indexed to the body surface area, RV EDVi, 120-140 ml/m^2) and 20% had moderate to severe RV dilation (RV EDVi 140-150 ml/m^2), while the remaining patients had normal or mildly dilated RV. Finally, 30% of patients had moderate pulmonary stenosis, with the RV to PA pressure gradient of $\geq$ 25 mmHg. The degree of RVOTO was evaluated based on the ratio of RV to LV ESP, where ratios $\geq$ 50% and < 50% were considered to represent high and low, respectively, degrees of RVOTO. The comparison of RV SV and outflow volume Q_{for} revealed mild TR in 4 patients.

The patients were divided into 3 groups according to the level of RVOTO and PR: low degree of RVOTO and at least moderate PR (group A); high degree of RVOTO and mild PR (group B); and high degree of RVOTO and at least moderate PR (group C). Groups A-C contained 9, 8, and 3 patients, respectively.

1.3.2 Model-derived ventricular contractility

We successfully calibrated the model for all patients before and after PVR. Figure 1.3 and Supplemental Figures 1.8-1.10 show the simulated cardiac cycles compared with data in

selected patients. Bland-Altman plots in Figure 1.4 and quantitative summary in Table 1.1 show the mean bias between the simulations and measurements before and after PVR.

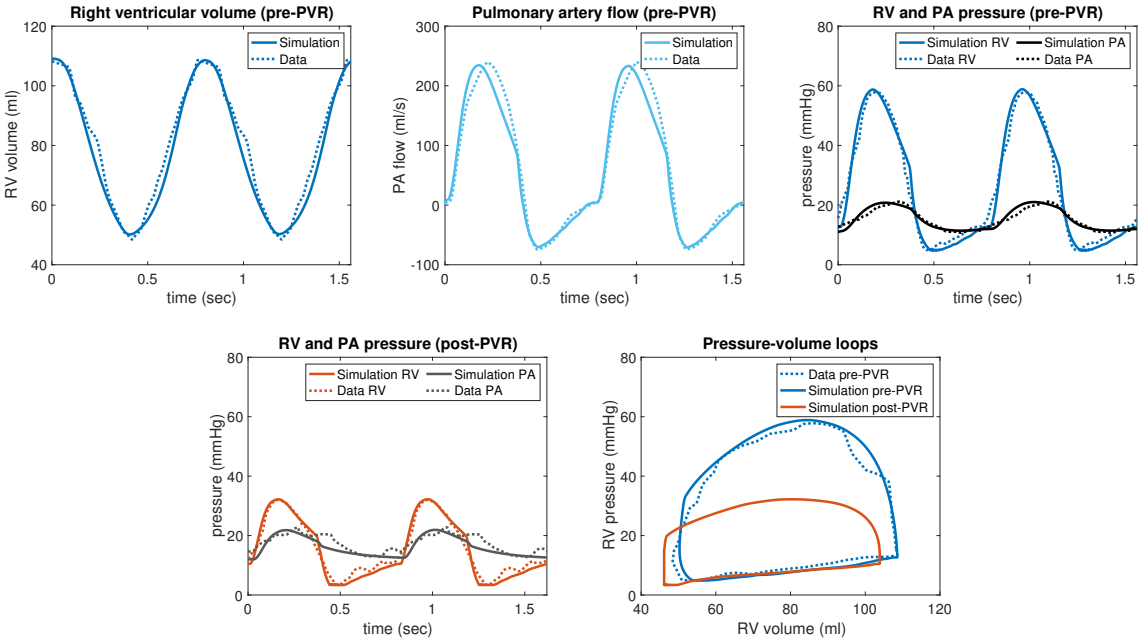

Figure 1.3: Measured data (dashed lines) and simulation (solid lines) for patient 16. PA, pulmonary artery; PVR, pulmonary valve repair; RV, right ventricle.

Table 1.1: Bland-Altman quantitative statistics summarizing the mean bias ± standard deviation and limits of agreement (95% confidence intervals) between simulations and measurements. EDVi, end-diastolic volume indexed to body surface area; ESP, end- systolic pressure; ESVi, end-systolic volume indexed to body surface area; PA, pulmonary artery; PVR, pulmonary valve replacement; Q_{back}, backward flow; Q_{for}, forward flow; RV, right ventricle.

	mean ± SD	95%-confidence interval
Pre-PVR		
RV EDVi (ml/m^2)	0.01 ± 0.04	-0.08 to 0.01
RV ESVi (ml/m^2)	-0.77 ± 1.41	-3.53 to 2.00
RV ESP (mmHg)	0.06 ± 1.10	-2.11 to 2.23
PA ESP (mmHg)	-0.08 ± 0.95	-1.93 to 1.78
PA Qfor (ml/cardiac cycle)	3.00 ± 5.40	-7.60 to 13.70
PA Qback (ml/cardiac cycle)	0.01 ± 5.00	-10.20 to 10.22
Post-PVR		
RV ESP (mmHg)	-0.05 ± 0.60	-1.23 to 1.13
PA ESP	0.41 ± 0.67	-0.90 to 1.72

Calibrating the model by using the data from a healthy population revealed the contractility of healthy RV to be in the range of 38-48 kPa. The values of RV contractility in all patients (assessed by models calibrated to pre- and post-PVR data) are plotted against RV ESP in Figure 1.5A. Pre- and post-PVR median contractilities were 66 and 51 kPa, respectively. Figure 1.5B shows a strong positive correlation ($R^2 = 0.95$; P <0.001) between the RV ESP and contractility rescaled by the ratio of myocardial wall thickness

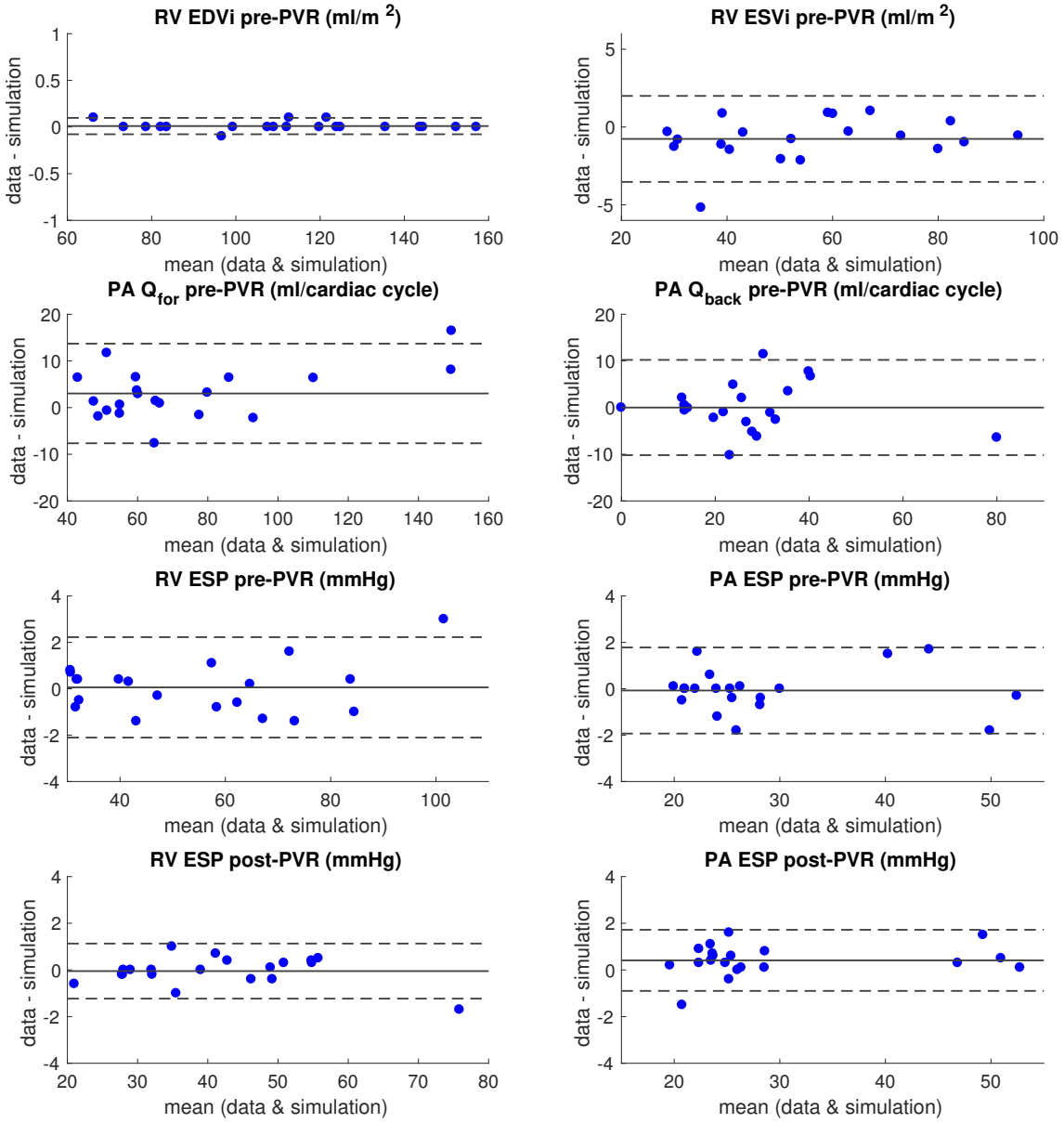

Figure 1.4: Bland-Altman plots for RV EDVi, ESVi, PA Qfor, Qback, RV ESP, PA ESP (all lines represent the mean of the difference between data and simulation, top and 95% prediction interval (± 1.96 times SD). EDVi, end-diastolic volume indexed to body surface area; ESP, end-systolic pressure; ESVi, end-systolic volume indexed to body surface area; PA, pulmonary artery; PVR, pulmonary valve replacement; Q_{back}, backward flow; Q_{for}, forward flow; RV, right ventricular.

over ventricular radius. Stroke work was calculated as the area encompassed within the simulated ventricular pressure-volume (P-V) loops and is plotted against RV ESP in Figure 1.5C. Pre- and post-PVR median stroke works were 327 and 233 mJ, respectively. The stroke works obtained from the healthy subjects were in the range of 103-150 mJ. The values of mean contractility and stroke work for each group, relative to the maximum values of the normal population, are presented in Table 1.2.

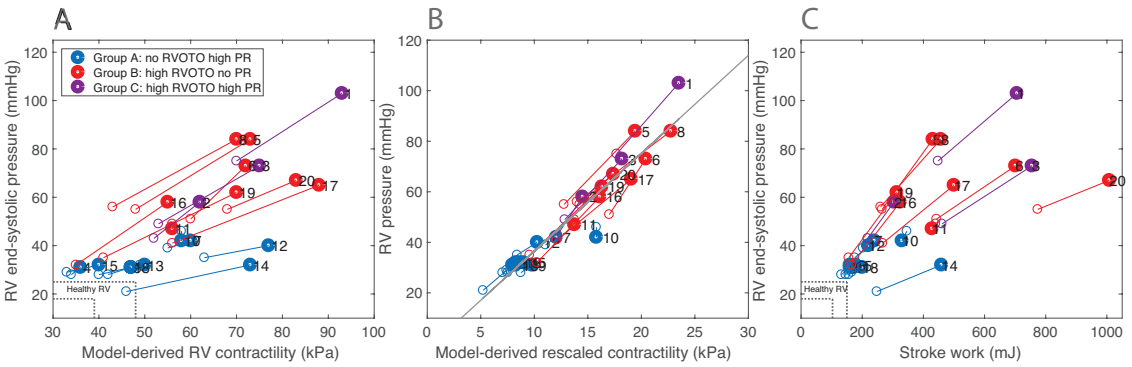

Figure 1.5: Model-derived right ventricular (RV) (A) contractility and (C) stroke work for each patient. Filled and empty circles correspond to pre- and post-PVR values, respectively. The number labels of the circles correspond to individual patients. The values for healthy RVs are represented by the area encompassed within the dashed lines. (B) RV contractility rescaled by the ratio of myocardial wall thickness over ventricular chamber radius against RV end-systolic pressure, where gray line is Pearson correlation with $R^2 = 0.95$ and $P < 0.05$. PR, pulmonary regurgitation; PVR, pulmonary valve replacement; RVOTO, right ventricular outflow tract obstruction.

Table 1.2: Median right ventricular (RV) contractility and relative contractility compared with normal RV contractility (48 kPa), and median RV stroke work and relative stroke work compared with normal RV stroke work (150 mJ). Group A: no right ventricular outflow tract obstruction (RVOTO) and high pulmonary regurgitation (PR), group B: high RVOTO and no PR, group C: high RVOTO and high PR. Significance is assumed at $P < 0.05$.

	Contractility (kPa)		Contractility with respect to normal		Stroke work (mJ)		Stroke work with respect to normal	
	Pre-PVR	Post-PVR	Pre-PVR	Post-PVR	Pre-PVR	Post-PVR	Pre-PVR	Post-PVR
Group A	50	46 (p=0.008)	4%	0%	200	166 (p=0.027)	34%	10%
Group B	71	52 (p=0.016)	48%	8%	444	266 (p=0.016)	196%	77%
Group C	75	53 (p=0.250)	56%	10%	706	448 (p=0.250)	370%	199%
All patients	66	51 (p=0.000)	38%	6%	327	233 (p=0.000)	118%	55%

1.3.3 Post-PVR changes in RV EDV and effective PA flow

The patient-specific post-PVR models were used to assess the changes of RV volumes and PA flow after PVR based on captured post-PVR invasive pressures. Figure 1.6 shows the model-derived changes of RV EDVi and PA Qeff. The average EDP decrease in our cohort was lower than that in the study by Lurz et al. [27]: 14.2% vs 26.5%. Consequently, the average EDV decrease was also lower: 3% decrease suggested by the model vs 12% reported by Lurz et al. The model suggested an increase of PA Q_{eff} after PVR, which fell between the pre-PVR values of Q_{for} and Q_{eff} – in line with Lurz et al.

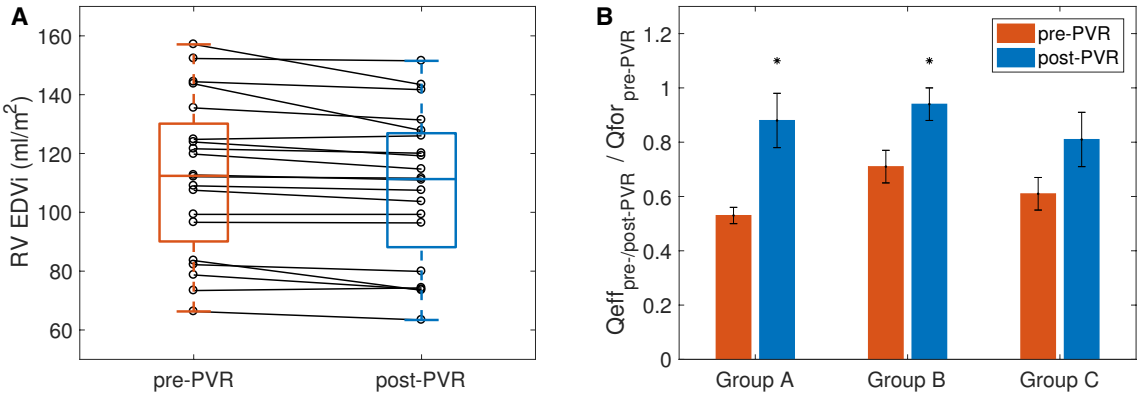

Figure 1.6: (A) Model-predicted post-pulmonary valve replacement (PVR) changes in right ventricular end-diastolic volumes indexed to body surface area (EDVi). Central line inside each box indicates the median, and the bottom and top edges of the boxes show 25th and 75th percentiles, respectively. Black circles connected by black lines show the EDVi change from before to after PVR for individual patients. (B) Post-PVR model- predicted change in effective flow (Q_{eff}) in each patient group. Orange bars: $Q_{\text{eff}_{\text{pre-PVR}}}/Q_{\text{for}_{\text{pre-PVR}}}$ corresponding to the complement of regurgitation fraction (1 - $Q_{\text{back}}/Q_{\text{for}}$), where Q_{for} and Q_{back} are forward and backward flows, respectively. Blue bars: $Q_{\text{eff}_{\text{post-PVR}}}$ (model) is scaled by $Q_{\text{for}_{\text{pre-PVR}}}$ (data) (consistently with the orange bars) to demonstrate model-predicted significant increase of $Q_{\text{eff}_{\text{post-PVR}}}$. Note that model-derived $Q_{\text{eff}}/Q_{\text{for}}$ = 1 for post-PVR (owing to the assumption of zero pulmonary regurgitation post-PVR). Asterisks indicate significant difference at $P < 0.05$.

1.4 Discussion

This study applied patient-specific biomechanical modeling on a group of patients with rTOF indicated for PVR. We aimed to assess whether the proposed data-model coupling framework provides any additional clinical indicators of the effects of PVR.

CMR- and pressure-derived clinical indicators suggested 3 groups of patients based on the grade of PR and severity of RVOTO. The patient-specific models created separately for pre- and post-PVR physiology revealed that PVR triggered an immediate adaptation of RV contractility for a majority of patients, with a decrease of the median contractility by 23%. Table 1.2 reveals that the patients with a high degree of RVOTO showed a larger contractility decrease (groups B and C) and the contractility of all patients decreased close to the normal values (Table 1.2 and Figure 1.5).

The stroke work represents the mechanical energy generated by the ventricle during a heartbeat. The analysis of P-V loops suggested that even though the patients with a high degree of RVOTO (groups B and C) experienced a significant decrease of the median stroke work (Table 1.2), the actual stroke work after PVR remained elevated owing to a limited decrease of RV pressure after PVR. The patients with predominantly PR and a low degree of RVOTO (group A) showed a decrease of the median stroke work by 17%. The resulting stroke work was only ∼10% above normal values (Table 1.2), thanks to the normal RV pressure after PVR.

The strong correlation between the ventricular pressure and the rescaled contractility is in line with Laplace's law of myocardial wall stress being directly proportional to the level of pressure developed in the chamber for a given geometry during ventricular systole. Thus, before PVR we observed higher levels of contractility in patients with increased RV systolic pressure and in those with dilated RVs (patients 12 and 14 from group A). The RV contractility decreased after PVR primarily owing to the release of RVOTO. The sole effect of regurgitation on the system was visible in the patients from group A. The median

contractility and stroke work in that group appeared to be only up to 4% and 34% higher, respectively, than a range of reference healthy RV contractility and stroke work (Table 1.2). This suggests that, in infants with TOF with borderline pulmonary valve annulus, inserting a transannular patch might be preferential, because the RV is likely to well tolerate the created PR. However, 2 patients with the most dilated RVs (RV EDVi > 140 mL/m^2) appeared to be the outliers, with pre-PVR contractilities of 77 and 73 kPa (patients 12 and 14, respectively). It is likely that before PVR, the majority of patients in group A had been preserving their cardiac output at moderately elevated myocardial stresses. Those with dilated RVs had been progressively becoming less efficient and had elevated metabolic demands. Therefore, our model revealed that the myocardial contractility was substantially increased in the patients with dilated RVs before PVR. However, the critical range of RV dilation is unclear from this study and is the subject of our ongoing work. Furthermore, we showed that the greatest reduction of contractility occurred because of removal of RVOTO, while removing the regurgitation itself did not lead to a significant immediate decrease of contractility in the majority of patients.

Not having post-PVR CMR prevented us from performing a detailed validation of our post-PVR models. However, a partial validation was possible thanks to the study by Lurz et al. [27], in which CMR was performed immediately after the intervention on the pulmonary valve. Our models showed a decrease of RV EDV for patients experiencing a decrease in RV EDP and an increase of PA Q_{eff} after PVR, both of which qualitatively match with the study of Lurz et al. The lower decrease of EDP (as measured in our patients compared with those of Lurz et al.) explains the lower EDV decrease in our group of patients.

1.4.1 Limitations

A number of limitations should be addressed. First, an assumption of spherical RV might have overestimated the contractility because the spherical shape is mechanically more efficient than a crescent shape. Figure 1.7 demonstrates the effect of interobserver variability in estimating RV myocardial mass: The difference between pre- vs post-PVR contractility were preserved in a relative sense, and this would be expected also if an accurate RV geometry was used. It is expected that the active stress developed in various parts of the RV varies (eg, inflow part may be very contractile, while the outflow will be hypo- or dyskinetic due to the passive transannular patch). Such a heterogeneity cannot be captured by our simplified model. However, our pilot study demonstrates that using such a modeling approach is directly feasible in the clinical setup. The level of complexity allows medical doctors to set up the patient-specific models. This may facilitate launching a large-scale and multisite clinical study counting hundreds of cases, which would be out of reach for a number of complex models.

Percutaneous PVR is mostly not used in patients with very dilated RVs and RVOTs, who rather undergo surgical PVR. In this pilot study we took advantage of the accessibility of measured pressures after PVR. However, we acknowledge that the population in this study was biased and did not allow for general conclusions regarding relative impact of PR and pulmonary stenosis over the whole range of this patient population. In a future study, we aim to use an estimation of RVOT pressure gradient based on the measured flow profile through the RVOT [28] and the estimated RV end-diastolic pressure according to the right atrial volume and flow through the tricuspid valve [29].

Another important concern is the time period of 4-6 months between the acquisition of CMR and catheterization data in this proof-of-concept work. The progressive RV remodeling might have caused an underestimation of the current RV volumes, which may in turn affect the predicted model-derived properties. Finally, the validation of our post-PVR

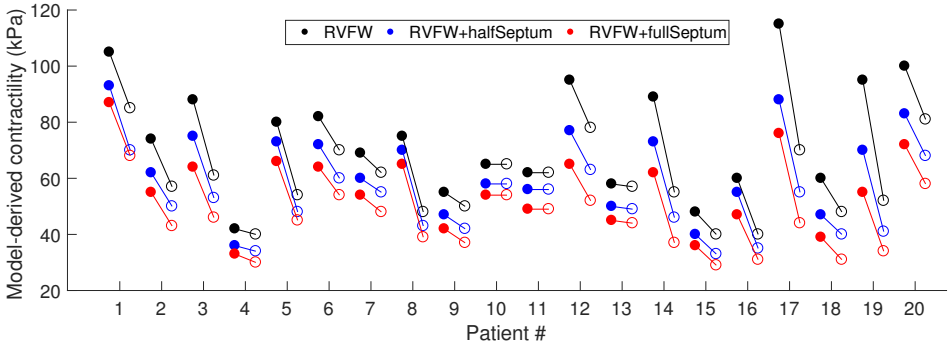

Figure 1.7: Sensitivity of the model-derived contractility to the variation of right ventricular (RV) mass. Pre- and post-pulmonary valve replacement (PVR) contractilities (filled and empty points, respectively) were calibrated for the following type of mass input for each patient: RV mass represented by RV free wall (RVFW; black points), RVFW mass increased by the mass of half septum mass (blue points), and RVFW with full septum (red points). Solid lines between the points show the decrease of the model-derived contractility after PVR.

model was limited by the absence of post-PVR CMR. In the future we aim to perform an additional CMR within 48 hours after PVR, which would be plausible for most patients. RV electromechanical dyssynchrony is another major pathophysiologic factor that can lead to further pathologic RV remodeling. Cardiac models with a detailed electrical component provide perspective in optimizing RV cardiac resynchronization therapy [30], and modeling could even contribute to the decision making of a possible combination of PVR and RV cardiac resynchronization therapy.

1.4.2 Future perspectives

In addition to RV contractility at rest, a reduced exercise capacity may play a significant role in the response to PVR and will be studied [14]. The present work demonstrates an application of models capturing an immediate state of the cardiovascular system to inform about the current physiologic state without explicitly considering the previous progress of ventricular remodeling. Models of long-term evolution [31; 32] have the potential to include information about the initial state of pathology, type of repair, and the evolution throughout the life of patient (Supplemental Table 1.4). They could also be useful in better understanding the reverse remodeling after PVR – a crucial step in predicting the long-term effect of PVR and subject of our ongoing research [33; 34]. Advanced imaging techniques such as the assessment of myocardial fiber directions by magnetic resonance diffusion tensor imaging35 could be considered in the future.

Even though the present study demonstrated a substantially increased work that the RV must exert in patients with residual RVOTO and therefore favors transannular patch in the case of borderline annulus size, we are aware that our proof-of-concept modeling study cannot have immediate implications on patient care. Furthermore, it is known that a mild-to-moderate stenosis in the early postoperative period may spontaneously regress and the strategy of preservation of annular function may be compatible with long-term relief of RVOTO.

1.5 Conclusion

Combination of computational models and clinical data is feasible in a cohort of patients with rTOF. The present study quantifies the level of RV overload with chronic valvular

disease and how the level of overloading decreases after intervention on the valve. Though not directly predicting who should undergo PVR and who should wait, we think our physiologic finding is of clinical interest as a step toward optimal clinical evaluation and management of patients with valvular heart disease. Furthermore, the need to aim for long-term relief of RVOTO is highlighted, perhaps prejudicing the initial surgical approach. Predictions based on coupling clinical data and biomechanical models have the potential to become part of clinical assessment to contribute to optimizing and personalizing the clinical management of every patient.

1.6 Supplemental Appendix. Additional Methodology

Detailed clinical information

Supplementary Table 1.3 shows patients' demographics and direct analysis of clinical data. Supplementary Table 1.4 summarizes clinical details about patients included in the study, namely the complicating features of the baseline anatomy, palliation (if any), type of repair, age of repair, possible re-intervention prior to the pulmonary valve replacement (PVR) and the type prosthesis used in percutaneous PVR (related to this study).

Description of the model

The model used in the present study is a biomechanical model of single heart cavity [18; 19] with the preload imposed from the measured pressure data in diastole, and connected to a Windkessel model of circulatory system [23] (schematics of the model is shown in Figure 1.2 of the main article body). The geometry and kinematics of the ventricle are reduced to a sphere with inner radius R and wall thickness d, while constitutive mechanical laws are preserved as in the full 3D heart model described in [24] and [20].

The displacement of the sphere in radial direction y and the intraventricular pressure P_{V} are the principal unknowns that the model is solving for. The variation of ventricular volume during the cardiac cycle and systolic wall thickening is then directly derived from the radius R (from the center of the cavity to the middle of ventricular wall (see Figure 1.2):

$$V = \frac{4}{3}\pi \left(R - \frac{d}{2}\right)^3, \tag{1.1}$$

where

$$R = R_0(1 + e_{\mathrm{fib}}), \qquad d = d_0(1 - e_{\mathrm{fib}})^{-2}, \qquad e_{\mathrm{fib}} = (R - R_0)/R_0, \tag{1.2}$$

with R_0 and d_0 being the ventricular radius and wall thickness at reference (stress-free) configuration.

The multiscale formulation of the model allows to capture the behavior of actin-myosin interaction at the fiber level and translate it into the whole organ performance [24; 20]. The constitutive behavior of myocardium is represented by a Hill-Maxwell rheological model [35]. It contains an active contractile component, that represents sliding of the myosin heads along actin filament, and a visco-elastic component accounting for the visco-elastic properties of surrounding connective tissue (collagen-rich components in myocardium). Physiological assumptions of mechano-chemical coupling of the actin-myosin complex in the sarcomere are translated into the mechanical system generating force. It was originally developed by A. F. Huxley [21] (see also recent work [22]). All myosin filaments in the sarcomere unit are considered as a series of springs with certain energy. The following system of ordinary differential equations describes the active stress (τ_c) and active stiffness (k_c) produced in each actin-myosin unit (by all myosin springs) at certain sarcomere extension (e_{fib}):

$$\begin{cases} \dot{k}_c = -(|u| + \alpha|\dot{e}_{\mathrm{fib}}|)k_c + n_0(e_{\mathrm{fib}})k_0|u|_+ \\ \dot{\tau}_c = -(|u| + \alpha|\dot{e}_{\mathrm{fib}}|)\tau_c + \dot{e}_{\mathrm{fib}}k_c + n_0(e_{\mathrm{fib}})\sigma_0|u|_+, \end{cases} \tag{1.3}$$

where $u(t)$ is an electrical activation function that represents intracellular calcium concentration levels and induces contraction (when $u > 0$) or relaxation. The maximum value of u was taken as 35 s^{-1} [36] and the minimum negative value within the range of -100 to -20 s^{-1} (depending on the rate of ventricular pressure decay in early relaxation).

The function $n_0(e_{\text{fib}}) \in [0,1]$ is the fraction of recruited myosin heads at a given sarcomere extension e_{fib} representing the Frank-Starling law [20]. The parameter α is a bridge destruction rate upon rapid change in length in the sarcomere [20]. The parameter σ_0 is the asymptotic active stress developed by the sarcomere during systole at a given inotropic level and under optimal fiber extension (when Frank-Starling function $n_0 = 1$). This parameter is referred in this work as the myocardial contractility.

The elastic component of the myocardium is modeled by the passive constitutive law inspired from [37] (see also detailed analysis in [38]) in the form of the exponential hyperelastic potential

$$W_e = C_0 e^{C_1(J_1-3)^2} + C_2 e^{C_3(J_4-1)^2}, \tag{1.4}$$

with material constants C_i, $i \in \{0,1,2,3\}$, representing the myocardial passive properties. They account for the behavior of ventricle when a given preload (internal pressure) is imposed – the so-called end-diastolic pressure-volume relationship (EDPVR). The reduced invariants of the right Cauchy-Green strain tensor $\underline{\underline{C}}$ are given by $J_1 = I_1 I_3^{-\frac{1}{3}}$ and $J_4 = I_4 I_3^{-\frac{1}{3}}$, where $I_1 = \text{tr}(\underline{\underline{C}})$, $I_3 = \det(\underline{\underline{C}})$, $I_4 = \tau_1 \cdot \underline{\underline{C}} \cdot \tau_1$ (with τ_1 being the unit vector in myocardial fiber direction). The overall dynamics is described by a Lagrangian formulation, where the aforementioned Cauchy-Green deformation tensor $\underline{\underline{C}}$ and Green-Lagrange strain tensor $\underline{\underline{e}}$ are defined by

$$\underline{\underline{C}} = \underline{\underline{F}}^T \cdot \underline{\underline{F}}, \qquad \underline{\underline{e}} = \frac{1}{2}(\underline{\underline{C}} - \underline{\underline{I}}), \tag{1.5}$$

where $\underline{\underline{F}} = \underline{\underline{I}} + \nabla \underline{y}$ is the deformation gradient with $\underline{y}$ being the displacement with respect to the stress-free reference configuration ($\underline{\underline{I}}$ stands for the identity tensor).

The viscous pseudo-potential is given by

$$W_v = \frac{\eta}{2}\text{tr}(\dot{\underline{\underline{e}}}^2), \tag{1.6}$$

where η is a viscous damping parameter.

The ventricle is connected with the circulation by coupling the pressures in the atrium, ventricle and outflow artery (P_{at}, P_{V} and P_{ar}) with the ventricular volume change $\dot{V}$ (by inflow or outflow of blood). The inflow via the tricuspid valve (TV) and outflow via the right ventricular outflow tract (RVOT) are controlled by diodes [24], which allow forward as well as pathological regurgitant backward flows (we recall Figure 1.2). These valve components allow to model pathological stenosis by increasing the resistance to forward flow $R^{\text{TV}}_{\text{for}}$ or $R^{\text{RVOT}}_{\text{for}}$ for TV or RVOT, respectively (which have minimal resistance under physiological conditions). Likewise, the regurgitation is modeled by decreasing the backward resistance $R^{\text{TV}}_{\text{back}}$ or $R^{\text{RVOT}}_{\text{back}}$ (for TV or RVOT, respectively), while very high resistances are used under physiological non-regurgitant regime (practically, zero back-conductance). The overall ventricular volume change $\dot{V}$ by inflow or outflow of blood is given by [24]:

$$\begin{cases} \dot{V} = \frac{(P_{\text{at}}-P_{\text{V}})}{R^{\text{TV}}_{\text{for}}} + \frac{(P_{\text{ar}}-P_{\text{V}})}{R^{\text{RVOT}}_{\text{back}}} & \text{, when} \quad P_{\text{v}} \leqslant P_{\text{at}} \qquad \text{(filling of ventricle)} \\ \dot{V} = \frac{(P_{\text{v}}-P_{\text{at}})}{R^{\text{TV}}_{\text{back}}} + \frac{(P_{\text{ar}}-P_{\text{v}})}{R^{\text{RVOT}}_{\text{back}}} & \text{, when} \quad P_{\text{at}} \leqslant P_{\text{v}} \leqslant P_{\text{ar}} \quad \text{(isovolumic contraction)} \\ \dot{V} = \frac{(P_{\text{ar}}-P_{\text{V}})}{R^{\text{RVOT}}_{\text{for}}} + \frac{(P_{\text{at}}-P_{\text{V}})}{R^{\text{TV}}_{\text{back}}} & \text{, when} \quad P_{\text{v}} \geqslant P_{\text{ar}} \qquad \text{(ejection).} \end{cases} \tag{1.7}$$

Finally, the peripheral circulation is represented by a two-stage Windkessel model [23] containing proximal resistance and capacitance R_{prox}, C_{prox} (representing the main and branch pulmonary arteries, with pressure P_{ar}), and distal resistance and capacitance R_{dist},

C_{dist} (representing the remaining pulmonary circulation, with pressure P_{dist} and terminal venous pressure P_{vs}), as depicted in Figure 2. The Windkessel system reads:

$$\begin{cases} C_{\text{prox}}\dot{P}_{\text{ar}} + (P_{\text{ar}} - P_{\text{dist}})/R_{\text{prox}} = Q \\ C_{\text{dist}}\dot{P}_{\text{dist}} + (P_{\text{dist}} - P_{\text{ar}})/R_{\text{prox}} = (P_{\text{vs}} - P_{\text{d}})/R_{\text{dist}}. \end{cases} \tag{1.8}$$

Model calibration

This section describes the model calibration procedure.

I Model calibration prior to pulmonary valve replacement

1 The pulmonary Windkessel model was adjusted independently of the heart model. The forward flow was imposed from the measured data into the two-stage Windkessel system, and proximal and distal resistance and capacitance elements were adjusted to match the arterial pressure waveform in the data.

2 The geometrical parameters for the heart model were obtained from the end-diastolic time frame of the short axis cine magnetic resonance image (end-diastolic volume and the right ventricular myocardial mass). The volume at reference configuration (V_{ref}), when zero intraventricular pressure is assumed, was prescribed using the phenomenological relation obtained experimentally in [25]. The volume V_{ref} (in ml) is given by

$$V_{\text{ref}} = EDV(0.6 - 0.006EDP),$$

with EDV being the measured end-diastolic volume in (ml) and EDP the measured end-diastolic ventricular pressure (in mmHg). The right ventricular (RV) mass was considered as the mass of the RV free wall increased by half of the interventricular septum. In the simplified geometry of the model, the measured RV mass directly provided the myocardial wall thickness at reference configuration of the model (d_0).

3 To calibrate the passive properties of myocardium (given by hyperelastic potential Eq. (1.4)), we followed [19] and used coefficients $C_0 = 665$ Pa, $C_1 = 2.4$ Pa, $C_2 = 103$ Pa and $C_3 = 5.5$ Pa (which were obtained to fit the experimentally measured end-diastolic pressure-volume relationship to a reference healthy human data). The passive potential Eq.(1.4) was then multiplied by a "stiffness multiplication factor" aiming for the simulated end-diastolic volume to match the measurement, once the measured end-diastolic pressure (preload) was imposed.

4 To calibrate the resistances $R_{\text{for}}^{\text{RVOT}}$ and $R_{\text{back}}^{\text{RVOT}}$, the pulmonary Windkessel model was connected to the heart model. The forward resistance $R_{\text{for}}^{\text{RVOT}}$ was adjusted to match the measured difference between RV and pulmonary artery (PA) end-systolic pressures. The initial guess (pre-calibration) of the value of $R_{\text{for}}^{\text{RVOT}}$ was made by taking

$$R_{\text{for}}^{\text{RVOT}} = (\bar{P}_{\text{V}} - \bar{P}_{\text{ar}})/Q_{\text{for}},$$

with $\bar{P}_{\text{V}}$ being the average RV pressure during systole, $\bar{P}_{\text{ar}}$ the average PA pressure during systole and Q_{for} the forward flow in PA. The backward resistance was adjusted to match the backward flow waveform in the data (decreased $R_{\text{back}}^{\text{RVOT}}$ value, if pulmonary regurgitation was present). After introducing the backflow into the system, the distal Windkessel parameters (R_{dist} and C_{dist}) were readjusted so that the simulated pressure decay matched the acquired pulmonary pressure waveform.

5 The backward resistance of the tricuspid valve $R_{\text{back}}^{\text{TV}}$ was adjusted in the patients with tricuspid regurgiation to match the level of regurgitation volume to the measurement [39].

6 The profile of the electrical activation function u in Eq. (1.3) was calibrated based on QRS and ST durations measured from the ECG.

7 The parameter of active contractility σ_0 in Eq. (1.3) was adjusted to match RV stroke volume and end-systolic pressure.

II Model calibration after pulmonary valve replacement

The datasets after pulmonary valve replacement (post-PVR) were limited to pressure waveforms of right-heart catheterization. In the absence of any post-PVR flow data, we assumed that non-significant pulmonary regurgitation was present after the intervention and excluded the possibility for the backflow by increasing the backward resistance $R_{\text{back}}^{\text{RVOT}}$. In addition, we assumed that the passive stiffness properties and reference volume (V_{ref}) did not change immediately after PVR.

The ventricular preload was prescribed according to the RV pressure measurement post-PVR. The forward resistance of the $R_{\text{for}}^{\text{RVOT}}$ was decreased to match the pressure gradient between RV and PA (which decreased due to elimination of RVOT obstruction) and the distal Windkessel parameters were modified to match the pressure decay of the post-PVR PA pressure waveform. Finally, the contractility σ_0 was adjusted to match the peak of RV end-systolic pressure.

Supplementary Table 1.5 provides model parameters in each patient-specific models. Figures 3 (main body of article) and Supplementary Figures 1.8-1.10 display RV pre- and post-PVR calibrations for selected patients.

Automatization of the model setup, would allow the performance of a sensitivity analysis [40] and is a necessary step to translate the present proof-of-concept work into clinical practice.

Model-derived relative stiffness

Supplementary Table 1.5 last column shows patient-specific tissue stiffness. The median stiffness in our cohort was 1.67 and in the healthy population [17] 1.10. The model-estimated tissue stiffness seem to reveal a stiffening of the right ventricular myocardium by around 50% above normal in the studied cohort. We remark that these results are preliminary due to the uncertainty in the estimation of reference volume in the right ventricle. Detailed study of passive tissue stiffness is out of scope of this work.

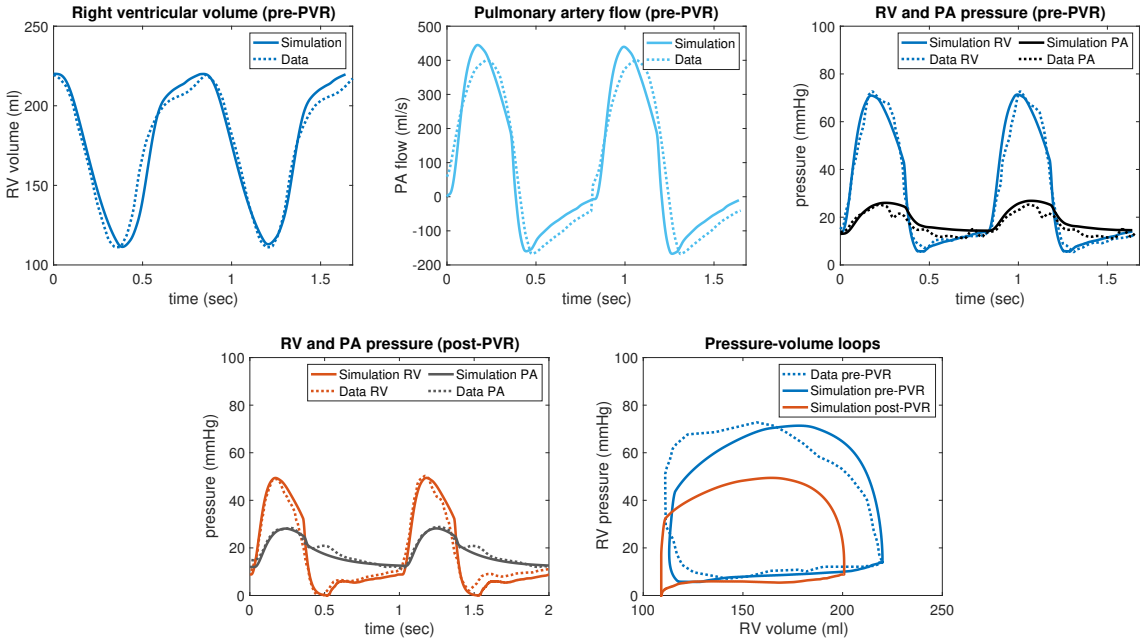

Figure 1.8: Measured data (dashed line) and simulation (solid line) for Patient #3.

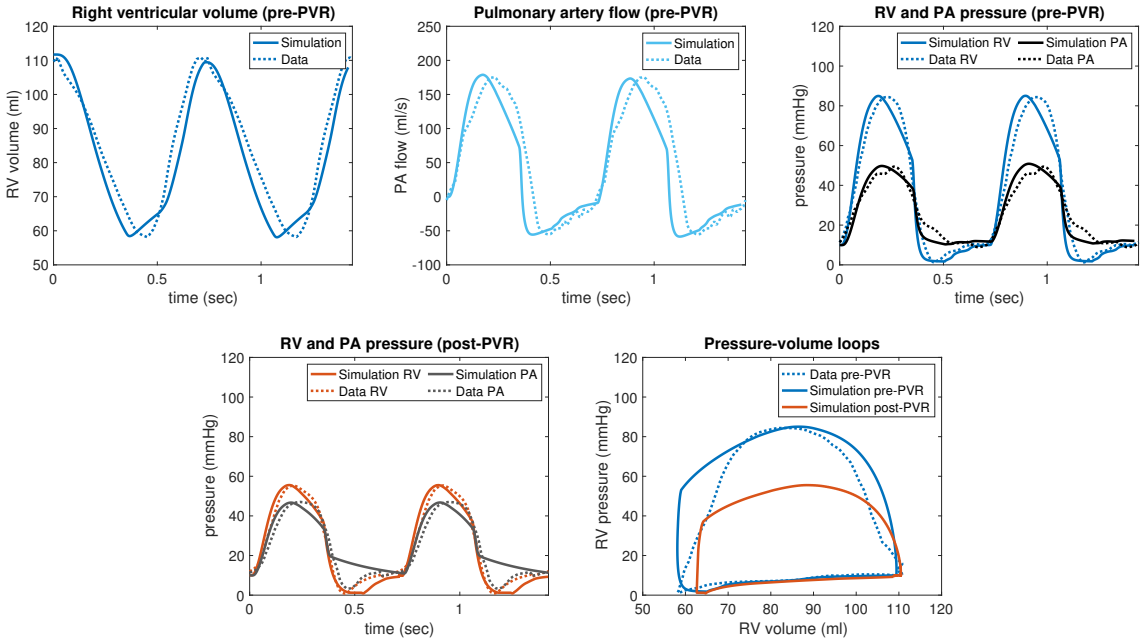

Figure 1.9: Measured data (dashed line) and simulation (solid line) for Patient #8.

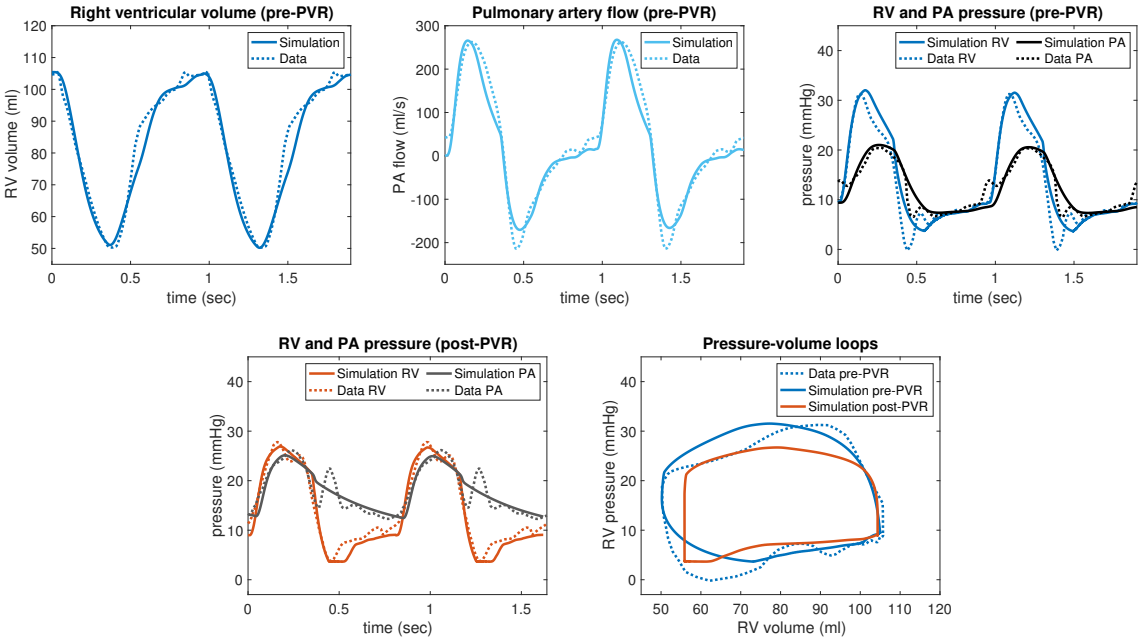

Figure 1.10: Measured data (dashed line) and simulation (solid line) for Patient #9.

				pre-PVR												post-PVR				
Patient #	age year	sex	BSA m^2	QRSd ms	HR beats/min	RV FW mass g	Septum mass g	RV iEDV ml/m^2	RV iESV ml/m^2	RV EF %	PR %	TR %	LV ESP mmHg	RV ESP mmHg	PA ESP mmHg	QRSd ms	HR beats/min	RV ESP mmHg	PA ESP mmHg	Group
1	12	F	1.21	0.165	61	70	26	136	83	39	47	-	-	103	45	0.147	58	75	50	C
2	8	M	0.86	0.137	63	40	16	120	60	50	36	-	85	58	28	0.098	67	43	26	C
3	13	M	1.4	0.166	72	85	41	157	79	50	39	-	90	73	25	0.147	59	49	29	C
4	11	F	0.97	0.158	64	44	18	122	63	48	58	-	77	31	23	0.12	79	28	24	A
5	9	F	0.99	0.137	85	70	20	144	95	34	29	-	91	84	49	0.098	86	55	51	B
6	11	F	1.34	0.086	70	70	25	107	40	63	29	-	101	73	28	0.09	71	51	24	B
7	8	M	0.87	0.126	81	33	12	113	40	65	46	10	69	42	24	0.126	68	39	25	A
8	8	F	0.99	0.159	85	70	18	112	60	47	30	11	89	84	49	0.156	84	56	47	B
9	11	F	0.97	0.16	64	35	18	109	52	53	59	-	76	31	20	0.145	75	28	26	A
10	11	F	1.34	0.089	74	66	19	99	32	68	29	-	105	42	24	0.093	67	46	26	A
11	17	M	2.23	0.165	61	69	28	73	29	61	0	18	87	47	21	0.151	61	49	24	B
12	6	M	0.84	0.129	87	25	15	152	85	44	47	-	99	40	26	0.129	91	35	26	A
13	8	M	1.18	0.117	87	31	13	97	49	49	46	-	-	32	25	0.115	86	32	25	A
14	16	F	2.02	0.133	59	47	26	144	73	49	49	-	96	32	25	0.104	58	21	21	A
15	26	F	1.69	0.147	67	47	19	79	38	51	35	10	93	32	24	0.133	68	29	24	A
16	17	F	1.64	0.163	75	55	23	66	29	56	21	-	88	58	21	0.164	74	32	23	B
17	15	M	1.52	0.129	74	40	28	84	30	64	24	-	76	65	22	0.11	79	41	22	B
18	11	F	1.17	0.096	95	37	27	124	68	45	47	-	78	31	20	0.101	88	28	20	A
19	13	F	1.29	0.146	79	33	29	82	43	48	29	-	86	62	30	0.135	76	35	29	B
20	19	F	2.1	0.129	75	84	42	125	53	58	29	-	85	67	41	0.12	50	55	53	B
Healthy	12		1.2	0.11	73	25	14	100	47	54	-	-	100	18-25	18-25	-	-	-	-	-

Table 1.3: Demographics and patients' characteristics derived from measured data prior to and after pulmonary valve replacement (pre-PVR and post-PVR, respectively). HR: heart rate; LV, RV and PA ESP: LV, RV and pulmonary artery end-systolic pressures; PR: pulmonary valve regurgitation fraction; QRSd: duration of QRS complex measured in ECG; RVFW mass: right ventricular free wall mass; RV EDVi and ESVi: RV end-diastolic and end-systolic volumes indexed to body surface area (BSA); RV EF: RV ejection fraction; TR: tricuspid valve regurgitation fraction.

Patient number	Anatomical complicating features	Palliation	Type of repair	Age of repair (years)	Re-intervention/ re-surgery	Type of prosthesis
1	Pulmonary atresia	BT shunt	Conduit	0.42	RPA angioplasty at 2 years	Melody PB10 20mm pulmonary valve at 12 years
2	Pulmonary atresia	–	Conduit	0.02	RPA angioplasty and conduit change at 6 months	Melody PB10 20mm pulmonary valve at 8 years
3	Pulmonary atresia	–	Conduit	0.04	–	Melody PB10 20mm pulmonary valve at 13 years
4	–	BT shunt	Transannular patch	0.75	–	Edwards Sapien 29mm XT valve at 11 years
5	DORV	BT shunt	Conduit	1.17	–	Melody PB10 20mm pulmonary valve at 9 years
6	–	–	Transannular patch	0.33	–	Edwards Sapien 26mm pulmonary valve at 11 years
7	Absent pulmonary valve		Conduit	0.02	Conduit replaced at 3 years	Edwards Sapien 23mm XT valve at 8 years
8	Pulmonary atresia	BT shunt	Conduit	1.17	Conduit replaced at 3 years	Melody PB10 20mm pulmonary valve at 8 years
9	–	–	Transannular patch	0.75	–	Edwards Sapien 29mm XT valve at 11 years
10	–	–	Transannular patch	0.33	–	Edwards Sapien 26mm pulmonary valve at 11 years
11	–	–	Conduit	0.83	Conduit replace at 3 years Bioprosthesis (8 years)	Melody PB10 20mm pulmonary valve valve at 17 years
12	–	–	Transannular patch	0.33	–	Edwards Sapien 23mm XT valve at 6 years
13	Pulmonary atresia	–	Conduit	0.02	–	Edwards Sapien 23mm XT valve at 8 years
14	–	–	Transannular patch	0.58	–	Edwards Sapien 23mm XT valve at 16 years
15	–	–	Conduit	0.58	Conduit revision at 12 years	Edwards Sapien 23mm XT valve at 26 years
16	Pulmonary atresia	–	Conduit	0.02	–	Melody 22mm pulmonary valve at 17 years
17	Pulmonary atresia	BT shunt	Conduit	0.75	–	Melody PB10 20mm pulmonary valve at 15 years
18	Pulmonary atresia	–	Conduit	0.02	–	Melody PB10 20mm pulmonary valve at 11 years
19	–	BT shunt	Conduit	0.17	Conduit replaced at 1 year and at 7 years	Melody PB10 20mm pulmonary valve at 13 years
20	–	–	Transannular patch	0.42		Melody 22mm pulmonary valve at 19 years

Table 1.4: Clinical details about patients included in the study. BT shunt, Blalock-Taussig shunt; DORV, double outlet right ventricle; RPA, right pulmonary artery.

Patient	$R_{\text{for}}^{\text{RVOT}}$		$R_{\text{back}}^{\text{RVOT}}$	Contractility		Relative tissue stiffness
#	pre-PVR ($\times 10^6 \frac{\text{Pa·s}}{\text{m}^3}$)	post-PVR ($\times 10^6 \frac{\text{Pa·s}}{\text{m}^3}$)	pre-PVR ($\times 10^6 \frac{\text{Pa·s}}{\text{m}^3}$)	pre-PVR (kPa)	post-PVR (kPa)	pre-/post-PVR
1	43.0	18.1	35.0	93	70	1.72
2	22.0	11.4	30.3	62	52	1.63
3	14.0	7.7	9.2	75	53	1.74
4	7.1	4.3	10.0	36	34	1.56
5	27.0	3.8	50.0	73	48	1.58
6	18.0	11.5	18.2	72	60	1.68
7	11.0	11.0	7.7	60	55	1.58
8	27.0	7.8	25.0	70	43	1.49
9	6.9	1.5	5.0	47	42	1.65
10	6.3	6.3	18.0	58	58	1.78
11	11.0	11.0	$2 \cdot 10^5$	56	56	1.53
12	8.1	7.7	8.3	77	63	1.95
13	3.8	3.8	3.3	50	49	1.72
14	2.3	0.1	5.7	73	46	2.50
15	5.0	4.0	14.3	40	33	1.75
16	22.0	5.5	15.4	55	35	1.67
17	18.0	7.9	22.2	88	56	1.63
18	5.3	5.0	7.7	47	40	1.50
19	22.0	3.7	30.3	70	41	1.66
20	7.7	0.8	14.3	83	68	1.78
Healthy	0.1	-	$2 \cdot 10^5$	38-48	–	1.10

Table 1.5: Main patient-specific parameters of the model and their changes after pulmonary valve replacement (PVR).

Bibliography

[1] H. W. Vliegen, A. van Straten, A. de Roos, A. A. Roest, P. H. Schoof, A. H. Zwinderman, J. Ottenkamp, E. E. van der Wall, and M. G. Hazekamp, "Magnetic resonance imaging to assess the hemodynamic effects of pulmonary valve replacement in adults late after repair of tetralogy of Fallot," *Circulation*, vol. 106, no. 13, pp. 1703–1707, 2002.

[2] M. A. Quail, A. Frigiola, A. Giardini, V. Muthurangu, M. Hughes, P. Lurz, S. Khambadkone, J. E. Deanfield, V. Tsang, and A. M. Taylor, "Impact of pulmonary valve replacement in tetralogy of Fallot with pulmonary regurgitation: a comparison of intervention and nonintervention," *The Annals of thoracic surgery*, vol. 94, no. 5, pp. 1619–1626, 2012.

[3] J. P. Bokma, M. M. Winter, T. Oosterhof, H. W. Vliegen, A. P. van Dijk, M. G. Hazekamp, D. R. Koolbergen, M. Groenink, B. J. Mulder, and B. J. Bouma, "Preoperative thresholds for mid-to-late haemodynamic and clinical outcomes after pulmonary valve replacement in tetralogy of Fallot," *European heart journal*, vol. 37, no. 10, pp. 829–835, 2016.

[4] H. H. Dave, E. R. V. Buechel, A. Dodge-Khatami, A. Kadner, V. Rousson, U. Bauersfeld, and R. Prêtre, "Early insertion of a pulmonary valve for chronic regurgitation helps restoration of ventricular dimensions," *The Annals of thoracic surgery*, vol. 80, no. 5, pp. 1615–1621, 2005.

[5] A. Frigiola, M. Hughes, M. Turner, A. Taylor, J. Marek, A. Giardini, T.-Y. Hsia, and K. Bull, "Physiological and phenotypic characteristics of late survivors of tetralogy of Fallot repair who are free from pulmonary valve replacement," *Circulation*, vol. 128, no. 17, pp. 1861–1868, 2013.

[6] J. S. Tweddell, P. Simpson, S.-H. Li, J. Dunham-Ingle, P. J. Bartz, M. G. Earing, and A. N. Pelech, "Timing and technique of pulmonary valve replacement in the patient with tetralogy of Fallot," in *Seminars in Thoracic and Cardiovascular Surgery: Pediatric Cardiac Surgery Annual*, vol. 15, pp. 27–33, Elsevier, 2012.

[7] J. Therrien, Y. Provost, N. Merchant, W. Williams, J. Colman, and G. Webb, "Optimal timing for pulmonary valve replacement in adults after tetralogy of Fallot repair," *The American journal of cardiology*, vol. 95, no. 6, pp. 779–782, 2005.

[8] T. Geva, "Repaired tetralogy of Fallot: the roles of cardiovascular magnetic resonance in evaluating pathophysiology and for pulmonary valve replacement decision support," *Journal of Cardiovascular Magnetic Resonance*, vol. 13, no. 1, pp. 1–24, 2011.

[9] A. M. Valente, K. Gauvreau, G. E. Assenza, S. V. Babu-Narayan, J. Schreier, M. A. Gatzoulis, M. Groenink, R. Inuzuka, P. J. Kilner, Z. Koyak, *et al.*, "Contemporary predictors of death and sustained ventricular tachycardia in patients with repaired tetralogy of Fallot enrolled in the INDICATOR cohort," *Heart*, vol. 100, no. 3, pp. 247–253, 2014.

[10] V. Wang, P. Nielsen, and M. Nash, "Image-based predictive modeling of heart mechanics," *Annual review of biomedical engineering*, vol. 17, pp. 351–383, 2015.

[11] R. Chabiniok, V. Y. Wang, M. Hadjicharalambous, L. Asner, J. Lee, M. Sermesant, E. Kuhl, A. A. Young, P. Moireau, M. P. Nash, *et al.*, "Multiphysics and multiscale modelling, data–model fusion and integration of organ physiology in the clinic: ventricular cardiac mechanics," *Interface focus*, vol. 6, no. 2, p. 20150083, 2016.

[12] L. Asner, M. Hadjicharalambous, R. Chabiniok, D. Peresutti, E. Sammut, J. Wong, G. Carr-White, P. Chowienczyk, J. Lee, A. King, *et al.*, "Estimation of passive and active properties in the human heart using 3D tagged MRI," *Biomechanics and modeling in mechanobiology*, vol. 15, no. 5, pp. 1121–1139, 2016.

[13] R. Chabiniok, P. Moireau, P.-F. Lesault, A. Rahmouni, J.-F. Deux, and D. Chapelle, "Estimation of tissue contractility from cardiac cine-MRI using a biomechanical heart model," *Biomechanics and modeling in mechanobiology*, vol. 11, no. 5, pp. 609–630, 2012.

[14] B. Ruijsink, K. Zugaj, J. Wong, K. Pushparajah, T. Hussain, P. Moireau, R. Razavi, D. Chapelle, and R. Chabiniok, "Dobutamine stress testing in patients with Fontan circulation augmented by biomechanical modeling," *PloS one*, vol. 15, no. 2, p. e0229015, 2020.

[15] M. Genet, C. T. Stoeck, C. Von Deuster, L. C. Lee, and S. Kozerke, "Equilibrated warping: Finite element image registration with finite strain equilibrium gap regularization," *Medical image analysis*, vol. 50, pp. 1–22, 2018.

[16] D. A. Castellanos, K. Škardová, A. Bhattaru, E. Berberoglu, G. Greil, A. Tandon, J. Dillenbeck, B. Burkhardt, T. Hussain, M. Genet, *et al.*, "Left ventricular torsion obtained using equilibrated warping in patients with repaired Tetralogy of Fallot," *Pediatric Cardiology*, pp. 1–9, 2021.

[17] N. Kawel-Boehm, A. Maceira, E. R. Valsangiacomo-Buechel, J. Vogel-Claussen, E. B. Turkbey, R. Williams, S. Plein, M. Tee, J. Eng, and D. A. Bluemke, "Normal values for cardiovascular magnetic resonance in adults and children," *Journal of Cardiovascular Magnetic Resonance*, vol. 17, no. 1, pp. 1–33, 2015.

[18] M. Caruel, R. Chabiniok, P. Moireau, Y. Lecarpentier, and D. Chapelle, "Dimensional reductions of a cardiac model for effective validation and calibration," *Biomechanics and modeling in mechanobiology*, vol. 13, no. 4, pp. 897–914, 2014.

[19] A. Le Gall, F. Vallée, K. Pushparajah, T. Hussain, A. Mebazaa, D. Chapelle, É. Gayat, and R. Chabiniok, "Monitoring of cardiovascular physiology augmented by a patient-specific biomechanical model during general anesthesia. A proof of concept study," *PloS one*, vol. 15, no. 5, p. e0232830, 2020.

[20] D. Chapelle, P. Le Tallec, P. Moireau, and M. Sorine, "Energy-preserving muscle tissue model: formulation and compatible discretizations," *International Journal for Multiscale Computational Engineering*, vol. 10, no. 2, 2012.

[21] A. F. Huxley, "Muscle structure and theories of contraction," *Prog. Biophys. Biophys. Chem*, vol. 7, pp. 255–318, 1957.

[22] F. Kimmig, D. Chapelle, and P. Moireau, "Thermodynamic properties of muscle contraction models and associated discrete-time principles," *Advanced Modeling and Simulation in Engineering Sciences*, vol. 6, no. 1, pp. 1–36, 2019.

[23] N. Stergiopulos, B. E. Westerhof, and N. Westerhof, "Total arterial inertance as the fourth element of the windkessel model," *American Journal of Physiology-Heart and Circulatory Physiology*, vol. 276, no. 1, pp. H81–H88, 1999.

[24] J. Sainte-Marie, D. Chapelle, R. Cimrman, and M. Sorine, "Modeling and estimation of the cardiac electromechanical activity," *Computers & structures*, vol. 84, no. 28, pp. 1743–1759, 2006.

[25] S. Klotz, I. Hay, M. L. Dickstein, G.-H. Yi, J. Wang, M. S. Maurer, D. A. Kass, and D. Burkhoff, "Single-beat estimation of end-diastolic pressure-volume relationship: a novel method with potential for noninvasive application," *American Journal of Physiology-Heart and Circulatory Physiology*, vol. 291, no. 1, pp. H403–H412, 2006.

[26] R. Chabiniok, P. Moireau, C. Kiesewetter, T. Hussain, R. Razavi, and D. Chapelle, "Assessment of atrioventricular valve regurgitation using biomechanical cardiac modeling," in *International Conference on Functional Imaging and Modeling of the Heart*, pp. 401–411, Springer, 2017.

[27] P. Lurz, J. Nordmeyer, V. Muthurangu, S. Khambadkone, G. Derrick, R. Yates, M. Sury, P. Bonhoeffer, and A. M. Taylor, "Comparison of bare metal stenting and percutaneous pulmonary valve implantation for treatment of right ventricular outflow tract obstruction: use of an x-ray/magnetic resonance hybrid laboratory for acute physiological assessment," *Circulation*, vol. 119, no. 23, pp. 2995–3001, 2009.

[28] H. Švihlová, J. Hron, J. Málek, K. Rajagopal, and K. Rajagopal, "Determination of pressure data from velocity data with a view toward its application in cardiovascular mechanics. part 1. theoretical considerations," *International Journal of Engineering Science*, vol. 105, pp. 108–127, 2016.

[29] S. F. Nagueh, C. P. Appleton, T. C. Gillebert, P. N. Marino, J. K. Oh, O. A. Smiseth, A. D. Waggoner, F. A. Flachskampf, P. A. Pellikka, and A. Evangelisa, "Recommendations for the evaluation of left ventricular diastolic function by echocardiography," *European Journal of Echocardiography*, vol. 10, no. 2, pp. 165–193, 2009.

[30] J. Janoušek, J. Kovanda, M. Ložek, V. Tomek, P. Vojtovič, R. Gebauer, P. Kubuš, M. Krejčíř, J. Lumens, T. Delhaas, *et al.*, "Pulmonary right ventricular resynchronization in congenital heart disease: acute improvement in right ventricular mechanics and contraction efficiency," *Circulation: Cardiovascular Imaging*, vol. 10, no. 9, p. e006424, 2017.

[31] M. Genet, L. C. Lee, B. Baillargeon, J. M. Guccione, and E. Kuhl, "Modeling pathologies of diastolic and systolic heart failure," *Annals of biomedical engineering*, vol. 44, no. 1, pp. 112–127, 2016.

[32] S. Göktepe, O. J. Abilez, and E. Kuhl, "A generic approach towards finite growth with examples of athlete's heart, cardiac dilation, and cardiac wall thickening," *Journal of the Mechanics and Physics of Solids*, vol. 58, no. 10, pp. 1661–1680, 2010.

[33] L. C. Lee, M. Genet, G. Acevedo-Bolton, K. Ordovas, J. M. Guccione, and E. Kuhl, "A computational model that predicts reverse growth in response to mechanical unloading," *Biomechanics and modeling in mechanobiology*, vol. 14, no. 2, pp. 217–229, 2015.

[34] F. Regazzoni, D. Chapelle, and P. Moireau, "Combining data assimilation and machine learning to build data-driven models for unknown long time dynamics—applications in cardiovascular modeling," *International Journal for Numerical Methods in Biomedical Engineering*, p. e3471, 2021.

[35] A. V. Hill, "The heat of shortening and the dynamic constants of muscle," *Proceedings of the Royal Society of London. Series B-Biological Sciences*, vol. 126, no. 843, pp. 136–195, 1938.

[36] M. Caremani, F. Pinzauti, M. Reconditi, G. Piazzesi, G. J. Stienen, V. Lombardi, and M. Linari, "Size and speed of the working stroke of cardiac myosin in situ," *Proceedings of the National Academy of Sciences*, vol. 113, no. 13, pp. 3675–3680, 2016.

[37] G. A. Holzapfel and R. W. Ogden, "Constitutive modelling of passive myocardium: a structurally based framework for material characterization," *Philosophical Transactions of the Royal Society A: Mathematical, Physical and Engineering Sciences*, vol. 367, no. 1902, pp. 3445–3475, 2009.

[38] M. Hadjicharalambous, R. Chabiniok, L. Asner, E. Sammut, J. Wong, G. Carr-White, J. Lee, R. Razavi, N. Smith, and D. Nordsletten, "Analysis of passive cardiac constitutive laws for parameter estimation using 3D tagged MRI," *Biomechanics and modeling in mechanobiology*, vol. 14, no. 4, pp. 807–828, 2015.

[39] R. Chabiniok, P. Moireau, C. Kiesewetter, M. T. Hussain, R. Razavi, and D. Chapelle, "Assessment of atrioventricular valve regurgitation using biomechanical cardiac modeling," *Functional Imaging and Modelling of the Heart - 9th International Conference, FIMH 2017, Proceedings: (LCNS)*, pp. 401–411, May 2017.

[40] L. Marx, M. A. Gsell, A. Rund, F. Caforio, A. J. Prassl, G. Toth-Gayor, T. Kuehne, C. M. Augustin, and G. Plank, "Personalization of electro-mechanical models of the pressure-overloaded left ventricle: fitting of windkessel-type afterload models," *Philosophical Transactions of the Royal Society A*, vol. 378, no. 2173, p. 20190342, 2020.

CHAPTER 2

Biomechanical modeling to evaluate the evolution of myocardial mechanical properties under different loading conditions

The purpose of this chapter was to explore the ability of the biomechanical model to predict the response of ventricular mechanics to the progressive decrease of the afterload in rTOF RVs that are predominantly affected by RVOTO. Patient-specific models pre-PVR created in chapter 1 were used, cessation of PV regurgitation and progressively decreasing RVOT resistance were assumed. Myocardial contractility was re-calibrated for the corresponding decrease in RVOT resistance. *In silico* relationships between the contractility and RVOT resistance post-PVR were built. The predictive value of these relationships was tested against the post-PVR models created from the actual post-PVR datasets in chapter 1. The resulting *in silico* relationships between contractility and RVOT resistance showed a linear form. *In silico* predicted contractility was in correspondence with post-PVR model-derived contractility. The chapter demonstrates that these relationships have the potential to inform clinicians about the hypothetical mechanical response of the ventricle based on the degree of pre-operative RVOTO.

Contents

Prediction of Ventricular Mechanics After Pulmonary Valve Replacement in Tetralogy of Fallot by Biomechanical Modeling: A Step Towards Precision Healthcare

Maria Gusseva[1,2], Tarique Hussain[3], Camille Hancock Friesen,[4], Gerald Greil[3], Dominique Chapelle[1,2], Radomír Chabiniok[1,2,3,5]

[1]Inria, Palaiseau, France
[2]LMS, Ecole Polytechnique, CNRS, Institut Polytechnique de Paris, Palaiseau, France
[3]Division of Pediatric Cardiology, Department of Pediatrics, UT Southwestern Medical Center, Dallas, TX
[4]Division of Pediatric Cardiothoracic Surgery, Department of Pediatrics, UT Southwestern Medical Center, Dallas, Texas, USA
[5]Department of Mathematics, Faculty of Nuclear Sciences and Physical Engineering, Czech Technical University in Prague, Prague, Czech Republic

Annals of Biomedical Engineering 49: 3339–3348 (2021)

Abstract

Clinical indicators of heart function are often limited in their ability to accurately evaluate the current mechanical state of the myocardium. Biomechanical modeling has been shown to be a promising tool in addition to clinical indicators. By providing a patient-specific measure of myocardial active stress (contractility), biomechanical modeling can enhance the precision of the description of patient's pathophysiology at any given point in time. In this work we aim to explore the ability of biomechanical modeling to predict the response of ventricular mechanics to the progressively decreasing afterload in repaired tetralogy of Fallot (rTOF) patients undergoing pulmonary valve replacement (PVR) for significant residual right ventricular outflow tract obstruction (RVOTO). We used 19 patient-specific models of patients with rTOF prior to pulmonary valve replacement (PVR), denoted as PSM_{pre}, and patient-specific models of the same patients created post-PVR (PSM_{post})—both created in our previous published work. Using the PSMpre and assuming cessation of the pulmonary regurgitation and a progressive decrease of RVOT resistance, we built relationships between the contractility and RVOT resistance post-PVR. The predictive value of such *in silico* obtained relationships were tested against the PSM_{post}, i.e. the models created from the actual post-PVR datasets. Our results show a linear 1-dimensional relationship between the *in silico* predicted contractility post-PVR and the RVOT resistance. The predicted contractility was close to the contractility in the PSM_{post} model with a mean ($\pm$ SD) difference of 6.5 ($\pm$ 3.0)%. The relationships between the contractility predicted by *in silico* PVR vs. RVOT resistance have a potential to inform clinicians about hypothetical mechanical response of the ventricle based on the degree of pre-operative RVOTO.

Keywords— myocardial contractility, ventricular overload, valvular heart disease, biomechanical modeling, valve replacement

2.1 Introduction

After initial repair of tetralogy of Fallot (TOF) pulmonary regurgitation (PR) and/or residual right ventricular outflow tract obstruction (RVOTO) detrimentally affect ventricular mechanical properties in the long-term. A chronic right ventricular (RV) volume and/or pressure overload leads to RV dilatation and/or hypertrophy. At the extent of the myocardial ability to compensate, the RV remodeling become pathologic and RV systolic and/or diastolic function may deteriorate. To avoid decompensated RV remodeling or to allow the RV to reverse-remodel back to normal size, patients undergo a pulmonary valve replacement (PVR). Timing of PVR is critical. PVR is ideally performed as late as possible because of the limited lifespan of an implanted valve [1], but before the myocardium undergoes significant irreversible changes. The ability to most accurately evaluate the current mechanical state of the myocardium and subsequently predict optimal timing of PVR is a subject of ongoing research. The sensitivity and specificity of the current clinical guidelines for PVR are limited and in practice post-PVR RV reverse-remodeling occurs in only 60% of patients [2]. The level of PR, RV dilatation (end-diastolic volume typically indexed to body surface area), and RV ejection fraction are often considered as the main clinical indicators for PVR [3; 4]. A recent observational cohort study has demonstrated that greater RV hypertrophy and higher levels of RV systolic pressures are strongly associated with irreversible remodeling and/or sudden death in tetralogy of Fallot patients after surgical repair (rTOF) [5]. It is therefore important to understand both the independent and combined effect of RV dilation and hypertrophy triggering factors (PR and RVOTO, respectively) on the evolution of RV mechanics.

Biomechanical modeling has been shown to be a promising tool for modeling '*in silico*' (a new term that has been coined to contrast to '*in vivo*') myocardial function. The short-term models (capturing single or a few cardiac beats) have been shown to be useful in predicting short-term effects of Cardiac Resynchronization Therapy [6; 7; 8]. Biomechanical modeling has also been proposed to assess the effect of pulmonary vasodilatation therapy in Fontan patients with early-stage heart failure [9].

In our recently published retrospective study [10] we demonstrated the ability of a biomechanical model to provide information about the current mechanical state of the myocardium in late rTOF patients prior to and immediately after PVR, while using the clinical data obtained pre- and post-PVR. In the present work we would like to explore the ability of these patient-specific models created from the pre-PVR data (PSM_{pre}) to predict the response of ventricular mechanics to PVR. Specifically, we aim to build a relationship between the myocardial contractility predicted *in silico* using PSM_{pre}, while decreasing the RVOT resistance (and subsequently decreasing RV-to-PA pressure difference, in clinical medicine often incorrectly called the pressure gradient). This will simulate the reduction of RVOTO during PVR when the valve is implanted. The predictive capability of such an *in silico* PVR will be assessed by comparing the predicted RV contractility with the contractility in the patient-specific models post-PVR (PSM_{post}) as reported in our previous work [10], where PSM_{post} and the associated contractility values were obtained when using the catheterization data measured after the actual PVR.

2.2 Methods

2.2.1 Patient-specific biomechanical models pre- and post-PVR

The creation of PSM_{pre} and PSM_{post} of the studied cohort has been reported previously [10]. Here, we provide only a brief description. We used a biomechanical model of the RV

cavity with simplified geometry (spherical ventricle with inner radius R and wall thickness d). The model developed by Caruel et al. [11] has been previously employed in various clinical studies [12; 13]. The constitutive mechanical properties of the myocardium are preserved as in the full 3D heart model [14].

The overall tissue-level mechanical behavior of the myocardium is described by a rheological model of Hill-Maxwell type [15] that allows to represent an active contractile component (actin-myosin unit) and a viscoelastic component (collagen-rich elements). The active behavior of the myocardium is modeled within A.F.Huxley's sliding filament theory [16; 17]. The myosin filaments within a sarcomere unit are considered as an element that produces active stress (τ_c) and active stiffness (k_c) at certain sarcomere extension (e_{fib}) with the following system of differential equations [18; 14]:

$$\begin{cases} \dot{k}_c = -(|u| + \alpha|\dot{e}_{\text{fib}}|)k_c + n_0(e_{\text{fib}})k_0|u|_+ \\ \dot{\tau}_c = -(|u| + \alpha|\dot{e}_{\text{fib}}|)\tau_c + \dot{e}_{\text{fib}}k_c + n_0(e_{\text{fib}})\sigma_0|u|_+, \end{cases} \tag{2.1}$$

where $u(t)$ is an electrical activation function that is related to intracellular calcium kinetics and induces contraction (when $u > 0$) or relaxation (when $u < 0$) of the myocardium. The parameter α is a bridge destruction rate upon rapid change in length in the sarcomere [14].The function $n_0(e_{\text{fib}}) \in [0, 1]$ is the representation of the Frank–Starling law that gives the fraction of recruited myosin heads at a given sarcomere extension (e_{fib}) [14]. The parameters σ_0 and k_0 are the active stress and stiffness developed by the sarcomere during systole under optimal fiber extension (e_{fib}), when $n_0 = 1$, reflecting the inotropic state [13]. The parameter σ_0 will be further referred to as contractility. The elastic part of passive behavior of the myocardium is modeled by the constitutive law inspired by Holzapfel and Ogden [19; 20] in the form of the hyperelastic potential:

$$W_e = C_0 e^{C_1(J_1-3)^2} + C_2 e^{C_3(J_4-1)^2}, \tag{2.2}$$

where C_i, $i \in 0, 1, 2, 3$ are material constants that account for the passive behavior of the ventricle under imposed preload pressure. The calibration of C_i to the given end-diastolic pressure (EDP) and volume provides the patient-specific end-diastolic pressure volume relationship (EDPVR). The overall dynamics of the system are given by a Lagrangian formulation, where $\underline{\underline{e}}$ is Green–Lagrange strain tensor and $J_{1,4}$ are the reduced invariants of the right Cauchy-Green strain tensor ($\underline{\underline{C}}$), that accounts for transversely isotropic behavior of the myocardium (for details see Refs. [11; 14; 20]).

The viscous part of the passive behavior is given by viscous pseudo-potential:

$$W_v = \frac{\eta}{2}\text{tr}(\dot{\underline{\underline{e}}}^2), \tag{2.3}$$

where η is a viscous damping parameter.

The ventricular cavity model was coupled with inlet and outlet valves to control the inflow from the tricuspid valve (TV) and outflow through the right ventricular outflow tract (RVOT). Both TV and RVOT were represented by a system of diodes with forward and backward resistances that allowed simulation of the required forward and backward flows in the corresponding compartments (Fig. 2.1). Thus, by increasing the resistance to forward flow ($R_{\text{for}}^{\text{TV}}$ and $R_{\text{for}}^{\text{RVOT}}$ for TV and RVOT, respectively) we can simulate valvular stenosis of a given grade. Likewise, by decreasing the backward resistances ($R_{\text{back}}^{\text{TV}}$ and $R_{\text{back}}^{\text{RVOT}}$ for TV and RVOT, respectively) we can model valvular regurgitation. The pressures in the atrium, ventricle and pulmonary artery (P_{at}, P_{RV} and P_{PA}, respectively) are coupled with a ventricular volume change $\dot{V}$ (inflow or outflow of blood) as described by Sainte-Marie et al [21].

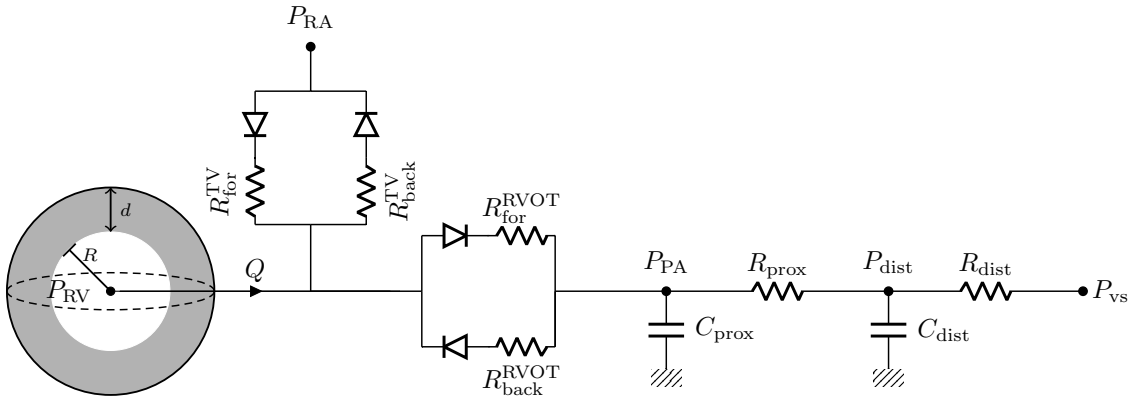

Figure 2.1: Reduced-order model of the right ventricle (RV) with inner radius R and wall thickness d: The ventricle is coupled to tricuspid valve (TV) and RV outflow tract (RVOT) via a system of diodes with forward and backward resistance ($R^{\mathrm{TV}}_{\mathrm{for}}$, $R^{\mathrm{TV}}_{\mathrm{back}}$ and $R^{\mathrm{RVOT}}_{\mathrm{for}}$, $R^{\mathrm{RVOT}}_{\mathrm{back}}$). The pulmonary circulation is represented by a Windkessel model with resistance and capacitance of proximal and distal arteries (R_{prox}, C_{prox}, and R_{dist}, C_{dist}, respectively). P_{RV} and P_{RA} are pressure in the RV and right atria, respectively. P_{PA} and P_{dist}, and P_{vs} are pressure in the proximal and distal pulmonary artery, and venous system, respectively.

$$\begin{cases} \dot{V} = \frac{(P_{\mathrm{at}}-P_{\mathrm{V}})}{R^{\mathrm{TV}}_{\mathrm{for}}} + \frac{(P_{\mathrm{ar}}-P_{\mathrm{V}})}{R^{\mathrm{RVOT}}_{\mathrm{back}}}, & \text{when} \quad P_{\mathrm{v}} \leqslant P_{\mathrm{at}} \\ \dot{V} = \frac{(P_{\mathrm{v}}-P_{\mathrm{at}})}{R^{\mathrm{TV}}_{\mathrm{back}}} + \frac{(P_{\mathrm{ar}}-P_{\mathrm{v}})}{R^{\mathrm{RVOT}}_{\mathrm{back}}}, & \text{when} \quad P_{\mathrm{at}} \leqslant P_{\mathrm{v}} \leqslant P_{\mathrm{ar}} \\ \dot{V} = \frac{(P_{\mathrm{ar}}-P_{\mathrm{V}})}{R^{\mathrm{RVOT}}_{\mathrm{for}}} + \frac{(P_{\mathrm{at}}-P_{\mathrm{V}})}{R^{\mathrm{TV}}_{\mathrm{back}}}, & \text{when} \quad P_{\mathrm{v}} \geqslant P_{\mathrm{ar}}. \end{cases} \tag{2.4}$$

The circulation system is represented by a two-stage Windkessel model [22], as is also depicted in Fig. 2.1.

In the present study, we will use $\mathrm{PSM}_{\mathrm{pre}}$ and $\mathrm{PSM}_{\mathrm{post}}$ of nineteen rTOF patients created in our previous work [10]. These models are given by the patient-specific parameters characterizing the circulation (proximal and distal resistance and capacitances R_{p}, R_{d}, C_{d}); the heart geometry and function (myocardial passive stiffness, active contractility), and RVOT mechanics (RVOT forward and backward resistances $R^{\mathrm{RVOT}}_{\mathrm{for}}$, $R^{\mathrm{RVOT}}_{\mathrm{back}}$). The detailed model calibrations are described in our previous work [10]. We remark that the ethical approvals in the study [10], in which the patient-specific models were created, were granted by the Institutional Review Boards of UT Southwestern Medical Center Dallas (STU-2020-0023) and UT Austin (IRB 2020-06-0128).

2.2.2 Post-PVR *in silico* prediction of contractility

The pre-PVR patient-specific models $\mathrm{PSM}_{\mathrm{pre}}$ were used to predict *in silico* the RV contractility after PVR. We assumed no PR after PVR (therefore we increased the backward RVOT resistance $R^{\mathrm{RVOT}}_{\mathrm{back}}$ to a large value). Sequentially, the RVOT resistance $R^{\mathrm{RVOT}}_{\mathrm{for}}$ was decreased to its minimum (representing no RVOTO assumed after PVR). For each value of $R^{\mathrm{RVOT}}_{\mathrm{for}}$ the ventricular contractility was recalibrated in the model to preserve pulmonary artery peak systolic pressure (PA PSP). This is in line with our observations made in this cohort [10] and another study using clinical data [23] and is detailed in Sec. 2.3.1. The RVOT pressure difference for the corresponding decrease of the $R^{\mathrm{RVOT}}_{\mathrm{for}}$ resistance was calculated by subtracting PA PSP from the simulated RV pressure. The *in silico* decrease of RVOT pressure difference was plotted against the corresponding values of *in silico* predicted contractility. The contractility in $\mathrm{PSM}_{\mathrm{post}}$ reported previously [10] (see Sec. 2.2.1) was

used to validate the *in silico* predicted contractility for a measured value of RVOT pressure difference post-PVR.

2.2.3 Statistical analysis

The changes in post-PVR RV and PA PSP were evaluated via the Wilcoxon signed-rank test at $p < 0.050$. The difference between the *in silico* predicted post-PVR contractility and the contractility in PSM_{post} was quantitatively evaluated via a Bland–Altman plot analysis. In addition, the *in silico* predicted contractility and the contractility in PSM_{post} were multiplied by the ratio of myocardial wall thickness over ventricular chamber radius—rescaled in accordance with the Laplace law. Pearson's correlations were built between the rescaled *in silico* predicted contractility, rescaled contractility in PSM_{post} and the post-PVR RV peak systolic pressure (RV PSP) at $p<0.050$.

2.3 Results

2.3.1 RV and PA peak systolic pressures in patient-specific models pre- and post-PVR

Patients were divided into 2 groups according to the level of RVOTO: low- and high-RVOTO groups based on RV-to-LV systolic pressure ratio. RVOTO was defined as low if the ratio of RV to LV peak systolic pressures was $< 50\%$ and high if the ratio was $\geqslant 50\%$. All patients from the low-RVOTO group had at least moderate PR (regurgitation fraction $> 30\%$), while the high-RVOTO patients had at least mild PR (regurgitation fraction $> 20\%$). There were n = 9 patients with low-RVOTO and n=10 patients with high-RVOTO. Complete clinical and hemodynamic characteristics of this patient cohort can be found in the supplementary material of published work [10].

Figure 2.2 shows RV PSP and PA PSP pre- and post-PVR in the low- and high-RVOTO groups. RV PSP showed insignificant post-PVR change ($p=0.133$) and a significant decrease ($p=0.004$) in low-RVOTO group and high-RVOTO group, respectively. In the low-RVOTO and high-RVOTO groups the median change of PA PSP was 2.0 and 1.0 mmHg, respectively. The analysis of pressure data in our patient cohort therefore showed an insignificant change of PA PSP post-PVR ($p=0.326$ for all patients).

2.3.2 *In silico* prediction of right ventricular contractility

Figures 2.3 and 2.4 show the *in silico* prediction of RV contractility for a sequential decrease of RVOT resistance (R_{for}^{RVOT}) in 4 patients from high- and 2 patients from low-RVOTO groups, respectively. *In silico* predictions of contractility for the remaining patients can be found in the Supplementary Figs. 2.6 and 2.7. With a decreasing level of R_{for}^{RVOT}, the RV contractility was decreasing along a line for all studied patients, creating a 1D patient-specific trajectory within the RV contractility-RVOT pressure difference space. The mean (± SD) *in silico* predicted contractility at 0 mmHg RVOT pressure difference for all patients was 36 (±) 9 kPa. Note that the range of healthy RV contractility was assumed to be 38–48 kPa [10].

Figure 2.5a shows a Bland–Altman plot of the difference between the *in silico* predicted contractility post-PVR and data-estimated contractility in PSM_{post} for the measured RVOT pressure difference post-PVR.

The mean (±SD) absolute difference between the *in silico* predicted contractility and the contractility in PSM_{post} in the low- and high-RVOTO group was 4.0 (±2.6) and 3.1 (±2.1) kPa, respectively. Pearson's correlation (R^2) for the *in silico* predicted contractility and

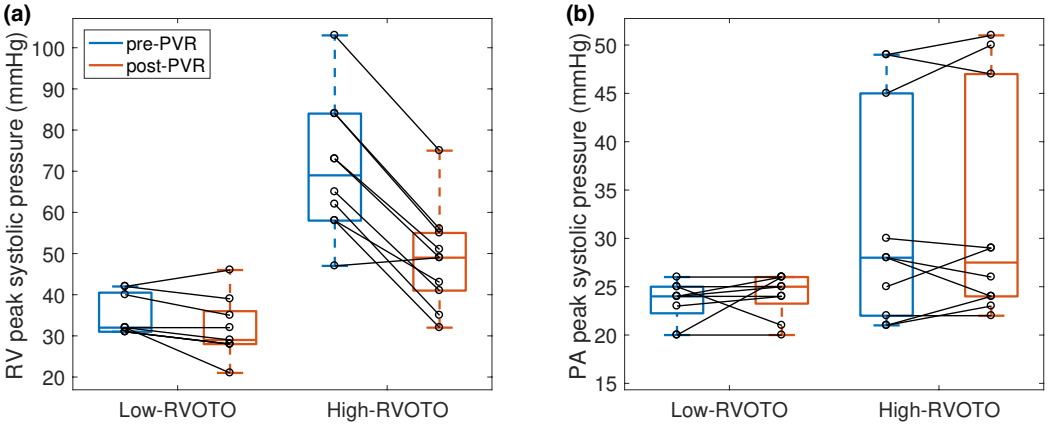

Figure 2.2: (a) right ventricular (RV) peak systolic pressure pre- and post-PVR. (b) pulmonary artery (PA) peak systolic pressure pre- and post-PVR. Central line inside the boxplots is the median, bottom and top edges of the boxes show 25th and 75th percentiles, respectively, the whiskers connect the most extreme data points not considered as outliers. Low-/High-RVOTO low/high right ventricular outflow tract obstruction patient groups.

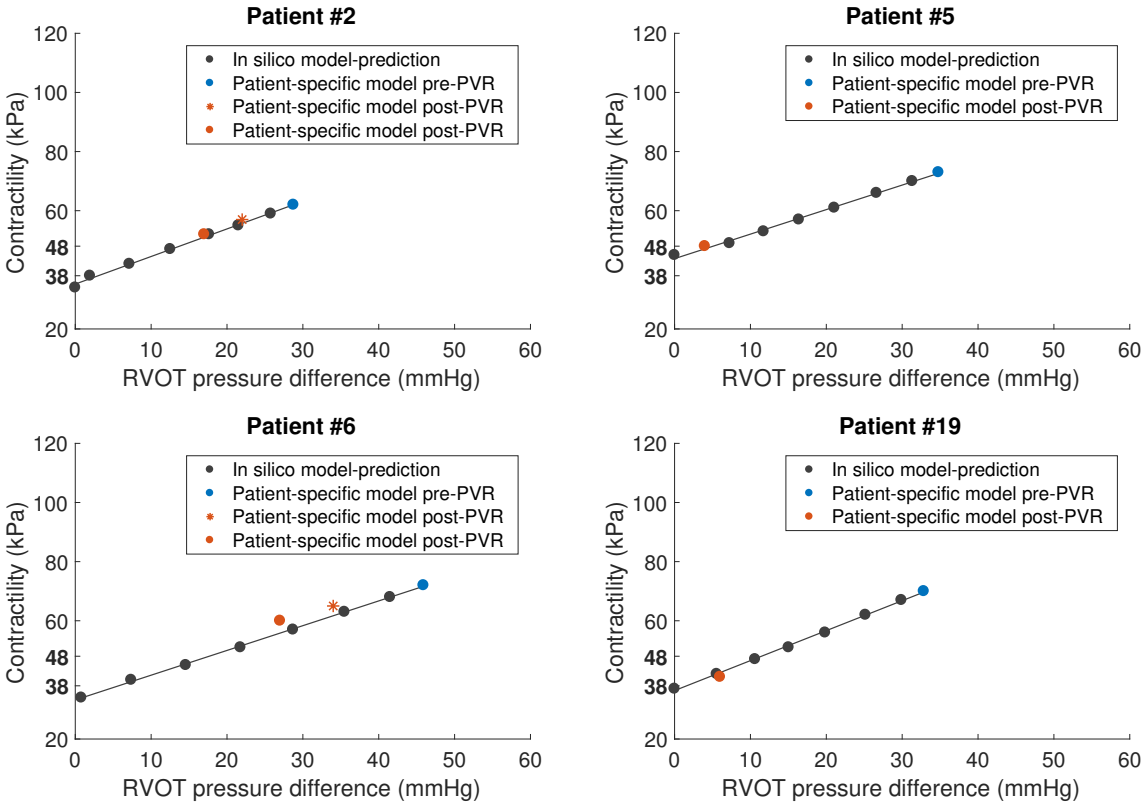

Figure 2.3: *In silico* prediction of right ventricular (RV) contractility post-PVR (black points) for selected patients from high right ventricular outflow tract obstruction (RVOTO) group. Filled blue and orange points are the contractilities in the pre- and post-PVR patient-specific models. Orange stars in patients #2 and #6 are additional post-PVR data-estimated contractility, where post-PVR pressures were acquired ∼2 h earlier than the final post-PVR pressure measurement (filled orange points). Healthy RV contractility was assumed to be 38-48 kPa [10].

for the contractility in PSM_{post} (both multiplied by the ratio of myocardial wall thickness over ventricular chamber radius according to Laplace's law) was 0.902 (p=0.000) and 0.910

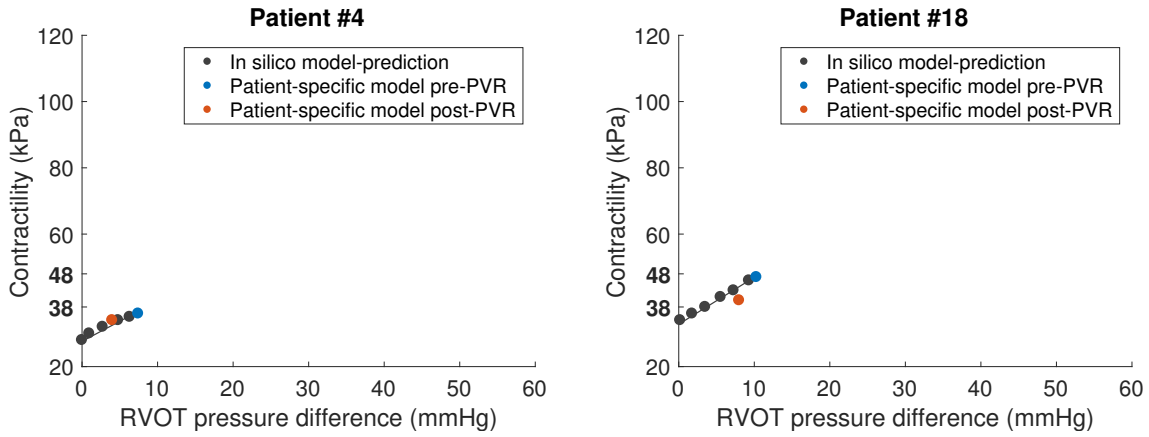

Figure 2.4: *In silico* prediction of right ventricular (RV) contractility post-PVR (black points) for selected patients from low right ventricular outflow tract obstruction (RVOTO) group. Filled blue and orange points are the contractilities in the pre- and post-PVR patient-specific models

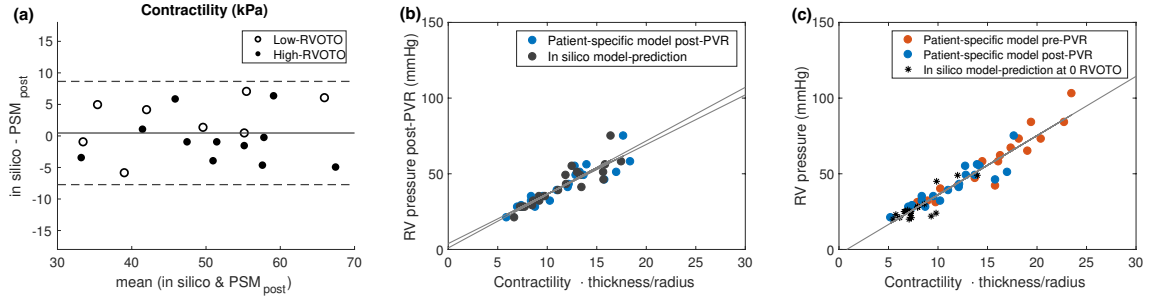

Figure 2.5: Quantitative difference between the contractility from *in silico* prediction and that from the post-PVR patient-specific models for a measured post-PVR right ventricular (RV) outflow tract pressure difference. A: Bland–Altman plot, solid horizontal line is the mean of the difference between the *in silico* predicted and contractility in the patient-specific model, top and bottom dashed horizontal lines are the limits of agreement at 95% prediction interval (±1.96 times standard deviation). B: Pearson's correlation for *in silico* predicted and the contractility in patient-specific model, while both are multiplied by the ratio of myocardial wall thickness over ventricular chamber radius (rescaled contractility) and measured RV peak systolic pressure post-PVR at $p < 0.05$. C: Pearson's correlation between the rescaled contractility and RV pressure. Orange and blue points are the pre- and post-PVR contractilities in the patient-specific models, respectively. Black stars are the *in silico* predicted contractility at zero mmHg RVOT pressure difference, R^2=0.954, p=0.000.

(p=0.000), respectively (Fig. 2.5b). Figure 2.5c shows Pearson's correlation for the *in silico* predicted contractility at 0 mmHg pressure difference and the contractility in pre- and post-PVR patient-specific models rescaled in accordance with the Laplace's law in relation to the RV PSP. R^2 for all values of contractility (orange, and blue points and black stars in Fig. 2.5c) is 0.954 (p=0.000). For the contractility at 0 mmHg pressure difference alone (black stars in Fig. 2.5c), R^2 is 0.850 (p=0.000).

2.4 Discussion

In this work we evaluated the predictive value of patient-specific biomechanical models created from patients' data prior to PVR in previously reported study [10] to establish model-predicted (*in silico*) changes in RV contractility post-PVR. We used an assumption that PA PSP was preserved post-PVR as it showed little or no variation in clinical data [10; 23]. We therefore gradually decreased the RVOT resistance and re-calibrated the

contractility to maintain PA PSP for each patient to represent the set of *in silico* predicted contractilities. We used the data-estimated contractility in PSM_{post}, also created in the previous study [10], to validate the *in silico* predicted contractility. For the majority of patients, the *in silico* predicted contractility fell close to the RV contractility in PSM_{post}. The mean (± SD) error in low- and high-RVOTO groups corresponded to 5.0 (±4.0)% and 4.0 (±3.0)% with respect to pre-PVR contractility, respectively. The difference between the *in silico* predicted contractility and the contractility in PSM_{post} on individual patient basis varied from negative (negative part of y-axis on Bland–Altman plot denoting the *in silico* predictions underestimating the contractility in PSM_{post}) to positive (positive part of y-axis, the *in silico* predictions overestimating the contractility from patient-specific models). These errors could be explained by the measurement uncertainties in the catherization pressure signals. In addition, different preload pressures imposed during the *in silico* PVR prediction vs. the preload used in the patient-specific models could have contributed to the discrepancy presented in the Bland–Altman plot: the *in silico* prediction did not assume any preload change from the pre-PVR RV end-diastolic pressure (EDP), while the actual post-PVR patient-specific models directly used the measured post-PVR pressures. However, as only a mild decrease of EDP post-PVR was observed, we expect that its effect on the post-PVR contractility will be small compared to that given by the decrease in RVOTO. We also evaluated the difference between the *in silico* predicted contractility values and the contractility in PSM_{post} rescaled with respect to the Laplace's law (Wall stress directly proportional to Pressure · chamber radius/wall thickness). Pearson's correlations between the rescaled contractility and measured RV pressure post-PVR — using either the *in silico* prediction or the in PSM_{post} — showed almost identical strong correlations (Fig. 2.5b). This suggests that the effect of the variation present in Bland–Altman plot is small with respect to the global mechanical properties of the ventricle for a given ventricular geometry.

We observe linearity of the relationship between the *in silico* predicted contractility and the RVOT resistance. In addition, these 1D relationships predict the contractility at 0 mmHg RVOT pressure difference to be in the range of healthy RV contractility [10] in all patients. In accordance with Laplace's law we plotted the rescaled *in silico* predicted contractility at 0 mmHg RVOT pressure difference against the pre-PVR PA PSP and combined that correlation with previously published Laplace's correlations of pre- and post-PVR data-estimated contractility in PSM_{pre} and PSM_{post}, respectively [10]. The combined correlation revealed a strong overall relationship. The return to a completely unobstructed RVOT may not be possible in some patients due to the residual RVOT gradient of at least 10–15 mmHg (as a result of placing a stented bioprosthesis). Nevertheless, the *in silico* predicted contractility at hypothetically minimal RVOT resistance also follows the Laplace's law of ventricular wall stress generation. This further strengthens the physiological relevance of the *in silico* predicted relationship between the contractility vs. RVOT resistance post-PVR for a given ventricular geometry.

Although the model used in this study is rather complex and nonlinear in various aspects (e.g. passive and active behavior of myocardium), the final finding is a nearly linear relationship between the *in silico* predicted contractility and the RVOT resistance throughout a wide range of the resistance values. As shown in Fig. 2.2, there is an insignificant change of PA PSP post-PVR. With the systolic PA pressure waveform being rather flat and PA PSP being close to PA end-systolic pressure (ESP), the pressure change between the start and end of ejection is nearly preserved post-PVR as well as the amount of ejected blood (stroke volume, SV). This was also observed in the clinical study of Lurz et al. [23], which suggested that the SV undergoes insignificant change immediately after PVR.

We can approximate SV by

$$\mathrm{SV} = \frac{\mathrm{RVPSP} - \mathrm{PAPSP}}{R_{\mathrm{for}}^{\mathrm{RVOT}}} \cdot t_{\mathrm{eject}}, \tag{2.5}$$

where t_{eject} stands for time of ejection. In the previous work [10] we demonstrated that model-derived contractility σ_0 is proportional to RV PSP via the Laplace law:

$$\mathrm{RVPSP} = 2\sigma_0 \frac{h}{r}, \tag{2.6}$$

where h and r are ventricular wall thickness and chamber radius, respectively. Assuming that SV is relatively unchanged immediately after the RVOTO release, by combining Eqs. (2.5) and (2.6) the linearity between σ_0 and RVOT resistance ($R_{\mathrm{for}}^{\mathrm{RVOT}}$) becomes apparent:

$$2\sigma_0 \frac{h}{r} = \frac{\mathrm{SV} \cdot R_{\mathrm{for}}^{\mathrm{RVOT}}}{t_{\mathrm{eject}}} + \mathrm{PAPSP}. \tag{2.7}$$

We hypothesize that the linearity between the *in silico* predicted contractility and the RVOT resistance observed in the current cohort of patients is determined by the preservation of SV immediately post-PVR. A larger cohort of patients containing both RVOTO and PR should be studied to elucidate if the preservation of the SV post-PVR and if the observed linearity consistently happens. Nevertheless, the contractility itself accounts for nonlinear active constitutive behavior of the myocardium and in the present modeling approach is an inherently patient-specific index of the inotropic state of the myocardium and our results support its prognostic significance.

It should be recognized that there are other mechanical models that could provide the representation of the internal myocardial stress. For example, a lumped-parameter model of the heart and circulation as in CircAdapt is an alternative patient-specific approach for modeling the stress–strain relationship of the myocardium and the interaction between ventricles and the vascular tree [24; 25; 26]. Even though CircAdapt models contain the interaction between the two ventricles and are fast in computation time (real time or close to real time), their micromechanical formulation does not account for sarcomere-level kinetics but is in the form of phenomenological myofiber-level stress–strain relationship. The family of 3D finite element models [14; 27; 28; 7] allows the investigation of regional wall mechanics (e.g. contractility [29; 30]), see also review articles [31; 32] and references therein. However, these are computationally expensive approaches, which limits their practical applicability in the investigation of large cohorts of patients in clinical settings. In the current work we ran 7 simulations per patient to establish the *in silico* relationships. This would be hardly achievable with a 3D model.

Overall, the *in silico* predicted relationship between the contractility and RVOT resistance demonstrates an immediate response of RV active mechanical properties to the varying afterload pressure. Our results suggest that after PVR the RVOT pressure difference and myocardial contractility will follow a nearly linear relationship (1D line). The linearity of pressure vs. contractility relationship could be used to inform about evolution of RV mechanics at a given level of RVOTO post-PVR and subsequently assist in planning the patient's intervention. Should the goal be to reduce the myocardial stress to a larger extent, the surgical procedure might be preferential as opposed to the percutaneous procedure that is known to typically result in a higher level of residual RVOT difference. The current workflow, however, cannot provide the exact estimate of post-PVR physiology. The level of RVOT resistance decrease may depend on a number of factors (e.g. actual morphology of RVOTO, type of prosthetic valve used, initial type of repair). Possibly, patient-specific

computational fluid dynamics simulations on the RVOT and PA could contribute to predict the decrease of the RV-to-PA pressure difference [33; 34; 35]. This is, however, out of scope of the current work.

The complete validation of the *in silico* predicted relationship between the post-PVR contractility and RVOT resistance is limited due to the limitation of the study [10], in which the only post-PVR measured pressures were available. In addition, the number of patients used in the present study is relatively small to draw universal conclusions regarding the response of RV mechanics to decreased RVOT pressure difference. Therefore, a detailed study with extended cohort of patients and simultaneous acquisition of pressure-volume data during the intervention (e.g. by a conductance catheter) is a natural follow-up to the present paper. The current modeling approach predicts an instantaneous change of ventricular mechanics at a given geometry in response to different levels of RVOTO whereas the long-term effect of PVR on the mechanical and morphological properties remain unknowable. In the future we propose to combine our prediction of immediate response to PVR with a kinematic growth theory framework [36; 37; 38; 39] or machine learning approach [40], which could include some distinct features obtained from advanced image data analysis constrained by a biomechanical model [41]. In particular, it will be interesting to study the morphological change of the ventricular cavity to mechanical unloading at several points along the predicted (1D) line, where a given change of intraventricular pressure with respect to pre-PVR could be considered as a stress-based unloading stimuli [42].

Biomechanical modeling has a potential to provide an insight into the evolution of RV mechanics. We have demonstrated the ability of the model to predict the mechanical response of the ventricle under progressive recovery of RV ESP through decreasing levels of RVOTO. Our results show a linear relationship between contractility and the level of RVOTO post- PVR. This step could contribute to the optimal clinical management for individual patients. The future objective would be to suggest what type of intervention (e.g. type or size of prosthesis, or percutaneous vs. surgical approach) would be the best for a given patient and combine with our ventricular-mechanics prediction. In the current paper we demonstrated the approach on the cohort of tetralogy of Fallot patient with pulmonary valve pathology and right ventricular overload. This type of model-derived predicted outcome may have relevant application even in other valvular pathologies (e.g. aortic valve pathologies).

ACKNOWLEDGMENTS

We would like to acknowledge Dr Philippe Moireau, Inria research team MΞDISIM, for the development of the cardiac simulation software CardiacLab used in this work. This work was supported by the Inria-UTSW Associated Team TOFMOD. It was also funded from by the W. B. & Ellen Gordon Stuart Trust, The Communities Foundation of Texas and by the Pogue Family Distinguished Chair (award to Dr F. Gerald Greil in February, 2015). The work was in addition supported by the Ministry of Health of the Czech Republic [NV19-08-00071]. Research reported in this publication was supported by Children's Health^{SM}, but the content is solely the responsibility of the authors and does not necessarily represent the official views of Children's Health^{SM}.

2.5 Appendix

Supplementary Figures 2.6-2.7 show the *in silico* prediction of right ventricular (RV) contractility post-PVR for all patients.

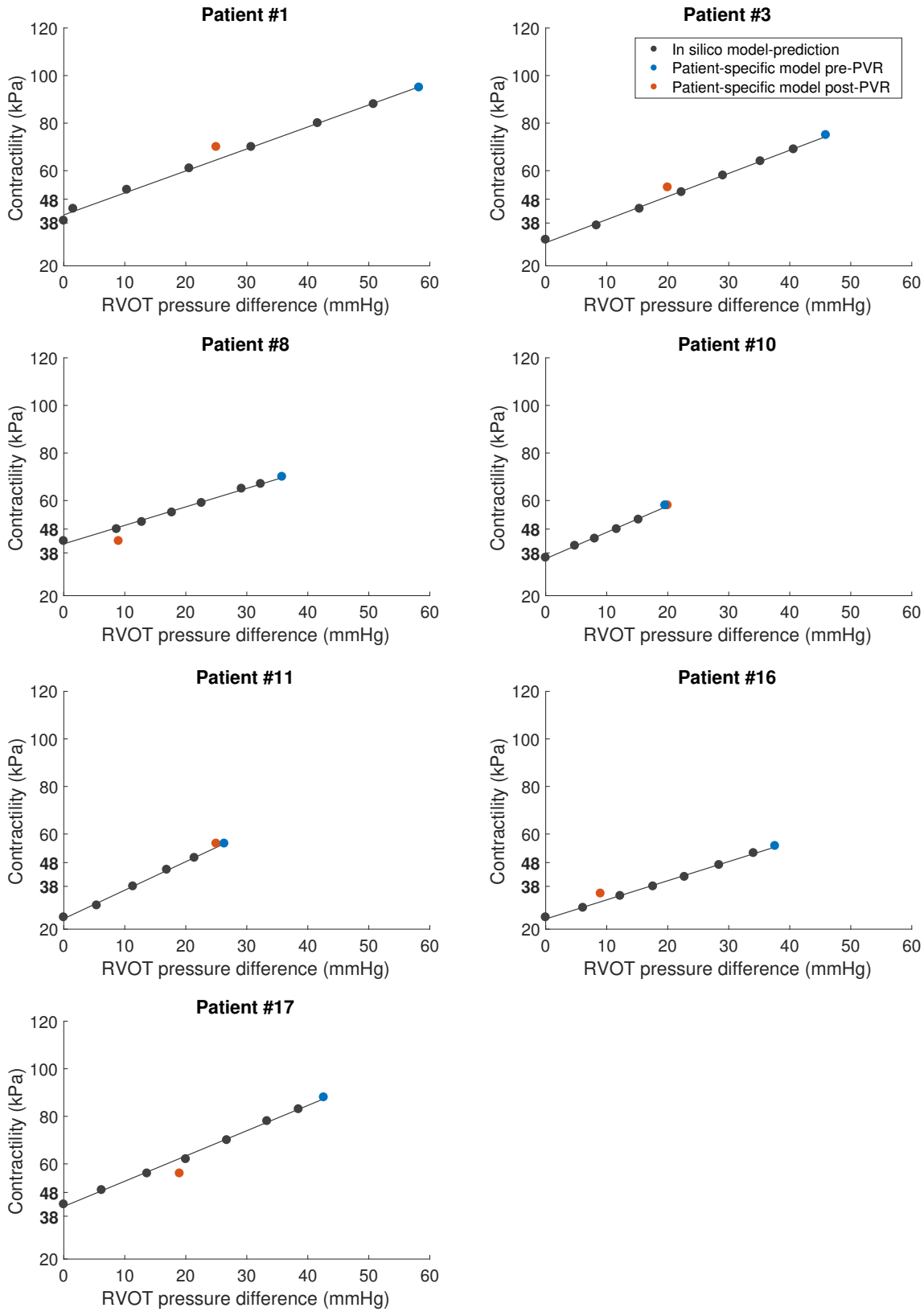

Figure 2.6: *In silico* prediction of right ventricular (RV) contractility post-PVR (black points) for the patients from high right ventricular outflow tract obstruction (RVOTO) group. Filled blue and orange points are the contractilities in the pre- and post-PVR patient-specific models, respectively.

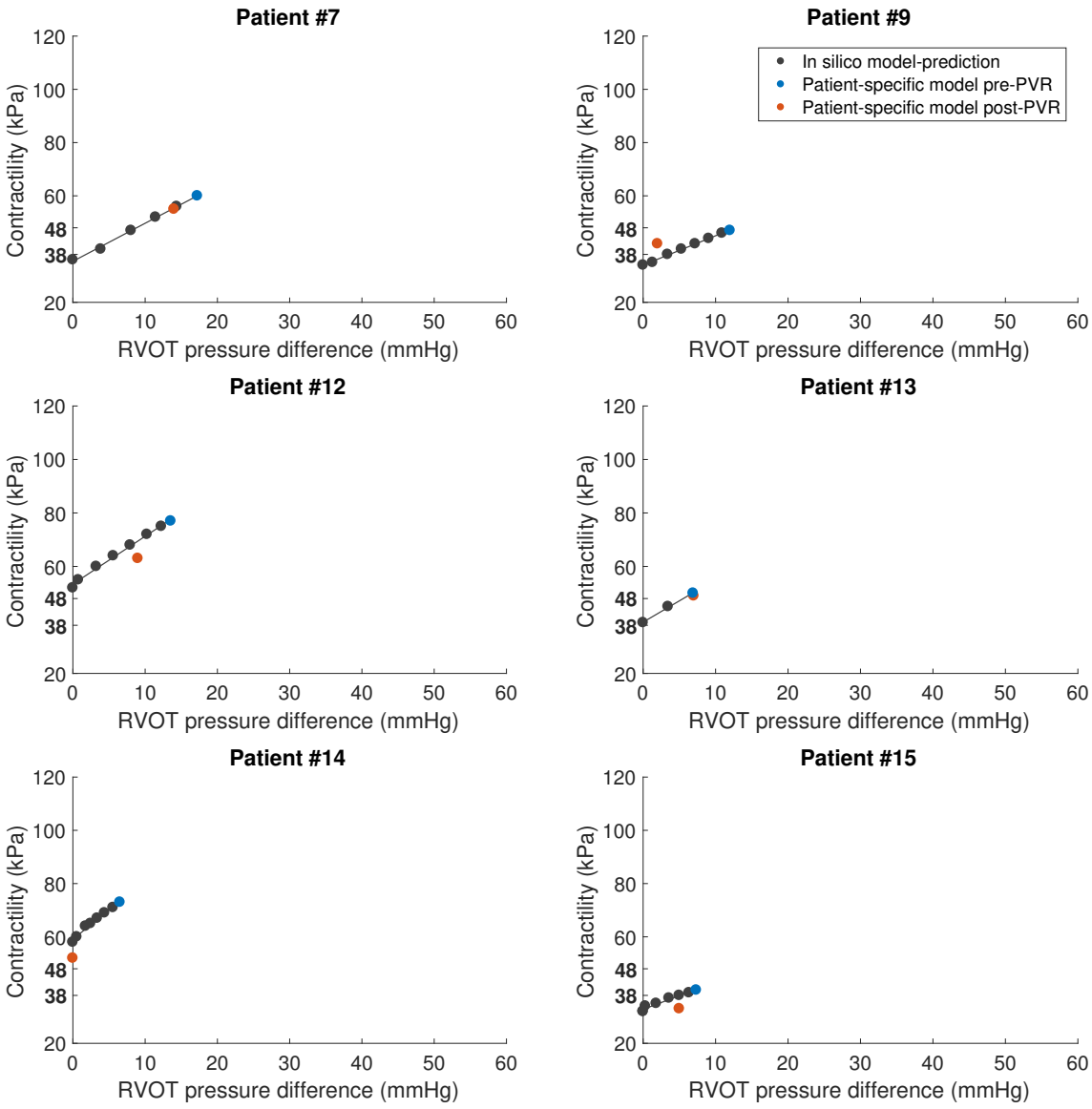

Figure 2.7: *In silico* prediction of right ventricular (RV) contractility post-PVR (black points) for the patients from low right ventricular outflow tract obstruction (RVOTO) group. Filled blue and orange points are the contractilities in the pre- and post-PVR patient-specific models, respectively.

Bibliography

[1] T. Oosterhof, F. J. Meijboom, H. W. Vliegen, M. G. Hazekamp, A. H. Zwinderman, B. J. Bouma, A. P. van Dijk, and B. J. Mulder, "Long-term follow-up of homograft function after pulmonary valve replacement in patients with tetralogy of Fallot," *European heart journal*, vol. 27, no. 12, pp. 1478–1484, 2006.

[2] M. A. Quail, A. Frigiola, A. Giardini, V. Muthurangu, M. Hughes, P. Lurz, S. Khambadkone, J. E. Deanfield, V. Tsang, and A. M. Taylor, "Impact of pulmonary valve replacement in tetralogy of Fallot with pulmonary regurgitation: a comparison of intervention and nonintervention," *The Annals of thoracic surgery*, vol. 94, no. 5, pp. 1619–1626, 2012.

[3] H. Baumgartner, "The Task Force on the Management of Grown-up Congenital

Heart Disease of the European Society of Cardiology (ESC): ESC Guidelines for the management of grown-up congenital heart disease (new version 2010)," *Eur Heart J*, vol. 31, pp. 2915–2957, 2010.

[4] T. Geva, "Repaired tetralogy of fallot: the roles of cardiovascular magnetic resonance in evaluating pathophysiology and for pulmonary valve replacement decision support," *Journal of Cardiovascular Magnetic Resonance*, vol. 13, no. 1, pp. 1–24, 2011.

[5] A. M. Valente, K. Gauvreau, G. E. Assenza, S. V. Babu-Narayan, J. Schreier, M. A. Gatzoulis, M. Groenink, R. Inuzuka, P. J. Kilner, Z. Koyak, *et al.*, "Contemporary predictors of death and sustained ventricular tachycardia in patients with repaired tetralogy of Fallot enrolled in the INDICATOR cohort," *Heart*, vol. 100, no. 3, pp. 247–253, 2014.

[6] J. Lumens, C.-P. S. Fan, J. Walmsley, D. Yim, C. Manlhiot, A. Dragulescu, L. Grosse-Wortmann, L. Mertens, F. W. Prinzen, T. Delhaas, *et al.*, "Relative impact of right ventricular electromechanical dyssynchrony versus pulmonary regurgitation on right ventricular dysfunction and exercise intolerance in patients after repair of tetralogy of Fallot," *Journal of the American Heart Association*, vol. 8, no. 2, p. e010903, 2019.

[7] S. A. Niederer, G. Plank, P. Chinchapatnam, M. Ginks, P. Lamata, K. S. Rhode, C. A. Rinaldi, R. Razavi, and N. P. Smith, "Length-dependent tension in the failing heart and the efficacy of cardiac resynchronization therapy," *Cardiovascular research*, vol. 89, no. 2, pp. 336–343, 2011.

[8] M. Sermesant, R. Chabiniok, P. Chinchapatnam, T. Mansi, F. Billet, P. Moireau, J.-M. Peyrat, K. Wong, J. Relan, K. Rhode, *et al.*, "Patient-specific electromechanical models of the heart for the prediction of pacing acute effects in CRT: a preliminary clinical validation," *Medical image analysis*, vol. 16, no. 1, pp. 201–215, 2012.

[9] B. Ruijsink, K. Zugaj, K. Pushparajah, and R. Chabiniok, "Model-based indices of early-stage cardiovascular failure and its therapeutic management in Fontan patients," in *International Conference on Functional Imaging and Modeling of the Heart*, pp. 379–387, Springer, 2019.

[10] M. Gusseva, T. Hussain, C. H. Friesen, P. Moireau, A. Tandon, C. Patte, M. Genet, K. Hasbani, G. Greil, D. Chapelle, *et al.*, "Biomechanical modeling to inform pulmonary valve replacement in tetralogy of Fallot patients after complete repair," *Canadian Journal of Cardiology*, 2021.

[11] M. Caruel, R. Chabiniok, P. Moireau, Y. Lecarpentier, and D. Chapelle, "Dimensional reductions of a cardiac model for effective validation and calibration," *Biomechanics and modeling in mechanobiology*, vol. 13, no. 4, pp. 897–914, 2014.

[12] A. Le Gall, F. Vallée, K. Pushparajah, T. Hussain, A. Mebazaa, D. Chapelle, É. Gayat, and R. Chabiniok, "Monitoring of cardiovascular physiology augmented by a patient-specific biomechanical model during general anesthesia. a proof of concept study," *PloS one*, vol. 15, no. 5, p. e0232830, 2020.

[13] B. Ruijsink, K. Zugaj, J. Wong, K. Pushparajah, T. Hussain, P. Moireau, R. Razavi, D. Chapelle, and R. Chabiniok, "Dobutamine stress testing in patients with fontan circulation augmented by biomechanical modeling," *PloS one*, vol. 15, no. 2, p. e0229015, 2020.

[14] D. Chapelle, P. Le Tallec, P. Moireau, and M. Sorine, "Energy-preserving muscle tissue model: formulation and compatible discretizations," *International Journal for Multiscale Computational Engineering*, vol. 10, no. 2, 2012.

[15] A. V. Hill, "The heat of shortening and the dynamic constants of muscle," *Proceedings of the Royal Society of London. Series B-Biological Sciences*, vol. 126, no. 843, pp. 136–195, 1938.

[16] A. F. Huxley, "Muscle structure and theories of contraction," *Prog. Biophys. Biophys. Chem*, vol. 7, pp. 255–318, 1957.

[17] F. Kimmig, D. Chapelle, and P. Moireau, "Thermodynamic properties of muscle contraction models and associated discrete-time principles," *Advanced Modeling and Simulation in Engineering Sciences*, vol. 6, no. 1, pp. 1–36, 2019.

[18] J. Bestel, F. Clément, and M. Sorine, "A biomechanical model of muscle contraction," in *International Conference on Medical Image Computing and Computer-Assisted Intervention*, pp. 1159–1161, Springer, 2001.

[19] M. Hadjicharalambous, R. Chabiniok, L. Asner, E. Sammut, J. Wong, G. Carr-White, J. Lee, R. Razavi, N. Smith, and D. Nordsletten, "Analysis of passive cardiac constitutive laws for parameter estimation using 3D tagged MRI," *Biomechanics and modeling in mechanobiology*, vol. 14, no. 4, pp. 807–828, 2015.

[20] G. A. Holzapfel and R. W. Ogden, "Constitutive modelling of passive myocardium: a structurally based framework for material characterization," *Philosophical Transactions of the Royal Society A: Mathematical, Physical and Engineering Sciences*, vol. 367, no. 1902, pp. 3445–3475, 2009.

[21] J. Sainte-Marie, D. Chapelle, R. Cimrman, and M. Sorine, "Modeling and estimation of the cardiac electromechanical activity," *Computers & structures*, vol. 84, no. 28, pp. 1743–1759, 2006.

[22] N. Stergiopulos, B. E. Westerhof, and N. Westerhof, "Total arterial inertance as the fourth element of the windkessel model," *American Journal of Physiology-Heart and Circulatory Physiology*, vol. 276, no. 1, pp. H81–H88, 1999.

[23] P. Lurz, J. Nordmeyer, V. Muthurangu, S. Khambadkone, G. Derrick, R. Yates, M. Sury, P. Bonhoeffer, and A. M. Taylor, "Comparison of bare metal stenting and percutaneous pulmonary valve implantation for treatment of right ventricular outflow tract obstruction: use of an x-ray/magnetic resonance hybrid laboratory for acute physiological assessment," *Circulation*, vol. 119, no. 23, pp. 2995–3001, 2009.

[24] T. Arts, T. Delhaas, P. Bovendeerd, X. Verbeek, and F. W. Prinzen, "Adaptation to mechanical load determines shape and properties of heart and circulation: the CircAdapt model," *American Journal of Physiology-Heart and Circulatory Physiology*, vol. 288, no. 4, pp. H1943–H1954, 2005.

[25] J. Lumens and T. Delhaas, "Cardiovascular modeling in pulmonary arterial hypertension: focus on mechanisms and treatment of right heart failure using the circadapt model," *The American journal of cardiology*, vol. 110, no. 6, pp. S39–S48, 2012.

[26] J. Lumens, T. Delhaas, B. Kirn, and T. Arts, "Three-wall segment (TriSeg) model describing mechanics and hemodynamics of ventricular interaction," *Annals of biomedical engineering*, vol. 37, no. 11, pp. 2234–2255, 2009.

[27] P. J. Hunter and B. H. Smaill, "The analysis of cardiac function: a continuum approach," *Progress in biophysics and molecular biology*, vol. 52, no. 2, pp. 101–164, 1988.

[28] A. D. McCulloch, B. H. Smaill, and P. J. Hunter, "Left ventricular epicardial deformation in isolated arrested dog heart," *American Journal of Physiology-Heart and Circulatory Physiology*, vol. 252, no. 1, pp. H233–H241, 1987.

[29] L. Asner, M. Hadjicharalambous, R. Chabiniok, D. Peresutti, E. Sammut, J. Wong, G. Carr-White, P. Chowienczyk, J. Lee, A. King, N. Smith, R. Razavi, and D. Nordsletten, "Estimation of passive and active properties in the human heart using 3D tagged MRI," *Biomechanics and Modeling in Mechanobiology*, vol. 15, no. 5, pp. 1121–1139, 2016.

[30] R. Chabiniok, P. Moireau, P.-F. Lesault, A. Rahmouni, J.-F. Deux, and D. Chapelle, "Estimation of tissue contractility from cardiac cine-MRI using a biomechanical heart model," *Biomechanics and modeling in mechanobiology*, vol. 11, no. 5, pp. 609–630, 2012.

[31] R. Chabiniok, V. Y. Wang, M. Hadjicharalambous, L. Asner, J. Lee, M. Sermesant, E. Kuhl, A. A. Young, P. Moireau, M. P. Nash, *et al.*, "Multiphysics and multiscale modelling, data–model fusion and integration of organ physiology in the clinic: ventricular cardiac mechanics," *Interface focus*, vol. 6, no. 2, p. 20150083, 2016.

[32] V. Wang, P. Nielsen, and M. Nash, "Image-based predictive modeling of heart mechanics," *Annual review of biomedical engineering*, vol. 17, pp. 351–383, 2015.

[33] F. Donati, S. Myerson, M. M. Bissell, N. P. Smith, S. Neubauer, M. J. Monaghan, D. A. Nordsletten, and P. Lamata, "Beyond bernoulli: improving the accuracy and precision of noninvasive estimation of peak pressure drops," *Circulation: Cardiovascular Imaging*, vol. 10, no. 1, p. e005207, 2017.

[34] R. Fučík, R. Galabov, P. Pauš, P. Eichler, J. Klinkovskỳ, R. Straka, J. Tintěra, and R. Chabiniok, "Investigation of phase-contrast magnetic resonance imaging underestimation of turbulent flow through the aortic valve phantom: Experimental and computational study using lattice boltzmann method," *Magnetic Resonance Materials in Physics, Biology and Medicine*, vol. 33, no. 5, pp. 649–662, 2020.

[35] H. Švihlová, J. Hron, J. Málek, K. Rajagopal, and K. Rajagopal, "Determination of pressure data from velocity data with a view toward its application in cardiovascular mechanics. Part 1. Theoretical considerations," *International Journal of Engineering Science*, vol. 105, pp. 108–127, 2016.

[36] M. Genet, L. C. Lee, B. Baillargeon, J. M. Guccione, and E. Kuhl, "Modeling pathologies of diastolic and systolic heart failure," *Annals of biomedical engineering*, vol. 44, no. 1, pp. 112–127, 2016.

[37] S. Göktepe, O. J. Abilez, and E. Kuhl, "A generic approach towards finite growth with examples of athlete's heart, cardiac dilation, and cardiac wall thickening," *Journal of the Mechanics and Physics of Solids*, vol. 58, no. 10, pp. 1661–1680, 2010.

[38] R. C. Kerckhoffs, J. H. Omens, and A. D. McCulloch, "A single strain-based growth law predicts concentric and eccentric cardiac growth during pressure and volume overload," *Mechanics research communications*, vol. 42, pp. 40–50, 2012.

[39] W. Kroon, T. Delhaas, T. Arts, and P. Bovendeerd, "Computational modeling of volumetric soft tissue growth: application to the cardiac left ventricle," *Biomechanics and modeling in mechanobiology*, vol. 8, no. 4, pp. 301–309, 2009.

[40] F. Regazzoni, D. Chapelle, and P. Moireau, "Combining data assimilation and machine learning to build data-driven models for unknown long time dynamics—Applications in cardiovascular modeling," *International Journal for Numerical Methods in Biomedical Engineering*, p. e3471, 2021.

[41] D. A. Castellanos, K. Škardová, A. Bhattaru, E. Berberoglu, G. Greil, A. Tandon, J. Dillenbeck, B. Burkhardt, T. Hussain, M. Genet, *et al.*, "Left ventricular torsion obtained using equilibrated warping in patients with repaired tetralogy of fallot," *Pediatric Cardiology*, pp. 1–9, 2021.

[42] L. C. Lee, M. Genet, G. Acevedo-Bolton, K. Ordovas, J. M. Guccione, and E. Kuhl, "A computational model that predicts reverse growth in response to mechanical unloading," *Biomechanics and modeling in mechanobiology*, vol. 14, no. 2, pp. 217–229, 2015.

CHAPTER 3

Model-assisted time-synchronization of clinical pressure-volume data

Clinical pressure-volume (P-V) data when acquired by different modalities (e.g. CMR and pressure catheter) are often subjected to time-synchronization errors. This yields acquired P-V loops with artificial shape, in particular skewed isovolumetric phases. These errors are inherent to data acquisition and data processing techniques. The prime motivation of this chapter was to develop a time-synchronization technique that could be directly employed in clinical settings, e.g. during a volume-challenge study (manipulating preload conditions of the heart via administration of fluid bolus) of patients with single-ventricle geometry prior to completing Fontan circulation. This chapter develops a model-assisted time-synchronization method for ventricular P-V signals from two types of data acquisition protocols: (1) P-V data with prospectively (N=24, single-ventricle patients) and (2) with retrospectively (N=45, predominantly rTOF left and right ventricular patients) ECG-triggered cine MRI sequences. The qualitative improvement of time-synchronized P-V loops is demonstrated by plotting the clinically acquired P-V loops and those obtained after the proposed time-synchronization. We use a metrics derived from cardiovascular physiology to demonstrate the physiologically meaningful quantitative improvement of time-synchronized P-V data. In particular, we statistically compare the original and time-synchronized maximum time derivative of time-varying elastance ($E(t)$) – ($dE/dt_{\max}$) – in relation to $\max(dP/dt)$ derived from the original pressure signals. The proposed time-synchronization method produced high-quality P-V loops yielding statistically more accurate indices of myocardial energetics – max value of time-varying elastance ($E_{\max}$) and stroke work (area encompassed within P-V loop). This chapter demonstrated an ability of the model to assist in clinical data treatment during pre-interventional planning for e.g. patients with single-ventricle geometry.

Contents

Time-synchronization of invasive cardiovascular magnetic resonance data using a biomechanical model for pressure-volume loop analysis

Maria Gusseva[1,2], Daniel A. Castellanos[3,4], Joshua S. Greer[3], Mohamed Abdelghafar Hussein[3,5], Keren Hasbani[6], Gerald Greil[3], Surendranath R. Veeram Reddy[3], Tarique Hussain[3], Dominique Chapelle[1,2], Radomír Chabiniok[1,2,3,7]

[1]Inria, Palaiseau, France
[2]LMS, Ecole Polytechnique, CNRS, Institut Polytechnique de Paris, Palaiseau, France
[3]Division of Pediatric Cardiology, Department of Pediatrics, UT Southwestern Medical Center, Dallas, TX
[4]Department of Cardiology, Boston Children's Hospital, Boston, MA, USA
[5]Pediatric department, Kafrelsheikh University, Kafr Elsheikh, Egypt
[6]Division of Pediatric Cardiology, Department of Pediatrics, Dell Medical School, UT Austin, TX
[7]Department of Mathematics, Faculty of Nuclear Sciences and Physical Engineering, Czech Technical University in Prague, Prague, Czech Republic

The material of this chapter was converted into an extended research letter to editor format and was accepted for publication in the Journal of Magnetic Resonance Imaging. Preliminary proof-of-concept study of the proposed methods was published as a conference paper in the Proc. of Functional Imaging and Modeling of Heart (FIMH).

Abstract

Background: Therapy planning benefits from assessment of myocardial energetics using ventricular pressure-volume (P-V) loops. The acquisition of P-V signals using cardiac MRI and intraventricular pressure is often subjected to time-synchronization errors yielding P-V diagrams with skewed isovolumetric phases.

Purpose: We aim to develop a universal time-synchronization method for the ventricular P-V signals, independent of the setup of MRI sequence, type of catheter and patients' pathophysiology, by using biomechanical cardiac modeling.

Study type: retrospective.

Population: Two groups of P-V data with prospectively (N=24) and retrospectively (N=45) ECG-triggered cine MRI.

Field strength / sequence: 1.5 T scanner. bSSFP cine sequence in prospective ECG-triggering (kt-BLAST factor 6, partial Fourier 0.625) and in retrospective ECG-gating (SENSE 2), both in temporal resolution 30ms.

Assessment: Ventricular time-varying elastance $E(t) = P(t)/V(t)$ was computed from original (orig) and time-synchronized (t-syn) data. The expected physiological relationship between $\max(dP/dt)$ and $\max(dE/dt)$ was statistically evaluated.

Statistical test: Linear regression models through the origin were fitted to investigate the difference between $\max(dP_{\mathrm{orig/t-syn}}/dt)$ and $\max(dE_{\mathrm{orig/t-syn}}/dt)$. Wilcoxon signed-rank tests at $p<0.05$ were conducted to assess the quantitative difference between $\max(dE_{\mathrm{orig}}/dt)$ and $\max(dE_{\mathrm{t-syn}}/dt)$. Standard error of regression coefficients ($\mathrm{SE}_{\mathrm{coef}}$) and coefficients of determination (R^2) of fitted models were computed. Original and time-synchronized values of $E_{\max}$ and stroke work were compared with Wilcoxon signed rank test at $p<0.05$.

Results: The shapes of time-synchronized P-V loops were qualitatively improved. Time-synchronized P-V signals showed statistically stronger relationship between $\max(dP/dt)$ and $\max(dE/dt)$ in terms of physiologically more relevant coefficient of linear regression model and decreased variance of $\max(dE/dt)$ with respect to $\max(dP/dt)$ (R^2 >0.88 in all patients). Time-synchronized and original $\max(dE/dt)$ were significantly different (p=0.00 in all patients). Time-synchronized stroke work was significantly higher than original stroke work (p=0.00 in all patients).

Data conclusion: The proposed time-synchronization method produces high-quality P-V loops from cine MRI combined with catheter-derived pressure recordings.

Keywords— time-synchronization of clinical data, pressure-volume loop, invasive cardiovascular magnetic resonance imaging, cardiovascular modeling, translational research

3.1 Introduction

Pressure-volume (P-V) loops provide a meaningful insight into myocardial energetics and their employment in the clinical practice is beneficial in a number of situations both for left and right ventricles (LV, RV), e.g. to investigate ventricular-arterial coupling [1; 2; 3] or to assess the myocardial function [4; 5]. For instance, patients with single ventricle geometry prior to completing a complex surgical intervention undergo a detailed assessment of the current mechanical state of the myocardium [6]. P-V loops can be reconstructed from invasive cardiovascular magnetic resonance imaging (iCMR) (simultaneous acquisition of catheter pressure and CMR volume) in order to assess the functionality of the heart [7]. However, the recorded pressure and volume tracings are not perfectly synchronous yielding P-V loops with artificial shapes (see Figure 3.1). While the acquired pressure data are aligned with respect to the R-wave of the ECG, in the acquisition of the cine magnetic resonance imaging (MRI) a number of factors could cause a suboptimal alignment of data with respect to the R-wave peak of patient's ECG. First, the acquisition of cine MRI data is performed typically over hundreds of cardiac cycles yielding a time-volume plot that represents an average cycle during the acquisition. Second, due to a strong magnetic field of the MR scanner, it is difficult to derive a standard ECG. The so-called ventriculogram (VCG) is used instead, even though the terminology is often slightly abused and the signal is called ECG (as we do in our paper). Typically, the most prominent peak in the VCG is automatically detected and used as a trigger point. Particularly, in patients with pathological QRS duration (e.g. in some patients with a bundle branch block the QRS duration may go even beyond 200 ms), a more prominent S or R' wave can be detected instead. Third, retrospective ECG gating, which is preferred for cine MRI, allows the whole cardiac cycle to be acquired (as opposed to prospective triggering, in which typically the first 30-50 ms and final 100 ms are missed). However, the retrospective reconstruction and associated temporal interpolation is yet another factor in the temporal offset of volume

data. Finally, the fluid-filled catheter could record the pressures with some delay due to inertia effect, which could vary depending on the catheter type and size [8].

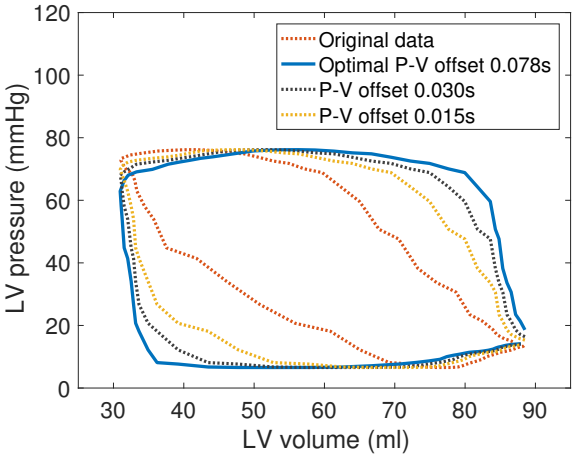

Figure 3.1: Illustration of the pressure-volume (P-V) offsets on the shape of the P-V loop in the measured data of left ventricle (LV) of a patient with repaired tetralogy of Fallot (#AF25 LV).

A complete synchronization of the P-V signals is possible when the data are acquired fully synchronously, for instance when using a conductance and pressure catheter. During iCMR procedures, as the time offset between the ventricular pressure and volume varies among patients due to the actual configuration of iCMR protocol (e.g. setup of the MRI sequence or the type and size of catheter used), the synchronization of corresponding cardiac phases in the P-V signals is typically performed manually. This approach relies on the isovolumic contraction and relaxation phases to be "perpendicular" to the x-axis in the P-V loop (we recall Figure 3.1). However, a manual synchronization can be suboptimal particularly in some clinical scenarios, e.g. for patients with valvular regurgitation where a clear appearance of isovolumic phases in P-V diagrams is lacking.

Due to the numerous factors contributing to the P-V dyssynchrony causing the P-V time-offset being different in each patient and acquisition, we aim to develop a universal time-synchronization procedure independent of a variability of the volume-pressure time-offset given by the individual patients and a given examination protocol. We use a biophysical model specific to a given patient and created using the acquired data. A recent methodological study [9] demonstrated the potential of such an approach to synchronize P-V signals in time [9]. Using the measured values of maximum and minimum ventricular pressure and volume, simplified patient-specific models of a cardiac cycle are created. These models provide synchronous pressure and volume waveforms, which can be used as a template to time-synchronize the measured data (see Figure 3.2). In the current work we aim to apply such a model-assisted time-synchronization technique on an extended cohort of patients: 24 P-V datasets of patients with single-ventricle geometry; 20 datasets of RVs; and 18 datasets of LVs, both in patients with tetralogy of Fallot after complete surgical repair (rTOF). We show the qualitative improvement by plotting the clinically acquired P-V loops and those obtained after the proposed time-synchronization. Since the ground truth synchronized data are not available in the cohort of patients undergoing CMR and pressure catheter exams, we use a metrics derived from cardiovascular physiology that demonstrates the physiologically meaningful quantitative improvement. Specifically, we statistically compare the original and time-synchronized maximum time derivative of time-varying elastance ($E(t)$)– $\max(dE/dt)$ – in relation to the maximum time derivative of pressure – $\max(dP/dt)$ – derived from the original pressure signals.

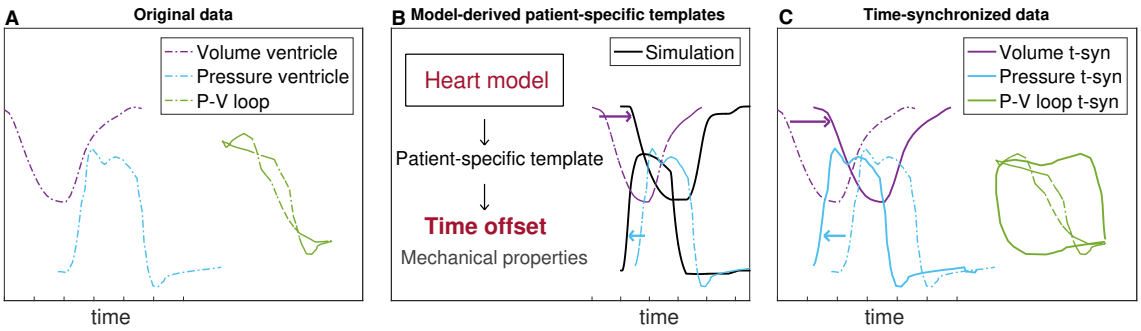

Figure 3.2: A: Distorted pressure-volume (P-V) loop due to the time offset between the acquired pressure and volume data illustrated on Patient AF24 LV from our study. B: Detection of the time offset by using patient-specific biomechanical model, simulating synchronous pressure and volume waveforms. C: Corrected P-V loop (solid line) reconstructed from the time-synchronized (t-syn) data.

3.2 Methods

3.2.1 Data

Datasets from two groups of patients were included in this study. The first group contained 10 patients with single-ventricle physiology prior to completing the Fontan circulation. The patients underwent an iCMR procedure where the catherization pressure and cine MRI were simultaneously acquired prior to and after a fluid bolus administration. Patients received 5 ml/kg within 1 or 2 fluid boluses. Ventricular volumes were measured using a prospectively ECG-triggered balanced steady-state free precession (bSSFP) cine sequence (kt-BLAST factor 6, partial Fourier 0.625, in order to shorten acquisition time in this volume-challenge study). The temporal resolution was ∼30 ms. In total, 24 pressure-volume (P-V) datasets from a baseline and post-bolus conditions were acquired. Additionally, most patients also had standard clinical cine MRI with retrospective ECG gating (SENSE 2, temporal resolution ∼30 ms) taken at baseline conditions. The second group consisted of 20 rTOF patients prior to the pulmonary valve replacement (PVR). CMR was acquired and reconstructed with standard settings and retrospective ECG gating (as described above). Catheter pressures were acquired in a separate session. In total 17 and 20 P-V datasets of left and right ventricles (LV, RV), respectively, were included in the study. We remark that two rTOF patients did not have LV pressure tracing and one had LV pressure tracing of an inferior quality. CMR ventricular volumes were processed using the CVI42 software (Circle Cardiovascular Imaging Inc., Calgary, Canada) and the motion tracking algorithm [10; 11]. The data collections for single-ventricle patients were performed under the ethical approval of the Institutional Review Boards of UT Southwestern Medical Center Dallas (STU 032017-061). The data collections for rTOF patients were performed under the ethical approvals of the Institutional Review Boards of UT Southwestern Medical Center Dallas (STU-2020-0023) and UT Austin (IRB 2020-06-0128). The IRBs waived the need for a consent to use the anonymized retrospective data.

An additional dataset with fully synchronous pressure and volume signals, acquired using a conductance P-V loop catheter in a pre-clinical study, was included as a verification case. Seven P-V loops were generated out of the single measured cardiac cycle: original P-V data (perfectly synchronous pressure and volume signals); and six P-V loops with imposing an artificial time offsets of ±50, ±100 and ±150 ms between the pressure and volume signals.

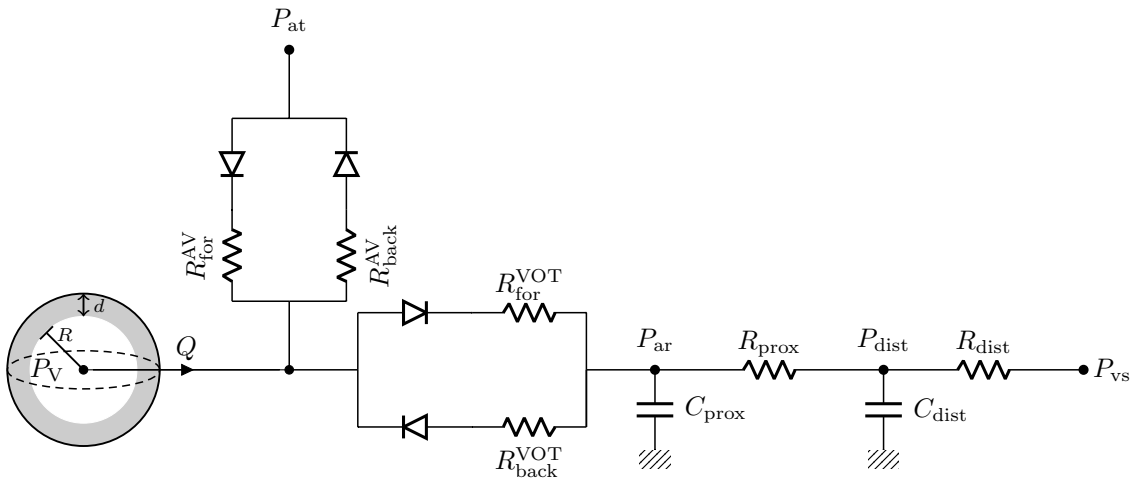

Figure 3.3: Coupling of the heart with atrioventricular and arterial valves via system of diodes and with circulation system represented by a two-stage Windkessel model. P_{at} , P_{V}, P_{ar}, P_{dist}, P_{vs} are pressures in atrium, ventricle, proximal artery, distal circulation and venous system, respectively; $R^{\mathrm{AV}}_{\mathrm{for}}$, $R^{\mathrm{AV}}_{\mathrm{back}}$ and $R^{\mathrm{VOT}}_{\mathrm{for}}$, $R^{\mathrm{VOT}}_{\mathrm{back}}$ are forward, backward resistances of atrioventricular valve and ventricular outflow tract, respectively. R_{prox}, C_{prox}, R_{dist}, C_{dist} are proximal and distal resistances and capacitances in Windkessel model.

3.2.2 Biomechanical model of the heart

We employed the biomechanical heart model described in [12]. This model was used in clinical research projects, such as [5; 13; 14]. A subject-specific model was created for each dataset in our study. Ventricular geometry and kinematics are reduced to a sphere with inner radius R and wall thickness d (Figure 3.16). Constitutive material laws that provide myocardial passive and active properties are preserved as in the full 3D heart model [15]. Myocardial passive stiffness is given by visco-elastic constitutive law [16]. Myocardial contractility is modeled within the A. F. Huxley sliding filament theory framework [17; 18] where mechano-chemical coupling of actin-myosin unit produces an active contraction of the sarcomere. The internal myocardial stresses (passive and active) are in mechanical equilibrium with external intraventricular cavity pressure. Globally, the ventricular cavity pressure and volume are an output of the model. The heart model is coupled with inlet and outlet valves that are described by a system of diodes to control an inflow from the atrioventricular (AV) valve and an outflow through the ventricular outflow tract (VOT) with corresponding forward and backward AV/VOT valve resistances, $R^{\mathrm{AV/VOT}}_{\mathrm{for}}$ and $R^{\mathrm{AV/VOT}}_{\mathrm{back}}$, as described in [19] and applied in a recent clinical study [14]. The circulation system is represented by a two-stage Windkessel model [20]. The model was made patient-specific by applying the following sequential calibration procedure [14]: Windkessel model parameters (resistances and capacitances), were adjusted to match maximum, minimum and dicrotic notch pressures in the outflow artery. Then, in the ventricular cavity model wall thickness and sphere radius were prescribed from cine MRI mass and EDV measurements. The stress-free reference configuration was derived as in the Klotz et al. study [21]. Ventricular preload was imposed from the measured end-diastolic pressure (EDP). Passive myocardial stiffness was adjusted to match measured EDV under imposed preload. Myocardial contractility was calibrated according to the measured stroke volume and end-systolic pressure in the ventricle.

3.2.3 Time-varying elastance

We perform a quantitative evaluation of the time-synchronized P-V loops with respect to the time-varying elastance (TVE) model of Suga et al. [22]. Time-varying elastance $E(t)$ is defined by

$$E(t) = \frac{P(t)}{V(t) - V_0} \tag{3.1}$$

with $P(t)$ and $V(t)$ being ventricular pressure and volume. In this work, the correction factor V_0 is taken as zero. Sunagawa and Sagawa [23] proposed that time derivative of ventricular pressure can be expressed in terms of time derivative of $E(t)$ and that in the isovolumetric phase the maximum derivative of ventricular pressure ($\max(dP/dt)$) is linearly related to the maximum derivative of $E(t)$ ($\max(dE/dt)$).

$$\max(dP/dt) = \max(dE/dt) \cdot (EDV - V_0). \tag{3.2}$$

The linearity of $\max(dP/dt)$ vs. end-diastolic volume (EDV) relationship with a slope corresponding to $\max(dE/dt)$ was experimentally detected in canine hearts by Little et al. [24]. Therefore, in the present work we consider the relationship between $\max(dP/dt)$ and $\max(dE/dt)$ as a quantitative measure of ventricular function during ejection.

3.2.4 Time-synchronization

Thanks to the biophysical and physiological behavior of the model, the simulated pressure and volume traces are synchronous and were therefore taken as templates to synchronize the original data in time. Optimal time offsets $t_{\text{offset}}^{\text{pressure}}$ and $t_{\text{offset}}^{\text{volume}}$ between the measured data and the model were derived by minimizing the criterion:

$$\min_{t_{\text{offset}}} \int_0^{t_{\text{end}}} (f(t) - g(t - t_{\text{offset}}))^2 dt, \tag{3.3}$$

where $f(t)$ represents the simulated ventricular pressure or volume; $g(t)$ is the measured ventricular pressure (volume); t_{end} is the end of the cardiac cycle in the measured data.

First, we applied the time-synchronization procedure on the dataset acquired by the conductance P-V loop catheter, in which the pressure-volume time offsets were manually imposed. The time-synchronized data were compared with the original fully synchronous acquisition to verify our approach.

Then, all clinical datasets with intraventricular pressure catheter and cine MRI-cardiac volumes were time-synchronized according to criterion given by eq. (3.3). P-V loops were constructed both for original and time-synchronized (t-syn) data. They were first assessed qualitatively. Secondly, the TVE function was computed for the original and t-syn data:

$$\begin{aligned} E_{\text{orig}}(t) &= \frac{P_{\text{orig}}(t)}{V_{\text{orig}}(t)}, \\ E_{\text{t-syn}}(t) &= \frac{P_{\text{t-syn}}(t)}{V_{\text{t-syn}}(t)}, \end{aligned} \tag{3.4}$$

where $P_{\text{orig/t-syn}}(t)$, $V_{\text{orig/t-syn}}(t)$ are ventricular cavity pressures and volumes as originally measured / time-synchronized, respectively. The time derivative of ventricular pressure can be expressed in terms of TVE [23] for the original or t-syn data, respectively:

$$\frac{P_{\text{orig/t-syn}}(t)}{dt} = \frac{dE_{\text{orig/t-syn}}(t)}{dt} \cdot V_{\text{orig/t-syn}}(t) + E_{\text{orig/t-syn}}(t) \cdot \frac{dV_{\text{orig/t-syn}}(t)}{dt}. \tag{3.5}$$

During the isovolumic contraction phase, dP/dt reaches its maximum value, $\max(dP/dt)$, and $V(t)$ is constant (equal to EDV) [24], hence:

$$\max(dP_{\mathrm{orig/t-syn}}/dt) = \max(\frac{dP_{\mathrm{orig/t-syn}}(t)}{dt}) = \max(\frac{dE_{\mathrm{orig/t-syn}}(t)}{dt}) \cdot EDV. \tag{3.6}$$

Original and time-synchronized values of maximum TVE: $E_{\max} = \max(P(t)/V(t))$, and stoke work: area encompassed within the P-V loop, were computed for each patient.

3.2.5 Statistical analysis

Considering the identity relationship in Eq. (3.6), a reference linear relationship through the origin with slope coefficient (Coef) equal to 1 was constructed. Then, linear regression models through the origin were fitted to investigate the difference between $\max(dP_{\mathrm{orig/t-syn}}/dt)$ computed directly from original/time-synchronized data and $\max(dP_{\mathrm{orig/t-syn}}/dt)$ expressed in terms of TVE of original/time-synchronized data (Eq. (3.6)). Coef of the fitted models of original/time-synchronized data were computed and compared with the reference linear regression model. Wilcoxon signed-rank tests at $p<0.05$ were conducted to assess the quantitative difference between $\max(dE_{\mathrm{orig}}/dt)$ and $\max(dE_{\mathrm{t-syn}}/dt)$. Standard error of regression coefficients (SE_{coef}) and coefficients of determination (R^2) of fitted models of original/time-synchronized data were computed. Original and time-synchronized values of $E_{\max}$ and stroke work were statistically compared with Wilcoxon signed rank test at $p<0.05$.

3.3 Results

Figure 3.4 shows pressure and volume waveforms from the dataset acquired by the conductance catheter with manually imposed time offsets. Our time-synchronization corrected the P-V loops within 0.002s of the imposed time offset, verifying the approach.

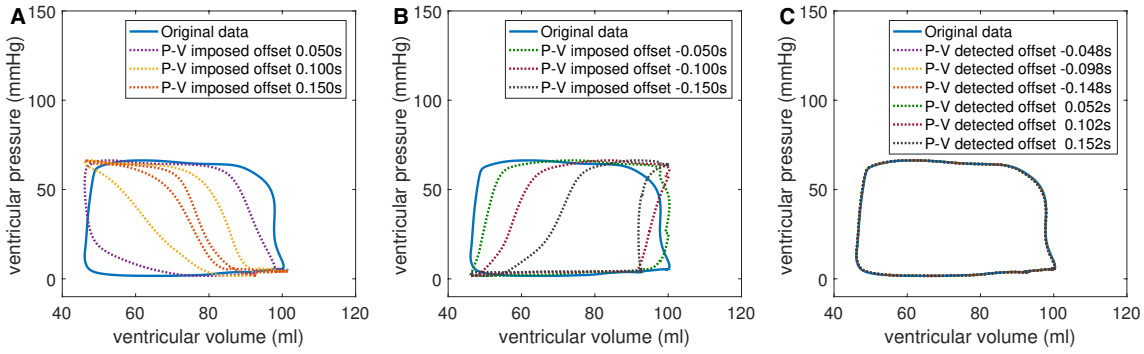

Figure 3.4: Verification of time-synchronization technique using conductive catheter pressure-volume (P-V) data. A: Original P-V loop from conductive catheter (solid blue line) and artificially imposed P-V time-offsets in positive direction (colored dotted lines). B: original P-V loop from conductive catheter (solid blue line) and artificially imposed P-V time-offsets in negative direction (colored dotted lines). C: model-detected P-V time-offsets imposed in A. Offsets are the difference between the pressure and volume in absolute values.

Figures 3.5 and 3.6 show ventricular pressure, volume and outflow from the ventricle acquired by pressure catheter and CMR, plotted together with the result of simulation. The measured data are plotted before and after the time-synchronization for single-ventricle

patient #10 (prospective ECG-gating) and rTOF RV patient #F05 (retrospective ECG-gating, 58% of pulmonary regurgitation), respectively. Figures 3.7 and 3.8 display the original and time-synchronized P-V loops for selected single-ventricle patients and rTOF patients (left and right ventricular data), respectively.

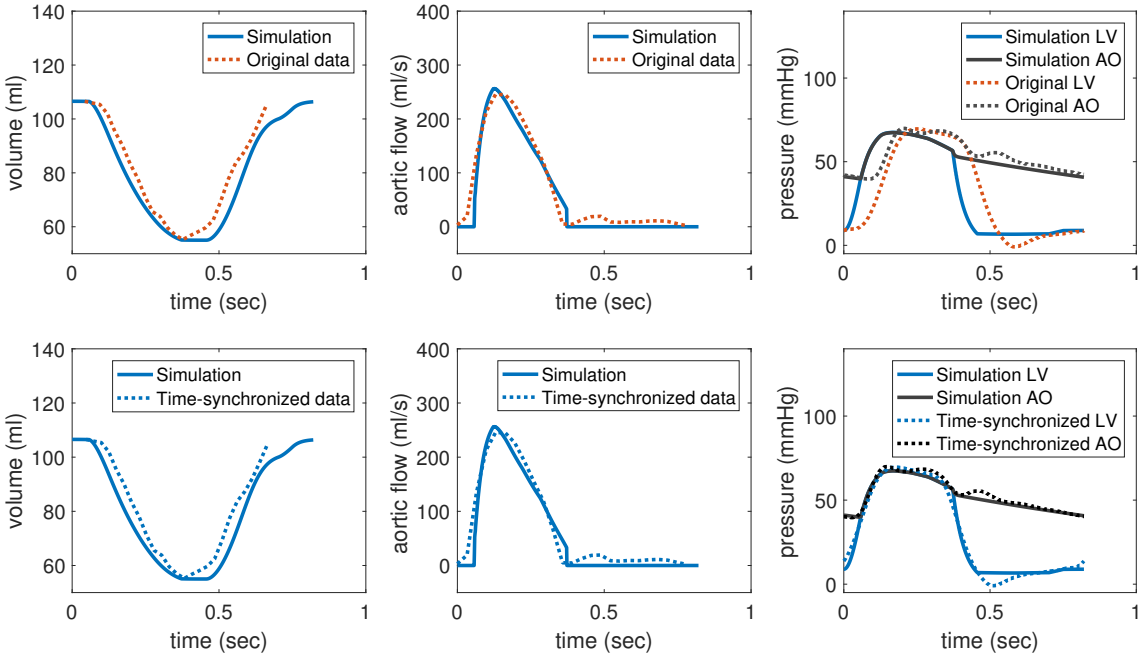

Figure 3.5: Example of measured data plotted together with simulation for single-ventricle patient #10 with prospective ECG-trigger. Top row: model calibration versus original (non-synchronized) data; bottom row: model calibration versus time-synchronized data. LV: left ventricle; AO: aorta.

Figure 3.9 shows the fitted linear regression models for original and time-synchronized signals in single-ventricle patients (panel A), rTOF LV and RV patient datasets (panels B-C). Table 3.1 summarizes statistics of linear regression models presented in Figure 3.9 and p-values of Wilcoxon signed-rank test for the difference between $\max(dE_{\text{orig}}/dt)$ and $\max(dE_{\text{t-syn}}/dt)$. The coefficients of linear regression models for $\max(dE_{\text{orig}}/dt)$ vs. $\max(dE_{\text{t-syn}}/dt)$ were: 1.279 vs. 1.040 in single-ventricle patients; 1.795 vs. 1.126 in rTOF LVs; and 1.615 vs. 1.180 in rTOF RVs. The difference between $\max(dE_{\text{orig}}/dt)$ and $\max(dE_{\text{t-syn}}/dt)$ was significant with p=0.000 in all three groups.

Table 3.1: Statistics for linear regression models of original and time-synchronized (t-syn) data, and a reference linear (ref.) model; and -values of Wilcoxon singed-rank test between original and t-syn data. Coef: regression coefficient; R^2: coefficient of determination; rTOF- LV/-RV: repaired tetralogy of Fallot left/right ventricle, respectively; SE_{coef}: standard error of the coefficient; W: Wilcoxon singed-rank test.

	Single-ventricle		rTOF-LV		rTOF-RV		ref.
	Original	T-syn	Original	T-syn	Original	T-syn	
Coef	1.279	1.040	1.795	1.126	1.615	1.180	1.000
SE_{coef}	0.039	0.012	0.087	0.026	0.064	0.023	0.000
R^2	0.774	0.963	0.626	0.881	0.712	0.912	1.000
W		0.000		0.000		0.000	

Table 3.2 shows the model-derived time offsets of single-ventricle patients at baseline,

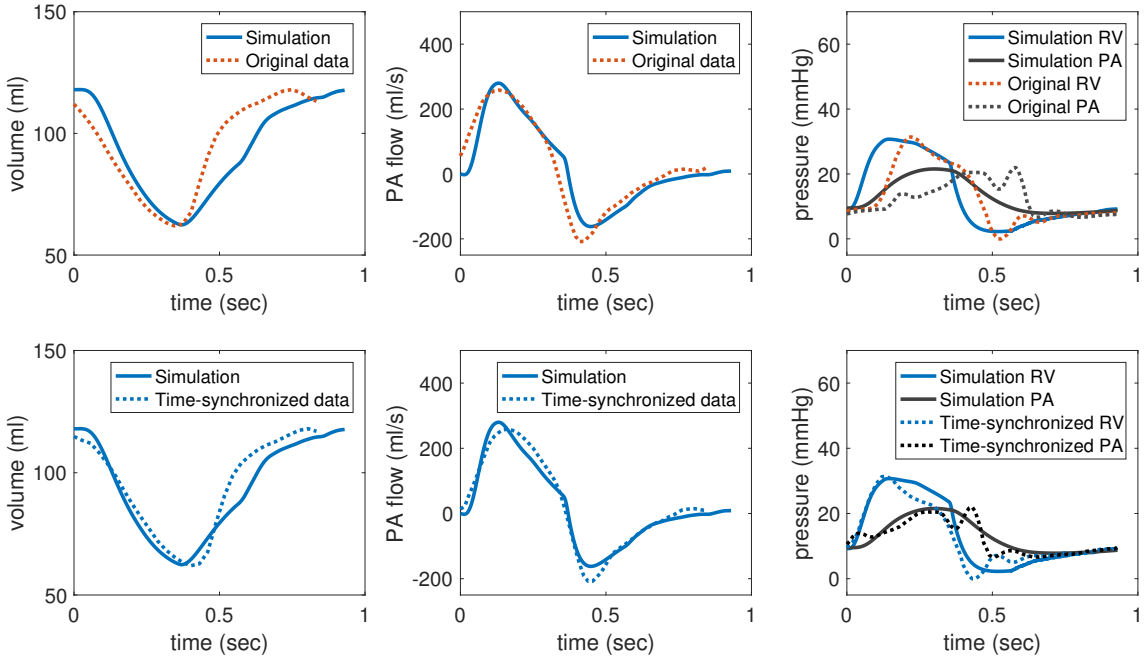

Figure 3.6: Example of measured data plotted together with simulation for right ventricle of rTOF patient #F05, who had pulmonary regurgitation (regurgitation fraction of 58%). Top row: model calibration versus original (non-synchronized) data; bottom row: model calibration versus time-synchronized data. RV: right ventricle; PA: pulmonary artery.

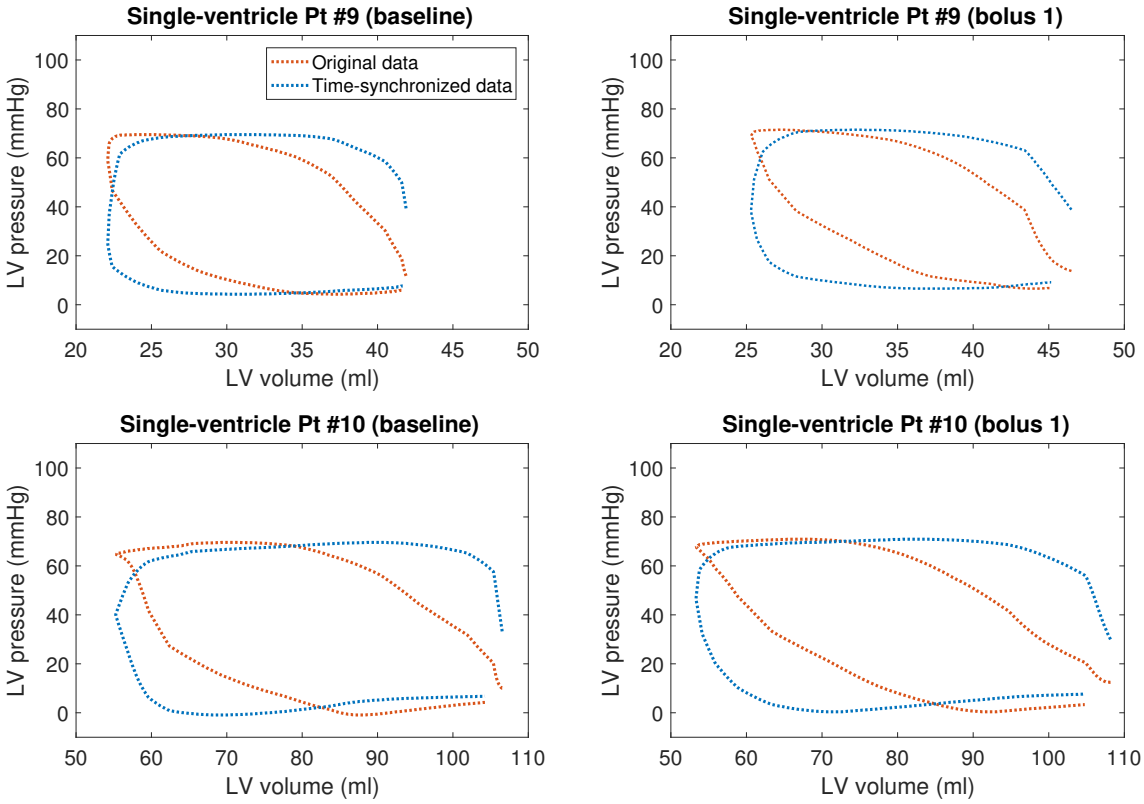

Figure 3.7: Pressure-volume loops for single-ventricle patients #9 and #10 at baseline and after administration of 5ml/kg fluid bolus (bolus 1), CMR is with prospective ECG-trigger.

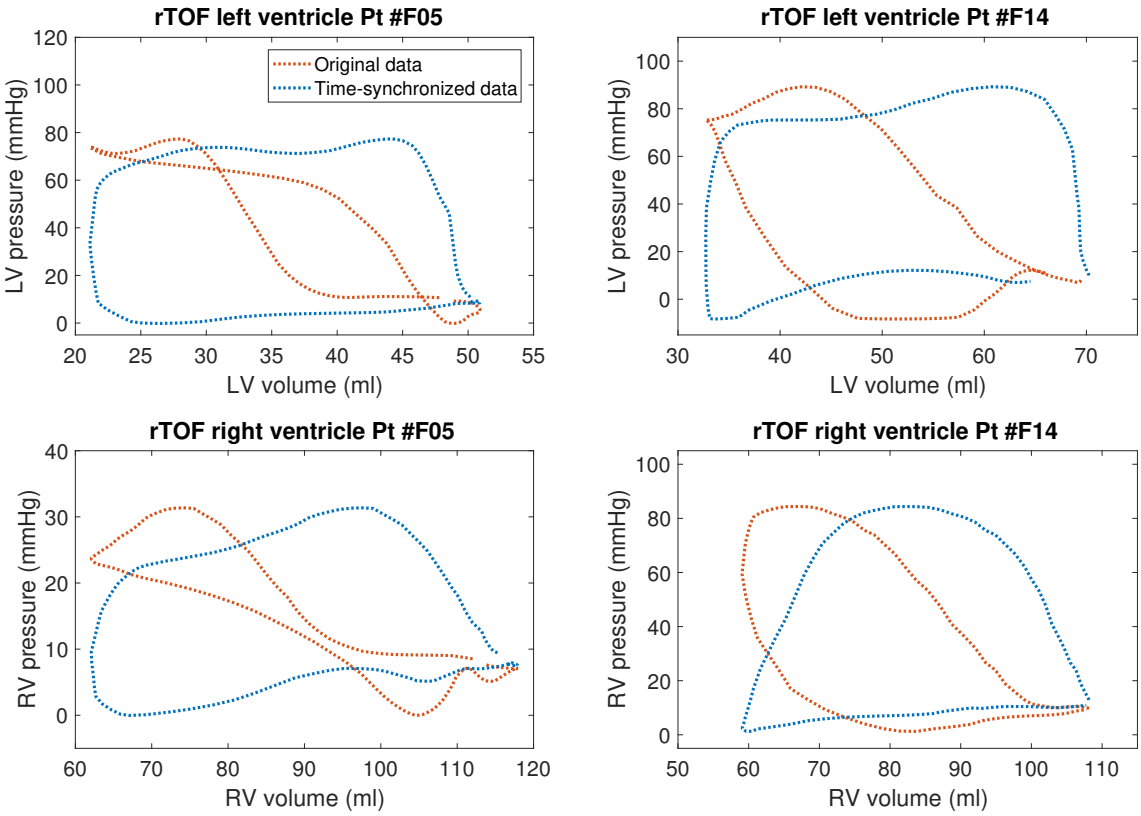

Figure 3.8: Pressure-volume loops for rTOF patients. Patient #F05 right ventricle (RV) contains 58% of pulmonary regurgitation. Patient #F14 RV contains 11% and 30% of tricuspid and pulmonary regurgitation, respectively.

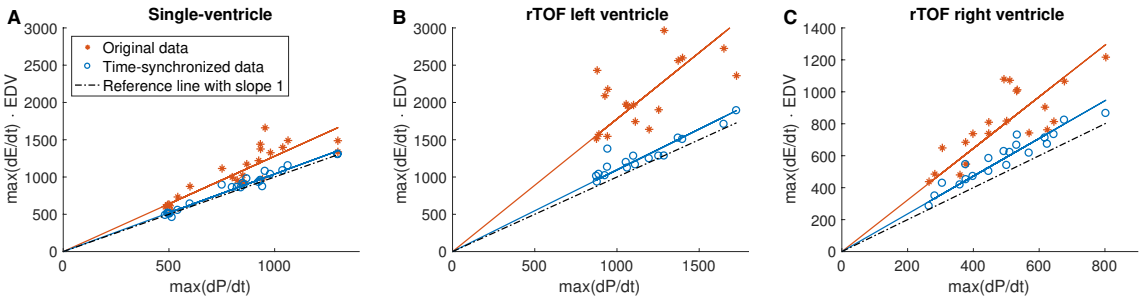

Figure 3.9: Linear regression models for original and time-synchronized data for single-ventricle patients (A), rTOF left venricle (rTOF-LV) (B), and rTOF right ventricle (rTOF-RV) (C). Dotted black line is a reference model with slope equal to 1.

bolus 1 and bolus 2 for prospective cine MRI sequence combined with catherization pressures, and that at baseline for retrospective cine MRI combined with the baseline catherization pressures. Mean (± SD) P-V offsets were 0.054 (± 0.021) s, 0.062 (± 0.026) s, and 0.063 (± 0.018) s in baseline, bolus 1 and 2, respectively (all using prospectively ECG-triggered cine MRI). Mean (± SD) P-V offsets in baseline with retrospective cine MRI were 0.079 (± 0.033) s. Table 3.3 shows the model-derived time offsets of left and right ventricles of rTOF patients, where mean (± SD) P-V offsets were 0.110 (± 0.039) s and 0.116 (± 0.032) s in LV and RV, respectively.

Table 3.2: Model-derived time offsets of pressure-volume data for single-ventricle patients with prospective ECG trigger (prosp) in three bolus conditions: baseline, bolus 1, and bolus 2; and retrospective ECG gating (retro) in baseline. QRSd: QRS duration; HR: heart rate; SD: standard deviation.

	QRSd (s)	HR (bpm)	Time-offsets (pressure-volume) (s)			
			Baseline prosp	Bolus 1 prosp	Bolus 2 prosp	Baseline retro
Pt #1	-	72	0.074	0.081	0.082	-
Pt #2	-	102	0.039	0.055	0.043	0.079
Pt #3	-	93	0.028	-	-	0.061
Pt #4	-	78	0.040	0.040	0.048	0.053
Pt #5	-	103	0.064	0.086	0.080	-
Pt #6	-	85	0.077	0.075	0.060	0.122
Pt #8	0.080	96	0.021	0.005	-	0.041
Pt #9	0.080	82	0.067	0.074	-	0.077
Pt #10	0.091	73	0.080	0.079	-	0.130
Pt #11	0.078	81	0.050	0.064	-	0.091
mean			0.054	0.062	0.063	0.079
SD			0.021	0.026	0.018	0.033

Figure 3.10 shows original and time-synchronized values of $E_{\max}$ and stroke work, where time-synchronized $E_{\max}$ was significantly lower (p=0.00 in all patients) and time-synchronized stroke work was significantly higher (p=0.00 in all patients) compared to those calculated from the original P-V data.

3.4 Discussion

The present study develops a time-synchronization technique for the P-V data by using patient-specific biomechanical models. The fully synchronous pre-clinical dataset allowed to verify the model-based synchronization. A small error in the detected time offset of 2 milliseconds was most likely caused by a slight model-data discrepancy given by: noise or other artifacts in the P-V data (which cannot be completely avoided in any type of data acquisition); and model imperfection (even though in line with biophysical and physiological principles, the model is only a representation of reality). Taking into account the fact that the temporal resolution of cine MRI – the core of presented work – is typically 20-30 ms, the detected offset of 2 ms (i.e. <10 % of temporal resolution) is negligible.

Then, we applied the method on two types of data acquisition protocols: iCMR P-V datasets, in which the pressure is acquired together either with highly-accelerated cine

Table 3.3: Model-derived time offsets for repaired tetralogy of Fallot (rTOF) left and right ventricle patients. CMR: cardiovascular magnetic resonance; Cath: catherization; LV: left ventricle; QRSd: QRS duration; HR: heart rate; RV: right ventricle; SD: standard deviation.

	QRSd (s)	HR (bpm)		Time-offsets (pressure-volume) (s)	
		CMR	Cath	rTOF-LV	rTOF-RV
Pt #F02	0.165	64	61	-	0.079
Pt #F03	0.137	66	63	0.128	0.059
Pt #F04	0.166	58	73	0.118	0.120
Pt #F05	0.158	68	64	0.148	0.130
Pt #F06	0.137	72	85	0.108	0.106
Pt #F07	0.086	70	70	0.061	0.086
Pt #F13	0.126	63	81	0.095	0.107
Pt #F14	0.159	72	85	0.088	0.094
Pt #F16	0.160	68	64	0.098	0.122
Pt #F17	0.089	60	80	-	0.091
Pt #F18	0.165	83	61	0.152	0.113
Pt #F19	0.129	88	87	0.100	0.098
Pt #F20	0.117	93	87	-	0.136
Pt #F21	0.133	81	59	0.098	0.141
Pt #F22	0.147	91	67	0.200	0.199
Pt #AF24	0.163	82	75	0.096	0.101
Pt #AF25	0.129	75	74	0.047	0.127
Pt #AF26	0.096	74	95	0.155	0.153
Pt #AF29	0.146	79	79	0.123	0.165
Pt #AF31	0.129	49	75	0.058	0.095
mean	0.140			0.110	0.116
SD	0.030			0.039	0.032

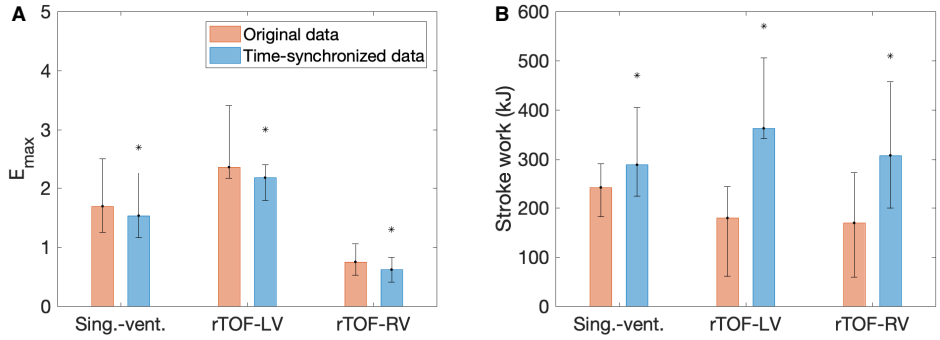

Figure 3.10: Boxplot of original and time-synchronized indices of myocardial function in each patient group. A: maximum values of time-varying elastance ($E_{\max}$). B: stroke work (area encompassed within the pressure-volume loop). Bars correspond to the medians, upper and lower error bars are 75th and 25th percentiles, respectively. Asterisks show significant difference of time-synchronized data with respect to the original at $p<0.05$. rTOF-LV/-RV: repaired tetralogy of Fallot left/right ventricle patients.

MRI using prospective ECG triggering (at baseline and post-fluid bolus), or with standard cine MRI in retrospective ECG gating (at baseline); and P-V data obtained during separate catheterization and CMR sessions (cine MRI in retrospective ECG gating). While the patients with single ventricles underwent the iCMR procedures, the sequential pressure catheter and CMR exam were performed for the patients with rTOF. Figures 3.7 and 3.8 demonstrate that the proposed time-synchronization qualitatively improves the shapes of P-V loops in both single-ventricle and rTOF patients. Figure 3.9 shows that the time-synchronization changes the slope of the relationship between $\max(dE_{\mathrm{t-syn}}/dt)\cdot EDV$ and $\max(dP_{\mathrm{t-syn}}/dt)$ closer to the reference linear model with the slope of 1. Furthermore, the time-synchronization decreases the variance of $\max(dE_{\mathrm{t-syn}}/dt)$ with respect to $\max(dP_{\mathrm{t-syn}}/dt)$ with R^2 >0.93 in all three groups and consequently shifts the original time-varying elastance to its more physiologically meaningful relationship. The time-synchronized value of maximum time-varying elastance ($E_{\max}$) could be later used as a surrogate measure of ventricular mechanical performance. Note that in rTOF patients in both LVs and RVs the slope of time-synchronized linear regression is above 1 by 13% and 18%, respectively. This could be due to the volumes acquired 3-4 months prior to the catheterization causing an underestimation of EDV with respect to the pressure signals. RVs, and to a lesser extent LVs, of rTOF patients undergo progressive remodeling (dilatation of the chamber and/or thickening of the myocardial wall) until the pressure is measured during the percutaneous PVR [25]. The relationship between $\max(dE/dt)\cdot EDV$ and $\max(dP/dt)$ (Eq. (3.6)) assumes constant EDV during isovolumic contraction. Some RVs in our cohort have a mild level of tricuspid valve regurgitation causing an imperfect isovolumic contraction. Therefore, the EDV variability is more prominent in the RVs than in LVs of the rTOF patients in our study. Since the tricuspid regurgitation is mild, we find this correlation reliable.

The model-detected P-V time offsets vary both between the patients and within individual datasets (e.g. between bolus conditions, or rTOF LV and RV datasets. Such a variability demonstrates that the image acquisition – with P-V synchronously measured or not – is subjected to time-synchronization errors and that those errors appear to be different during every new acquisition. In single-ventricle patients with cine MRI acquired with prospective ECG-trigger the time offsets are of the order of 2-3 MRI time frames (Table 3.2). In single-ventricle patients at baseline when the additional retrospectively ECG-gated cine MRI were combined with pressures, the offsets became 3-4 cine MRI time frames. In

rTOF patients the offsets are of the order of 3-5 frames (Table 3.3). The pathologically long QRS duration was observed in rTOF patients, mean (± SD) QRSd is 0.137 (± 0.025) s, which could have increased the uncertainty in detecting the R-peak by the MR scanner. Also, errors associated with the temporal interpolation when reconstructing from the retrospectively ECG-gated sequence could have increased the P-V offset. Our study therefore confirms that when combining intraventricular catherization and CMR procedures, the temporal errors in P-V signals are associated with CMR acquisition and reconstruction techniques. In particular, temporal resolution, the type of ECG trigger / gating (prospective vs. retrospective), averaging over hundreds of cycles, and detection of R-peak from a wide QRS complex might have contributed to the detected P-V offsets in the studied datasets. This also substantiate developing a universal model-based time-synchronization.

The multiscale biomechanical model employed in this work has been previously used in a number of patient-specific applications, e.g. in planning of cardiac resynchronization therapy [26]. The model was also directly coupled with in vivo cine MRI via data assimilation [27]. These works demonstrate its compatibility with real cardiology data, including physiologically relevant timings of cardiac phases. We acknowledge that alternative cardiac models with adequate representation of P-V changes could be employed for the proposed synchronization method. The advantage of using physiologically compatible cardiac models, e.g. [15; 28], is that such models can be coupled with datasets with complex hemodynamics. The model could represent inflow and/or outflow valve mechanics, such as valvular regurgitation and/or stenosis [14; 29] and account for the mechanics of circulatory system such as pulmonary/systemic vasoconstriction in pulmonary/systemic hypertension. Figure 3.8 (bottom row) demonstrates the effect of tricuspid and pulmonary regurgitation on the shape of RV P-V loops in rTOF patients. The regurgitation on either valve suppresses the corresponding isovolumic phases. This would limit the ability to time-synchronize such datasets, if the criterion for the time synchronization was solely the constant ventricular volume during the isovolumic phases. The proposed time-synchronization template provided by the model is a solution suitable even in patients with valvular pathologies.

We remark that, furthermore, the biophysical model (thanks to the predictive capability) substitutes for the missing part of the cardiac cycle, as can be seen in the time-volume plots acquired by cine MRI in prospective ECG trigger (Figure 3.5 left). We also appreciate that the model used for this study was demonstrated to be easily deployed in clinical environment and directly used by physicians [5; 13; 30]. The proposed time-synchronization method is not limited neither to the presented data acquisition protocols nor to the P-V signals themselves, and could be utilized in a variety of clinical scenarios, e.g. when catherization is combined with transthoracic echocardiography [5], or to synchronize aortic pressure-flow loops [31].

The study demonstrates that time-synchronization of P-V data yields a more physiological relationship of TVE where the time-synchronized value of $E_{\max}$ is significantly lower than the non-synchronized one. Suga et al. demonstrated in [22] on invasive data from canine hearts that the maximum value of ventricular TVE ($E_{\max}$) is a load independent measure of ventricular contractility. Subsequent studies consistently showed its applicability across species (e.g. in pigs [32] or human patients [33; 34]. Therefore, the maximum value of TVE is commonly used as a surrogate measure of myocardial contractility [2; 35], and the time-synchronization of P-V data is therefore crucial for an accurate and reproducible detailed assessment of the ventricular systolic function. Finally, Figure 3.10 shows a significant difference between the stroke work between synchronized and non-synchronized data. The plot demonstrates the need of synchronizing the data to derive correct values of important quantities of ventricular energetics. While the actual ground truth is not known, the indirect evidence by the elastance-derived metrics and the qualitative amelioration of

the P-V loops, gave a confidence to our method of data synchronization.

While the biomechanical model was used in this work only to synchronize the measured P-V data, the model itself has a physiological significance and could provide additional information of clinical interest. The high-quality PV-loops can therefore be combined e.g. with physiological parameters of myocardial contractility, periphery vascular resistance or ventriculo-arterial coupling [5; 13; 14], to give some examples.

3.4.1 Limitations

There are a number of limitations of the study. First of all, CMR and pressure catheter exams do not provide the ground truth measurement of P-V loop. This is why we employed a metrics based on time-varying elastance and demonstrated that the proposed time synchronization is significantly ameliorating the P-V loop, as is reflected by this measure commonly used in cardiac physiology. We used only one fully synchronous dataset obtained by the conductance to verify our approach. However, the synchronicity of simulated pressure and volume of our physiologically and biophysically based model was validated in our previous clinical studies: with full 3D model [26] and with reduced-order model [5; 13; 14]. We also name the limitation of this small-scale study being a single-observer only.

3.4.2 Conclusion

Clinical scenarios that necessitate high-quality P-V loops for the therapy planning can benefit from the proposed model-based time-synchronization of P-V signals. The modeling framework is fast in computation time and can be directly employed in clinical settings. The method is universal for the variety of P-V data acquisition protocols and pathologies. It is efficient for both simultaneously and sequentially acquired cine MRI and pressure data, i.e. it makes the use of P-V loops available to all centers and not only to those with dedicated and costly pressure and conductance catheter simultaneous P-V loop systems. It could be also adapted to other imaging protocols (e.g. echocardiography, or dynamic CT) combined with catherization data. In conclusion, the proposed method applies the model to contribute to the planning of complex interventions and, thanks to the biophysical and physiological background of the models, it can consequently augment the possibilities of the optimal clinical management.

3.5 Appendix 1: Extended research letter to editor

Time-synchronization of interventional cardiovascular magnetic resonance data using a biomechanical model for pressure-volume loop analysis

Maria Gusseva[a,b], Daniel A. Castellanos[c], Joshua S. Greer[d], Mohamed Abdelghafar Hussein[d,e], Keren Hasbani[f], Gerald Greil[d], Surendranath R. Veeram Reddy[d], Tarique Hussain[d], Dominique Chapelle[a,b], Radomír Chabiniok[a,b,d,g]

[a]Inria, Palaiseau, France
[b]LMS, Ecole Polytechnique, CNRS, Institut Polytechnique de Paris, Palaiseau, France
[c]Department of Cardiology, Boston Children's Hospital, Boston, MA, USA
[d]Division of Pediatric Cardiology, Department of Pediatrics, UT Southwestern Medical Center, Dallas, TX
[e]Pediatric department, Kafrelsheikh University, Kafr Elsheikh, Egypt
[f]Division of Pediatric Cardiology, Department of Pediatrics, Dell Medical School, UT Austin, TX
[g]Department of Mathematics, Faculty of Nuclear Sciences and Physical Engineering, Czech Technical University in Prague, Prague, Czech Republic

Accepted to the Journal of Magnetic Resonance Imaging (2022),
https://doi.org/10.1002/jmri.28216

3.5.1 Introduction

Pressure-volume loops (PV loops) provide a meaningful insights into myocardial energetics [6; 7]. Pressure-volume (P-V) data is often acquired by different modalities and subject to time-synchronization errors yielding skewed shapes of PV diagrams (Figure 3.11 (A)). A temporal dyssynchrony could be associated with cardiac magnetic resonance imaging (MRI) acquisition and reconstruction techniques: the temporal resolution of the scanner, the type of ECG trigger / gating (prospective vs. retrospective), averaging over cardiac cycles, and detection of R-peak from a wide QRS complex [9]. In addition, some delays could arise from the inertia effect of the fluid-filled catheter that varies depending on the catheter type and size [8].

A complete synchronization of the P-V signals is possible when using an intraventricular conductance catheter. In other settings, a manual delineation of the isovolumic phases may be performed. However, such an approach can be suboptimal, e.g. in patients with valvular regurgitation due to the absence of clear isovolumic phases. We aim to develop a time-synchronization technique that is independent of the data acquisition methods or patients' pathophysiology by using patient-specific biomechanical model derived waveforms to detect P-V offsets in the measured data. Our previous study demonstrated the potential of such an approach on P-V data acquired sequentially (volumetric data during cardiac MRI followed by pressure data during cardiac catheterization) without valvular regurgitation [9]. In the present study we aim to extend the method for simultaneously acquired P-V data

(i.e. during interventional cardiac MRI) and for patients with pulmonary regurgitation (i.e. right ventricles of patients with repaired tetralogy of Fallot, rTOF).

3.5.2 Methods

3.5.2.1 Data

Datasets from two groups of patients were included in the study. The first group contained 10 patients with single-ventricle physiology undergoing interventional cardiac MRI within the pre-Fontan assessment. P-V were acquired simultaneously at baseline and immediately after fluid administration providing 24 P-V datasets. Fluid boluses were administered either as a single 5 ml/kg bolus or as two 2.5 ml/kg boluses. A highly-accelerated prospective ECG-triggered cine bSSFP sequence (kt-BLAST factor 5, partial Fourier 0.625, slice thickness 10 mm, spatial resolution 2.4 x 2.4 x 10 mm) was used. Another group contained patients with rTOF with 17 left and 20 right ventricular P-V datasets (rTOF-LV and rTOF-RV, respectively). A retrospective ECG-gated cine bSSFP sequence (SENSE 2, spatial resolution 2 x 2 x 10 mm) was used. Catheter pressures were sequentially acquired during pulmonary valve replacement therapy. Temporal resolution was 30 ms in both groups and all acquisitions. A motion tracking algorithm [11] was used to obtain time-vs.-volume signals from cardiac MRI.

3.5.2.2 Biomechanical heart model

We employed a biomechanical heart model of a single heart cavity where the geometry and kinematics of the ventricle are represented by sphere [12] with constitutive mechanical laws describing active (contractile) and passive (viscoelastic) behavior of the myocardium. To model a cardiac cycle in patient-specific manner model parameters were tuned such that simulated waveforms corresponded to the maximum and minimum pressure and volume for a given patient (see e.g. [13]).

3.5.2.3 Time synchronization

The model was used as a template for temporal synchronization of original P-V data. We assumed that synchronicity of simulated P-V traces is given by the biophysical and physiological formulation of the model. We minimized the distance between data and model waveforms (Figure 3.11 (B)) to detect the corresponding time offsets for $t_{\text{offset}}^{\text{pressure}}$ and $t_{\text{offset}}^{\text{volume}}$:

$$\min_{t_{\text{offset}}} \int_0^{t_{\text{end}}} (f(t) - g(t - t_{\text{offset}}))^2 dt, \tag{3.7}$$

where $f(t)$ and $g(t)$ are the simulated and original ventricular pressure or volume, respectively; t_{end} is the end of the cardiac cycle in the original data. Total P-V time offset was given by:

$$t_{\text{offset}}^{\text{P-V}} = abs(t_{\text{offset}}^{\text{pressure}} - t_{\text{offset}}^{\text{volume}}) \cdot \tag{3.8}$$

PV loops were constructed for original and time-synchronized (t-syn) data. Quantitative evaluation of t-syn traces was derived from time-varying elastance (TVE). TVE [22], defined as $E(t) = P(t)/V(t)$, was computed from original and t-syn data, where $P(t)$ and $V(t)$ are ventricular pressures and volumes, respectively. According to TVE the isovolumic phase could be described as [24; 23]:

$$\max(dP/dt) = \max(dE/dt) \cdot EDV, \tag{3.9}$$

where $\max(dP/dt)$ and $\max(dE/dt)$ are maximum time derivatives of ventricular pressure and elastance, respectively, end-diastolic volume (EDV) is assumed to be constant during isovolumic contraction. We confronted $\max(dE/dt)$ derived from original and t-syn data ($\max(E_{\mathrm{orig}}/dt)$ and $max(E_{\mathrm{t-syn}}/dt)$, respectively) with respect to the $\max(dP/dt)$ of the original pressure waveforms via linear regression analysis. Note that $\max(dP/dt)$ does not change with time-synchronization.

Finally, the original, t-syn and model-derived values of maximum TVE (i.e. $E_{\max} = \max[P(t)/V(t)]$), and stroke work (i.e. area encompassed within the PV loop) were computed for each patient and statistically compared with Wilcoxon signed rank test at $p < 0.05$.

3.5.3 Results

Figure 3.11 (D-F) shows t-syn PV loops for selected patients from all groups. The slope coefficients of linear regressions models ($Coef$) of $\max(dE_{\mathrm{orig}}/dt)$ vs. $\max(dE_{\mathrm{t-syn}}/dt)$ in single-ventricle patients were 1.279 vs. 1.040; in rTOF LVs 1.795 vs. 1.126; and in rTOF RVs 1.615 vs. 1.180 (Figure 3.12).

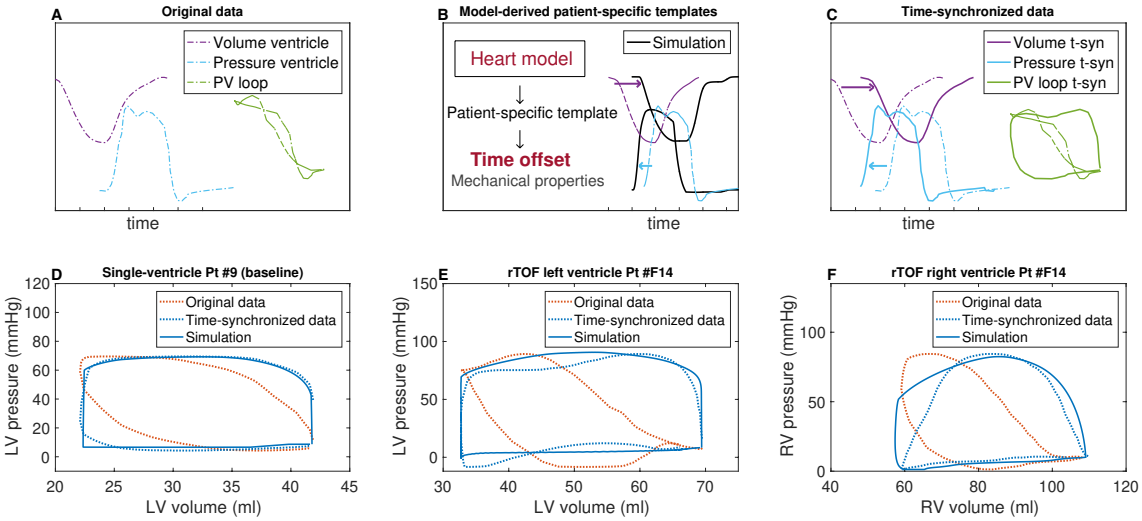

Figure 3.11: Model-assisted time-synchronization of clinical pressure-volume data. A: Distorted pressure-volume loop (PV loop) due to the time offset between the acquired pressure and volume data illustrated on rTOF left ventricle Pt #AF24 from our study. B: Detection of the time offset by using patient-specific biomechanical model, simulating synchronous pressure and volume waveforms. C: Corrected PV loop (solid line) reconstructed from the time-synchronized (t-syn) data D: PV loops for single-ventricle patient #9 at baseline (cine MRI is prospectively ECG-triggered). E-F: PV loops for rTOF patient left and right ventricles (rTOF-LV and -RV, respectively), rTOF-RV Pt #F14 contains 11% and 30% of tricuspid and pulmonary regurgitation, respectively.

Mean (± SD) model-derived P-V offsets of single-ventricle patients were 0.059 (± 0.022) s; of rTOF-LVs and rTOF-RVs 0.110 (± 0.039) s and 0.116 (± 0.032) s, respectively.

T-syn vs. original $E_{\max}$ ($p = 0.000$) and stroke work ($p = 0.000$) were significantly lower in all patients. The difference for model-derived vs. time-synchronized (1) $E_{\max}$ was not significant in all three groups ($p > 0.050$ in all patients), (2) stroke work was not significant for single-ventricle and rTOF LV ($p > 0.050$ in both groups) and significant for rTOF RV patients ($p = 0.000$), Figure 3.13.

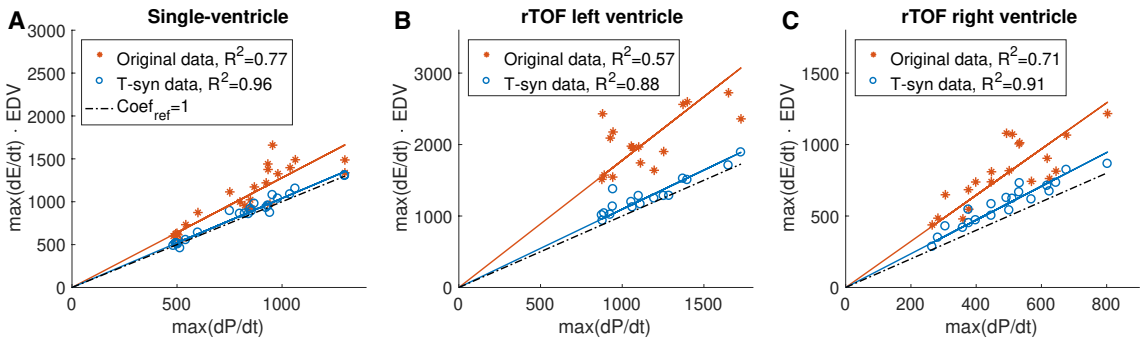

Figure 3.12: Linear regression models for original and time-synchronized (t-syn) data for single-ventricle patients (A), rTOF left ventricle (B), and rTOF right ventricle (C). Dotted black line is a reference linear model with slope ($Coef_{\mathrm{ref}}$) equal to 1. R^2: coefficients of determination of linear regression models.

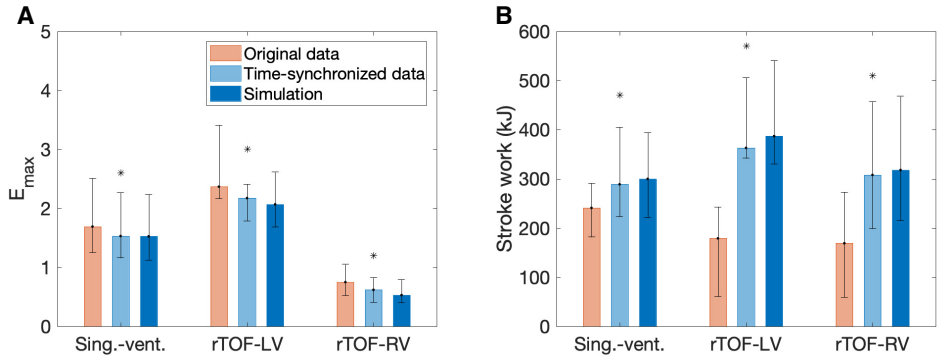

Figure 3.13: Boxplot of original and time-synchronized indices of myocardial function in each patient group. A: maximum values of time-varying elastance (E_{max}). B: stroke work (area encompassed within the pressure-volume loop). Bars correspond to the medians, upper and lower error bars are 75th and 25th percentiles, respectively. Asterisks show significant difference of time-synchronized data with respect to the original at $p < 0.05$. rTOF-LV/-RV: repaired tetralogy of Fallot left/right ventricle patients, respectively.

3.5.4 Discussion

We developed a biomechanical model-assisted time-synchronization technique for clinical P-V data. Time-synchronization qualitatively improves the shapes of PV loops in all patients. Quantitative improvement of t-syn data was demonstrated via stronger TVE relationship during isovolumic phase. In addition to that t-syn values of E_{max} and stroke work were significantly different from the non-synchronized ones. Therefore, time-synchronization of P-V data is crucial to derive meaningful values for ventricular energetics.

This model can replace noisy data traces, thus overcoming errors associated with data acquisition and/or processing protocols (e.g. missing part of the cardiac cycle, noise in the data, or non-physiological over-/undershoot in pressure measurements).

Acknowledgments

We would like to acknowledge Dr Philippe Moireau, Inria research team MΞDISIM, for the development of the cardiac simulation software CardiacLab used in this work.

Grant Support

This work was supported by the Inria-UTSW Associated Team TOFMOD. It was also funded from by the W. B. & Ellen Gordon Stuart Trust, The Communities Foundation of Texas and by the Pogue Family Distinguished Chair (award to Dr F. Gerald Greil in February, 2015). The work was in addition supported by the Ministry of Health of the Czech Republic [NV19-08-00071]. Research reported in this publication was supported by Children's HealthSM, but the content is solely the responsibility of the authors and does not necessarily represent the official views of Children's Health^{SM}.

Ethics approval and consent to participate

The data collections for single-ventricle patients were performed under the ethical approvals of the Institutional Review Boards of UT Southwestern Medical Center Dallas (STU 032017-061). The data collections for rTOF patients were performed under the ethical approvals of the Institutional Review Boards of UT Southwestern Medical Center Dallas (STU-2020-0023) and UT Austin (IRB 2020-06-0128). The IRBs waived the need for a consent to use the anonymized retrospective data.

3.6 Appendix 2: Conference proceeding of Functional Imaging and Modeling of Heart FIMH 2021

Model-assisted time-synchronization of cardiac MR image and catheter pressure data

Maria Gusseva[1,2],Joshua S. Greer[3], Daniel A. Castellanos[3,4], Mohamed Abdelghafar Hussein[3,5], Gerald Greil[3], Surendranath R. Veeram Reddy[3], Tarique Hussain[3], Dominique Chapelle[1,2], Radomír Chabiniok[1,2,3,6]

[1]Inria, Palaiseau, France
[2]LMS, Ecole Polytechnique, CNRS, Institut Polytechnique de Paris, Palaiseau, France
[3]Division of Pediatric Cardiology, Department of Pediatrics, UT Southwestern Medical Center, Dallas, TX
[4]Department of Cardiology, Boston Children's Hospital, Boston, MA, USA
[5]Pediatric department, Kafrelsheikh University, Kafr Elsheikh, Egypt
[6]Department of Mathematics, Faculty of Nuclear Sciences and Physical Engineering, Czech Technical University in Prague, Prague, Czech Republic

FIMH2021, doi.org/10.1007/978-3-030-78710-3_35

Abstract

When combining cardiovascular magnetic resonance imaging (CMR) with pressure catheter measurements, the acquired image and pressure data need to be synchronized in time. The time offset between the image and pressure data depends on a number of factors, such as the type and settings of the MR sequence, duration and shape of QRS complex or the type of catheter, and cannot be typically estimated beforehand. In the present work we propose using a biophysical heart model to synchronize the left ventricular (LV) pressure and volume (P-V) data. Ten patients, who underwent CMR and LV catheterization, were included. A biophysical model of reduced geometrical complexity with physiologically substantiated timing of each phase of the cardiac cycle was first adjusted to individual patients using basic morphological and functional indicators. The pressure and volume waveforms simulated by the patient-specific models were then used as templates to detect the time offset between the acquired ventricular pressure and volume waveforms. Time-varying ventricular elastance was derived from clinical data both as originally acquired as well as when time-synchronized, and normalized with respect to end-systolic time and maximum elastance value ($E^N_{\text{orig}}(t)$, $E^N_{\text{t-syn}}(t)$, respectively). $E^N_{\text{t-syn}}(t)$ was significantly closer to the experimentally obtained $E^N_{\text{exp}}(t)$ published in the literature ($p<0.05$, L^2 norm). The work concludes that the model-driven time-synchronization of P-V data obtained by catheter measurement and CMR allows to generate high quality P-V loops, which can then be used for clinical interpretation.

Keywords— interventional cardiovascular magnetic resonance imaging, cardiovascular modeling, time-synchronization of clinical data, pressure-volume loops, personalized medicine, translational research

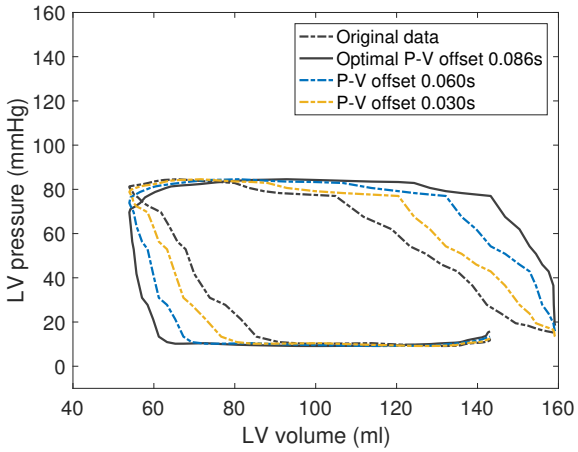

Figure 3.14: Illustration of the pressure-volume (P-V) offsets on the shape of the P-V loop in the measured data.

3.6.1 Introduction

The analysis of intraventricular pressure-volume (P-V) loops contributes to the detailed assessment of the heart function and can be employed when planning a complex intervention. Combining the catheter pressure measurement with cardiovascular magnetic resonance imaging (CMR) yields rich morphological and functional datasets of the current state of patients' pathology. However, the recorded ventricular pressures and volumes are often not precisely synchronous, even during a simultaneous acquisition, which affects the shape of the P-V loop (see Fig. 3.14). There are three principal reasons for this P-V dyssynchrony:

I Data of cine MRI are obtained over a number of cardiac cycles and the reconstructed time-volume plot therefore represents an average cycle during the acquisition.

II The detection of R-peak in the strong magnetic field of MRI is known to be challenging, particularly in patients with a pathological QRS complex in whom the S wave or R' wave (e.g. in some right bundle branch block patients) may be detected instead. This leads into the time offset up to the QRS duration.

III The fluid-filled catheter is known to record the pressure changes with some delay, which varies depending e.g. on the catheter size.

The time offset caused by these points varies among the patients and practically cannot be predicted beforehand. In this work we propose to create biophysical models of a reduced complexity using the patient-specific information of the maximum and minimum ventricular volume and pressure provided by the CMR and catheter data. These models will then be used as a template for the time-synchronization of the measured P-V data (see the pipeline depicted in Fig. 3.15). Qualitative assessment will be carried out by plotting the P-V loops using the original and the time-synchronized pressure and volume waveforms. The quantitative comparison will be performed by comparing the generated ventricular time-varying elastance functions with the experimentally obtained time-varying elastance published by Suga et al. [22]. Furthermore, some functional characteristics of the cardiovascular system not directly visible in the data can be obtained thanks to using a patient-specific biophysical model.

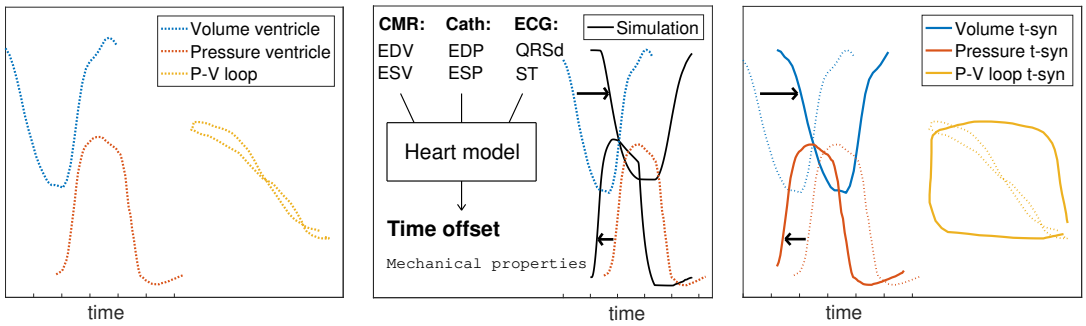

(a) Original data (b) Patient-specific model (c) Time-synchronizion

Figure 3.15: Time-synchronization pipeline. (a) Original pressure-volume (P-V) data; (b) Patient-specific time offset detected by the model (black arrows); (c) Time offset detected in (b) applied on original P-V data in (a) to obtain time-synchronized (t-syn) P-V data (solid lines). ED/ESV: end-diastolic/-systolic volumes (ventricle); ED/ESP: end-diastolic/-systolic pressures (ventricle); ECG: electrocardiogram timings.

3.6.2 Methods

3.6.2.1 Data

Datasets of left ventricles of ten patients with repaired tetralogy of Fallot (rTOF) were included in the study. The data collections were performed under the ethical approvals of the Institutional Review Board of UT Southwestern Medical Center Dallas (STU-2020-0023). The IRB waived the need for a consent to use the anonymized retrospective data. Cine MRI data with retrospective ECG gating (with parallel factor SENSE=2, temporal resolution ∼30 ms) covering both ventricles and phase-contrast flow through the aortic valve were acquired. The ventricular volumes from cine MRI were obtained using the CVI42 software (Circle Cardiovascular Imaging Inc., Calgary, Canada) combined with the motion tracking algorithm of [10]. The catherization was performed in a separate session after CMR. A left-heart cathether was advanced into aorta and left ventricle, where the pressures were recorded during a breath-hold.

3.6.2.2 Biophysical heart model

A reduced-complexity biomechanical model of left ventricle (LV) and systemic circulation was employed [12]. The schematics of the model is depicted in Fig. 3.16. The geometry and kinematics of the ventricle are reduced to a sphere with an inner radius R and a wall thickness d, while the constitutive mechanical laws are preserved as in the full 3D heart model [15; 19]. The mechanical behavior of the myocardium is described by a rheological model of Hill-Maxwell type [36] that contains an active contractile component (actin-myosin complex) and a visco-elastic component (collagen-rich elements in the surrounding connective tissue). The active component is represented within Huxley's sliding filament theory [17; 18]. All myosin filaments in the sarcomere unit are considered as a series of springs, with active stress (τ_c) and active stiffness (k_c) produced for sarcomere extension (e_{fib}) given by, see [15]:

$$\begin{cases} \dot{k}_c = -(|u| + \alpha|\dot{e}_{\text{fib}}|)k_c + n_0(e_{\text{fib}})k_0|u|_+ \\ \dot{\tau}_c = -(|u| + \alpha|\dot{e}_{\text{fib}}|)\tau_c + \dot{e}_{\text{fib}}k_c + n_0(e_{\text{fib}})\sigma_0|u|_+, \end{cases} \tag{3.10}$$

where $u(t)$ is an electrical activation function representing intracellular calcium kinetics that induces contraction (when $u > 0$) or relaxation ($u < 0$) of the myocardium (Fig. 3.16b).

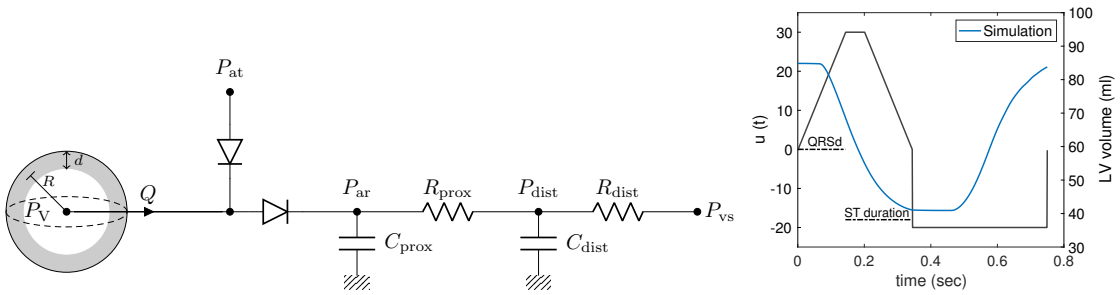

(a) Biomechanical model (b) Activation function

Figure 3.16: (a) Coupling of the heart with atrioventricular and arterial valves via system of diodes and with circulation system represented by a two-stage Windkessel model. $P_{at}, P_V P_{ar}, P_{dist}, P_{vs}$ stand for pressures in left atrium, left ventricle, aorta, distal systemic circulation and venous system; $R_{prox}, C_{prox}, R_{dist}, C_{dist}$ are proximal and distal resistances and capacitances in Windkessel model; (b) Electrical activation function $u(t)$ (black line) with imposed timings of duration of QRS and ST segment from electrocardiogram measurements.

The parameter α is a bridge destruction rate upon rapid change in length in the sarcomere [15]. The parameter σ_0 is the active stress developed by the sarcomere during systole under optimal extension e_{fib}, and $n_0(e_{\text{fib}}) \in [0, 1]$ represents the Frank-Starling law [15]. The parameter σ_0 will be further referred to as the contractility.

The model was turned into patient-specific regime according to the sequential calibration procedure described in [5]. Briefly, the 2-stage Windkessel model was adjusted by imposing the flow measured by phase-contrast MRI aiming to match the maximum and minimum aortic pressure and the pressure at the dicrotic notch. Then, the LV wall thickness and the ventricular volume were prescribed according to the cine MRI. The model stress-free configuration was assumed as in the experimental data of [21]. The ventricular preload was prescribed from the measured end-diastolic ventricular pressure. Passive myocardial properties were calibrated to match the measured end-diastolic volume under imposed preload. Myocardial contractility was adjusted to match the measured stroke volume. Patient-specific parameters adjusted during this process, therefore were in the Windkessel model: distal and proximal resistances of the circulation, distal capacitance of the circulation; in the heart model: myocardial stiffness and contractility. Ventricular stroke work was calculated as the area encompassed within the model-derived P-V loop.

3.6.2.3 Time-synchronization

Thanks to the biophysical and physiological character of the model, the timing of the cardiac phases was considered as a reference. The simulated waveforms were therefore used as templates to time-synchronize the original data to find an optimal time offset t_{offset} between the measured data and the model, minimizing the criterion:

$$\min_{t_{\text{offset}}} \int_0^{t_{\text{ES}}} (f(t) - g(t - t_{\text{offset}}))^2 dt, \tag{3.11}$$

where $f(t)$ represents the simulated LV pressure or volume; $g(t)$ represents the measured ventricular pressure (volume); t_{ES} is the time of end-systole in the data.

The P-V loops were constructed by using both original and time-synchronized waveforms. Time-varying elastance was computed for the original and time-synchronized data as:

$$E_{\text{orig/t-syn}}(t) = \frac{P_{\text{orig/t-syn}}(t)}{V_{\text{orig/t-syn}}(t)}, \tag{3.12}$$

Table 3.5: Model-derived time offsets and biophysical parameters. QRSd: QRS duration; MRI: magnetic resonance imaging; Cath: catherization; R_{dist}: distal resistance of the circulation.

		Heart rate		Time offsets	Mechanical indicators		
	QRSd	MRI	Cath	Pressure-volume	Contractility	Stroke work	R_{dist}
	s	bpm	bpm	s	kPa	mJ	$\times 10^8$Pa $\times$ s/m^3
Pt #1	0.089	70	74	0.081	95	698	1.05
Pt #2	0.165	83	61	0.142	85	853	0.52
Pt #3	0.129	88	87	0.139	86	367	1.55
Pt #4	0.133	81	59	0.098	100	893	0.85
Pt #5	0.147	91	67	0.139	73	467	1.60
Pt #6	0.163	82	75	0.120	73	462	1.40
Pt #7	0.129	75	74	0.106	67	445	0.90
Pt #8	0.096	74	95	0.161	56	304	1.10
Pt #9	0.146	79	79	0.158	48	328	1.30
Pt #10	0.129	49	75	0.086	80	907	0.54

where $P_{\text{orig/t-syn}}(t)$, $V_{\text{orig/t-syn}}(t)$ are LV pressures and volumes as originally measured / time-synchronized. The time-varying elastances were then double-normalized in time (with respect to the end-systolic time t_{ES}) and with respect to the maximal elastance value, as in Suga et al. [22]:

$$E^N(\bar{t}) = \frac{E(\bar{t} \cdot t_{\text{ES}})}{\max(E)}. \tag{3.13}$$

3.6.2.4 Statistical analysis

The distances between the normalized time-varying elastance obtained from the original, time-synchronized data, respectively (E^N_{orig}, $E^N_{\text{t-syn}}$, respectively) and the experimentally obtained E^N_{exp} (by Suga et al. [22]) were compared using the L^2 norm over the whole cardiac cycle, i.e. relative distance RD is given by

$$\text{RD}(E^N_{\text{orig/t-syn}}, E^N_{\text{exp}}) = \frac{||E^N_{\text{orig/t-syn}} - E^N_{\text{exp}}||_{L^2}}{||E^N_{\text{exp}}||_{L^2}}. \tag{3.14}$$

Wilcoxon signed-rank tests at $p<0.05$ were conducted to assess the difference between $\text{RD}(E^N_{\text{orig}}, E^N_{\text{exp}})$ and $\text{RD}(E^N_{\text{t-syn}}, E^N_{\text{exp}})$.

3.6.3 Results

Fig. 3.17 shows an example of the patient-specific model and the model-based time-synchronization for Patient #6. Fig. 3.18 displays P-V loops for selected patients, while using original or time-synchronized pressure and volume waveforms. Fig. 3.19(a) shows for patient #6 $E^N_{\text{orig/t-syn}}(\bar{t})$ (original and time-synchronized data, respectively), in comparison with the experimentally obtained $E^N_{\text{exp}}(\bar{t})$. Median $\text{RD}(E^N_{\text{orig}}, E^N_{\text{exp}})$ and $\text{RD}(E^N_{\text{t-syn}}, E^N_{\text{exp}})$ (original and time-synchronized data for all patients) were 0.16 and 0.03, respectively, as shown in Fig. 3.19(b). According to the Wilcoxon signed-rank test, $E^N_{t-syn}(\bar{t})$ was significantly closer to $E^N_{\text{exp}}(\bar{t})$ ($p<0.05$). Table 3.5 shows the time offsets for all patients detected by the proposed procedure between original and time-synchronized data. Table 3.5 (right columns) shows examples of patient-specific quantities derived by the model characterizing the functional state of the heart and circulation system.

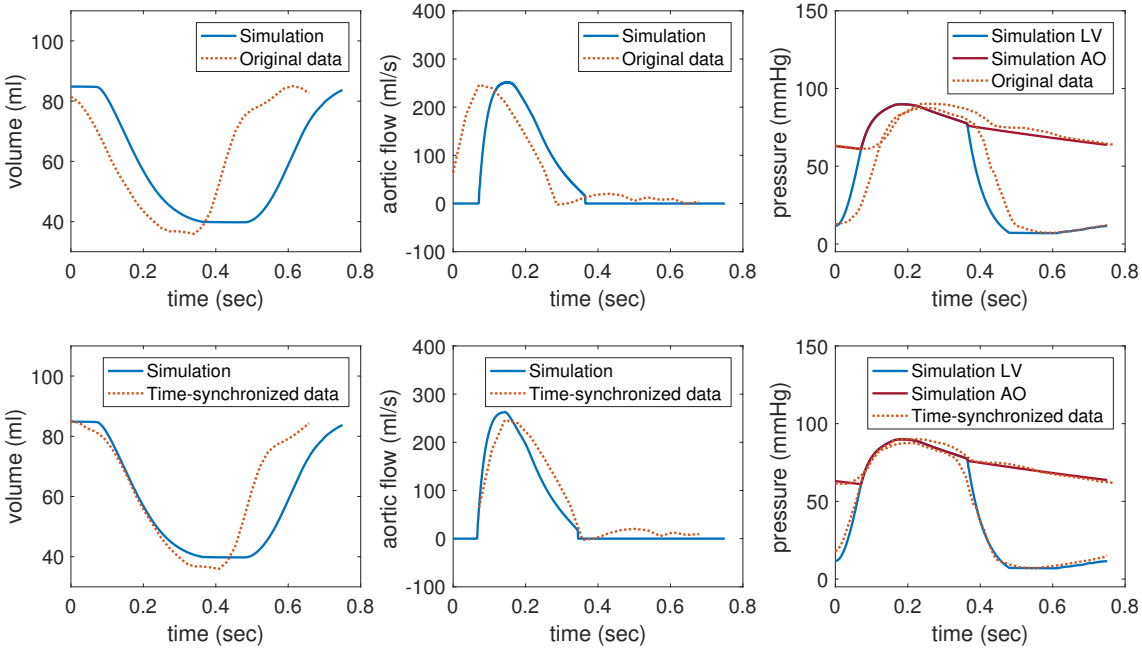

Figure 3.17: Example of data-model coupling for Patient #6. Top: model calibration versus original (non-synchronized) data; bottom: model calibration versus time-synchronized data.

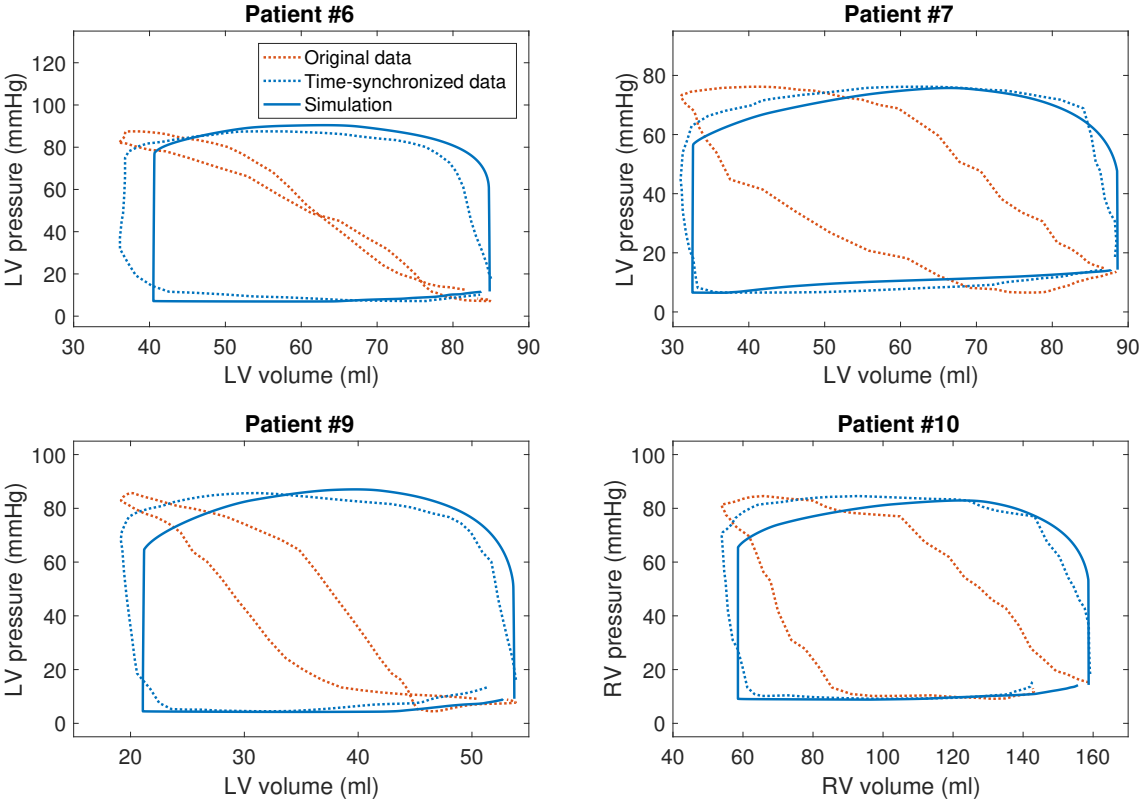

Figure 3.18: Pressure-volume loops for selected patients.

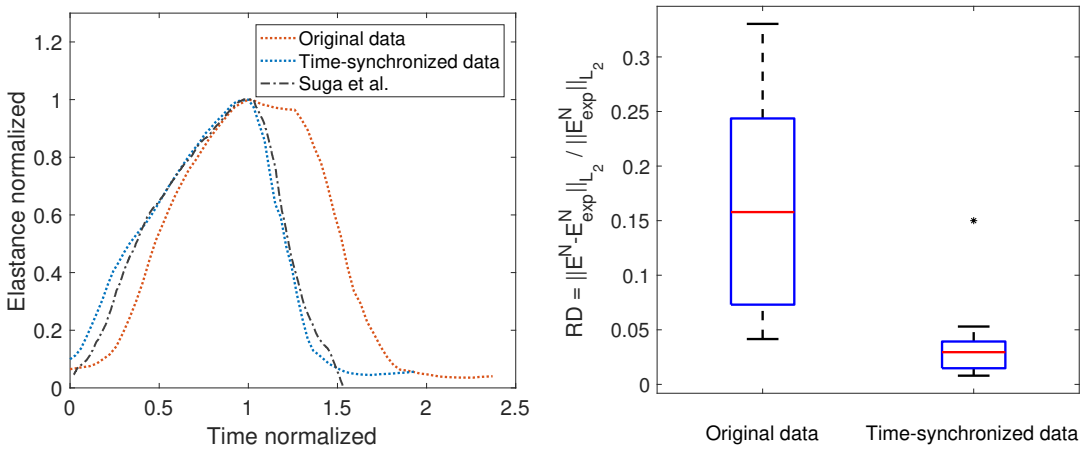

(a) Normalized elastance Patient #6

(b) Relative distance all patients

Figure 3.19: (a) Normalized elastance for a selected patient versus elastance in [22] (b) Boxplots of relative distance (RD) of normalized elastance between original/time-synchronized data and the elastance in [22] for all patients. Central line inside the boxes indicates the median, and the bottom and top edges of the boxes show the 25th and 75th percentiles, respectively. The star indicates significant difference at $p<0.05$.

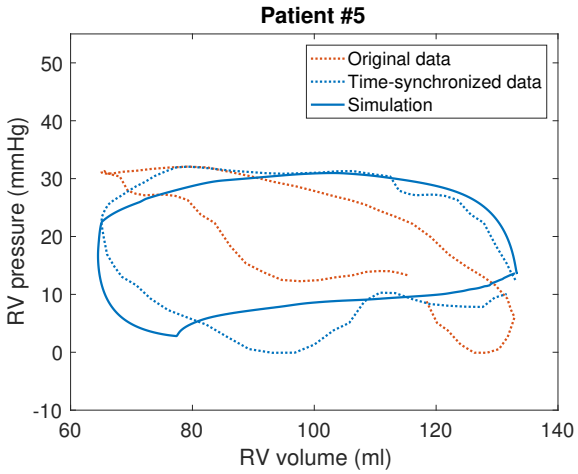

Figure 3.20: Pressure-volume loops for right ventricle of patient #5 with 11% and 30% of tricuspid and pulmonary regurgitation, respectively.

3.6.4 Discussion

In this work we developed a time-synchronization protocol for the ventricular pressure obtained by catheter measurement and volume from cine MRI using a patient-specific computational model. Fig. 3.18 shows a qualitative improvement of the P-V loops after time-synchronizing the pressure and volume data. The box plot in Fig. 3.19 shows that in all 10 patients the shape of normalized time-varying elastance obtained from time-synchronized P-V data is substantially closer to the experimentally measured curve [22]. This suggests that the time-synchronization restores the time-varying elastance to give a physiologically more meaningful relationship. Even though the time-varying elastance obtained in [22] was obtained in dogs, some data obtained in other animal species (e.g. pigs [32]) or even from invasive measurements in human patients [33; 34] suggest their compatibility with [22]. Therefore, in the present work we assumed the normalized time-varying elastance [22] to be a physiological representative of ventricular pressure-volume relationship. The time offsets detected by the model appeared to vary among the patients (Table 3.5) demonstrating that the same offset cannot be applied to all patients even though the same setup of MR acquisition was used. The offsets between P-V data were between 0.081 and 0.161 s, what is in the order of the QRS duration in all patients in our study. In addition to that in patients #2, #4, #5, #10 the difference between MRI and pressure heart rates was more that 30%. Therefore we hypothesize that when combining MRI and catherization techniques the offsets in the P-V data might be associated with several factors: wide QRS complex, difference in the heart rates, and an error in the order of temporal resolution of the MRI (0.020-0.030s).

The model employed in this work was a biomechanical model incorporating physiology of muscle contraction built on various spatial scales. Of note, any other heart model with adequate timings of P-V change could be used as a template in the proposed time-synchronization method. The advantage of using our model [15] is that it can also account for the valvular mechanics (inflow and/or outflow valve regurgitation, see [29]) and hence can be used for time-synchronization of the ventricles with more complicated physiology. Fig. 3.20 shows an example of model-assisted time-synchronization of the right ventricle of Patient #5 with 11% and 30% of tricuspid and pulmonary regurgitation, respectively, where the absence of isovolumic phases would have limited the ability to yield a physiological P-V loop without using a model as a resynchronization template. In addition, the advantage of using a truly biophysical model is that it provides, as a "side effect", additional patient-specific mechanical indicators of various compartments of the cardiovascular system (some examples are displayed in Table 3.5). Those may not be directly visible in the data but are clinically relevant. For instance, myocardial contractility characterizes the functionality of the ventricle, the stroke work can provide information about myocardial energetics, and the distal resistance of the circulation system is an important indicator of a functional state or cardiovascular health in a variety of pathologies. The proposed time-synchronization strategy is not limited neither to the CMR & catherization data acquisition protocol nor to the ventricular pressure & volume data itself, and could be utilized in the variety of patients' data. It can be used e.g. to time-synchronize data acquired in an interventional CMR suite (iCMR, [7]). Moreover, the model can substitute e.g. a missing part of the cardiac cycle in the volume waveform (typically, in highly accelerated cine MRI in prospective ECG trigger).

3.6.5 Conclusion

Time-synchronization of data using patient-specific biophysical modeling can be applied when combining various imaging techniques (echoardiography, dynamic CT, or CMR) and/or

when imaging is combined with catherization data. The proposed modeling framework is fast in computational time and can be employed in clinical settings allowing to plot high-quality P-V loops and extract some useful functional indices of the cardiovascular system.

Acknowledgments

The authors acknowledge the support of the Associated Team TOFMOD, created between Inria France and UT Southwestern Medical Center Dallas. The work was also funded in part by the W.B. & Ellen Gordon Stuart Trust, The Communities Foundation of Texas and by the Pogue Family Distinguished Chair (awarded to Dr F. Gerald Greil in February, 2015). In addition, we would like to acknowledge Dr Philippe Moireau, Inria research team MΞDISIM, for the development of the cardiac simulation software CardiacLab used in this work. Research reported in this publication was supported by Children's Health^{SM} but the content is solely the responsibility of the authors and does not necessarily represent the official views of Children's Health^{SM}.

Bibliography

[1] K. Tello, A. Dalmer, J. Axmann, R. Vanderpool, H. A. Ghofrani, R. Naeije, F. Roller, W. Seeger, N. Sommer, J. Wilhelm, *et al.*, "Reserve of right ventricular-arterial coupling in the setting of chronic overload," *Circulation: Heart Failure*, vol. 12, no. 1, p. e005512, 2019.

[2] H. Latus, W. Binder, G. Kerst, M. Hofbeck, L. Sieverding, and C. Apitz, "Right ventricular–pulmonary arterial coupling in patients after repair of tetralogy of Fallot," *The Journal of thoracic and cardiovascular surgery*, vol. 146, no. 6, pp. 1366–1372, 2013.

[3] C. McCabe, P. A. White, S. P. Hoole, R. G. Axell, A. N. Priest, D. Gopalan, D. Taboada, R. MacKenzie Ross, N. W. Morrell, L. M. Shapiro, and J. Pepke-Zaba, "Right ventricular dysfunction in chronic thromboembolic obstruction of the pulmonary artery: a pressure-volume study using the conductance catheter," *Journal of Applied Physiology*, vol. 116, pp. 355–363, Feb. 2014. Publisher: American Physiological Society.

[4] O. Gaemperli, P. Biaggi, R. Gugelmann, M. Osranek, J. J. Schreuder, I. Bühler, D. Sürder, T. F. Lüscher, C. Felix, D. Bettex, *et al.*, "Real-time left ventricular pressure-volume loops during percutaneous mitral valve repair with the MitraClip system," *Circulation*, vol. 127, no. 9, pp. 1018–1027, 2013.

[5] A. Le Gall, F. Vallée, K. Pushparajah, T. Hussain, A. Mebazaa, D. Chapelle, É. Gayat, and R. Chabiniok, "Monitoring of cardiovascular physiology augmented by a patient-specific biomechanical model during general anesthesia. A proof of concept study," *PloS one*, vol. 15, no. 5, p. e0232830, 2020.

[6] J. Wong, K. Pushparajah, A. de Vecchi, B. Ruijsink, G. F. Greil, T. Hussain, and R. Razavi, "Pressure-volume loop-derived cardiac indices during dobutamine stress: a step towards understanding limitations in cardiac output in children with hypoplastic left heart syndrome," *International Journal of Cardiology*, vol. 230, pp. 439–446, Mar. 2017.

[7] S. R. V. Reddy, Y. Arar, R. Abou Zahr, V. Gooty, J. Hernandez, A. Potersnak, P. Douglas, Z. Blair, J. S. Greer, S. Roujol, *et al.*, "Invasive cardiovascular magnetic resonance (iCMR) for diagnostic right and left heart catheterization using an MR-conditional guidewire and passive visualization in congenital heart disease," *Journal of Cardiovascular Magnetic Resonance*, vol. 22, no. 1, pp. 1–11, 2020.

[8] A. de Vecchi, R. E. Clough, N. R. Gaddum, M. C. M. Rutten, P. Lamata, T. Schaeffter, D. A. Nordsletten, and N. P. Smith, "Catheter-induced errors in pressure measurements in vessels: an in-vitro and numerical study," *IEEE transactions on bio-medical engineering*, vol. 61, pp. 1844–1850, June 2014.

[9] M. Gusseva, J. S. Greer, D. A. Castellanos, M. A. Hussein, G. Greil, S. R. Veeram Reddy, T. Hussain, D. Chapelle, and R. Chabiniok, "Model-Assisted Time-Synchronization of Cardiac MR Image and Catheter Pressure Data," in *Functional Imaging and Modeling of the Heart* (D. B. Ennis, L. E. Perotti, and V. Y. Wang, eds.), Lecture Notes in Computer Science, (Cham), pp. 362–372, Springer International Publishing, 2021.

[10] M. Genet, C. T. Stoeck, C. von Deuster, L. C. Lee, and S. Kozerke, "Equilibrated warping: Finite element image registration with finite strain equilibrium gap regularization," *Medical Image Analysis*, vol. 50, pp. 1–22, 2018. Publisher: Elsevier.

[11] D. Castellanos, K. Skardova, A. Bhattaru, G. Greil, A. Tandon, J. Dillenbeck, B. Burkhardt, T. Hussain, M. Genet, and R. Chabiniok, "Left ventricular torsion obtained using equilibrated warping in patients with repaired Tetralogy of Fallot.," *Pediatric Cardiology*, 2021.

[12] M. Caruel, R. Chabiniok, P. Moireau, Y. Lecarpentier, and D. Chapelle, "Dimensional reductions of a cardiac model for effective validation and calibration," *Biomechanics and Modeling in Mechanobiology*, vol. 13, pp. 897–914, Aug. 2014. Publisher: Springer Verlag.

[13] B. Ruijsink, K. Zugaj, J. Wong, K. Pushparajah, T. Hussain, P. Moireau, R. Razavi, D. Chapelle, and R. Chabiniok, "Dobutamine stress testing in patients with Fontan circulation augmented by biomechanical modeling," *PLOS ONE*, vol. 15, p. e0229015, Feb. 2020. Publisher: Public Library of Science.

[14] M. Gusseva, T. Hussain, C. H. Friesen, P. Moireau, A. Tandon, C. Patte, M. Genet, K. Hasbani, G. Greil, D. Chapelle, and R. Chabiniok, "Biomechanical Modeling to Inform Pulmonary Valve Replacement in Tetralogy of Fallot Patients after Complete Repair," *Canadian Journal of Cardiology*, June 2021.

[15] D. Chapelle, P. Le Tallec, P. Moireau, and M. Sorine, "Energy-preserving muscle tissue model: formulation and compatible discretizations," *International Journal for Multiscale Computational Engineering*, vol. 10, no. 2, 2012.

[16] G. A. Holzapfel and R. W. Ogden, "Constitutive modelling of passive myocardium: a structurally based framework for material characterization," *Philosophical Transactions of the Royal Society A: Mathematical, Physical and Engineering Sciences*, vol. 367, no. 1902, pp. 3445–3475, 2009.

[17] A. F. Huxley, "Muscle structure and theories of contraction," *Progress in Biophysics and Biophysical Chemistry*, vol. 7, pp. 255–318, 1957.

[18] F. Kimmig, D. Chapelle, and P. Moireau, "Thermodynamic properties of muscle contraction models and associated discrete-time principles," *Advanced Modeling and Simulation in Engineering Sciences*, vol. 6, no. 1, pp. 1–36, 2019.

[19] J. Sainte-Marie, D. Chapelle, R. Cimrman, and M. Sorine, "Modeling and estimation of the cardiac electromechanical activity," *Computers & Structures*, vol. 84, pp. 1743–1759, Nov. 2006.

[20] N. Stergiopulos, B. E. Westerhof, and N. Westerhof, "Total arterial inertance as the fourth element of the windkessel model," *The American Journal of Physiology*, vol. 276, pp. H81–88, Jan. 1999.

[21] S. Klotz, I. Hay, M. L. Dickstein, G.-H. Yi, J. Wang, M. S. Maurer, D. A. Kass, and D. Burkhoff, "Single-beat estimation of end-diastolic pressure-volume relationship: a novel method with potential for noninvasive application," *American Journal of Physiology-Heart and Circulatory Physiology*, vol. 291, pp. H403–H412, July 2006. Publisher: American Physiological Society.

[22] H. Suga, K. Sagawa, and A. A. Shoukas, "Load Independence of the Instantaneous Pressure-Volume Ratio of the Canine Left Ventricle and Effects of Epinephrine and Heart Rate on the Ratio," *Circulation Research*, vol. 32, pp. 314–322, Mar. 1973. Publisher: American Heart Association.

[23] K. Sunagawa and K. Sagawa, "Models of ventricular contraction based on time-varying elastance," *Critical Reviews in Biomedical Engineering*, vol. 7, pp. 193–228, Mar. 1982.

[24] W. C. Little, "The left ventricular dP/dtmax-end-diastolic volume relation in closed-chest dogs.," *Circulation Research*, vol. 56, pp. 808–815, June 1985. Publisher: American Heart Association.

[25] T. Geva, "Repaired tetralogy of Fallot: the roles of cardiovascular magnetic resonance in evaluating pathophysiology and for pulmonary valve replacement decision support," *Journal of Cardiovascular Magnetic Resonance: Official Journal of the Society for Cardiovascular Magnetic Resonance*, vol. 13, p. 9, Jan. 2011.

[26] M. Sermesant, R. Chabiniok, P. Chinchapatnam, T. Mansi, F. Billet, P. Moireau, J. M. Peyrat, K. Wong, J. Relan, K. Rhode, M. Ginks, P. Lambiase, H. Delingette, M. Sorine, C. A. Rinaldi, D. Chapelle, R. Razavi, and N. Ayache, "Patient-specific electromechanical models of the heart for the prediction of pacing acute effects in CRT: a preliminary clinical validation," *Medical Image Analysis*, vol. 16, pp. 201–215, Jan. 2012.

[27] R. Chabiniok, P. Moireau, P.-F. Lesault, A. Rahmouni, J.-F. Deux, and D. Chapelle, "Estimation of tissue contractility from cardiac cine-MRI using a biomechanical heart model," *Biomechanics and Modeling in Mechanobiology*, vol. 11, pp. 609–630, May 2012.

[28] T. Arts, T. Delhaas, P. Bovendeerd, X. Verbeek, and F. W. Prinzen, "Adaptation to mechanical load determines shape and properties of heart and circulation: the CircAdapt model," *American Journal of Physiology. Heart and Circulatory Physiology*, vol. 288, pp. H1943–1954, Apr. 2005.

[29] R. Chabiniok, P. Moireau, C. Kiesewetter, M. T. Hussain, R. Razavi, and D. Chapelle, "Assessment of atrioventricular valve regurgitation using biomechanical cardiac modeling," *Functional Imaging and Modelling of the Heart - 9th International Conference, FIMH 2017, Proceedings: (LCNS)*, pp. 401–411, May 2017.

[30] R. Waugh, M. A. Hussein, J. Weller, K. Sharma, G. Greil, J. Kahn, T. Hussain, and R. Chabiniok, "Cardiac Modeling for Multisystem Inflammatory Syndrome in Children (MIS-C, PIMS-TS)," in *International Conference on Functional Imaging and Modeling of the Heart*, pp. 435–446, Springer, 2021.

[31] C. Mekkaoui, P. H. Rolland, A. Friggi, M. Rasigni, and T. G. Mesana, "Pressure-flow loops and instantaneous input impedance in the thoracic aorta: another way to assess the effect of aortic bypass graft implantation on myocardial, brain, and subdiaphragmatic perfusion," *The Journal of Thoracic and Cardiovascular Surgery*, vol. 125, pp. 699–710, Mar. 2003.

[32] F. Seemann, P. Arvidsson, D. Nordlund, S. Kopic, M. Carlsson, H. Arheden, and E. Heiberg, "Noninvasive Quantification of Pressure-Volume Loops From Brachial Pressure and Cardiovascular Magnetic Resonance," *Circulation. Cardiovascular Imaging*, vol. 12, p. e008493, Dec. 2019.

[33] H. Senzaki, C.-H. Chen, and D. A. Kass, "Single-Beat Estimation of End-Systolic Pressure-Volume Relation in Humans," *Circulation*, vol. 94, pp. 2497–2506, Nov. 1996. Publisher: American Heart Association.

[34] A. Le Gall, F. Vallée, D. Chapelle, and R. Chabiniok, "Minimally-invasive estimation of patient-specific end-systolic elastance using a biomechanical heart model," in *FIMH 2019 - 10th Functional Imaging and Modelling of the Heart*, (Bordeaux, France), June 2019.

[35] A. Schmeisser, T. Rauwolf, A. Ghanem, T. Groscheck, D. Adolf, F. Grothues, K. Fischbach, O. Kosiek, C. Huth, S. Kropf, *et al.*, "Right heart function interacts with left ventricular remodeling after CRT: A pressure volume loop study," *International journal of cardiology*, vol. 268, pp. 156–161, 2018.

[36] A. V. Hill, "The heat of shortening and the dynamic constants of muscle," *Proceedings of the Royal Society of London. Series B - Biological Sciences*, vol. 126, pp. 136–195, Oct. 1938. Publisher: Royal Society.

CHAPTER 4

Conceptual link between model-derived measures of ventricular contractility and clinically accepted surrogate measures of ventricular systolic performance

Translation of novel model-derived indices into clinical practice necessitates their validation against existing clinically accepted biomarkers. In this chapter the goal is to explore a conceptual link between data- and model-derived indices of ventricular contractility. Time-synchronized datasets and calibrated models of all patients from Chapter 3 were used to (1) build statistical relationships between the aforemetioned indices, and (2) statistically compare model- and data-derived $\max(dP/dt)$. In addition, a thorough literature review on the clinical relevance of the presented indices of cardiac systolic function was performed. The results (1) showed significant correlation between all model- and data-derived indices, and (2) emphasized a potential application of model-derived $\max(dP/dt)$ as a model-based data filter of noisy values of clinical $\max(dP/dt)$. A literature review demonstrated that (1) the gold standard measure of ventricular contractility is challenging to use with the current physiological and biomechanical knowledge, and (2) some clinical scenarios might benefit from combining several indices of contractile performance.

Contents

4.1 Introduction

Myocardial contractility is often described by myocardial inotropic state. Myocardial inotropy is the potential of the myocardium to generate an optimal level of force during systole in a steady state and on a beat-to-beat basis. It is a specific characteristic of an organ-level performance of the heart to develop an optimal level of force that is required to pump the blood into the arterial network during ventricular systole. Pathological conditions due to substantial tissue-level remodeling could diminish an overall inotropy of the myocardium. This could lead to an inability of the heart to maintain an adequate bodily blood supply and if sustained to organ failure. Therefore, to optimize the diagnostics and treatment of cardiac pathologies it is important to have accurate measures of myocardial inotropy (contractility) that are able to characterize the functional state of the heart.

Myocardial inotropic state can be measured during the two points throughout the cardiac systole: (1) during isovolumic phase when the ventricle is building pressure against the closed arterial and atrioventricular valves and the rate of tension development reaches its maximum, and (2) at the end of ejection when the maximum level of stress is generated for given loading conditions to push all the blood into the circulation. The maximum rate of pressure development during isovolumic systole ($\max(dP/dt)$) is a surrogate measure of the maximum rate of tension development within the myocardium [1; 2; 3; 4; 5]. The end of ejection and the associated level of myocardial stress has been characterized by the maximum value of time-varying elastance ($E_{\max}$). In the sequel we will introduce the theoretical relationship between $\max(dP/dt)$ and $E_{\max}$.

4.1.1 $E_{\max}$ as a measure of ventricular pump function during systole

The time-varying elastance model ($E(t)$) of Suga et al [6] describes ventricular systolic pump function in terms of variation in instantaneous ratio of pressure versus volume during the cardiac cycle. It determines the ability of ventricular chamber to generate systolic pressure and flow against given vascular impedance [7]. Recall:

$$E(t) = \frac{P(t)}{V(t) - V_0}, \tag{4.1}$$

with $P(t)$ and $V(t)$ being ventricular pressure and volume. In this work, similar to Chapter 3 the correction factor V_0 is taken as zero.

The time-varying elastance model has been shown to be valid for a variety of species: dogs [6; 8], pigs [9], and humans [10; 11]. Suga and colleagues [6; 8] have demonstrated that the normalization of $E(t)$ curve by its peak amplitude ($E_{\max}$) and the time to peak amplitude ($t_{\max}$) among studied ventricles yields a single normalized elastance curve ($E^N(\bar{t})$) with unique shape regardless of the canine ventricle studied. $E^N(\bar{t})$ was shown to be independent of loading conditions, heart rate and contractile state:

$$E^N(\bar{t}) = \frac{E(\bar{t} \cdot t_{\max})}{E_{\max}}. \tag{4.2}$$

Hence:

$$E(t) = E_{\max} * E^N(\bar{t}), \tag{4.3}$$

where

$$E_{\max} = \frac{P_{ES}}{V_{\mathrm{ES}}}, \tag{4.4}$$

with P_{ES} and V_{ES} being end-systolic pressure and volume, respectively.

The characteristic parameters of time-varying elastance curve are $E_{\max}$ and $t_{\max}$, the latter characterizing the time of end systole [6]. $E_{\max}$ is independent from loading conditions and is sensitive to the changes in inotropic state of the myocardium [6; 8; 12] and is therefore considered as a surrogate measure of contractility.

4.1.2 Conceptual link between E_{max} and max(dP/dt)

Senzaki et al. [10] demonstrated in human LV's that mean $E^N(\bar{t})$ curves appeared to have the same shape despite different disease conditions, afterload, preload and inotropic states (Figure 4.1).

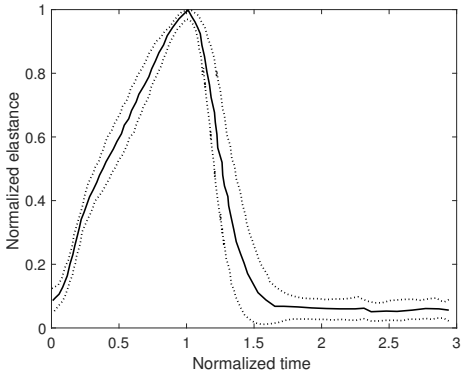

Figure 4.1: Averaged normalized elastance curve ($E^N(\bar{t})$) for the cohort of 78 human left ventricles, where 15 patients were normal heart and 63 contained various forms of chronic heart disease. Solid line is the mean and dashed lines are the ± 1 standard deviation. Adapted from [10]

Figure 4.1, reproduced from Senzaki et al. [10], shows that the least variance of the normalized elastance for the studied cohort of 78 patients (15 normal heart and 63 various forms of chronic heart disease) occurred in two points of cardiac cycle: (1) early contraction (isovolumic phase) and (2) just before the end of systole, suggesting that a time-varying elastance model could systematically predict the chamber performance at these two characteristic time points. Similar conclusion was reached in animal study by Little in 1985 [13] who showed that max(dP/dt) can be expressed in terms of maximum time derivative of $E(t)$ (max(dE/dt)) during isovolumetric systole assuming that end-diastolic volume (EDV) is constant. Recall from Chapter 3:

$$\max(dP/dt) = \max(dE/dt) * EDV\cdot \tag{4.5}$$

In addition the time-varying elastance model predicts that max(dE/dt) is proportional to $E_{\max}$ via time differentiation of eq. (4.3):

$$\max(dE/dt) = (E_{\max}/t_{\max}) * \max(dE^N/d\bar{t})\cdot \tag{4.6}$$

The value of $E^N(\bar{t})$ was shown to be preserved across canine [6; 8] and human [10] ventricles. The maximum value of the derivative of $E^N(\bar{t})$ should also be constant – k:

$$\max(dE/dt) = (E_{\max}/t_{\max}) * k\cdot \tag{4.7}$$

Little [13] invasively obtained max(dP/dt) vs. EDV relationship via acute preload reduction by caval occlusion in closed chest canine LV's and compared it with P_{ES} vs. V_{ES} relationship (where the slope is equal to $E_{\max}$). It was found that (1) max(dP/dt) vs. EDV relationship was described by straight line and the slope of this line was equivalent to

max(dE/dt), and (2) in response to positive inotropic stimulation both max(dE/dt) and E_{max} significantly increased. Similar proportionality between the slopes of the relationships between max(dP/dt) vs. EDV and P_{ES} vs. V_{ES} was demonstrated in another study by [14]. Therefore, the time-varying elastance model has the potential to provide a conceptual link between dynamics of contraction occurring in isovolumic phase and end of ejection.

4.1.3 Model-derived contractility

The biomechanical model-derived contractility represents a maximum inotropic stress generated by the myocardium during systole. It is derived from Huxley's sliding filament theory of actin-myosin dynamics that are integrated into the Hill-Maxwell rheological law to model the overall tissue-level contraction (see Appendix in Chapter 1). In Chapters 1 and 2 we have demonstrated the potential of the model-derived contractility to characterize RV function before and after pulmonary valve replacement in patient-specific manner. The model-derived contractility (rescaled by the ratio of ventricular wall thickness over chamber radius) was in agreement with the Laplace's law and has been previously shown to correlate with max(dP/dt) in [15].

4.1.4 Objectives

Translation of novel model-derived indices into clinical practice necessitates their validation against existing clinically accepted biomarkers. The first aim of this chapter is to explore a conceptual link between data- and model-derived indices of ventricular contractility. The following associated relationships between data- and model-derived indices will be quantitatively evaluated: (1) $E(t)$ vs. data- and model-derived max(dP/dt), (2) model-derived contractility vs. data-derived max(dP/dt), and (3) model-derived contractility vs. data-derived E_{max}.

Clinically acquired max(dP/dt) might not always be available due to the absence of continuous pressure signal or due to the high level of noise present in the acquisition of the pressure signal. Therefore, the second aim is to explore the the potential of model-derived max(dP/dt) to act as a model-based 'data-filter'. We will statistically evaluate the difference between data- and model-derived max(dP/dt) with respect to their relationship with data-derived E_{max}.

4.2 Methods

4.2.1 Data

Three groups of patients were included in this study. Time-synchronized datasets from Chapter 3 were used: N=16 single-ventricle patients, N=17 rTOF LV patients, and N=20 rTOF RV patients. The catheters used to collect pressure signals in three patients' groups were: in single ventricle and rTOF RV patients 6-French Arrow, Balloon Wedge-Pressure Catheter (Teleflex Medical Headquarter International, Ireland, Model #: AI-07124 or AI-07126), and in rTOF LV patients 4F 90cm Pigtail 4-French non-braided pigtail catheter (Angiodynamics, Soft-Vu, Amsterdam, The Netherlands).

4.2.2 Time-varying elastance and max(dP/dt)

To explore the relationship between E_{max} and max(dP/dt) we used the time-varying elastance model according to which max(dP/dt) should be related to E_{max} via eqs. (4.5) and (4.7):

$$\frac{\max(dP/dt)}{EDV} = (E_{\max}/t_{\max}) * k\cdot \tag{4.8}$$

4.2.3 Myocardial contractility and max(dP/dt) from patient-specific biomechanical models.

For single-ventricle and rTOF RV patients we used the calibrated models from Chapters 3 and 1, respectively. For rTOF LV patients the same biomechanical model described in detail in the Chapter 1 was used to calibrate the model (see description of calibration procedure in the Appendix of Chapter 1). Briefly, the following patient-specific parameters of the circulation were adjusted: proximal resistance, distal resistance and capacitance. EDV and ventricular mass were used to derive the reference volume and mean wall thickness. End-diastolic pressure was imposed to calibrate patient-specific parameters of myocardial wall thickness from hyperelastic law (eq. (1.4) in Chapter 1). Finally, myocardial contractility was calibrated to match measured end-systolic pressure and volume (ESP and ESV, respectively) in the data. Intraventricular pressure is the output of the model that is given by the principle of virtual work. Model-derived pressure-vs-time waveform was differentiated in time to obtain the maximum value of its derivative $\max(dP/dt^{\text{model}})$.

4.2.4 Quantitative analysis of the relationships between the data- and model-derived measures of contractility

Data-derived measures of ventricular contractility were $E_{\max}$ and $\max(dP/dt^{\text{data}})$, and model-derived measures were $\max(dP/dt^{\text{model}})$ and contractility. The following associated relationships were built:

I Linear regression model through the origin for $E_{\max}/t_{\max}$ vs. $\max(dP/dt^{\text{data/model}})$ /EDV (eq. (4.8)) at $p < 0.050$. Note that in the sequel this relationship will be referred to as $E_{\max}$ vs. $\max(dP/dt^{\text{data/model}})$ relationship. The reference value of k in this relationship was assumed be k_{ref}=$\max(dE^N/d(\bar{t}))$, where $\max(dE^N/d(\bar{t}))$=2.3 as suggested by Senzaki et al. [10] for a human ventricle.

II Pearson's correlation between model-derived contractility rescaled by the ratio of myocardial wall thickness over chamber radius (in accordance with Laplace's law) and $\max(dP/dt^{\text{data/model}})$ at $p < 0.050$.

III Pearson's correlation between $\max(dP/dt^{\text{data/model}})$ and ventricular ESP in the data at $p < 0.050$. Bland-Altman plots were constructed to quantitatively evaluate the difference between $\max(dP/dt^{\text{data}})$ and $\max(dP/dt^{\text{model}})$.

IV Pearson's correlation between model-derived rescaled contractility and $E_{\max} \cdot EDV$ at $p < 0.050$.

4.3 Results

4.3.1 Relationship between $E_{\max}$ and max($dP/dt^{\text{data/model}}$)

The mean (± SD) $E_{\max}$ in three patients groups was: 1.92 (± 1.13) mmHg/ml, 2.23 (± 0.82) mmHg/ml, and 0.61 (± 0.25) mmHg/ml in single-ventricle, rTOF LV and rTOF RV, respectively. The mean (± SD) $t_{\max}$ in three patients groups was: 0.27 (± 0.04) s, 0.32 (± 0.03) s and 0.27 (± 0.05) s in single-ventricle, rTOF LV and rTOF RV, respectively.

Figure 4.2 shows fitted linear regression models for the relationships between $E_{\max}/t_{\max}$ vs. $\max(dP/dt^{\text{data/model}})$/EDV in single-ventricle, rTOF LV and RV patients. Table 4.1 summarizes quantitative statistics of the fitted regression models. In all three groups R^2 of data- vs. model-derived $E_{\max}$ vs. $\max(dP/dt)$ relationships were 0.87 vs. 0.98 in single-ventricle patients, 0.60 vs. 0.82 in rTOF LV patients, and 0.72 vs. 0.86 in rTOF RV patients. The mean (± SD) coefficients of data- vs. model-derived $E_{\max}$ vs. $\max(dP/dt)$ relationships were 1.66 (±0.28) vs. 2.25 (±0.20), respectively, in single-ventricle group; 2.16 (±0.61) vs. 2.28 (±0.32), respectively, in rTOF LV group; 1.68 (±0.47) vs. 1.72 (±0.28), respectively, in rTOF RV group.

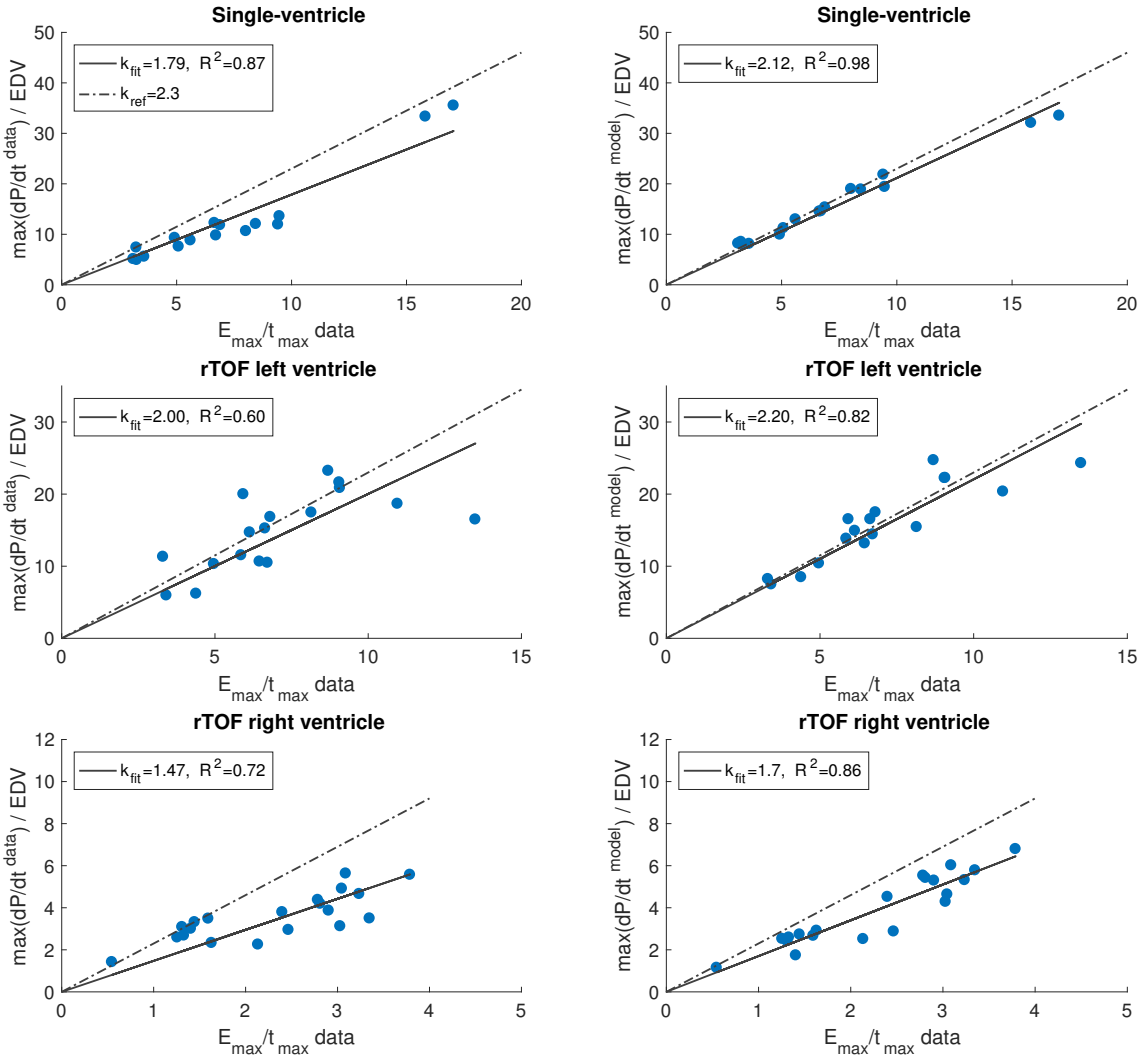

Figure 4.2: Linear regression models for the relationships between time-varying elastance given by the data and maximum time derivative of ventricular pressure given by the data ($\max(dP/dt^{\text{data}})$) and that provided by the model ($\max(dP/dt^{\text{model}})$) in single-ventricle, rTOF left and right ventricle patients. EDV: end-diastolic volume; $E_{\max}$: maximum time-varying elastance; $t_{\max}$: time of occurrence of $E_{\max}$; k_{fit}: coefficient of the fitted linear regression model: k_{ref}: reference coefficient equal to 2.3 derived from Senzaki et al. normalized time-varying elastance curve [10]; R^2: coefficient of determination at $p < 0.05$.

Table 4.1: Statistics for linear regression models for the relationships between data-derived time-varying elastance and data- and model-derived maximum time derivative of ventricular pressure, $\max(dP/dt^{\text{data}})$ and $\max(dP/dt^{\text{model}})$, respectively, in single-ventricle, rTOF left (LV) and right ventricle (RV) patients. k_{fit}: regression coefficient; $SE_{k_{\text{fit}}}$: standard error of the coefficient; R^2: coefficient of determination.

	$\max(dP/dt^{\text{data}})$				$\max(dP/dt^{\text{model}})$			
	k_{fit}	$SE_{k_{\text{fit}}}$	R^2	p-value	k_{fit}	$SE_{k_{\text{fit}}}$	R^2	p-value
Single-vent.	1.79	0.09	0.87	0.00	2.12	0.04	0.98	0.00
rTOF LV	2.00	0.14	0.60	0.00	2.20	0.09	0.82	0.00
rTOF RV	1.47	0.08	0.72	0.00	1.70	0.06	0.86	0.00

4.3.2 Relationship between contractility and max($dP/dt^{\text{data/model}}$)

Figure 4.3 shows Pearson's correlations between model-derived rescaled contractility and $\max(dP/dt^{\text{data}})$ and $\max(dP/dt^{\text{model}})$. R^2 between contractility and $\max(dP/dt^{\text{data}})$ were 0.80 (p=0.00), 0.55 (p=0.02) and 0.80 (p=0.00) in single-ventricle, rTOF LV, and rTOF RV patients, respectively.

4.3.2.1 Difference between data- and model-derived max(d/Pdt)

Mean $\max(dP/dt^{\text{data}})$ (± SD) was 821 (± 247) mmHg, 1157 (± 262) mmHg, and 484 (± 144) mmHg in single-ventricle, rTOF LV and rTOF RV groups, respectively. Mean arterial diastolic pressure (± SD) was 47.8 (± 6.3) mmHg, 52.4 (± 7.6) mmHg, and 11.8 (± 2.2) mmHg in single-ventircle, rTOF LV, and rTOF RV patient groups, respectively.

Figure 4.4 and Table 4.2 show the Bland-Altman statistics for the difference between $\max(dP/dt^{\text{data}})$ and $\max(dP/dt^{\text{model}})$. The mean (± SD) difference was -272 (± 168) mmHg, -78 (± 221) mmHg and -40 (±118) mmHg in single-ventricle, rTOF LV and rTOF RV patients, respectively.

Figure 4.5 shows Pearson's correlations between ventricular ESP and $\max(dP/dt^{\text{data/model}})$, where R^2 of data- vs. model-derived relationships were 0.84 (p=0.00) vs. 0.91 (p=0.00), 0.66 (p=0.00) vs. 0.83 (p=0.00), and 0.77 (p=0.00) vs. 0.95 (p=0.00) in single-ventricle, rTOF LV, and rTOF RV patients, respectively.

Table 4.2: Bland-Altman quantitative statistics showing the mean bias ± standard deviation (SD) and limits of agreement at 95%-confidence interval (CI) (± 1.96 times standard deviation) between data- and model-derived $\max(dP/dt)$ in mmHg.

	mean ± SD	95% - CI
Single-vent.	-274 ± 168	-601 to 57
rTOF LV	-78 ± 221	-511 to 357
rTOF RV	-40 ± 118	-271 to 190

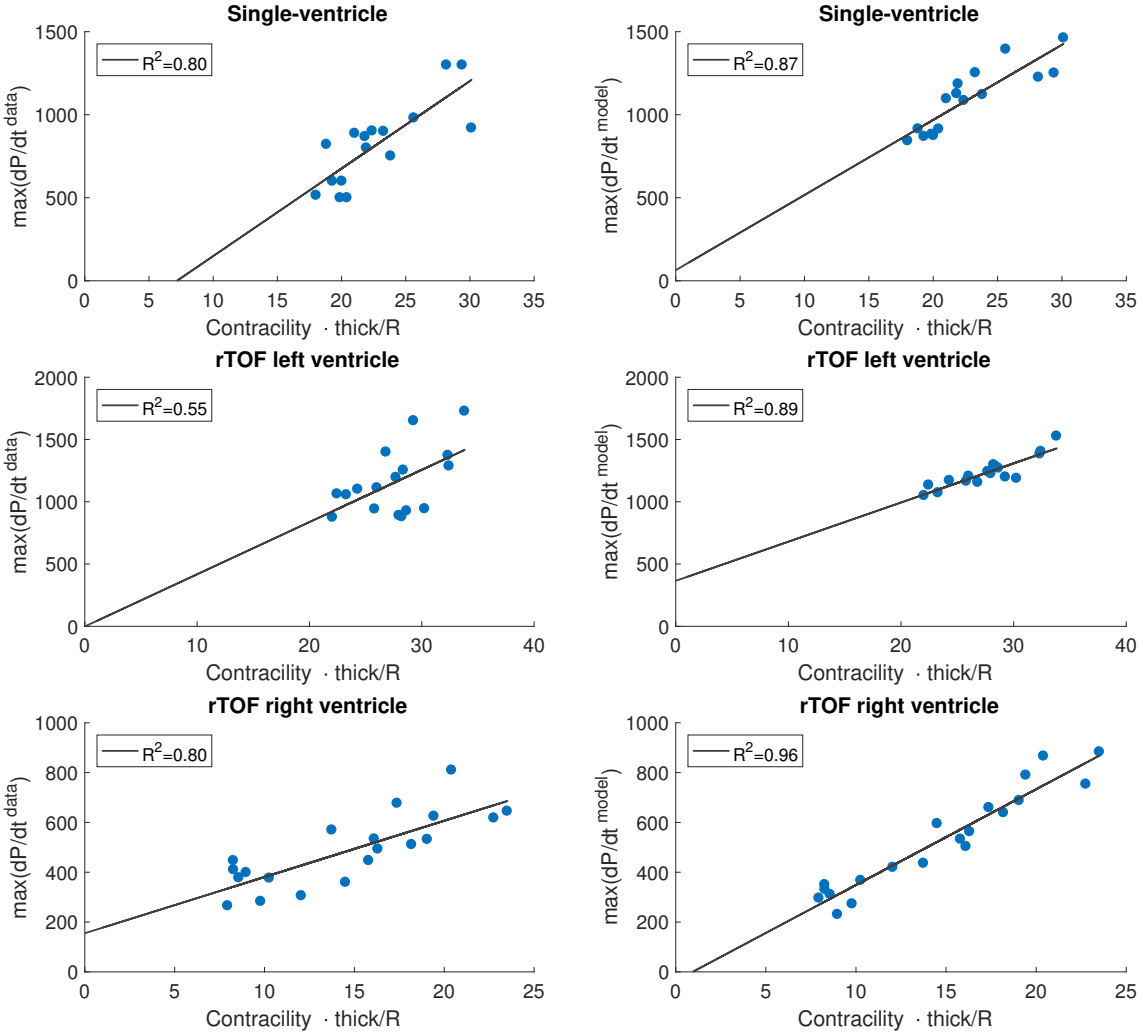

Figure 4.3: Pearson's correlations between model-derived contractility rescaled by the ratio of ventricular wall thickness over chamber radius and maximum time derivative of ventricular pressure given by the data ($\max(dP/dt^{\text{data}})$) and that provided by the model ($\max(dP/dt^{\text{model}})$) in single-ventricle (top row), rTOF left (middle row) and right ventricle (bottom row) patients. R^2: Pearson's coefficient at $p < 0.05$.

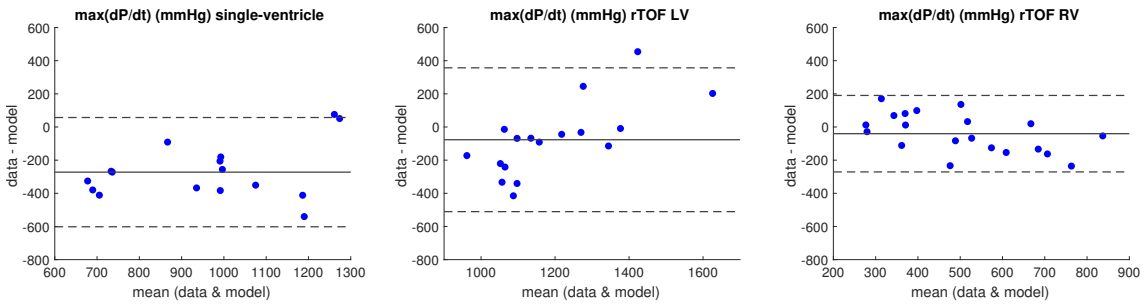

Figure 4.4: Bland-Altman plots for the difference between data- and model-derived $\max(dP/dt)$ in single-ventricle (left), rTOF left (middle) and right ventricle (right) patients. Solid horizontal line is the mean of the difference between data- and model-derived $\max(dP/dt)$. Top and bottom dashed horizontal lines are the 95 % prediction interval ($\pm$ 1.96 standard deviation). LV: left ventricle; RV: right ventricle.

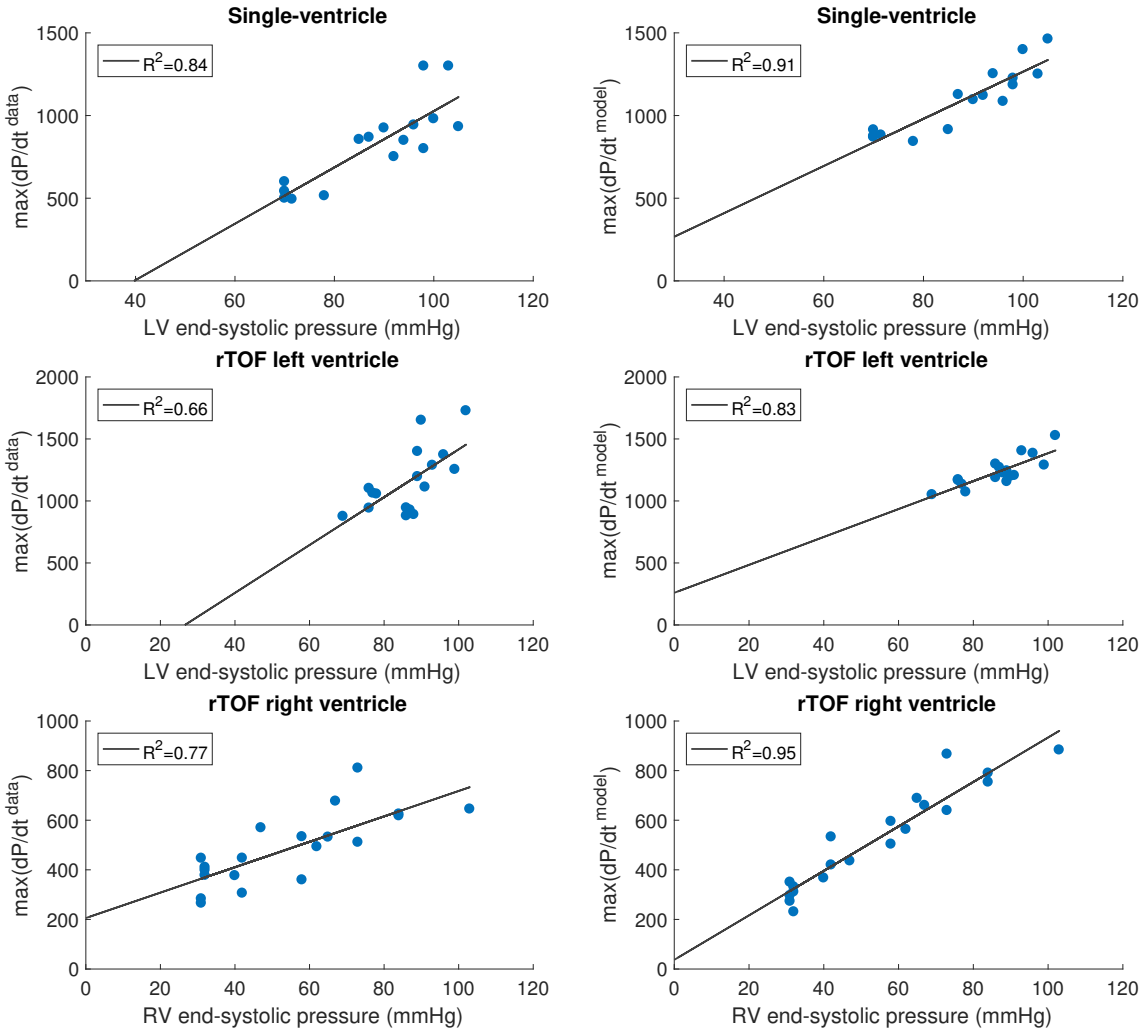

Figure 4.5: Pearson's correlations between ventricular end-systolic pressure and data-/ model-derived maximum time derivative of ventricular pressure ($\max(dP/dt^{\mathrm{data/model}})$) in single-ventricle (top row), rTOF left (middle row) and right ventricle (bottom row) patients. LV: left ventricle; RV: right ventricle; R^2: Pearson's coefficient at $p < 0.05$.

4.3.3 Relationship between contractility and $E_{\max}$

Figure 4.6 shows Pearson's correlations between model-derived contractility rescaled by the ratio of ventricular wall thickness over chamber radius and maximum time-varying elastance ($E_{\max}$) divided by EDV. R^2 was 0.89 (p=0.00), 0.78 (p=0.00), and 0.97 (p=0.00) in single-ventricle, rTOF LV and rTOF RV patients' groups, respectively.

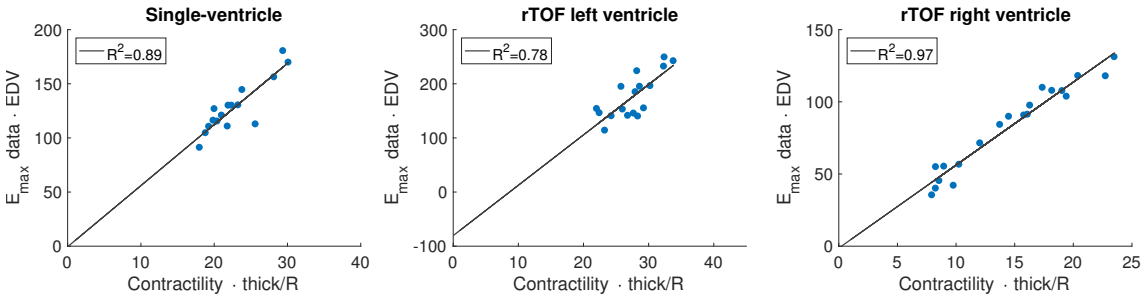

Figure 4.6: Pearson correlations between model-derived contractility rescaled by the ratio of ventricular wall thickness over chamber radius and maximum time-varying elastance ($E_{\max}$) divided by end-diastolic volume (EDV) in single-ventricle (left), rTOF left (middle) and right ventricle (right) patients. R^2: Pearson's coefficient at $p < 0.05$.

4.4 Discussion

The aim of the present chapter was to explore a conceptual link between data- and model-derived surrogate measures of ventricular contractility. The main findings were:

- $E_{\max}$ vs. $\max(dP/dt^{\text{data}})$: strong relationship in single-ventricle, and moderate relationships in rTOF LV and rTOF RV patients' groups
- $E_{\max}$ vs. $\max(dP/dt^{\text{model}})$: strong relationship in all three patients' groups
- contractility vs. $\max(dP/dt^{\text{data}})$: strong relationship in single-ventricle and rTOF RV patients, and moderate relationship in rTOF LV patients.
- contractility vs. $E_{\max}$: strong relationship in all patients' groups.

4.4.1 Quantitative link between $E_{\max}$ and $\max(dP/dt)$

Linear regression analysis of the relationship between $E_{\max}$ vs. $\max(dP/dt^{\text{data}})$ were strong and significant in single-ventricle group, and moderate and significant in rTOF LV and RV groups substantiating the correspondence of pressure-volume data with the elastance model of Suga [8]. Similarly in the relationship between $E_{\max}$ vs. $\max(dP/dt^{\text{model}})$ the strongest relationship with the least variance was observed in single-ventricle group. In single-ventricle patients pressure-volume data were simultaneously acquired whereas in rTOF LV and RV patients pressure-volume data were recorded in separate sessions (volumes 3-4 months prior to catherization). As already acknowledged in Chapter 3 volume data might be underestimated with respect to the pressure data in rTOF patients as both ventricles are progressively remodeling until the catherization is performed.

Linear regression models for the relationships of $E_{\max}$ vs. $\max(dP/dt^{\text{data/model}})$ in Figure 4.2 suggest that model-derived $\max(dP/dt)$ quantitatively strengthens $E_{\max}$ vs. $\max(dP/dt)$ relationship yielding higher values of R^2 and lower values of SE_{fit} in all patients. In addition model-derived $\max(dP/dt)$ shifted k_{fit}-coefficients ($k_{\text{fit}} = 2.12$, $k_{\text{fit}} =$

2.20 and $k_{\text{fit}} = 1.70$ in single-ventricle, rTOF LV, and rTOF RV, respectively) closer to the k-coefficient reported in the literature: $k_{\text{ref}} = 2.3$ in Senzaki et al. [10] (human), $k_{\text{suga}} = 2.4$ in Suga et al [6] (canine), and $k = 2.2 \pm 0.7$ in the study by Little [13] (canine).

The k_{fit}-coefficient in rTOF RV group was lower compared to that in single-ventricle and rTOF LV groups. Anatomical and physiological characteristics that are inherent to the RV — crescent geometry, greater regional wall variation, mechanical coupling with the LV— might contribute to the observed difference in $E_{\max}$ vs. $\max(dP/dt)$ relationship between rTOF LVs and RVs. Suga and colleagues [7; 6; 8] originally proposed the time-varying elastance concept for the description of LV systolic pump function. Later, a number of researcher showed the validity of time-varying elastance for the characterization of RV systolic performance. Maughan et al [16], in canine RVs, Dell'Italia et al. [17] and Brown et al. [18], in human RVs, invasively derived time-varying elastance and demonstrated that (1) the linear relationship between pressure and volume at any given point in time within the cardiac cycle for the range of imposed preload and afterload conditions, (2) the maximum slope of these linear relationships ($E_{\max}$) was sensitive to the imposed changes in the inotropic state. Thus, assuming that the time-varying elastance model is valid for RV the lower k_{fit}-coefficient of rTOF RV $E_{\max}$ vs. $\max(dP/dt^{\text{model}})$ relationship might signify that for a given level of $E_{\max}$ RV generates a lower $\max(dP/dt)$ compared to that in the rTOF LV. The diastolic pressure in the pulmonary circulation is lower than in the systemic (e.g. in our cohort pulmonary artery diastolic pressure was by 40 mmHg lower than that in the aorta of rTOF), therefore during RV isovolumetric systole semilunar valve opens at lower pressures and the peak rate of achieved pressure increase is also lower [2]. Also, RV contractile behaviour could be determined by the mechanical dependence of RV systolic pump function from LV contraction as demonstrated by [19; 20; 21] and extensively discussed in the review by [22]. Oboler et al. [19] and [21] in canine heart and Feneley et al. [20] in human hearts demonstrated that in the conditions of induced dyssynchronous ventricular contraction (e.g. RV pressure derivative becomes double peaked and LV remains single peaked) either peak I or peak II of RV dP/dt (depending on the conditions of ventricular assynchrony) becomes temporally coincident with the peak of LV dP/dt. In addition to that [21] showed that RV dP/dt peak that is coincident with LV dP/dt peak is significantly greater in magnitude than the other RV dP/dt peak. Since the ventricles anatomically share the fibers via septum and pericardial sac [23; 24] the tension that is developed by the LV contraction could be transmitted to RV via common fibers. LV could consequently contribute to the total tension that is developed by the RV during systole. Finally, a lower k_{fit}-coefficient in rTOF RV might be a marker of a pathological state of the ventricle. Recall that RVs in the present dataset are severely affected by pulmonary valve regurgitation and/or stenosis. Therefore, lower k_{fit}-coefficient might be associated with the remodeling of the RV myocardium due to long-term exposure to pulmonary valve regurgitation and/or stenosis and associated depressed ventricular systolic function. However, more extensive RV data are required in order to distinguish whether anatomical characteristics of the RV or pathological hemodynamic conditions contribute to the lower k_{fit} values observed in the present chapter.

4.4.2 Data- and model-derived max(dP/dt)

In single-ventricle patients model-derived $\max(dP/dt)$ appeared to be systematically over-estimated with respect to the data-derived $\max(dP/dt)$. In rTOF patient groups the difference between data- and model-derived $\max(dP/dt)$ in LV is more prominent than in RV (Bland-Altman plot on Figure 4.4). The ground truth for $\max(dP/dt)$ is however not known. Therefore the observed difference between data- and model-derived $\max(dP/dt)$

could be associated with both the noise present in the catherization pressure signals and modeling errors. Firstly, fluid-filled catheters are subjected to inertia artefacts that arise due to their design (i.e. a column of fluid that fills the catheter) and that distort a pressure wave to certain extent as it travels inside the probe altering the shape of the recorded waveform [25]. The catheter-induced artefacts present in the acquired signal depend on catheter size and type [26] and become exaggerated once the pressure time derivative is computed [27]. Hence, rTOF LV pressure recordings could be more noisy than the rTOF RV recordings as different types of catheters were used. Secondly, model induced errors might also play a role. The observed overestimation of model-derived $\max(dP/dt)$ might be due to the model being less accurate for the description of single-ventricular mechanics. In particular, an assumption of the spherical ventricular shape might be less appropriate for single-ventricle patients. This patient cohort was not homogeneous with some patients having systemic left and some systemic right ventricle. Therefore, the further investigation of modeling errors need to be performed.

4.4.3 Quantitative interdependence between the surrogate measures of ventricular contractility

The correlation between model-derived contractility and data-derived $\max(dP/dt)$ was strong and significant in single-ventricle and rTOF RV patients, and moderate and significant in rTOF LV patients. A weaker correlation in rTOF LV could be due to the noisy pressure signals as acknowledged above. Strong correlations between model-derived contractility and data-derived $E_{\max} \cdot EDV$ were observed in all patients' groups. Therefore, model-derived contractility is in correspondence with the clinically accepted surrogate measures of contractility: one that represents the rate of tension development and the other systolic pump function of the heart. As outlined in Section 4.1.2 time-varying elastance model conceptually links the contractile performance during isovolumetric systole with that of end-ejection. Significant relationships between (1) $E_{\max}$ and $\max(dP/dt^{\text{data/model}})$ and (2) between model-derived contractility and $\max(dP/dt^{\text{data/model}})$ both substantiate that contractile performance of the heart during isovolumetric contraction is linked to that at the end of systole. Therefore, we hypothesize that muscle ability to develop tension is likely to be proportional to its ability to generate the end-systolic level of tension for a given ventricular geometry. Garcia et al [28] investigated the interaction between $\max(dP/dt)$ and $E_{\max}$ in porcine LVs under different afterload conditions and contractile states and concluded that $E_{\max}$ was the main determinant of the changes in $\max(dP/dt)$. Gleason et al [27] proposed that in the conditions of chronic exposure to pressure overload the ventricle adapts its rate of tension development in similar fashion as it adapts its ability to develop maximum tension. Gleason et al [27] found a good correlation between $\max(dP/dt)$ and ESP (our data also showed a significant correlation between $\max(dP/dt)$ and ESP, Figure 4.5). Sandler et al [29] and Spann et al. [30] discovered that when ventricular sustains chronic elevation of ESP ventricular wall increases in mass, but the tension per unit of myocardial mass remains constant. In the view of these findings [27; 29] and others [31; 32; 33] it has been proposed that mechanism of adaptive hypertrophy maintains the tension per unit of myocardial mass constant whilst ventricular wall is adding myocardial muscle units in order to sustain increased contractile demand. Therefore, it is possible that in the increased hemodynamic loading the rate of tension development is also maintained constant per unit of myocardial mass as a results of adaptive ventricular hypertrophy [27] .

4.4.4 Clinical implications

Identifying reliable, reproducible and predictive indices of myocardial contractility for clinical use has been a subject of translational and clinical research for many years. It is particularly challenging to derive load independent measures of myocardial performance that could characterize the changes in myocardial material properties and predict the onset of tissue-level irreversible remodelling.

Since 1970s time-varying elastance has been recognized as a physiologically relevant concept to index organ-level cardiac performance. Changes in chamber elastance (in particular $E_{\max}$) are assumed to represent a net effect of changes of myocardial material properties (i.e. stiffness, contractility, contractile to eleastic element ratio) and chamber structural properties that together determine venticular pumping ability [34]. Even though some researchers have shown the efficiency of $E_{\max}$ to characterize the pathological state of the myocardium [35; 36; 37] and to evaluate cardiac performance in response to various therapeutic interventions (in LV: [38; 39; 40; 37], and in RV [41]) its clinical use remains to be limited. Firstly, an estimation of $E_{\max}$ is technically demanding as it pertains fitting linear regression to several end-systolic pressure-volume points that are typically acquired by varying preload via e.g. inferior vena cava occlusion, whilst latter could be dangerous in some pathological conditions. Some alternative methods exist to estimate $E_{\max}$ from single-beat pressure-volume measurement using systolic time intervals and normalized elastance curve ($E^{\mathrm{N}}(\bar{t})$) with invasive [10; 42] and noninvasive [43] pressure acquisitions. Le Gall et al [11] argued, however, that such methods are too sensitive to their parameters (e.g. there is high probability of error in measured $t_{\max}$ that could render an inaccurate estimation of $E_{\max}$ from $E^{\mathrm{N}}(\bar{t})$). Le Gall et al. [11] proposed biomechanical model-assisted estimation of patient-specific elastance from single-beat echocardiographic flow and catherization pressure data. The model allows to vary loading conditions *in silico* rendering several points on ESPVR to estimate $E_{\max}$. Secondly, the assumption of ESPVR non-linearity might not be universally correct [44]. The linearity of the ESPVR has been shown to be violated in the hearts subjected to regional coronary occlusion [45] where the slope appeared to be convex to the volume axis. Another group of studies have demonstrated contractility-dependent curvilinearity of ESPVR on *in situ* canine left ventricles [46; 47; 48]: at higher contractile states ($E_{\max} > 7$ mmHg/ml) ESPVR was concave to volume axis, and at lower ($E_{\max} < 3.5$ mmHg/ml) it was convex (note that in these studies the values of $E_{\max}$ were calculated with V_0). These studies however concluded that in the physiological inotropic range of contractility in the *in vivo* heart the ESPVR is linear [46; 47; 48]. In addition to that the linearity of human RV elastance has been questioned as the wide range of resting $E_{\max}$ values and the varying V_0 throughout the contraction was reported by [17; 18] in normotensive RVs. Nevertheless, lack of linearity should not be interpreted against the validity of varying-elastance model to describe systolic performance of a given heart at a given inotropic state [44]. Instead, the potential nonlinearity should be considered depending on the operating range of pressure-volume data and when interpreting the data for intra-subject comparison [18; 44]. Thirdly, in extreme pathological scenarios time-varying elastance might be an inadequate model. Vandenberghe et al [49] showed that in patients with advanced heart failure with inserted mechanical circulatory support (e.g. LV assist device patients) obtained time-varying elastance curves showed high variation in amplitude on beat-to-beat basis due to interaction between the heart and ventricular assist device. Simple elastance model where pressure is determined by the instantaneous volume and that assumes that hemodynamics are internally regulated by the heart and cardiovascular system cannot account for complex heart-to-device interaction where the heart is subjected to extreme loading condition that are suddenly changing on beat-to-beat

basis. Such cases justify a need for a more complex microstructurally oriented modeling approaches such as [50] that are able to track cardiac performance in real time [51; 52].

Since early 1960s the maximum rate of pressure increase has been proposed as a surrogate measure of contractility that from phenomenological point of view represents velocity of fiber shortening. Even though it is highly sensitive to changes in inotropic state [53; 54; 55; 1; 56; 57], it has been shown to be dependent on a number of organ-level factors. (1) Max(dP/dt) is highly preload dependent via Frank-Starling mechanism (length-dependent affinity of binding of Ca^{2+} to troponin-C and the numbers of cross-bridges cycling) [55; 58; 59]. Therefore to account for length-dependent effect the correction of max(dP/dt) by EDV was introduced [13]. The relationship between max(dP/dt) vs. EDV (with slope of max(dE/dt) see Section 4.1.2) was found to be more sensitive to acute changes in contractility than $E_{\max}$ [14; 60]. (2) Max(dP/dt) is dependent on the diastolic pressure in the arterial system [55; 59]. Max(dP/dt) occurs just before the opening of the semilunar valve, thus, if ventricle is building a pressure against lower load (e.g. diastolic pressure in the pulmonary circulation) its ability to generate maximum pressure is reduced during isovolumetric systole. At the onset of opening of the semilunar valve the work generated by the ventricle is distributed into the pushing the blood into the arterial tree and the rate of pressure rise decreases. (3) Max(dP/dt) is subjected to chronotropic effect, increased heart rate causes the increased concentration of Ca^{2+} in the sarcoplasmic reticulum of the myocardium and consequently increases the rate of myocardial activation (so-called 'Treppe' effect originally discovered by Bowditch in 1871 [61]) [62; 27; 55]. (4) The manner of ventricular activation could affect the muscle ability to build force. In clinical studies it was shown that left bundle brunch block slows down max(dP/dt) [20]. Similarly, in our *in silico* simulations we demonstrated that increased duration of QRS complex tends to decrease max(dP/dt) (Figure 4.7 in Appendix). Finally, an *in silico* effect of the level of the atrioventricular (AV) valve regurgitation on max(dP/dt) appeared to be small (Figure 4.8 in Appendix).

Preload, arterial diastolic pressure, and heart rate could be altered by interventions and vary in resting state between the patients. Therefore, the inotropic effect of the contractility change as indexed by max(dP/dt) could be hidden especially when comparing on inter-subject basis [55]. However, due to an excellent sensitivity of max(dP/dt) to changes in inotropic state it has been viewed as a fair measure of contractility when the variation in preload, diastolic arterial pressure and heart rate could be relatively controlled. A number of studies with patients undergoing cardiac resynchronization therapy (CRT) demonstrated the potential of max(dP/dt) to evaluate the acute response to the therapy and predict the incidence of heart failure or mortality in 1 year following the implantation of the CRT device [57; 63; 56]. The predictors of the long-term response were either the baseline or the acute max(dP/dt) post CRT implantation, whilst the level of relative response of max(dP/dt) to CRT (e.g. baseline max(dP/dt) divided by acute max(dP/dt)) did not correlate with the long-term outcome [63; 56]. These results support the ability of max(dP/dt) to evaluate the contractile state within individual patients and not between the patients.

Model-derived contractility is a measure of maximum inotropic stress developed by the myocardium during systole. During the calibration the model is sequentially coupled to patient-specific measurements of heart rate, QRS duration, end-diastolic and end-systolic pressures and volumes in the arteries (only pressures) and ventricle. Therefore, the calibrated value of contractility is a function of the patient-specific levels of preload and afterload conditions rendering the comparison between the subjects possible. In Chapter 1 we assessed the ability of model-derived contractility to evaluate the current state of the myocardium of the rTOF patients pre- and post-PVR. In Chapter 2 we explored the ability of the model to predict an *in silico* mechanical response of the myocardium to

different afterload conditions post-PVR in the hypothetical absence of post-PVR data. We demonstrated that model-derived contractility could augment clinical indicators of patients' pathology and inform clinicians about the level of myocardial contractility in response to varying afterload conditions. Our results show that the current model has the potential to provide personalized assessment of myocardial function. We acknowledge, that a long-term prognostic value of the model-derived contractility is yet to be determined. Only recently the current modeling approach started to be employed with real patients' data in [64; 15; 11; 52; 65; 66], where no long-term follow-up data were available. A translation of the novel model-derived indexes into clinical practise necessities their validation against the existing clinically accepted biomarkers of myocardial function. In the current chapter we established strong correlations between model-derived contractility and $\max(dP/dt^{\text{data}})$ and $E_{\max}$ substantiating the physiological relevance of the model-derived contractility to describe systolic performance of the heart.

4.4.5 Model-derived max(dP/dt) as a model-based data filter

Our results showed that model-derived $\max(dP/dt)$ is statistically more equivalent to the data-derived $E_{\max}$. This suggests that model-derived $\max(dP/dt)$ quantitatively strengthens the relationship between contractile performance of isovolumetric phase and end of ejection. $\text{Max}(dP/dt)$ acquired in clinical settings is a continuous variable that is highly subjected to measurement artefacts. Hence, even tiny fluctuations of the probe during pressure acquisition are exaggerated once the first derivative of the pressure is computed. Model-derived $\max(dP/dt)$ is calculated from the pressure signal that is an output of the model at a given time-step of the cardiac cycle simulation (e.g. in the current model it is 0.001 s). Therefore, model-derived $\max(dP/dt)$ has a potential to be used (1) as a filter for the noisy pressure signals, so-called 'model-based data filtering', and (2) as an index of isovolumic contraction in the conditions when clinical acquisition of the contentious pressure wave is either too noisy or not available at all. The function of model-derived $\max(dP/dt)$ as a data-filter should be further explored by fitting *in silico* noise to the the model-derived pressure signal and subsequently comparing the *in silico* and model-derived $\max(dP/dt)$.

4.4.6 Limitations

The results of the current chapter are subjected to some limitations. In the calculation of $E(t)$ the volume correction factor V_0 was not considered. In human heart the value of V_0 was shown to be relatively small, 18 ± 16 ml in LVs by Starling et al. [67] and 10 ± 19 ml in RV by Karunanithi et al. [68]. Starling et al. [67] showed a good correlation between E_{max} taken from $E(t)$ model with V_0 and that without ($R^2 = 0.90$). In comparison to the reported values in the literature for E_{max} that are taken from $E(t)$ model with V_0 the $E_{\max}$ values in the current chapter are likely to be systematically underestimated. In human LVs Starling et al. [67] showed that mean values for E_{max} without V_0 are by 35% lower than E_{max} with V_0, and in human RVs E_{max} without V_0 was by 68% lower than E_{max} with V_0 [18]. In the future the calculation of E_{max} that contains the correction for V_0 could be performed via model-assisted estimation of patient-specific elastance as shown by Le Gall et al. [11]. The limitations that are inherent to the model-derived contractility were already addressed in Chapters 1 and 2.

4.5 Concluding remarks

In this chapter we demonstrated the correspondence of data-derived indices of myocardial contractility ($E_{\max}$ and $\max(dP/dt)$) with model-derived contractility and $\max(dP/dt)$. Considering the complexity and hierarchical nature of the heart function and limited availability of measurable quantities *in vivo* the gold standard measure of ventricular contractility cannot be yet advised. Some clinical scenarios might benefit from combining several indices of contractile performance for the assessment of the effects of the intervention. Whilst the plausibility of the data- and model-derived myocardial indices to assess acute changes has been recognized more research is needed to elucidate their long-term predictive value. Finally, we suggested a potential application of $\max(dP/dt)$ as a model-based data filter of clinical $\max(dP/dt)$.

4.6 Appendix

In silico effect of (1) QRS duration and (2) AV valve regurgitation on $\max(dP/dt^{\text{model}})$ was investigated. In three selected patient-specific models from each patient group in the activation function of the heart we prescribed the duration of QRS from 0.08 to 0.150 s, preserved all other parameters and re-calculated the corresponding values of $\max(dP/dt^{\text{model}})$. Similarly, an *in silico* effect of AV valve regurgitation was investigated by decreasing by imposing the regurgitation on AV valve from 10 % to 50 % (via decreasing the value of AV valve resistance in the model). Preserving all other parameters we re-calculated the corresponding values of $\max(dP/dt^{\text{model}})$.

4.6.1 In silico effect of QRS duration on max(dP/dt)

Figure 4.7 shows an *in silico* effect of increasing the duration of QRS complex on $\max(dP/dt^{\text{model}})$ in three selected patient-specific models from single-ventricle, rTOF LV and RV patients groups. Increasing QRSd from 0.08 s to 0.150 s resulted in the 27%, 27% and 30 % decrease of the $\max(dP/dt)$ in single-ventricle, rTOF LV and rTOF RV selected patient-specific models, respectively.

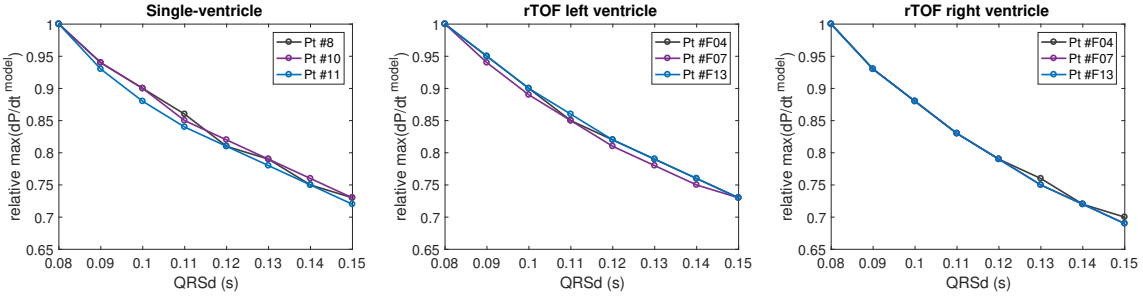

Figure 4.7: *In silico* effect of increasing QRS duration (QRSd) on $\max(dP/dt)$ in three selected patient-specific models from single-ventricle (left), rTOF left (middle) and right ventricle (right) patients groups, respectively. $\text{Max}(dP/dt)$ was rescaled by the value of patient-specific model-derived $\max(dP/dt)$ obtained at QRSd of 0.08 s.

The mean (± SD) QRSd in our patients' cohort was 0.082 (± 0.006) in single-ventricle patients, 0.140 (± 0.030) in rTOF LV and RV patients.

4.6.2 In silico effect of atrioventricular valve regurgitation on max(dP/dt)

Figure 4.8 shows an *in silico* effect of increasing AV valve regurgitation on max(dP/dt^{model}) in three selected patient-specific models from single-ventricle, rTOF LV and rTOF RV patient groups. Increasing AV valve regurgitation to 50 % resulted in 10% , 12% and 15% decrease of max(dP/dt^{model}) in single-ventricle, rTOF LV and rTOF RV patients, respectively.

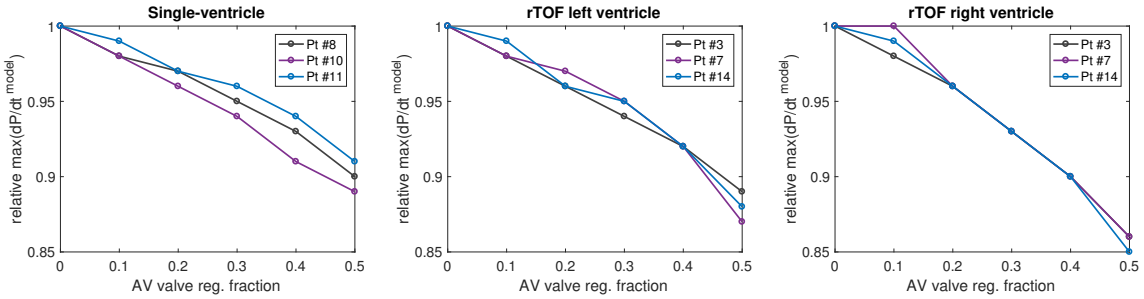

Figure 4.8: *In silico* effect of increasing atrioventricular (AV) valve regurgitation fraction on max(dP/dt^{model}) in three selected patient-specific models from single-ventricle (left), rTOF left (middle) and right ventricle (right) patients groups, respectively. max(dP/dt^{model}) was rescaled by the value of max(dP/dt^{model}) obtained at QRSd of 0.08 s.

Bibliography

[1] F. Mahler, J. Ross, R. A. O'Rourke, and J. W. Covell, "Effects of changes in preload, afterload and inotropic state on ejection and isovolumic phase measures of contractility in the conscious dog," *The American Journal of Cardiology*, vol. 35, pp. 626–634, May 1975.

[2] D. T. Mason, J. F. Spann, and R. Zelis, "Quantification of the contractile state of the intact human heart: Maximal velocity of contractile element shortening determined by the instantaneous relation between the rate of pressure rise and pressure in the left ventricle during isovolumic systole," *The American Journal of Cardiology*, vol. 26, pp. 248–257, Sept. 1970.

[3] D. T. Mason, E. Braunwald, J. W. Covell, E. H. Sonnenblick, and J. R. John Ross, "Assessment of Cardiac Contractility," *Circulation*, July 1971.

[4] H. W. Paley, I. G. McDonald, J. Blumenthal, J. Mailhot, and G. W. Modin, "The effects of posture and isoproterenol on the velocity of left ventricular contraction in man: The reciprocal relationship between left ventricular volume and myocardial wall force during ejection on mean rate of circumferential shortening," *The Journal of Clinical Investigation*, vol. 50, pp. 2283–2294, Nov. 1971.

[5] W. W. Parmley, J. James F. Spann, R. R. Taylor, and E. H. Sonnenblick, "The Series Elasticity of Cardiac Muscle in Hyperthyroidism, Ventricular Hypertrophy, and Heart Failure," *Proceedings of the Society for Experimental Biology and Medicine*, vol. 127, no. 2, pp. 606–609, 1968.

[6] H. Suga, K. Sagawa, and A. A. Shoukas, "Load Independence of the Instantaneous Pressure-Volume Ratio of the Canine Left Ventricle and Effects of Epinephrine and Heart Rate on the Ratio," *Circulation Research*, Mar. 1973.

[7] H. Suga, "Theoretical analysis of a left-ventricular pumping model based on the systolic time-varying pressure/volume ratio," *IEEE Transactions on Biomedical Engineering,*, vol. 18, 1971.

[8] H. Suga and K. Sagawa, "Instantaneous Pressure-Volume Relationships and Their Ratio in the Excised, Supported Canine Left Ventricle," *Circulation Research*, July 1974.

[9] F. Seemann, P. Arvidsson, D. Nordlund, S. Kopic, M. Carlsson, H. Arheden, and E. Heiberg, "Noninvasive Quantification of Pressure-Volume Loops From Brachial Pressure and Cardiovascular Magnetic Resonance," *Circulation: Cardiovascular Imaging*, 2019.

[10] H. Senzaki, C. H. Chen, and D. A. Kass, "Single-beat estimation of end-systolic pressure-volume relation in humans. A new method with the potential for noninvasive application.," *Circulation*, vol. 94, pp. 2497–2506, Nov. 1996.

[11] A. Le Gall, F. Vallée, D. Chapelle, and R. Chabiniok, "Minimally-Invasive Estimation of Patient-Specific End-Systolic Elastance Using a Biomechanical Heart Model," in *Functional Imaging and Modeling of the Heart*, pp. 266–275, Springer, Cham, June 2019.

[12] M. R. Starling, "Responsiveness of the maximum time-varying elastance to alterations in left ventricular contractile state in man," *American Heart Journal*, vol. 118, pp. 1266–1276, Dec. 1989.

[13] W. C. Little, "The left ventricular dP/dtmax-end-diastolic volume relation in closed-chest dogs.," *Circulation Research*, June 1985.

[14] W. C. Little, A. Rassi, and G. L. Freeman, "Comparison of effects of dobutamine and ouabain on left ventricular contraction and relaxation in closed-chest dogs.," *The Journal of Clinical Investigation*, vol. 80, pp. 613–620, Sept. 1987.

[15] B. Ruijsink, K. Zugaj, J. Wong, K. Pushparajah, T. Hussain, P. Moireau, R. Razavi, D. Chapelle, and R. Chabiniok, "Dobutamine stress testing in patients with Fontan circulation augmented by biomechanical modeling.," *PLoS ONE*, vol. 15, no. 2, p. e0229015, 2020.

[16] W. L. Maughan, A. A. Shoukas, and K. S. Circulation, "Instantaneous pressure-volume relationship of the canine right ventricle.," *Am Heart Assoc*, 1979.

[17] L. J. Dell'Italia and R. A. Walsh, "Application of a time varying elastance model to right ventricular performance in man.," *Cardiovascular research*, vol. 22, pp. 864–874, Dec. 1988.

[18] K. A. Brown and R. V. Ditchey, "Human right ventricular end-systolic pressure-volume relation defined by maximal elastance.," *Circulation*, July 1988.

[19] A. A. Oboler, J. F. Keefe, W. H. Gaasch, J. S. Banas, and H. J. Levine, "Influence of left ventricular isovolumic pressure upon right ventricular pressure transients.," *Cardiology*, vol. 58, no. 1, pp. 32–44, 1973.

[20] M. P. Feneley, T. P. Gavaghan, D. W. Baron, J. A. Branson, P. R. Roy, and J. J. Morgan, "Contribution of left ventricular contraction to the generation of right ventricular systolic pressure in the human heart.," *Circulation*, Mar. 1985.

[21] R. J. Damiano, J. L. Cox, J. E. Lowe, and W. P. Santamore, "Left ventricular pressure effects on right ventricular pressure and volume outflow," *Catheterization and Cardiovascular Diagnosis*, vol. 19, pp. 269–278, Apr. 1990.

[22] M. K. Friedberg and A. N. Redington, "Right versus left ventricular failure: differences, similarities, and interactions.," *Circulation*, vol. 129, pp. 1033–1044, Mar. 2014.

[23] B. K. Slinker and S. A. Glantz, "End-systolic and end-diastolic ventricular interaction.," *The American journal of physiology*, vol. 251, pp. H1062–75, Nov. 1986.

[24] D. Sanchez-Quintana, R. H. Anderson, and S. Y. Ho, "Ventricular myoarchitecture in tetralogy of Fallot.," *Heart*, vol. 76, pp. 280–286, Sept. 1996.

[25] J. R. B. Krovetz, L J and S. D. Goldbloom, "Limitation of Correction of Frequency Dependent Artefact in Pressure Recordings Using Harmonic Analysis," *Circulation*, Nov. 1974.

[26] A. de Vecchi, R. E. Clough, N. R. Gaddum, M. C. Rutten, P. Lamata, T. Schaeffter, D. A. Nordsletten, and N. P. Smith, "Catheter-induced errors in pressure measurements in vessels: an in-vitro and numerical study," *IEEE Transactions on Biomedical Engineering*, vol. 61, no. 6, 2014.

[27] E. B. Gleason, W L and, "Studies on the first derivative of the ventricular pressure pulse in man," *Journal of Clinical Investigation*, 1962.

[28] M. I. Monge Garcia, Z. Jian, J. J. Settels, C. Hunley, M. Cecconi, F. Hatib, and M. R. Pinsky, "Performance comparison of ventricular and arterial dP/dtmax for assessing left ventricular systolic function during different experimental loading and contractile conditions," *Critical Care*, vol. 22, pp. 1–12, Dec. 2018.

[29] H. Sandler and H. T. Dodge, "Left Ventricular Tension and Stress in Man," *Circulation Research*, Aug. 1963.

[30] J. F. Spann Jr, R. A. Buccino, E. H. Sonnenblick, and E. Braunwald, "Contractile State of Cardiac Muscle Obtained from Cats with Experimentally Produced Ventricular Hypertrophy and Heart Failure," *Circulation Research*, Sept. 1967.

[31] C. Grant, D. G. Greene, and I. L. Bunnell, "Left ventricular enlargement and hypertrophy: A clinical and angiocardiographic study," *The American Journal of Medicine*, vol. 39, no. 6, pp. 895–904, 1965.

[32] W. Grossman, D. Jones, and L. P. McLaurin, "Wall stress and patterns of hypertrophy in the human left ventricle.," *The Journal of Clinical Investigation*, vol. 56, pp. 56–64, July 1975.

[33] W. Grossman, F. Haynes, and S. S. Paraskos, "Alterations in preload and myocardial mechanics in the dog and in man," *Circulation Research*, 1972.

[34] D. Burkhoff, I. Mirsky, and H. SUGA, "Assessment of systolic and diastolic ventricular properties via pressure-volume analysis: a guide for clinical, translational, and basic researchers," *American Journal of Physiology-Heart and Circulatory Physiology*, Aug. 2005.

[35] S. Sasayama and H. Asanoi, "Coupling between the heart and arterial system in heart failure," *The American Journal of Medicine*, vol. 90, no. 5, Supplement 2, pp. S14–S18, 1991. Ibopamine: A new pharmacotherapeutic approach to heart failure.

[36] H. Ishihara, M. Yokota, T. Sobue, and H. Saito, "Relation between ventriculoarterial coupling and myocardial energetics in patients with idiopathic dilated cardiomyopathy," *Journal of the American College of Cardiology*, Feb. 1994.

[37] M. R. Starling, M. M. Kirsh, D. G. Montgomery, and M. D. Gross, "Mechanisms for left ventricular systolic dysfunction in aortic regurgitation: Importance for predicting the functional response to aortic valve replacement," *Journal of the American College of Cardiology*, Mar. 1991.

[38] J. Gorcsan, T. A. Gasior, W. A. Mandarino, L. G. Deneault, B. G. Hattler, and M. R. Pinsky, "Assessment of the immediate effects of cardiopulmonary bypass on left ventricular performance by on-line pressure-area relations.," *Circulation*, vol. 89, pp. 180–190, Jan. 1994.

[39] J. J. Schreuder, J. D. Biervliet, E. T. van der Velde, K. ten Have, A. D. van Dijk, N. G. Meyne, and J. Baan, "Systolic and diastolic pressure-volume relationships during cardiac surgery.," *Journal of cardiothoracic and vascular anesthesia*, vol. 5, pp. 539–545, Dec. 1991.

[40] J. J. Schreuder, A. Castiglioni, F. Maisano, P. Steendijk, A. Donelli, J. Baan, and O. Alfieri, "Acute decrease of left ventricular mechanical dyssynchrony and improvement of contractile state and energy efficiency after left ventricular restoration.," *The Journal of Thoracic and Cardiovascular Surgery*, vol. 129, pp. 138–145, Jan. 2005.

[41] I. John Gorcsan, S. Murali, P. J. Counihan, W. A. Mandarino, and R. L. Kormos, "Right Ventricular Performance and Contractile Reserve in Patients With Severe Heart Failure," *Circulation*, Dec. 1996.

[42] T. Shishido, K. Hayashi, K. Shigemi, T. Sato, M. Sugimachi, and K. Sunagawa, "Single-beat estimation of end-systolic elastance using bilinearly approximated time-varying elastance curve.," *Circulation*, vol. 102, pp. 1983–1989, Oct. 2000.

[43] C.-H. Chen, B. Fetics, E. Nevo, C. E. Rochitte, K.-R. Chiou, P.-A. Ding, M. Kawaguchi, and D. A. Kass, "Noninvasive single-beat determination of left ventricular end-systolic elastance in humans," *Journal of the American College of Cardiology*, Dec. 2001.

[44] D. A. Kass, W. M. Circulation, and 1988, "From'Emax'to pressure-volume relations: a broader view.," *Am Heart Assoc*, 1988.

[45] K. Sunagawa, W. L. Maughan, and K. Sagawa, "Effect of regional ischemia on the left ventricular end-systolic pressure-volume relationship of isolated canine hearts.," *Circulation Research*, Feb. 1983.

[46] T. Noda, C. P. Cheng, P. P. De Tombe, and W. C. Little, "Curvilinearity of LV end-systolic pressure-volume and dP/dtmax-end-diastolic volume relations," *American Journal of Physiology-Heart and Circulatory Physiology*, Sept. 1993.

[47] D. A. Kass, R. Beyar, E. Lankford, M. Heard, and W. Maughan, "Influence of contractile state on curvilinearity of in situ end-systolic pressure-volume relations.," *Circulation*, 1989.

[48] D. Burkhoff, S. Sugiura, D. T. Yue, and K. Sagawa, "Contractility-dependent curvilinearity of end-systolic pressure-volume relations," *American Journal of Physiology-Heart and Circulatory Physiology*, June 1987.

[49] S. Vandenberghe, P. Segers, P. Steendijk, B. Meyns, R. A. E. Dion, J. F. Antaki, and P. Verdonck, "Modeling Ventricular Function during Cardiac Assist: Does Time-Varying Elastance Work?," *ASAIO Journal*, vol. 52, no. 1, p. 4, 2006.

[50] E.-j. Kim and M. Capoccia, "Synergistic Model of Cardiac Function with a Heart Assist Device," *Bioengineering*, vol. 7, p. 1, Mar. 2020.

[51] D. Chapelle, P. Le Tallec, P. Moireau, and M. Sorine, "An energy-preserving muscle tissue model: formulation and compatible discretizations," *International Journal for Multiscale Computational Engineering*, vol. 10, no. 2, pp. 189–211, 2012.

[52] A. Le Gall, F. Vallée, K. Pushparajah, T. Hussain, A. Mebazaa, D. Chapelle, É. Gayat, and R. Chabiniok, "Monitoring of cardiovascular physiology augmented by a patient-specific biomechanical model during general anesthesia. A proof of concept study," *PLoS ONE*, vol. 15, p. e0232830, May 2020.

[53] A. G. Wallace, N. S. Skinner, and J. H. Mitchell, "Hemodynamic determinants of the maximal rate of rise of left ventricular pressure.," *The American journal of physiology*, vol. 205, pp. 30–36, July 1963.

[54] R. R. Taylor, J. W. Covell, and J. Ross, "Influence of the thyroid state on left ventricular tension-velocity relations in the intact, sedated dog.," *The Journal of Clinical Investigation*, vol. 48, pp. 775–784, Apr. 1969.

[55] D. T. Mason, "Usefulness and limitations of the rate of rise of intraventricular pressure (dp/dt) in the evaluation of myocardial contractility in man," *The American Journal of Cardiology*, vol. 23, pp. 516–527, Apr. 1969.

[56] M. D. Bogaard, P. Houthuizen, F. A. Bracke, P. A. Doevendans, F. W. Prinzen, M. Meine, and B. M. van Gelder, "Baseline left ventricular dP/dtmax rather than the acute improvement in dP/dtmax predicts clinical outcome in patients with cardiac resynchronization therapy," *European Journal of Heart Failure*, vol. 13, pp. 1126–1132, Oct. 2011.

[57] G. S. Nelson, C. W. Curry, B. T. Wyman, A. Kramer, J. Declerck, M. Talbot, M. R. Douglas, R. D. Berger, E. R. McVeigh, and D. A. Kass, "Predictors of Systolic Augmentation From Left Ventricular Preexcitation in Patients With Dilated Cardiomyopathy and Intraventricular Conduction Delay," *Circulation*, June 2000.

[58] H.-G. Zimmer, "Who Discovered the Frank-Starling Mechanism?," *Physiology*, Oct. 2002.

[59] R. L. Hamlin and C. del Rio, "dP/dtmax — A measure of 'baroinometry'," *Journal of Pharmacological and Toxicological Methods*, vol. 66, no. 2, pp. 63–65, 2012. Ninth Annual Focused Issue on Methods in Safety Pharmacology.

[60] W. C. Little, C. P. Cheng, M. Mumma, Y. Igarashi, J. Vinten-Johansen, and W. E. Johnston, "Comparison of measures of left ventricular contractile performance derived from pressure-volume loops in conscious dogs.," *Circulation*, Nov. 1989.

[61] H. Bowditch, "On the peculiarities of excitability which the fibres of cardiac muscle show," *Translated by Schaefer J, Deppert W, Lie RK, Lohff B, Noble MIM. In The Interval Force Relationship of the Heart: Bowditch Revisited ed Noble MIM and Seed WA*, pp. 3–42, 1871.

[62] S. Sarnoff, J. Mitchell, J. Gilmore, and J. Remensnyder, "Homeometric Autoregulation in the Heart," *Circulation Research*, Sept. 1960.

[63] H. Suzuki, M. Shimano, Y. Yoshida, Y. Inden, T. Muramatsu, Y. Tsuji, N. Tsuboi, H. Hirayama, R. Shibata, and T. Murohara, "Maximum Derivative of Left Ventricular Pressure Predicts Cardiac Mortality After Cardiac Resynchronization Therapy," *Clinical Cardiology*, vol. 33, pp. E18–E23, Dec. 2010.

[64] R. Chabiniok, P. Moireau, C. Kiesewetter, T. Hussain, R. Razavi, and D. Chapelle, "Assessment of atrioventricular valve regurgitation using biomechanical cardiac modeling," in *International Conference on Functional Imaging and Modeling of the Heart*, pp. 401–411, Springer, 2017.

[65] M. Gusseva, T. Hussain, C. H. Friesen, P. Moireau, A. Tandon, C. Patte, M. Genet, K. Hasbani, G. Greil, D. Chapelle, and R. Chabiniok, "Biomechanical Modeling to Inform Pulmonary Valve Replacement in Tetralogy of Fallot Patients after Complete Repair.," *Canadian Journal of Cardiology*, June 2021.

[66] M. Gusseva, J. S. Greer, D. A. Castellanos, M. A. Hussein, G. Greil, S. R. Veeram Reddy, T. Hussain, D. Chapelle, and R. Chabiniok, "Model-assisted time-synchronization of cardiac mr image and catheter pressure data," in *Functional Imaging and Modeling of the Heart* (D. B. Ennis, L. E. Perotti, and V. Y. Wang, eds.), (Cham), pp. 362–372, Springer International Publishing, 2021.

[67] M. R. Starling, R. A. Walsh, L. J. Dell'Italia, G. B. Mancini, J. C. Lasher, and J. L. Lancaster, "The relationship of various measures of end-systole to left ventricular maximum time-varying elastance in man.," *Circulation*, July 1987.

[68] M. K. Karunanithi, J. Michniewicz, S. E. Copeland, and M. P. Feneley, "Right ventricular preload recruitable stroke work, end-systolic pressure-volume, and dP/dtmax-end-diastolic volume relations compared as indexes of right ventricular contractile performance in conscious dogs.," *Circulation Research*, June 1992.

Conclusions and perspectives

Conclusions

Patients with CHD are particularly in demand of personalized healthcare solutions. Standard clinical biomarkers are limited in their ability to provide specific descriptions of advanced pathological states. This could lead to mistaken conclusions regarding the functional capacity of their cardiovascular system [1; 2; 3] and inability to define a correct timing for certain interventions. The knowledge of internal mechanical characteristics of the heart and vasculature could potentially enhance our understanding of the pathological profile of CHDs. With a growing potential of computational models to provide a detailed mechanical (geometrical) description of various compartments of the cardiovascular system a possibility to deploy a model-assisted diagnosis is becoming more and more evident.

The main goal of this thesis was to demonstrate the potential of biomechanical modeling to assist in clinical decision-making related to the management of patients with CHD. In particular, the goal was to develop scientific evidence to support the translation of biomechanical modeling to the clinical environment. The ability to fully exploit such goals largely depends on the collaborative potential of the research environment. The availability of clinical data is often a limiting factor in translational research. In this PhD work such a barrier was overcome thanks to the close collaboration between the modeling team at Inria and the department of pediatric cardiology at UTSW. In addition, a constant clinical outlook on the evolution of the applied modeling framework guided the development of our research.

We employed a previously developed multi-scale biomechanical model [4] with a geometry reduced to a spherical shape [5]. The model represents the mechanical behavior of a single ventricular cavity that is coupled to the circulatory system via a system of diodes and Windkessel model. The system of diodes contains forward and backward components allowing to include forward and backward flow through the arterial valve, respectively [6]. We demonstrated the potential of this model to provide an enhanced mechanical description of the RVs of patients with rTOF that are subjected to PV regurgitation and/or RVOTO. In particular, we showed an ability of this model (1) to evaluate the 'current mechanical state' of the RVs prior to and after PVR, and (2) to predict the evolution of RV mechanics under different loading conditions. In addition we showed an application of the model to provide a rigorous clinical data treatment of a variety of data acquisition protocols. This further extends the spectrum of clinical problems that could be optimized by means of patient-specific biomechanical modeling.

The results of this PhD work could be summarized in the following categories.

I: Patient-specific mechanical description of the right ventricle and pulmonary circulatory system

Model-derived contractility provided an insight into the mechanical state of the RV subjected to different hemodynamic conditions. Thanks to the valvular component in the model the calibration of the myocardial contractility considered the presence of PV regurgitation and RVOTO. Thus, we could assess the influence of independent and combined effects of PV regurgitation and RVOTO on RV functional state. Our results demonstrated that patients with predominant RVOTO experience higher levels of contractility pre-PVR and higher levels of contractility decrease post-PVR compared to those with predominant PV regurgitation. In addition, we have demonstrated the ability of the model to predict the mechanical response of the ventricle under progressive recovery of RV PSP through decreasing levels of RVOTO. We derived *in silico* relationships between myocardial contractility and RVOTO that appeared to be linear. These relationships demonstrated an immediate response of the

cardiac contractility to a given decrease in RVOTO.

Overall, we could quantify the level of RV overload and how the level of overloading could decrease after intervention on the valve. Even though our study is not able to provide the cut-off values of ventricular overload (when myocardial remodeling becomes irreversible) we speculate that revealed mechanical insight into the RV function could contribute to the optimal clinical management of patients with valvular pathologies. For example, if the need to aim for long-term relief of RVOTO is highlighted, the surgical approach of valve replacement might be preferential. The *in silico* relationship between contractility and RVOTO could be interpreted as a 'virtual experimental tool' for testing various post-PVR loading conditions. This could further contribute to the choice of the type of intervention on the valve (e.g. type or size of prosthesis, or percutaneous vs. surgical approach).

II: Model-assisted pressure-volume time-sychronization to optimize patients diagnostics

We developed a model-assisted time-synchronization technique of clinical P-V signals that is universal w.r.t. data acquisition protocols. The universality of the approach is determined by the model ability (1) to represent the physiological timing of the events of the cardiovascular system, (2) to integrate multiple data inputs, and (3) to represent ventricular mechanics considering the valvular regurgitation (i.e. the shape of the simulated P-V accounts for valvular mechanics). The time-synchronized P-V loops were qualitatively improved yielding physiologically more meaningful measures of ventricular energetics (e.g. $E_{\max}$ and stroke work).

Clinical scenarios that necessitate high-quality P-V loops for the therapy planning can benefit from the proposed model-based time-synchronization of P-V signals. The modeling framework is fast in computation time and can be directly employed in clinical settings. The applicability of the method for both simultaneously and sequentially acquired CMR and pressure data makes the use of P-V loops available to all centers and not only to those with dedicated and costly pressure and conductance catheters for simultaneous P-V loop systems. The proposed method applies the model to contribute to the planning of complex interventions and, thanks to the biophysical and physiological background of the models, it can consequently augment the possibilities of optimal clinical management.

The developed model-assisted time-synchronization belongs to the 'model-constrained' data processing techniques. We proposed a novel approach to align the data 'in time' while there are a number of model-constrained techniques to register data in space [7; 8; 9].

III: Correspondence of model-derived indices of myocardial contractility with clinically accepted measures of systolic performance

We have demonstrated the correspondence of data-derived indices of myocardial contractility (E_{max} and $\max(dP/dt)$) with model-derived contractility and $\max(dP/dt)$. A physiological validation of novel model-derived indices is one of the necessary steps in their translation to a clinical usage. In addition, we confronted data- and model-derived $\max(dP/dt)$. We suggested a potential application of $\max(dP/dt)$ as a model-based data filter of clinical $\max(dP/dt)$, The latter could be either (1) not available at all due to the absence of continuous intraventicular pressure signal; or (2) too noisy. The noise is inherent to the pressure acquisition itself and is amplified once the time derivative is computed.

A thorough literature review on clinical relevance of the data- and model-derived measures of contractility showed that the gold standard measure of ventricular contractility is challenging to use with the current physiological and biomechanical knowledge. This further substantiates a need for (1) a rigorous validation of the existing model-based

indicators and (2) a continued search for other biomechanical model-based indices of myocardial function. In addition, the literature review emphasized that some clinical scenarios might benefit from combining several indices of contractile performance.

Perspectives

Having obtained a detailed mechanical description of the RV myocardial function pre- and post-PVR of patients with rTOF, a natural perspective of these results will be to further explore a functional characteristic of the myocardium in terms of (1) myocardial energetics, (2) contractile reserve, (3) long-term evolution of contractility post-PVR, and (4) biventricular (i.e. RV-LV) interaction.

Myocardial energetics

A decreased contractility and stroke work post-PVR suggest a possible decrease in the myocardial metabolic and oxygen demand. Myocardial oxygen consumption was not evaluated but could be in principle measured by the Fick principle (from arterial and coronary sinus oxygen concentration) or via the ammonia positron emission tomography [10].

Contractile reserve

A knowledge of the contractile reserve of the patients could help to understand the functional limits of the heart. We could normalize patient-specific contractility indices obtained in Chapter 1 by the corresponding maximum contractility value to stratify the level of severity of pre-PVR contractility among patients. In addition, the level of contractile reserve itself could be an independent index of cardiac functionality [11], and could be used to access the response to PVR. Previous works have quantified the contractile reserve during dobutamine stress testing using the current 0D model [12] or time-varying elastance [13]. A similar methodology could be directly transferred to the patients with rTOF.

Automatization of the model setup

To date there exists a variety of biomechanical modeling approaches allowing a realistic simulation of myocardial mechanics in pathophysiological conditions. However, the validation of these models against *in vivo* patients data has not been extensively performed on large patients cohorts (> 100 subjects) [14]. Efficient methods enabling automatic parameter estimation could substantially contribute to the translation of the models into clinical practice. These methods could make large scale clinical studies possible and enable the sensitivity analysis of the novel model-derived indices. Some parameter estimation techniques have the potential to be integrated into an applied modeling pipeline, e.g. [15; 16; 17; 18; 19].

In this thesis patient-specific parameters were adjusted manually by following a sequential calibration of the corresponding model compartments. By using automated parameter identification a similar study could be extended to a larger cohort of patients (e.g. > 100 subjects). We particularly envision to run the model with more data of RVs of patients with rTOF solely affected by PV regurgitation. In Chapter 1 we have observed that 2 patient with dilated RVs (iEDV > 150 ml/m^2) from the group predominantly affected by PV regurgitation were outliers due to the high contractility. This suggests there might be an association between the level of RV dilatation and contractility. With only 9 patients in that group we could not investigate such a relationship. More patients data coupled to the

current 0D model could possibly provide a richer mechanical insight of the effect of PV regurgitation on the RV health.

Long-term remodeling of the myocardium

We showed that the biomechanical model employed in this thesis could be an efficient tool in characterizing immediate mechanical properties of the cardiovascular system. The results of Chapters 1 and 2 were interpreted without explicitly considering the previous or future progress of ventricular remodeling. The state of the myocardial health of patients with rTOF is however constantly evolving in time both prior to and after PVR. Therefore, in the future we propose to combine our modeling approach with models capturing a long-term evolution of cardiac mechanics. In particular, the kinematic growth theory framework [20; 21; 22] allows to simulate growth and remodeling of the myocardium. This theory assumes that changes in ventricular shape and size occur in response to the applied stress- and/or strain-based mechanical stimuli. Thus, various studies have modeled concentric and/or eccentric cardiac growth (as well as reverse growth) in terms of the chronic changes in ventricular morphology in response to e.g. simulated aortic stenosis and mitral valve regurgitation [23], simulated diastolic and systolic heart failure [24], and unloading of the left ventricle (i.e. a strain-driven reverse myocardial growth) [25]. The simulation results of these studies showed a good agreement with the image data of patients. The kinematic growth theory allows to study a consequence of growth (reverse growth) on organ morphology but does not capture an evolution of intrinsic tissue mechanical properties (i.e. myocardial contractility and stiffness).

We hypothesize that patients with rTOF could notably benefit from a modeling tandem combining the current patient-specific instantaneous model with the models of cardiac growth. Models of long-term evolution have the potential to include information about the initial state of pathology, type of repair, and the evolution throughout the life of patient. They could also be useful in better understanding the reverse remodeling after PVR – a crucial step in predicting the long-term effect of PVR.

The interpretation of the model-derived post-PVR indicators obtained in Chapter 1 could be enhanced by the model of reverse myocardial growth (such as [25]). As a perspective study of Chapter 2 we propose to investigate the morphological change of the ventricular cavity to mechanical unloading at several points along the predicted line, where a given change of intraventricular pressure with respect to pre-PVR could be considered as a stress-based unloading stimulus.

Synergetic approaches in modeling of cardiovascular disease

Digital tools that could aid clinical decision-making do not only reside within the mechanical models. Data-driven models (i.e. based on statistical and machine learning techniques) have proved their utility and robustness to identify unseen trends from large data cohorts that are of prognostic significance. For example, in application to rTOFs statistical shape modeling studies quantified the level of RV remodeling in terms of the association between morphological indices (i.e. global and regional RV dilatation, outflow tract bulging) and the level of PV regurgitation [26; 27]. A recent study by Mauger et al. [28] quantified the relationship between the biventricular shape variation and the severity of PV regurgitation. These studies assume that tissue-level remodeling is translated to the geometrical alterations of the ventricular cavity. Therefore, the associated statistical relationships between the morphological indices are interpreted as representative of the underlying changes in tissue functional capacity. The approach seems to be promising in (1) identifying global trends

in the population and (2) stratifying anatomical variability among patients. It is however limited in explaining the functional state of the outliers from the population templates [26].

An employment of a synergetic modeling approach in creation of digital medicine tools has been recently proposed [29]. It implies to combine data-driven and mechanical models in order to tackle clinical problems from a broader perspective [30]. For example, an application of this thesis combining current biomechanical model with aforementioned statistical shape modeling approaches [26; 27; 28] could provide tissue-level mechanical insight into revealed statistical relationships between the level of RV dilatation and PV regurgitation. In addition such a synergy could potentially describe the functional state of the population outliers revealed by the shape models (e.g. such as in [26]).

From a global perspective model synergies could be used to create population atlases that combine geometrical and mechanical indices of a variety of cardiovascular diseases. For example, considering the UK Biobank [31] as a source of population data, the machine learning algorithms could be used to classify and identify geometrical biomarkers of specific cardiac phenotypes. Then, each phenotype could be studied by means of biomechanical models (such as the model deployed in this thesis) in a patient-specific manner. The aim could be to obtain a range of patient-specific biomechanical parameters of the observed geometrical variability within a given phenotype. Biomechanical model-based description of the population phenotypes could in turn (1) broaden our knowledge of the key pathophysiological mechanisms, (2) enable *in silico* trails for the therapy development, and (3) provide prognosis of the effects of therapeutic interventions [29].

Indirect ventricular coupling via coupled model of two ventricles

In this thesis we primarily focused on the model-based analysis of the RV function of patients with rTOF. However, in patients with rTOF RV dysfunction often impairs LV systolic and diastolic performance [32; 33]. Some studies indeed suggest that the degree of LV dysfunction might be of prognostic significance and deterministic of exercise capacity in rTOFs [34; 35; 36].

In patients with rTOF LV dysfunction arises secondarily to RV volume and pressure overload. This is likely to be attributed to the biventricular coupling (i.e. anatomical and mechanical interdependence). The two ventricles are encapsulated by the common pericardial sac and share their fibers via the septum and subepicardial layers. During every cardiac beat both contraction and relaxation of the ventricular chambers are determined by such an interdependence. Thus, during cardiac systole the LV has been found to substantially contribute to RV contraction [37; 38; 39]. The total diastolic LV motion is constrained by the level of RV dilation due to the limited ability of the pericardial sac to stretch [38]. For example, reduced diastolic wall strain was found in the LVs of rTOFs with high level of RV volume overload [40; 41]. The reduced ability of LV to stretch during diastole leads to the decreased LV preload. This in turn could lead to a decrease in LV cardiac output via (1) reduced LV EDV, and (2) reduced ESV via Frank-Starling mechanism (i.e. length dependent decrease in the ability of the myocytes to develop maximum force).

The mechanisms that link RV dysfunction to a decrease in LV function remain poorly understood. Therefore, we hypothesize that extending the current model of single-ventricle to a coupled model of two ventricles (LV and RV) and two circulatory systems (pulmonary and systemic) could provide a tool to investigate the ventricular interdependence in patients with rTOF. In particular, we aim to investigate indirect ventricular coupling – e.g. the effect of RV output on LV preload pre- and post-PVR in terms of changes in LV EDV and myocardial contractility. After the removal of PV regurgitation from the RV during PVR the effective PA flow (Q_{eff}) increases [42]. Recall that in Chapter 1 we showed a model-

predicted increase in effective pulmonary flow (Q_{eff}) immediately post-PVR. Therefore, the volume of blood that fills the LA and LV should also increase. A number of studies showed an immediate increase in LV EDV immediately post-PVR [42; 35]. Therefore, we hypothesize that increased PA Q_{eff} is associated with increased LV EDV post-PVR via indirect ventricular coupling – an effect that we would aim to reproduce with a coupled model. A description of an envisioned 4-cavity closed-loop model of two ventricles and two circulatory systems as well as some preparatory work can be found in the Appendix A.

Final conclusions

This thesis demonstrated that biomechanical modeling could be deployed in a clinical environment to address various types of problems. The biomechanical model provides a common framework to integrate multiple datasets from individual patients. In application to patients with rTOF suffering from ventricular overload we have demonstrated that the current framework could assist in evaluating the response to the intervention and potentially advise a type of intervention on the valve. Moreover, this type of model-predicted outcome could be directly translated to the population of patients with other valvular pathologies (e.g. aortic valve stenosis). In addition, we demonstrated the potential of the model to provide 'model-constrained' data-processing of the variety of data acquisition protocols.

Models can facilitate the transition from population-based clinical decision-making (i.e. derived from empirical evidence-based clinical studies) to a patient-specific care. Predictions based on coupling clinical data and biomechanical models have the potential to become part of clinical assessment to contribute to optimizing and personalizing the clinical management of every patient.

Bibliography

[1] M. A. Quail, A. Frigiola, A. Giardini, V. Muthurangu, M. Hughes, P. Lurz, S. Khambadkone, J. E. Deanfield, V. Tsang, and A. M. Taylor, "Impact of Pulmonary Valve Replacement in Tetralogy of Fallot With Pulmonary Regurgitation: A Comparison of Intervention and Nonintervention," *The Annals of Thoracic Surgery*, vol. 94, no. 5, pp. 1619–1626, 2012.

[2] C. Lee, Y. M. Kim, C.-H. Lee, J. G. Kwak, C. S. Park, J. Y. Song, W.-S. Shim, E. Y. Choi, S. Y. Lee, and J. S. Baek, "Outcomes of Pulmonary Valve Replacement in 170 Patients With Chronic Pulmonary Regurgitation After Relief of Right Ventricular Outflow Tract Obstruction: Implications for Optimal Timing of Pulmonary Valve Replacement," *Journal of the American College of Cardiology*, Sept. 2012.

[3] C. Ince, "Personalized physiological medicine," *Critical Care*, vol. 21, pp. 27–33, Dec. 2017.

[4] D. Chapelle, P. L. Tallec, P. Moireau, and M. Sorine, "Energy-preserving muscle tissue model: formulation and compatible discretizations," *International Journal for Multiscale Computational Engineering*, vol. 10, no. 2, pp. 189–211, 2012.

[5] M. Caruel, R. Chabiniok, P. Moireau, Y. Lecarpentier, and D. Chapelle, "Dimensional reductions of a cardiac model for effective validation and calibration," *Biomechanics and Modeling in Mechanobiology*, vol. 13, pp. 897–914, Aug. 2014.

[6] J. Sainte-Marie, D. Chapelle, R. Cimrman, and M. Sorine, "Modeling and estimation of the cardiac electromechanical activity," *Computers & Structures*, vol. 84, pp. 1743–1759, Nov. 2006.

[7] D. Rueckert, L. I. Sonoda, C. Hayes, D. L. Hill, M. O. Leach, and D. J. Hawkes, "Nonrigid registration using free-form deformations: application to breast MR images," *IEEE transactions on medical imaging*, vol. 18, no. 8, pp. 712–721, 1999.

[8] J.-M. Peyrat, H. Delingette, M. Sermesant, C. Xu, and N. Ayache, "Registration of 4D cardiac CT sequences under trajectory constraints with multichannel diffeomorphic demons," *IEEE transactions on medical imaging*, vol. 29, no. 7, pp. 1351–1368, 2010.

[9] J. Schaerer, C. Casta, J. Pousin, and P. Clarysse, "A dynamic elastic model for segmentation and tracking of the heart in MR image sequences," *Medical Image Analysis*, vol. 14, no. 6, pp. 738–749, 2010.

[10] R. Slart, R. Tio, P. Van Der Vleuten, T. Willems, D. Lubbers, R. Dierckx, and D. van Veldhuisen, "Myocardial perfusion reserve and contractile pattern after beta-blocker therapy in patients with idiopathic dilated cardiomyopathy," *Journal of Nuclear Cardiology*, vol. 17, no. 3, pp. 479–485, 2010.

[11] R. Morimoto, T. Okumura, A. Hirashiki, H. Ishii, T. Ichii, S. Aoki, K. Furusawa, H. Hiraiwa, T. Kondo, N. Watanabe, *et al.*, "Myocardial contractile reserve predicts left ventricular reverse remodeling and cardiac events in dilated cardiomyopathy," *Journal of cardiology*, vol. 70, no. 4, pp. 303–309, 2017.

[12] B. Ruijsink, K. Zugaj, J. Wong, K. Pushparajah, T. Hussain, P. Moireau, R. Razavi, D. Chapelle, and R. Chabiniok, "Dobutamine stress testing in patients with Fontan circulation augmented by biomechanical modeling," *PloS one*, vol. 15, no. 2, p. e0229015, 2020.

[13] J. Wong, K. Pushparajah, A. de Vecchi, B. Ruijsink, G. F. Greil, T. Hussain, and R. Razavi, "Pressure–volume loop-derived cardiac indices during dobutamine stress: a step towards understanding limitations in cardiac output in children with hypoplastic left heart syndrome," *International journal of cardiology*, vol. 230, pp. 439–446, 2017.

[14] S. Niederer, Y. Aboelkassem, C. D. Cantwell, C. Corrado, S. Coveney, E. M. Cherry, T. Delhaas, F. H. Fenton, A. Panfilov, P. Pathmanathan, *et al.*, "Creation and application of virtual patient cohorts of heart models," *Philosophical Transactions of the Royal Society A*, vol. 378, no. 2173, p. 20190558, 2020.

[15] S. Longobardi, A. Lewalle, S. Coveney, I. Sjaastad, E. K. Espe, W. E. Louch, C. J. Musante, A. Sher, and S. A. Niederer, "Predicting left ventricular contractile function via Gaussian process emulation in aortic-banded rats," *Philosophical Transactions of the Royal Society A*, vol. 378, no. 2173, p. 20190334, 2020.

[16] L. Marx, M. A. Gsell, A. Rund, F. Caforio, A. J. Prassl, G. Toth-Gayor, T. Kuehne, C. M. Augustin, and G. Plank, "Personalization of electro-mechanical models of the pressure-overloaded left ventricle: fitting of Windkessel-type afterload models," *Philosophical Transactions of the Royal Society A*, vol. 378, no. 2173, p. 20190342, 2020.

[17] J. Mineroff, A. D. McCulloch, D. Krummen, B. Ganapathysubramanian, and A. Krishnamurthy, "Optimization framework for patient-specific cardiac modeling," *Cardiovascular engineering and technology*, vol. 10, no. 4, pp. 553–567, 2019.

[18] P. Moireau, D. Chapelle, and P. Le Tallec, "Filtering for distributed mechanical systems using position measurements: perspectives in medical imaging," *Inverse problems*, vol. 25, no. 3, p. 035010, 2009.

[19] R. Chabiniok, P. Moireau, P.-F. Lesault, A. Rahmouni, J.-F. Deux, and D. Chapelle, "Estimation of tissue contractility from cardiac cine-MRI using a biomechanical heart model," *Biomechanics and modeling in mechanobiology*, vol. 11, no. 5, pp. 609–630, 2012.

[20] E. K. Rodriguez, A. Hoger, and A. D. McCulloch, "Stress-dependent finite growth in soft elastic tissues.," *Journal of Biomechanics*, vol. 27, pp. 455–467, Apr. 1994.

[21] W. Kroon, T. Delhaas, T. Arts, and P. Bovendeerd, "Computational modeling of volumetric soft tissue growth: application to the cardiac left ventricle," *Biomechanics and Modeling in Mechanobiology*, vol. 8, pp. 301–309, Aug. 2009.

[22] S. Göktepe, O. J. Abilez, and E. Kuhl, "A generic approach towards finite growth with examples of athlete's heart, cardiac dilation, and cardiac wall thickening," *Journal of the Mechanics and Physics of Solids*, vol. 58, no. 10, pp. 1661–1680, 2010.

[23] R. C. P. Kerckhoffs, J. Omens, and A. D. McCulloch, "A single strain-based growth law predicts concentric and eccentric cardiac growth during pressure and volume overload.," *Mechanics research communications*, vol. 42, pp. 40–50, June 2012.

[24] M. Genet, L. C. Lee, B. Baillargeon, J. M. Guccione, and E. Kuhl, "Modeling Pathologies of Diastolic and Systolic Heart Failure.," *Annals of biomedical engineering*, vol. 44, pp. 112–127, Jan. 2016.

[25] L. C. Lee, M. Genet, G. Acevedo-Bolton, K. Ordovas, J. M. Guccione, and E. Kuhl, "A computational model that predicts reverse growth in response to mechanical unloading.," *Biomechanics and Modeling in Mechanobiology*, vol. 14, pp. 217–229, Apr. 2015.

[26] T. Mansi, I. Voigt, B. Leonardi, X. Pennec, S. Durrleman, M. Sermesant, H. Delingette, A. M. Taylor, Y. Boudjemline, G. Pongiglione, *et al.*, "A statistical model for quantification and prediction of cardiac remodelling: Application to tetralogy of fallot," *IEEE transactions on medical imaging*, vol. 30, no. 9, pp. 1605–1616, 2011.

[27] B. Leonardi, A. M. Taylor, T. Mansi, I. Voigt, M. Sermesant, X. Pennec, N. Ayache, Y. Boudjemline, and G. Pongiglione, "Computational modelling of the right ventricle in repaired tetralogy of Fallot: can it provide insight into patient treatment?," *European Heart Journal–Cardiovascular Imaging*, vol. 14, no. 4, pp. 381–386, 2013.

[28] C. A. Mauger, S. Govil, R. Chabiniok, K. Gilbert, S. Hegde, T. Hussain, A. D. McCulloch, C. J. Occleshaw, J. Omens, J. C. Perry, *et al.*, "Right-left ventricular shape variations in tetralogy of Fallot: associations with pulmonary regurgitation," *Journal of Cardiovascular Magnetic Resonance*, vol. 23, no. 1, pp. 1–14, 2021.

[29] J. Corral-Acero, F. Margara, M. Marciniak, C. Rodero, F. Loncaric, Y. Feng, A. Gilbert, J. F. Fernandes, H. A. Bukhari, A. Wajdan, *et al.*, "The 'Digital Twin' to enable the vision of precision cardiology," *European heart journal*, vol. 41, no. 48, pp. 4556–4564, 2020.

[30] F. Regazzoni, D. Chapelle, and P. Moireau, "Combining data assimilation and machine learning to build data-driven models for unknown long time dynamics—Applications in cardiovascular modeling," *International Journal for Numerical Methods in Biomedical Engineering*, p. e3471, 2021.

[31] "The UK Biobank." https://www.ukbiobank.ac.uk/, 2015.

[32] C. S. Broberg, J. Aboulhosn, F.-P. Mongeon, J. Kay, A. M. Valente, P. Khairy, M. G. Earing, A. R. Opotowsky, G. Lui, D. R. Gersony, *et al.*, "Prevalence of left ventricular systolic dysfunction in adults with repaired tetralogy of Fallot," *The American journal of cardiology*, vol. 107, no. 8, pp. 1215–1220, 2011.

[33] M. Śpiewak, Ł. A. Małek, J. Petryka, Ł. Mazurkiewicz, M. Marczak, E. K. Biernacka, M. Kowalski, P. Hoffman, M. Demkow, J. Miśko, *et al.*, "Factors associated with biventricular dysfunction in patients with repaired tetralogy of Fallot," *Kardiologia Polska (Polish Heart Journal)*, vol. 72, no. 7, pp. 631–639, 2014.

[34] A. Ghai, C. Silversides, L. Harris, G. D. Webb, S. C. Siu, and J. Therrien, "Left ventricular dysfunction is a risk factor for sudden cardiac death in adults late after repair of tetralogy of Fallot," *Journal of the American College of Cardiology*, vol. 40, no. 9, pp. 1675–1680, 2002.

[35] M. Vezmar, R. Chaturvedi, K.-J. Lee, C. Almeida, C. Manlhiot, B. W. McCrindle, E. M. Horlick, and L. N. Benson, "Percutaneous Pulmonary Valve Implantation in the Young 2-Year Follow-Up," *JACC-Cardiovascular Interventions*, vol. 3, pp. 439–448, APR 2010.

[36] A. M. Valente, K. Gauvreau, G. E. Assenza, S. V. Babu-Narayan, J. Schreier, M. A. Gatzoulis, M. Groenink, R. Inuzuka, P. J. Kilner, Z. Koyak, *et al.*, "Contemporary predictors of death and sustained ventricular tachycardia in patients with repaired

tetralogy of Fallot enrolled in the INDICATOR cohort," *Heart*, vol. 100, no. 3, pp. 247–253, 2014.

[37] M. P. Feneley, T. P. Gavaghan, D. W. Baron, J. A. Branson, P. Roy, and J. Morgan, "Contribution of left ventricular contraction to the generation of right ventricular systolic pressure in the human heart.," *Circulation*, vol. 71, no. 3, pp. 473–480, 1985.

[38] B. K. Slinker and S. A. Glantz, "End-systolic and end-diastolic ventricular interaction," *American Journal of Physiology-Heart and Circulatory Physiology*, vol. 251, no. 5, pp. H1062–H1075, 1986.

[39] D. Sanchez-Quintana, R. H. Anderson, and S. Y. Ho, "Ventricular myoarchitecture in tetralogy of Fallot.," *Heart*, vol. 76, no. 3, pp. 280–286, 1996.

[40] F. P. Fernandes, C. Manlhiot, S. L. Roche, L. Grosse-Wortmann, C. Slorach, B. W. McCrindle, L. Mertens, P. F. Kantor, and M. K. Friedberg, "Impaired left ventricular myocardial mechanics and their relation to pulmonary regurgitation, right ventricular enlargement and exercise capacity in asymptomatic children after repair of tetralogy of fallot," *Journal of the American Society of Echocardiography*, vol. 25, no. 5, pp. 494–503, 2012.

[41] C. m. Yu, W. s. Wong, V. y. Li, and Y. f. Cheung, "Left ventricular stiffness in adolescents and young adults with repaired tetralogy of Fallot," *Scientific reports*, vol. 7, no. 1, pp. 1–7, 2017.

[42] P. Lurz, J. Nordmeyer, V. Muthurangu, S. Khambadkone, G. Derrick, R. Yates, M. Sury, P. Bonhoeffer, and A. M. Taylor, "Comparison of Bare Metal Stenting and Percutaneous Pulmonary Valve Implantation for Treatment of Right Ventricular Outflow Tract Obstruction," *Circulation*, vol. 119, pp. 2995–3001, June 2009.

Appendix A: Coupled model of two ventricles and two circulatory systems

As a persective of this thesis we would like to investigate an indirect right- and left-ventricular (RV-LV) coupling in patients with rTOF. We aim to address an immediate effect of pulmonary valve replacement (PVR) on LV by means of a 4-cavity closed loop model.

Coupled model of two ventricles and two circulatory systems

We aim to create a 4-cavity closed-loop model with the following constituents: (1) ventricular cavities are represented by the 0D model [1]; (2) atrial cavities by the time-varying elastance model [2]; and (3) valvular components by the system of diodes; and (4) circulation systems by the lumped-parameter model with associated resistance and capacitance of the distal and proximal parts.

In the sequel we present a description of an atrial component in the 4-cavity model. In this model we aim to simulate simultaneous LV and RV contraction and the effect of circulatory system hemodynamics on ventricular mechanics. The goal of the atria in this setup is to provide a realistic ventricular filling. Therefore, we chose a phenomenological description of atrial mechanics – time-varying elastance model [2] – to simulate the flow that fills the ventricles as a result of active atrial contraction. First, we calibrated a 0D model [1] of the atria to *in silico* healthy left atrial dataset obtained from a population study of [3]. Then, we derived a time-varying elastance function from the simulated atrial pressure-volume (P-V) loop that was used an input for the biomechanicaly-derived time-varying elastance model of the atrial cavity [4].

In silico atrial pressure-volume loop

The atrial role in the cardiac cycle can be split into three functional phases [5]:

I Reservoir phase: atria act as a reservoir for blood during ventricular contraction. Passive filling of the atria by the venous return. Atrioventricular (AV) valves are closed.

II Conduit phase: atria act as a conduit that passively fills the ventricle during initial filling period. The phase initiates with the opening of the AV valves.

III Pump phase: atria actively pump the blood into the ventricles at the end of the filling period. Active atrial contraction contributes 15-30 % of total ventricular filling.

The data representative of a healthy left atrial function are presented in Table A1.

Table A1: Healthy left atrial *in silico* dataset. Volume data are the weighted means of healthy left atria from the population study of [3].

V_{max} (ml)	89.00	maximum volume achieved during reservoir phase
V_{min} (ml)	41.00	minimum volume achieved during pump phase
Wall thickness (mm)	2.73	
P_{max} (mmHg)	8.00	maximum pressure achieved during pump phase
P_{min} (mmHg)	2.00	preload for the atrial model (venous pressure)
P-wave (ms)	0.80	depolarization of the atria
PR-section (ms)	0.10	repolarization of the atria

We created a 0D model of the atria to represent the active atrial contraction during the pump phase. The calibration of the atrial model followed the calibration procedure as it is described for the ventricle in the Appendix of Chapter 1. Briefly, the following ingredients were adjusted:

I The afterload for the atria was given by a Windkessel model. Low resistance parameters were set such that simulation was periodic.

II Atrial cavity mass was derived from the atrial wall thickness given by [3].

III Preload pressure (i.e. pressure in the atrium at the end of the conduit phase) was assumed to be 2 mmHg. Atrial stiffness was adjusted to match the *in silico* V_{max}.

IV Forward and backward resistances of the outflow valve were set to the default values to represent no outflow valve obstruction and regurgitation, respectively.

V Electrical activation function was created based on the physiological timings of the duration of atrial depolarization (i.e. equal to 0.08 s) and repolarization (i.e. equal to 0.10 s).

VI Atrial contractility was adjusted to match the *in silico* V_{min}.

The simulation cycle was initiated by the active contraction of the atrium (pump phase). Time-varying elastance – $E(t) = P(t)/V(t)$ – was derived from the simulated pressure-volume loop.

Figure A1 shows the simulated atrial pressure-volume (P-V) loop and the associated time-varying elastance. We remark that ventricular filling happens during the conduit and pump phases of the atrial cycle. During the reservoir phase atrium is decoupled from the ventricle since the AV valve is closed. Therefore, we were particularly interested in reproducing the mechanical behavior of the conduit and pump phases. Our results show a good agreement with *in silico* atrial data. In addition the calculated volume integrals of the conduit and pump phases were 28.96 ml and 12.78 ml, respectively. This suggests that in the simulated 0D model the pump phase contributes 30 % to the total ventricular filling (i.e. given by the sum of the volume of blood of conduit and pump phases).

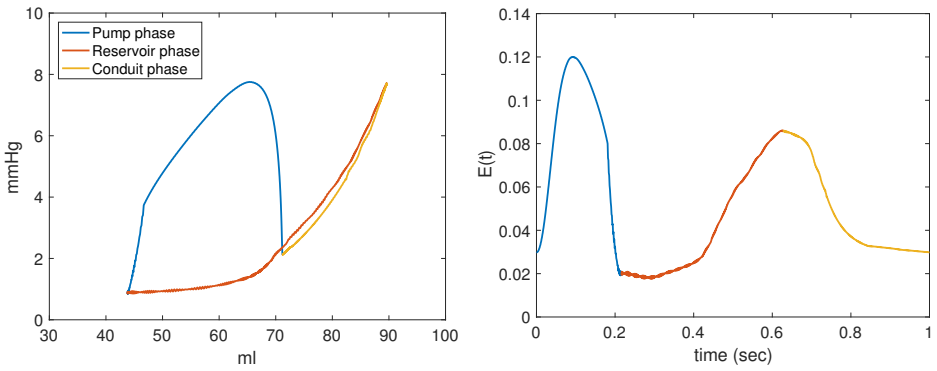

(a) Pressure-volume loop (b) Time-varying elastance

Figure A1: *In silico* atrial pressure-volume loop and the associated time-varying elastance.

Atrial time-varying elastance model

Instead of using a multi-scale description of the cavity mechanics (e.g. atria or ventricle) as provided by a 0D model, the mechanics of contraction could be represented by the time-varying elastance (E(t)) model and a passive filling by end-diastolic pressure volume relationship (EDPVR) – given by the hyperelastic potential eq. (1.4) as shown by Le Gall et al. [4]:

$$\begin{cases} P(t) = E(t) + \eta_{\mathrm{V}}^{\mathrm{s}} \dot{V}(t) & \text{systole} \\ P(t) = \mathrm{EDPVR}(t) + \eta_{\mathrm{V}}^{\mathrm{d}} \dot{V}(t), & \text{diastole} \end{cases} \tag{4.9}$$

where $\eta_{\mathrm{V}}^{\mathrm{s}} \dot{V}(t)$ and $\eta_{\mathrm{V}}^{\mathrm{d}} \dot{V}(t)$ are the penalty terms introduced for numerical stability for systole and diastole, respectively.

We run a biomechanically-derived time-varying elastance model (VEM) of the atria as described by Eq. (4.9). The systolic part was represented by the time-varying elastance of the pump phase derived from the 0D atrial model (Figure A1(b), blue part of the curve), and the diastolic part by the calibrated EDVPR of the atrial 0D model. Figure A2 shows the output of the VEM in comparison with the output of the 0D model of *in silico* atrium. Figure A2 demonstrates that VEM model can accurately reproduce the atrial mechanics. VEM is therefore an optimal modeling choice for a representation of atrial mechanics in the closed-loop 4-cavity model.

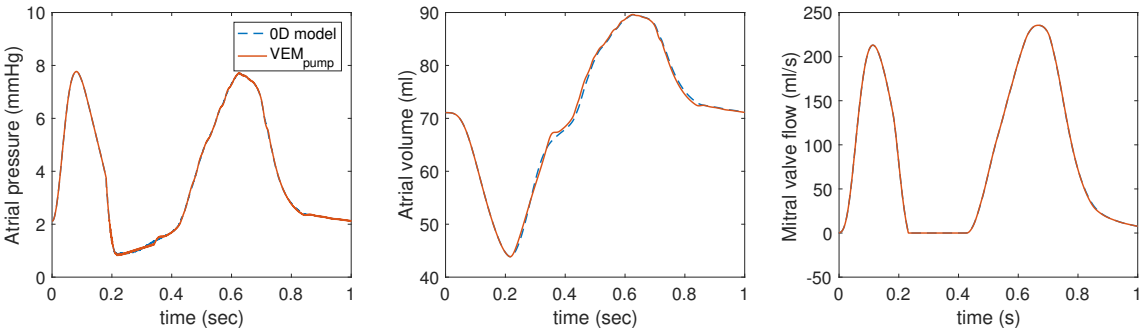

Figure A2: Simulation results of the time-varying elastance ($\mathrm{VEM}_{\mathrm{pump}}$) model of the atrium (orange solid lines) in comparison to the 0D model of the atrium (blue dotted lines).

Bibliography

[1] M. Caruel, R. Chabiniok, P. Moireau, Y. Lecarpentier, and D. Chapelle, "Dimensional reductions of a cardiac model for effective validation and calibration," *Biomechanics and Modeling in Mechanobiology*, vol. 13, pp. 897–914, Aug. 2014.

[2] H. Suga, K. Sagawa, and A. A. Shoukas, "Load independence of the instantaneous pressure-volume ratio of the canine left ventricle and effects of epinephrine and heart rate on the ratio," *Circulation research*, vol. 32, no. 3, pp. 314–322, 1973.

[3] N. Kawel-Boehm, A. Maceira, E. R. Valsangiacomo-Buechel, J. Vogel-Claussen, E. B. Turkbey, R. Williams, S. Plein, M. Tee, J. Eng, and D. A. Bluemke, "Normal values for cardiovascular magnetic resonance in adults and children," *Journal of Cardiovascular Magnetic Resonance*, vol. 17, pp. 1–33, Dec. 2015.

[4] A. Le Gall, F. Vallée, D. Chapelle, and R. Chabiniok, "Minimally-invasive estimation of patient-specific end-systolic elastance using a biomechanical heart model," in *FIMH 2019 - 10th Functional Imaging and Modelling of the Heart*, (Bordeaux, France), June 2019.

[5] A. Pironet, P. C. Dauby, S. Paeme, S. Kosta, J. G. Chase, and T. Desaive, "Simulation of Left Atrial Function Using a Multi-Scale Model of the Cardiovascular System," *PLoS ONE*, vol. 8, p. e65146, June 2013.

ECOLE DOCTORALE

Titre : Modélisation biomécanique cardiovasculaire personnalisée pour améliorer l'interprétation des données cliniques et aider à planifier les interventions chez les patients atteints de cardiopathie congénitale

Mots clés : modélisation biomécanique, contractilité du myocarde, surcharge ventriculaire, cardiopathie valvulaire, cardiopathie congénitale, synchronisation temporelle des données cliniques, médecine personnalisée

Résumé : Cette thèse de doctorat est une recherche interdisciplinaire qui porte sur la modélisation biomécanique appliquée du système cardiovasculaire chez les patients atteints de cardiopathies congénitales. L'objectif est d'explorer le potentiel de la modélisation biomécanique pour aider à la prise de décision clinique.
Tout d'abord, nous avons exploré la capacité d'un modèle biomécanique précédemment développé à améliorer l'interprétation des données cliniques pour les patients atteints de tétralogie de Fallot après réparation (TOFr) avant et après le remplacement de la valve pulmonaire (RVP). Des modèles personnalisés du ventricule droit (VD) et de la circulation pulmonaire ont été construits pour 20 sujets avant et après le RVP à l'aide de données obtenues par résonance magnétique cardiovasculaire (RMC) et par cathéter de pression. Ces modèles ont été soumis aux effets de la régurgitation de la valve pulmonaire (VP) et/ou de l'obstruction du canal de sortie du VD (RVOT). Les modèles ont fourni des indices de contractilité myocardique personnalisés avant et après la RPV. Les résultats ont montré une diminution de la contractilité chez tous les patients après la RVP. Les patients présentant une obstruction prédominante de l'RVOT ont connu une diminution plus importante de la contractilité, alors que l'arrêt de la régurgitation elle-même n'a pas entraîné de réduction significative de la contractilité. Après cette étude détaillée de la pathophysiologie des VD surchargés avant et après la RVP, nous avons exploré la capacité du modèle à prédire la réponse de la mécanique ventriculaire lors de la diminution progressive de la post-charge des VD chez les patients atteints de TOFr. Des modèles pré-PVR personnalisés ont été utilisés et l'arrêt de la régurgitation PV et la diminution progressive de la résistance RVOT ont été supposés. Les relations in silico résultantes entre la contractilité et la résistance de l'RVOT après la RVP sont apparues linéaires et cohérentes avec celles données par les modèles post-RVP spécifiques aux patients.
Pour les patients dont le cœur est constitué d'un seul ventricule et qui subissent une RMC combinée à un cathéter de pression (dans le cadre de la planification d'une chirurgie complexe), le modèle a été utilisé pour synchroniser dans le temps les données de pression du cathéter et les volumes ventriculaires obtenus par RMC. Cette synchronisation temporelle assistée par le modèle produit des boucles P-V de haute qualité qui donnent des indices plus précis de l'énergétique cardiaque (valeur maximale de l'élastance variable dans le temps ($E_{\max}$) et du travail systémique) et qui pourraient donc être utilisés pour améliorer l'interprétation clinique.
Enfin, nous avons comparé les indices de $E_{\max}$ et de la dérivée temporelle maximale de la pression ventriculaire, max(dP/dt), obtenus directement à partir des mesures cliniques, avec la contractilité et le max(dP/dt) dérivés du modèle. Tous les indices dérivés des données et du modèle ont montré une bonne concordance. De plus, une application potentielle du max(dP/dt) dérivé du modèle comme filtre de données basé sur le modèle a été soulignée.
Dans l'ensemble, cette thèse a démontré (1) la capacité de la modélisation biomécanique à fournir des indices mécaniques supplémentaires de la fonction ventriculaire et leur évolution dans différentes conditions de charge, ce qui pourrait contribuer à la planification d'une thérapie optimale ; (2) une application du modèle pour fournir un traitement robuste des données cliniques d'une variété de protocoles d'acquisition de données ; et (3) une correspondance des indices dérivés du modèle avec des mesures de substitution de la contractilité acceptées cliniquement. En conclusion, cette thèse a montré que la modélisation biomécanique pouvait être déployée dans un environnement clinique pour résoudre divers types de problèmes en médecine personnalisée.

Title : Patient-specific cardiovascular biomechanical modeling to augment interpretation of clinical data and assist planning interventions for patients with congenital heart disease

Keywords : biomechanical modeling, myocardial contractility, ventricular overload, valvular heart disease, congenital heart disease, time-synchronization of clinical data, personalized medicine

Abstract : This PhD thesis is an interdisciplinary research that deals with applied biomechanical modeling of the cardiovascular system in patients with congenital heart diseases. The aim is to explore the potential of biomechanical modeling to assist in clinical decision-making.
First, we explored the ability of a previously developed biomechanical model to augment the interpretation of clinical data for patients with tetralogy of Fallot after repair (rTOF) prior to and after pulmonary valve replacement (PVR). Patient-specific models of the right ventricle (RV) and pulmonary circulation were built for 20 subjects pre- and post-PVR using cardiovascular magnetic resonance (CMR) and pressure catheter data. These models were subjected to the effects of pulmonary valve (PV) regurgitation and/or RV outflow tract (RVOT) obstruction. The models provided patient-specific indices of myocardial contractility pre- and post-PVR. The results showed a decrease of contractility in all patients post-PVR. Patients with predominantly RVOT obstruction experienced a higher level of contractility decrease whereas ceasing the regurgitation itself did not lead to a significant reduction in contractility. After this detailed study of pathophysiology of the overloaded RVs pre- and post-PVR, we explored the ability of the model to predict the response of ventricular mechanics when progressively decreasing the afterload of the RVs in patients with rTOF. Pre-PVR patient-specific models were used and cessation of PV regurgitation and progressive decrease of RVOT resistance were assumed. The resulting in silico relationships between the contractility and RVOT resistance post-PVR appeared to be linear, and consistent with that given by the patient-specific post-PVR models.
For patients with single-ventricle hearts undergoing CMR combined with a pressure catheter (as part of planning for complex surgery), the model was used to synchronize in time the catheter-pressure data and the ventricular volumes obtained by CMR. This model-assisted time-synchronization produces high quality P-V loops that yield more accurate indices of myocardial energetics (maximum value of time-varying elastance ($E_{\max}$) and stroke work) and hence could be used to ameliorate the clinical interpretation.
Finally, we compared the indices of $E_{\max}$ and maximum time derivative of ventricular pressure, max(dP/dt), when obtained directly from the clinical measurements vs. model-derived contractility and max(dP/dt). All data- and model-derived indices showed a good agreement. In addition, a potential application of model-derived max(dP/dt) as a model-based data filter was emphasized.
Overall, this thesis demonstrated (1) an ability of biomechanical modeling to provide additional mechanical indices of ventricular function and their evolution under different loading conditions, which has the potential to contribute into the planning of optimal therapy; (2) an application of the model to provide robust clinical data processing of a variety of data acquisition protocols; and (3) a correspondence of model-derived indices with clinically accepted surrogate measures of contractility. In conclusion, this thesis showed that biomechanical modeling could be deployed in a clinical environment to address various types of problems towards the delivery of personalized healthcare solutions.

Institut Polytechnique de Paris
91120 Palaiseau, France